Michael Graupner

Induction and Maintenance of Synaptic Plasticity

Laboratoire de Neurophysique et Physiologie - Paris
Max-Planck-Institut für Physik komplexer Systeme - Dresden

Spécialité Physique
Université Pierre et Marie Curie
Paris VI
France

Institut für Theoretische Physik
Fakultät Mathematik und Naturwissenschaften
Technische Universität Dresden
Germany

Induction and Maintenance of Synaptic Plasticity

Dissertation

submitted in partial satisfaction

of the requirements for the academical degrees

Docteur de l'Université Pierre et Marie CURIE

Doctor rerum naturalium (Dr. rer. nat.)

presented by

Michael Graupner

Born August 9th, 1977 in Annaberg-Buchholz, Germany

Laboratoire de Neurophysique et Physiologie

Max-Planck-Institut für Physik komplexer Systeme

August 2008

Submitted December 21$^{\text{th}}$, 2007
Defended in June 2008 in front of the committee composed of (alphabetical order)

- Dr. Nicolas Brunel (Paris - France, P)
- Prof. Dr. Stéphane Charpier (Paris - France, P)
- Prof. Dr. Wulfram Gerstner (Lausanne - Switzerland, P)
- Prof. Dr. Frank Jülicher (Dresden - Germany, P, D)
- Prof. Dr. Roland Ketzmerick (Dresden - Germany, D)
- Prof. Dr. Clemens Laubschat (Dresden - Germany, D)
- Priv.-Doz. Dr. Günter Plunien (Dresden - Germany, D)
- Dr. Mark van Rossum (Edinburgh - United Kingdom, P)
- Prof. Dr. Petra Schwille (Dresden - Germany, D)

(P in brackets indicates presence during the thesis defense in Paris June 18$^{\text{th}}$, 2008; D in brackets signifies presence during the presentation of results in Dresden June 20$^{\text{th}}$, 2008)

To my Parents
Marianne and Klaus-Peter

Acknowledgments

Learning and memory consolidation are life long processes - shaped by many people and influenced by numerous experiences. For the past four years I am grateful to all those who have taken the time and effort to teach, discuss, and elucidate the many facets of science and career therein.

The person who contributed most to my scientific development in these years is Nicolas Brunel, my supervisor in Paris. I am thankful to him for teaching me all the facets of developing, examining and communicating a scientific project. His innate ability to focus on the essentials and his perfectionism led me to discover how to study a question with true scientific rigor. I am glad for having had the possibility to work with Nicolas.

I would like to thank Daniel Zytnicki for having given me the possibility to work in his laboratory in Paris. I am also indebted to Frank Jülicher who agreed to become my supervisor in Dresden. Thanks to him I had the opportunity to continue my thesis in the framework of a cotutelle (binational promotion). As a consequence, I was able to work with Benjamin Lindner in the MPI-PKS in Dresden for some time. I want to thank Benjamin for his help.

Significant help and advice during my first steps towards the thesis project were provided to me by Michael Meyer-Hermann to whom I am thankful.

I furthermore want to express my special thanks to Gerhard Soff who actively supported the initiation of this thesis project. He tragically passed away in December 2004.

Coming to Paris without speaking one word of French was not difficult thanks to the friendly welcome I experienced in the Laboratoire de Neurophysique et Physiologie. I want to thank all the members of the lab for the friendly atmosphere I experienced during the four years I have been working there. Monique Commercy and in particular Hervé Suaudeau have furthermore kindly helped me to tackle all the administrative and computer related issues during this time. I want to thank Marin Manuel, Kosuke Hamaguchi and Stéphane Jacobs for the enjoyable and constructive ambiance in the office we shared. I will also not forget Elie Berda who always brightened me up by his genuine cheerfulness.

I appreciated a lot the proximity to experimental neurophysiologists who were working on the opposite side of the hallway in the Laboratoire de Physiologie Cérébrale. Amongst those I am indebted to David DiGregorio and Thomas Otis for the many helpful discussions I had with them on the biology of synaptic function.

I want to thank Bernhard Chesnau and Sandrine Le Moigne who did patiently work out the cotutelle contract between the Technische Universität Dresden and the Université Pierre et Marie Curie in Paris.

On a more practical side, I want to thank all the organizations which supported the project of the thesis financially. These are: the Deutsche Akademische Austausch Dienst (DAAD), the Ministère des Affaires étrangères du Gouvernement Français, the Agence Nationale de la Recherche (ANR) Neurosciences and the Centre National de la Recherche Scientifique (CNRS).

The process of learning requires periods of memory consolidation. During the many such periods, I was lucky for having had friends with whom I had a wonderful time in Paris and Dresden. I want to thank them for the countless joyful and precious moments. In particular, I am thankful for the Buddy's (Brandon Stell) help with "tryin' to find reverse on a Soviet tank" (-The Big Lebowski; written and directed by Joel and Ethan Coen).

I am touched by the loving care of my parents Marianne and Klaus-Peter Graupner. I want to thank them with all my heart for being a nearly endless source of support throughout my PhD and all my studies.

All the people named here and many others have helped me directly and indirectly to do the work presented in this thesis. In light of all this support and help I feel privileged and grateful.

Abstract

Synaptic long-term modifications following neuronal activation are believed to be at the origin of learning and long-term memory. Recent experiments suggest that these long-term synaptic changes are all-or-none switch-like events between discrete states of a single synapse. The biochemical network involving calcium/calmodulin-dependent protein kinase II (CaMKII) and its regulating protein signaling cascade has been hypothesized to durably maintain the synaptic state in form of a bistable switch. Furthermore, it has been shown experimentally that CaMKII and associated proteins such as protein kinase A and calcineurin are necessary for the induction of long-lasting increases (long-term potentiation, LTP) and/or long-lasting decreases (long-term depression, LTD) of synaptic efficacy. However, the biochemical mechanisms by which experimental LTP/LTD protocols lead to corresponding transitions between the two states in realistic models of such networks are still unknown.

We present a detailed biochemical model of the calcium/calmodulin-dependent autophosphorylation of CaMKII and the protein signaling cascade governing the dephosphorylation of CaMKII. As previously shown, two stable states of the CaMKII phosphorylation level exist at resting intracellular calcium concentrations. Repetitive high calcium levels switch the system from a weakly- to a highly phosphorylated state (LTP). We show that the reverse transition (LTD) can be mediated by elevated phosphatase activity at intermediate calcium levels. It is shown that the CaMKII kinase-phosphatase system can qualitatively reproduce plasticity results in response to spike-timing dependent plasticity (STDP) and presynaptic stimulation protocols. A reduced model based on the CaMKII system is used to elucidate which parameters control the synaptic plasticity outcomes in response to STDP protocols, and in particular how the plasticity results depend on the differential activation of phosphatase and kinase pathways and the level of noise in the calcium transients.

Our results show that the protein network including CaMKII can account for (i) induction - through LTP/LTD-like transitions - and (ii) storage - due to its bistability - of synaptic changes. The model allows to link biochemical properties of the synapse with phenomenological 'learning rules' used by theoreticians in neural network studies.

Résumé

Les modifications synaptiques à long terme induites par des activités neuronales sont supposées être à l'origine de l'apprentissage et de la mémoire à long terme. Des expériences suggèrent que les modifications synaptiques à long terme sont des événements tout-ou-rien de type interrupteur entre des états distincts d'une synapse. Le réseau biochimique comprenant la protéine kinase II calcium-calmoduline dépendante (CaMKII) et la cascade de signalisation de protéines associées ont été supposées maintenir durablement des états synaptiques sous la forme d'un interrupteur bistable. Des expériences ont montré que CaMKII et des protéines associées comme la protéine kinase A et la calcineurine sont indispensables pour l'induction d'augmentations à long terme (long-term potentiation, LTP) et/ou de diminutions à long terme (long-term depression, LTD) de l'efficacité synaptique. Cependant, les mécanismes biochimiques par lesquels des protocoles experimentaux de LTP/LTD conduisent à des transitions correspondantes entre les deux états dans un modèle réaliste d'un tel réseau restent à clarifier.

Nous présentons un modèle détaillé biochimique de l'autophosphorylation calcium-calmoduline dépendante de CaMKII et de la cascade de signalisation de protéines qui contrôle la déphosphorylation de CaMKII. Comme il a été montré précédemment, deux états stables du niveau de phosphorylation de CaMKII existent à la concentration de calcium de base. Une transition de l'état faiblement phosphorylé vers l'état fortement phosphorylé est évoquée par une augmentation de concentration calcique suffisamment longue et importante (LTP). Nous montrons que la transition inverse (LTD) peut être évoquée par une augmentation de l'activité de phosphatases à des concentrations calciques intermédiaires. Ce modèle peut reproduire qualitativement des résultats de plasticité en réponse au protocole de 'spike-timing dependent plasticity (STDP)' et au protocole de stimulation purement présynaptique. Un modèle réduit est utilisé afin de mieux comprendre les paramètres qui contrôlent les modifications synaptiques provoquées par le protocole de STDP, et comment en particulier elles dépendent de l'activation différentielle des voies de phosphatases et de kinases et du niveau de bruit dans les transients calciques.

Ces résultats montrent que le réseau de protéines considéré incluant CaMKII peut expliquer (i) l'induction - par des transitions LTP/LTD - et (ii) le maintien - dû à la bistabilité - des changements synaptiques. Ils permettent de relier le propriétés biochimiques des synapses avec les 'règles d'apprentissage' phénoménologiques utilisées par les théoriciens dans des études de réseaux de neurones.

Zusammenfassung

Synaptische Langzeitveränderungen, die durch neuronale Aktivität hervorgerufen werden, sind höchstwahrscheinlich die neuronalen Grundbausteine des Lernvermögens und des Langzeitgedächtnisses. Experimentelle Ergebnisse zeigen, dass diese synaptischen Veränderungen schalterartige Übergänge im Sinne von alles-oder-nichts zwischen diskreten Zuständen einer einzelnen Synpase sind. Es wird angenommen, dass das biochemische Netzwerk einschließlich der Calcium/Calmodulin-abhängigen Proteinkinase II (CaMKII) und der zugehörigen Proteinsignalkaskade den synaptischen Zustand in Form eines bistabilen Schalters dauerhaft aufrechterhalten kann. Experimente zeigen darüber hinaus, dass CaMKII und assoziierte Proteine wie die Proteinkinase A und Calcineurin unabdingbar sind für die Hervorrufung von langanhaltenden Erhöhungen (long-term potentiation, LTP) und/oder langanhaltenden Verringerungen (long-term depression, LTD) der synaptischen Übertragungseffizienz. Die biochemischen Mechanismen, mittels derer experimentelle LTP/LTD Protokolle zu entsprechenden Übergängen zwischen den zwei Zuständen in realischen Modellen solcher Proteinnetzwerke führen, sind indessen unbekannt.

Wir präsentieren ein detailliertes Modell der Calcium/Calmodulin-abhängigen Autophosphorylierung von CaMKII und der Proteinsignalkaskade, die die Dephosphorylierung von CaMKII reguliert. Es ist zuvor demonstriert worden, dass zwei stabile Zustände des CaMKII Phosphorylierungsgrades bei Calcium-Ruhekonzentration existieren können. Wiederholte hohe Calciumkonzentrationen überführen das System vom gering phosphorylierten- in den stark phosphorylierten Zustand (LTP). Wir zeigen, dass der umgekehrte Übergang durch eine erhöhte Phosphataseaktivität im Bereich moderater Calciumkonzentrationen hervorgerufen werden kann (LTD). Darüber hinaus wird demonstriert, dass das CaMKII Kinase-Phosphatase System experimentell gewonnene synaptische Plastizitätsresultate, hervorgerufen durch ‘Spike-timing dependent plasticity (STDP)’- und presynaptische Stimmulationsprotokolle, qualitativ reproduzieren kann. Ein reduziertes Modell, dass auf dem CaMKII-System basiert, erlaubt uns besser zu verstehen, welche Parameter die durch STDP Stimmulierung hervorgerufenen Plastizitätsresultate kontrollieren und im Speziellen, in welcher Art und Weise die Plastizitätsresultate von der differenziellen Aktivierung von Phosphatasen und Kinasen und des Fluktuationsgrades der Calciumtransienten abhängen.

Unsere Untersuchungen zeigen, dass das betrachtete Proteinnetzwerk einschließlich CaMKII (i) die Induzierung - durch LTP/LTD Übergänge - und (ii) die Speicherung - aufgrund seiner Bistabilität - synaptischer Veränderungen erklären kann. Das Modell erlaubt darüber hinaus, eine Verbindung zwischen den biochemischen Eigenschaften einer Synapse und den phenomeologischen ‘Lernregeln’, wie sie in neuronalen Netzwerkstudien benutzt werden, herzustellen.

Contents

If the Lord Almighty had consulted me
before embarking on creation I should have
recommended something simpler.

Alphonso X (Alphonso the Wise), 1221-1284
King of Castile and Leon (attributed)

1 Introduction

Induction and maintenance of long-lasting synaptic changes has stimulated research since long-term potentiation (LTP) - a long-lasting increase in excitatory synaptic transmission efficacy - was first discovered by Lømo (Bliss and Lømo 1973). A few years later the reverse effect, long-term depression (LTD) - a long-lasting decrease in excitatory synaptic weight - was found again in the hippocampus by Lynch et al. (1977). Such synaptic plasticity events are thought to be related to learning and memory consolidation since a large body of evidence has been gathered demonstrating that both, synaptic plasticity and learning as well as memory, rely on similar mechanisms (Whitlock et al. 2006). Moreover, the blockade of specific molecules or of specific interactions between molecules has been demonstrated to impair learning and memory tasks as well as to prevent the induction of LTP/LTD in such animals (see Morris et al. (1986), Abraham and Mason (1988), for example). Despite the large number of molecules which have been identified to particitate in or modulate synaptic plasticity, especially in the hippocampus, the exact molecular mechanisms by which changes in synaptic efficacy are induced and maintained over time remain elusive.

Numerous experiments have shown how synaptic efficacy can be increased (LTP) or decreased (LTD) by presynaptic firing rate (Dudek and Bear 1992), by presynaptic firing paired with postsynaptic holding potential (Artola et al. 1990; Ngezahayo et al. 2000) or by spike timing of pre- and postsynaptic neurons (spike-timing dependent plasticity, STDP) (Markram et al. 1997; Magee and Johnston 1997; Bi and Poo 1998), to name some of the most common induction protocols. Such long-term modifications involve changes in the presynaptic release probability of the neurotransmitter glutamate (Bekkers and Stevens 1990; Malinow and Tsien 1990) or alternatively, changes in the number or the phosphorylation state or both of α-amino-3-hydroxyl-5-methyl-4-isoxazole-propionate acid (AMPA) receptors in the postsynaptic membrane (Davies et al. 1989; Manabe et al. 1992). These modifications of the synaptic state are typically recorded at the soma and are characterized by an increase (in case of LTP) or decrease (in case of LTD) of amplitude, slope, or size of the excitatory postsynaptic potential (EPSP). These changes show typically a continuous character. The signal at the soma is, however, a summation of EPSPs emerging from single, activated synapses. Recent experiments on putative single synaptic connections suggest that LTP and LTD are embodied as all-or-none switch like events at the level of a single synapse (Petersen et al. 1998; O'Connor et al. 2005b; Bagal et al. 2005). In other words, a single synapse can be seen as a bistable system storing one bit of information imprinted by synaptic plasticity. The downstream mechanisms which allow synaptic changes to last beyond hours, days, or even weeks - the so called "late-phase" of long-term modifications - involve structural remodeling, protein synthesis and gene transcription. Signaling molecules such as protein kinase A, calcium/calmodulin-dependent protein kinase II (CaMKII) and mitogen-activated protein kinase (MAPK) have been identified to be involved in the "early-phase" (< 60 min) providing the linkage to the "late-phase" of long-term modifications (Malenka and Bear 2004). How the biochemical apparatus involving these proteins can give rise to two stable synaptic states and how LTP/LTD stimulation protocols can move the synapse from one state to another is the subject of ongoing biological, and mathematical research.

Experimental protocols evoking synaptic long-term modifications have led to phenomenological models that capture one or several aspects of the linkage between pre- and postsynaptic activity (the timing of the pre-and postsynaptic spikes) and the evoked synaptic plasticity (Gerstner et al. 1996; Song et al. 2000; Senn et al. 2001; Abarbanel et al. 2003; Gerstner and Kistler 2002; Pfister and Gerstner 2006). These models, however, do not describe biochemical mechanisms of induction of synaptic changes but compute the synaptic weight based on spike times only. How the evoked state is maintained is generally not addressed in these models. A more biological approach involves the modeling of synaptic voltage- (Abarbanel et al. 2002) and calcium dynamics (Karmarkar et al. 2002; Karmarkar and Buonomano 2002; Shouval et al. 2002; Abarbanel et al. 2003) in response to synaptic activity. Experimentally, the level and time course of postsynaptic calcium elevations has been shown to be a necessary and sufficient signal for plasticity (Neveu and Zucker 1996; Yang et al. 1999; Cho et al. 2001; Mizuno et al. 2001; Nevian and Sakmann 2006). In the models, the calcium time course (Shouval et al. 2002; Abarbanel et al. 2003; Cai et al. 2007) or the maximal amplitude (Karmarkar et al. 2002) is read out by effective mechanisms conveying the calcium concentration level into synaptic changes: low calcium levels do not cause any changes, intermediate calcium levels decrease synaptic weight and high calcium levels increase synaptic weight. However, it has been shown difficult to reproduce the qualitative shape of plasticity results evoked by STDP spike-pair stimulation protocols in such models. In particular, a second range of LTD emerged at large positive time differences between the pre- and the postsynaptic spike in these models in contrast to experimental results suggesting no synaptic changes in this region. Stochastic properties of synaptic transmission (Shouval and Kalantzis 2005) or two distinct calcium pools triggering different readout mechanisms (Karmarkar et al. 2002) are suggested to reconcile these models with experimental data. The effective readout mechanisms of the calcium level are replaced by an artifical calcium detector system resembling the pathways associated with CaMKII in a model by Rubin et al. (2005). The complex readout mechanism allows to qualitatively and even quantitatively reproduce experimental plasticity outcomes. However, the components and rate constants of the proposed signaling cascade have no biological counterparts and the whole system is designed to bridge the gap between calcium dynamics and experimental observed plasticity result in response to STDP protocols. Whether realistic biochemical signaling cascades known to be involved in LTP/LTD induction lead to similar results remains to be shown.

Another line of research addresses the issue of maintenance of the evoked synaptic state during the early phase of LTP/LTD. The idea that this could be achieved by means of a bistable synaptic switch first expressed by Crick (1984) received recent experimental support by experiments showing that Schaffer collateral - CA1 neuron synapses in the hippocampus show all-or-none switch like transitions between two stable states (Blitzer et al. 1998; O'Connor et al. 2005b), a DOWN state with low efficacy and an UP state with high efficacy. Such binary switches could emerge from clusters of interacting receptors in the synaptic membrane (Shouval 2005), from positive feedback loops in extensive protein networks (Bhalla and Iyengar 1999; Hayer and Bhalla 2005) or from signaling cascades influencing CaMKII autophosphorylation and dephosphorylation (Lisman 1985; Zhabotinsky 2000; Okamoto and Ichikawa 2000; Miller et al. 2005). In the latter case, the models resolve details of CaMKII's peculiar protein function as opposed to protein networks taking into account protein-protein interactions only. CaMKII has received particular attention since experimental evidence has accumulated showing that CaMKII takes a key position in hippocampal learning and memory as well as LTP induction (Giese et al. 1998). CaMKII activation is governed by calcium/calmodulin binding and is prolonged beyond fast-decaying calcium transients by its autophosphorylation (Fink and Meyer 2002). Autophosphorylation of CaMKII at the residue theronine-286 in the autoregulatory domain (Thr^{286}) occurs after calcium/calmodulin binding to neighboring subunits in the CaMKII holoenzyme ring and enables the enzyme to remain autonomously active after dissociation of calcium/calmodulin (Hanson and Schulman 1992). In turn, as long as CaMKII stays activated, it is reversibly translocated to a postsynaptic density (PSD)-bound state where it interacts with multiple LTP related partners structurally organizing protein anchoring assemblies and therefore potentially delivering AMPA receptors to the cell surface (Shen and Meyer 1999; Hayashi et al. 2000; Lisman et al. 2002; Fink and Meyer 2002; Colbran 2004). The direct phosphorylation of the AMPA receptor GluR1 subunit by active CaMKII enhances AMPA channel function (Mammen et al. 1997; Derkach et al. 1999). The network involving CaMKII is particularly appealing in terms of learning and memory maintenance since N-methyl-D-aspartate receptor (NMDA-R)-dependent LTP requires calcium/calmodulin activation of CaMKII, potentially expressed by the phosphorylation level or the number of AMPA receptors, or both (Giese et al. 1998; Lisman et al. 2002; Bliss et al. 2003; Lisman 2003; Colbran 2004; Irvine et al. 2006). However, the role of CaMKII beyond LTP induction remains controversial. Autonomous activity of CaMKII increases only transiently following induction of LTP, hence inhibitors of CaMKII autonomous activity have no effect on the expression of LTP once LTP has been induced (Chen et al. 2001; Yang et al. 2004; Lengyel et al. 2004). In contrast, Sanhueza et al. (2007) show that a noncompetitive inhibitor of CaMKII can reverse LTP and they suggest that a component of synaptic memory is attributable to CaMKII in CA1 region synapses. Finally, there is experimental evidence for the involvement of proteins associated with CaMKII activity (cyclic adenosine monophosphate (cAMP)-regulated protein kinase A (PKA), protein phosphatase 1 (PP1) and calcineurin) in LTP and LTD (Mulkey et al. 1994; Blitzer et al. 1998; Morishita et al. 2001; Morishita et al. 2005). Furthermore, induction protocols of long-term modifications, such as STDP stimulation, for example, has been shown to rely on kinase (CaMKII) and phosphatase (calcineurin) activation (Wang et al. 2005; O'Connor et al. 2005a). It should be noted that multiple mechanisms supporting LTP/LTD induction and expression are likely to be present in synapses of different regions – we focus here on synapses for which the above statements have been shown to apply, *e.g.* the CA3-CA1 Schaffer collateral synapse (see review by Cooke and Bliss (2006)).

Modeling studies on CaMKII and associated pathways show that the system could be indeed bistable in a range of calcium concentrations including the resting level – a necessary requirement for the maintenance of long term changes (Lisman 1985; Zhabotinsky 2000; Okamoto and Ichikawa 2000; Hayer and Bhalla 2005). In such models, the two states correspond to two stable phosphorylation levels of the CaMKII protein for a given calcium concentration, *i.e.* a weakly- (DOWN) and a highly-phosphorylated state (UP). Miller et al. (2005) and Hayer and Bhalla (2005) show that such a switch can remain stable on very long time scales (years) in the presence of protein turnover and receptor trafficking, respectively. A transition from the DOWN to the UP state which could underlie long-term potentiation (LTP) can be induced by a sufficiently large and prolonged increase in calcium concentration. However, the opposite transition which could underlie depotentiation or LTD only occurs under unrealistic conditions, for example decrease of calcium concentration below resting level. Furthermore, it has not been considered how these biochemical network models behave in response to calcium transients evoked by experimental protocols that are known to induce synaptic plasticity. Rubin et al. (2005) reproduce experimental results on STDP using a model detector system which qualitatively resembles the protein network influencing CaMKII, but this model does not exhibit bistability. Other studies on biochemical signal transduction pathways including CaMKII show that the AMPA receptor activity can reproduce bidirectional synaptic plasticity as a function of calcium (D'Alcantara et al. 2003; Castellani et al. 2005). However, realistic stimulation protocols are not investigated in these models and again, they do not show bistability.

In this thesis, we consider a realistic model of protein interactions associated with CaMKII autophosphorylation through calcium/calmodulin and dephosphorylation by protein phosphatase 1 in the postsynaptic density (PSD). We first study the steady-state phosphorylation properties of CaMKII with respect to calcium and changing levels of PP1 activity. Conditions are elaborated for which the system allows for 'LTP' and 'LTD' transitions in reasonable ranges of calcium concentrations. We then demonstrate the ability of the CaMKII system to perform LTP- or LTD-like transitions in response to STDP stimulation protocols. We expose the CaMKII system to calcium transients evoked by pairs of pre- and postsynaptic spikes with a given time lag and show that short positive time lags evoke transitions from the DOWN to the UP state and short negative time lags lead to transitions from the UP to the DOWN state. Additionally, during exposure to the STDP stimulation protocol, different parts of the protein signaling cascade are blocked and the resulting plasticity results are compared with results of corresponding experimental assays. We demonstrate furthermore that the CaMKII model qualitatively reproduces experimental plasticity outcomes for presynaptic stimulation protocols. Transition results in response to stimulation protocols including purely pre- or purely postsynaptic spike pairs with different time lags are shown to evoke LTD or LTP transitions, respectively. These results can be readily tested by experiments.

In chapter IV, we study a simplified version of the CaMKII kinase-phosphatase system. Similar investigations on the calcium- and PP1 activity-dependent phosphorylation steady-states as well as on the transition behavior are performed. The simplification that the CaMKII ring has only two subunits rather than six gives some insights which apply in turn for more realistic models.

In the last part of the thesis, we simplify further the CaMKII kinase - phosphatase system with the objective of extracting and understanding basic defining features of a bistable synapse. In this reduced model which exhibits bistability, two processes representing CaMKII phosphorylation by kinases and dephosphorylation by phosphatases are differentially activated by calcium transients. Possible transition results between the stable UP and DOWN states and the influence of noise on those are examined for different experimental stimulation protocols known to induce synaptic changes. We show in particular that the activation of kinases and phosphatases with respect to calcium mainly influences the qualitative transition results in response to STDP spike-pair stimulation protocols and how this is affected by different noise levels. The reduced model generalizes across previous models and elaborates common features required to account for known experimental data. Differences in plasticity outcomes evoked by similar stimulation protocols across different brain regions are related to possible biological differences.

2

Introduction to synaptic plasticity

2.1 Structure of neurons

The nervous system consists of two different cells types: nerve cells (*neurons*) and glial cells (*neuroglia*). There exists approximately 100 billion neurons in the nervous system whereas the number of glial cells exceeds the number of neurons about 10 to 50 times. The functional task of neurons is the processing and transmission of signals. Their every aspect - their size, shape, cellular organization, development, and organization within the nervous system - is shaped by their specific functions of receiving, organizing and transmitting information. The connections between neurons occur through *synapses*, the sites where the information is transmitted from one nerve cell to the other. Though glial cells are not involved directly in signaling, they play critical roles in controlling the environment of the nerve cells, supporting the nerve cell structure and serve as insulation in form of myelin.

Although neurons have various morphologies within and across brain regions, they all share similar constituents, which identify them as neurons. The neuron, like all other cells, is bound by a plasma membrane. The membrane encloses the cytoplasm with the nucleus, which accommodates the genes, consisting of the DNA and its associated proteins. The cell body - the *soma* - contains beside the nucleus the membrane organelles responsible for the synthesis and processing of cellular proteins. Depending on their function the extensions emerging from the cell body can be classified in *axons* and *dendrites*.

On average, one to nine dendrites emerge from the soma and then divide successively to a highly branched dendritic tree with specific characteristics for each neuronal population. They are morphologically distinct from axons by their irregular outline, by their diameter which decreases along their branches, by the acute angles between the branches and by their ultrastructural characteristics (Hammond 1996).

Axons are distinguished from dendrites by their smooth appearance, their uniform diameter along their entire extent and their ultrastructural characteristics. They generally emerge at the initial segment expanding from the soma but sometimes at the level of a primary dendrite. Axons can transport electrical signals over a range from 0.1 mm up to 2 m to the *presynaptic terminal*. Over that range axons are divided into one or several collaterals which form right angles with the main axon giving rise to multiple terminals. The axon and its collaterals may be surrounded by a sheath, the myelin sheath. Myelin sheaths are formed by glial cells and act as isolator.

The number of connections that a neuron forms can be extraordinarily large. Single cortical neurons receive signals from over $10,000$ input synapses (DeFelipe and Fariñas 1992), while Purkinje cells in the cerebellum receive up to $100,000$ inputs (Palay and Chan-Palay 1974; Ito 1984) onto the surface of dendrites, *dendritic spines* and the soma. Dendritic spines are small membranous extrusions that protrude from a dendrite and form one half of a synapse, the other half being the presynaptic terminal. Spines have a bulbous head which is connected to the parent dendrite through a thin spine neck. This part constitutes the main receptive area of neurons. In order to respond to afferent information spines and dendrites either have direct junctions with the previous neuron (electrical synapse or gap junction), or express receptors and other proteins necessary to convert the incoming chemical signal into an electrical signal (chemical synapse). The *postsynaptic density* (PSD) expressed in chemical synapses concentrates and organizes neurotransmitter receptors to respond rapidly to neurotransmitter in the synaptic cleft. The structure and composition of the PSD is believed to play a major role in synaptic plasticity (see below). A picture of a pyramidal cell from the rabbit cerebral cortex is shown in the middle column of Fig. 2.1.

In spite of the general plan of cellular organization that most neurons share, they exist in an extraordinary variety of sizes and shapes. This diversity allows flexibility in signal processing and spatial organization of synaptic connections.

2.2 Signaling between neurons

Ions - such as K^+, Na^+, Cl^-, Ca^{2+} - are unequally distributed across the neuron membrane and the membrane is selectively permeable for these ions. Proteins in the membrane called transporters and pumps use metabolic energy to actively transport ions in and out of the cell giving rise to this ion concentration gradient across the membrane. As a consequence, a difference in electrical potential of about $60 - 70$ mV exists across the surface membrane of neurons. These ion con-

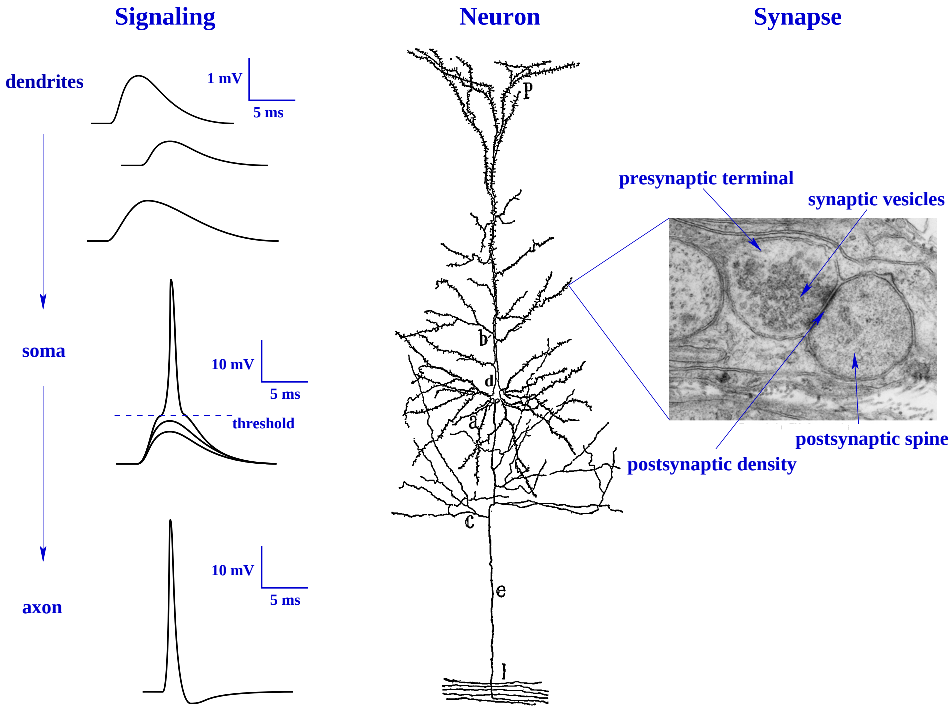

Figure 2.1: Electrical signal transport in a neuron, a pyramidal cell from the rabbit cerebral cortex and a transmission electron microscope picture of a synapse ***Signaling.*** The propagation of membrane depolarizations from the dendritic tree to the soma and further along the axon is schematized on the left hand side. Excitatory synaptic transmissions evoke excitatory postsynaptic potentials (EPSPs) of different sizes and durations (3 examples are shown). These EPSPs propagate to the soma. If the integrated signal of all incoming EPSPs exceeds a certain threshold at the soma, an action potential (AP) is triggered. This AP travels along the axon to nerve terminals projecting to postsynaptic neurons. ***Neuron.*** A pyramidal cell from the rabbit cerebral cortex is shown in the middle. This cell type has an elaborate dendritic tree. A massive, long dendrite arises from the soma and ends as a tuft of small branches in a more superficial layer or, more generally, in a molecular layer. All the little dots at the dendritic tree characterize spines. The Golgi method is used to stain and visualize the neuron. The different parts are indicated by letters: a: basal dentrides, b: dendritic tuft and its branches, c: axon collateral, d: soma, e: long axon and l: white matter (picture adapted from (Cajal 1995)). ***Synapse.*** The electron micrograph of an excitatory synapses is shown on the right hand side. The presynaptic terminal contains many small synaptic vesicles filled with neurotransmitters. Neurotransmitters are released at the synaptic junction (darkly stained areas) by the fusion of these vesicles with the plasma membrane. The neurotransmitters then bind to receptors of the postsynaptic density formed on the postsynaptic spine (picture taken from the website of City of Hope National Medical Center, 1500 E. Duarte Road, Duarte, CA 91010, USA, www.cityofhope.org/ November 10th, 2007).

centraion gradients represent a form of stored energy used by neurons to generate electrical signals.

The signals in a neuron result from the opening and closing of *ion channels*. These are transmembrane proteins which facilitate the passive flow of specific ions across the membrane along their electrochemical gradient. The flow of ions through the channels constitute a current that changes the membrane potential resulting in *depolarizations* or *hyperpolarizations* of the resting potential. These changes vary in time and space and represent electrical signals. See the schematic depiction of the signal transport along the neuron in the left column of Fig. 2.1.

The connections between neurons are formed by synapses. Chemical synapses use neurotransmitter in order to bridge the synaptic cleft and provide signal transmission. In contrast, electrical synapses or gap junctions are characterized by the apposition of the plasma membrane of the connected neurons. In this case, the ions flow directly from one cell to another without the use of transmitter. This work will consider synaptic plasticity observed at chemical synapses exclusively.

Neurotransmitter expelled at the presynaptic terminal of a chemical synapse diffuse into the synaptic cleft. Binding of neurotransmitter to the receptive surface at the extracellular space results in either a depolarization or a hyperpolarizations of the postsynaptic transmembrane potential, referred to as *postsynaptic potential* (PSP, see left hand column of Fig. 2.1). Which one of the two is observed depends on the type of neurotransmitter and receptors and on the momentary state of the postsynaptic neuron. The resulting signal encodes the input information in its size and shape and is therefore an analog signal. The synaptic potential travels along the dendrite and changes its size according to the active and passive properties of the dendrite (Sjöström et al. 2008). All incoming signals are propagated towards the soma and are integrated there. If at any moment the local potential at the initial segment of the soma exceeds a certain depolarization threshold, an action potential is triggered which travels down the axon. Depolarizations increase the probability of generating an action potential and are therefore called excitatory, whereas hyperpolarizations have the opposite effect and act in an inhibitory fashion.

Action potentials are brief, stereotyped depolarizations with amplitudes up to 110 mV which convey signals rapidly and efficiently over long distances. In contrast to the graduated postsynaptic potentials, action potentials are actively self-propagating and they maintain their shape. The stereotyped property of all action potential is achieved by an “all-or-none” reaction at the initial segment once the threshold is passed. Action potentials encode information by their occurrence, namely by their frequency, and not by their shape. Their duration is of the order of 1 ms. The propagation of action potentials into presynaptic nerve terminals triggers a signal cascade which finally leads to transmitter secretion. Furthermore, action potentials actively backpropagate into the dendrites of many neuronal types, providing a retrograde signal of neuronal output to the dendritic tree.

This alternating chain of electrical and chemical signals provides the capacity of efficient, fast information transport, and at the same time assures that the signal transmission between neurons can be subject to activity-dependent changes. In other words, since the signal transmission at the synapse involves a plethora of ions, proteins and interactions, every aspect of transmission can be altered through changes of the participating entities (see next chapter).

The purpose of this section is to provide a general and short overview of the composition and function of neurons within the nervous system and to introduce terms used in later sections. The above outlined signal transmission is applicable to the vast majority of neurons. However, it is not accurate in detail for all neurons. The books of Hall (1992), Hammond (1996) and Kandel et al. (1996) should be mentioned for further readings.

2.3 Synaptic plasticity in the hippocampus

This work is based on the fact that synapses can change their transmission efficacy in an activity-dependent manner. The assumption that this so-called synaptic plasticity is the basis of information storage in the central nervous system emerged about a century ago following the proposition by Santiago Ramón y Cajal that networks of neurons communicate with each other at specialized junctions which Charles Scott Sherrington called synapses in 1897. At this time, this was in conflict with the conclusion drawn by Golgi that nervous tissue was a continuous reticulum (or web) of interconnected cells. Electron microscopy later showed that a plasma membrane completely enclosed each neuron, supporting Cajal's theory, and weakening Golgi's reticular theory. The capacity of the brain to translate experiences into a seemingly infinite numbers of memories that can last for decades has been attributed to long-lasting, activity-dependent changes of synaptic efficacy. These ideas were first refined theoretically in the late 1940s by Hebb (1949) and Konorski (1948). They postulated a coincidence-detection rule for the synapse. That means that the synapse gets strengthened whenever the two connected nerve cells are active at the same time. However, they did not propose a rule leading to weakening of the synapse.

Activity-dependent changes were first discovered experimentally in the mammalian brain by Lømo in 1966 and the first characterization of long-lasting potentiation got published later together with Bliss (Bliss and Lømo 1973). As expected from the anatomical structure of the hippocampus, single electrical pulses to the perforant pathway emanating from the enthorhinal cortex elicit an excitatory postsynaptic potential (EPSP, a depolarization of the cell membrane resting at around

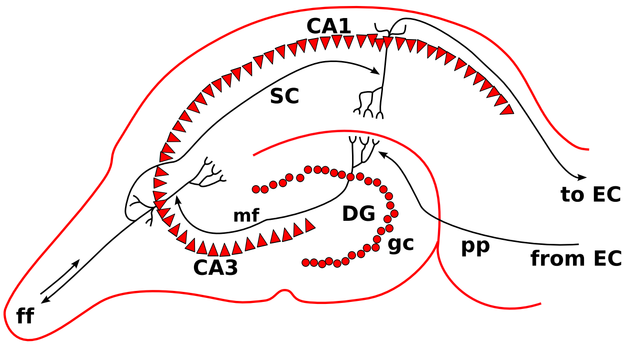

Figure 2.2: Scheme of the hippocampal network from a tansverse point of view. The hippocampus is a part of the forebrain, located in the medial temporal lobe. It belongs to the limbic system and plays major roles in short term memory and spatial navigation. The hippocampus forms principally a uni-directional network with input from the enthorhinal cortex (EC) that forms connections with granule cells (gc) in the dentate gyrus (DG) and CA3 pyramidal neurons via the perforant path (pp). CA3 neurons also receive input from the DG via the mossy fibres (mf). They send axons to CA1 pyramidal cells via the Schaffer collateral pathway (sc), as well as to CA1 cells in the contralateral hippocampus via the associational commissural pathway (ac). CA1 neurons also receive input directly from the perforant path and send axons back to the EC via the subiculum forming a loop.

-70 mV of the order of ~ 1 mV) recorded extracellularly from granule cells in the dentate gyrus (see Fig. 2.2). Repetitive high-frequency trains of electrical stimuli (tetani) applied to the perforant pathway lead to stronger, prolonged excitatory postsynaptic potentials in the dentate gyrus in the anesthetized rabbit. This effect is called long-term potentiation (LTP) and characterizes changes which last at least up to 60 min during *in vitro* experiments. The first experiments on synaptic plasticity were performed in anesthetized animals. Skrede and Westgaard (1971) introduced hippocampal slice preparations in which 400 - 500 μm thick transverse slices allow an easy access to the hippocampal circuitry. It is especially in the cornus ammonis 3 (CA3) and cornus ammonis 1 (CA1) pyramidal subfields regions where the majority of work on LTP and LTD has been conducted *in vitro* (see Fig. 2.2).

Besides its longevity, other characteristics of LTP have been identified by numerous experiments since its discovery. First, LTP is an input-specific process: a pathway can be potentiated without changing neighboring inactive inputs to the same postsynaptic cell (Andersen et al. 1980; Barrionuevo and Brown 1983). Since the average number of input synapses is 10,000 for a cortical cell (DeFelipe and Fariñas 1992) and up to 200,000 for Purkinje cells in the cerebellum (Palay and Chan-Palay 1974; Ito 1984), this feature ensures a large storage capacity. Second, LTP is associative. This means that a weak stimulation which is not by itself sufficient to evoke LTP, can become potentiating through association with a strong tetanus (McNaughton et al. 1978; Levy and Steward 1979). In terms of memory formation, this mechanism could ensure the association of related events or entities in the outside world. It is noteworthy that these characteristics have been predicted theoretically by Hebb long before their experimental validation (Hebb 1949).

Since its first discovery, LTP has been found at all excitatory synapses in the hippocampus and in a variety of other neural structures such as the cerebral cortex (Fox 2002), cerebellum (Salin et al. 1996; Lev-Ram et al. 2002), amygdala (Chapman et al. 1990), spinal cord (Ji et al. 2003) and many others. Induction and maintenance of synaptic long-term modifications have some common features in all these systems. Afferent action potentials invade the presynaptic terminal and trigger stochastic glutamate release into the synaptic cleft. Glutamate binds to postsynaptically positioned NMDA receptors, amongst other receptors. This event alone evokes a small calcium influx which is restricted to the postsynaptic spine and mediated by NMDA-R (Koester and Sakmann 1998) since at potentials close to the membrane resting potential (~ -70 mV) the NMDA receptor is almost completely blocked by magnesium ions (Nowak et al. 1984; Jahr and Stevens 1990). However, if the presynaptic input is paired with strong depolarization of the postsynaptic cell or back-propagating action potentials, the voltage-dependent magnesium block is expelled from the cation channel allowing a large influx of sodium as well as calcium ions into the neuron. The calcium influx is crucial since it is thought to initiate LTP and LTD induction (Lynch et al. 1983; Malenka et al. 1988; Yang et al. 1999; Zucker 1999). Intracellular calcium in turn activates calcium-sensitive signaling cascades such as pathways involving calcium/calmodulin-dependent protein kinase II or the cyclic adenosine monophosphatase (cAMP) (see below). These molecules initiate LTP/LTD expression mechanisms either locally, by phosphorylating receptors, or by signaling to the cell nucleus via transcription factors to alter gene expression (Goelet et al. 1986; Alberini et al. 1995).

However, the molecular processes underlying induction pathways and expression mechanisms of LTP and LTD vary from synapse to synapse. In the hippocampus, for example, at the mossy fiber - CA3 pyramidal cell synapse (see Fig. 2.2) the N-methyle-D-aspartate (NMDA) sub-class of glutamate receptors is not required for LTP induction (Harris and Cotman 1986). The site of LTP expression at this synapse is primarily presynaptic (Weisskopf and Nicoll 1995). In contrast, at perforant path - dentate gyrus granule cell (Morris et al. 1986; Errington et al. 1987) and Schaffer collateral - CA1 pyramidal cell synapses (Collingridge et al. 1983) (see Fig. 2.2), LTP induction is mediated by NMDA receptors. In these synapses, the NMDA receptor (NMDA-R) detects the coincidence of pre- and postsynaptic activity. Furthermore, the site of LTP expression at both synapses seems to primarily postsynaptic (McNaughton 1982; Manabe et al. 1992). However, recent experiments at CA3 - CA1 synapses raise the possibility that potentiation could be a two-step process with different locuses of the expression site (Ward et al. 2006). The first potentiating protocol moves the synapse from a silent to an unsilenced state through postsynaptic appearance of functional α-amino-3-hydroxy-5-methyl-4-isoxazolepropionic acid (AMPA) receptors (Liao et al. 1995), while the second potentiating protocol of formerly unsilenced synapses leads to an increase in release probability of neurotransmitter from the presynaptic site (Kuhnt and Voronin 1994; Ward et al. 2006). Despite common features, the perforant path - dentate gyrus granule cell and Schaffer collateral - CA1 pyramidal cell synapses are distinguishable in terms of the signaling mechanisms leading to the LTP expression state, as CaMKII signaling is required at the latter but not at the former (Zhang et al. 2005; Cooke et al. 2006). LTP is supported by cyclic AMP-dependent signaling at the perforant path - dentate gyrus granule cell synapse (Cooke et al. 2006). Due to the wealth of molecular mechanisms underlying synaptic plasticity in different regions of the brain, we focus on the Schaffer collateral - CA1 synapse for which LTP/LTD exhibits common characteristics with glutamatergic, excitatory synapses throughout the mammalian brain (Kirkwood et al. 1993).

2.4 Stimulation protocols evoking LTP/LTD

In the first experiments on synaptic activity-dependent long-term modifications, high-frequency trains of electrical stimuli delivered to afferents were employed to induce long-term potentiation (one or more trains at $10-20$ Hz for $10-15$ sec or 100 Hz for $3-4$ sec; Bliss and Lømo (1973)). Numerous other stimulation protocols have been shown to be able to evoke LTP and LTD in experimental preparations ever since. Whether or not these paradigms reflect patterns of activity used to encode experiences in the brain of a living organism is the subject of ongoing discussions. Some of the most common experimental paradigms are described in this section.

Dunwiddie and Lynch (1978) could show that LTD is evoked with the same presynaptic stimulation protocol as used by Lømo and Bliss but lower stimulation frequency (1 Hz). In a more comprehensive study, Dudek and Bear (1992) showed that presynaptic stimulation at low frequencies (900 presynaptic stimuli at $1 < f < 10$ Hz) evokes long-term depression in Schaffer collateral - CA1 neuron connections. Furthermore, they observed LTP for frequencies larger than 10 Hz, similar to the early results by Bliss and Lømo (1973) on the perforant pathway. No changes were observed for $f < 1$ Hz (Dudek and Bear 1992) (see Fig. 2.3*A* and *C* for an illustration of the plasticity results obtained by Dudek and Bear (1992)).

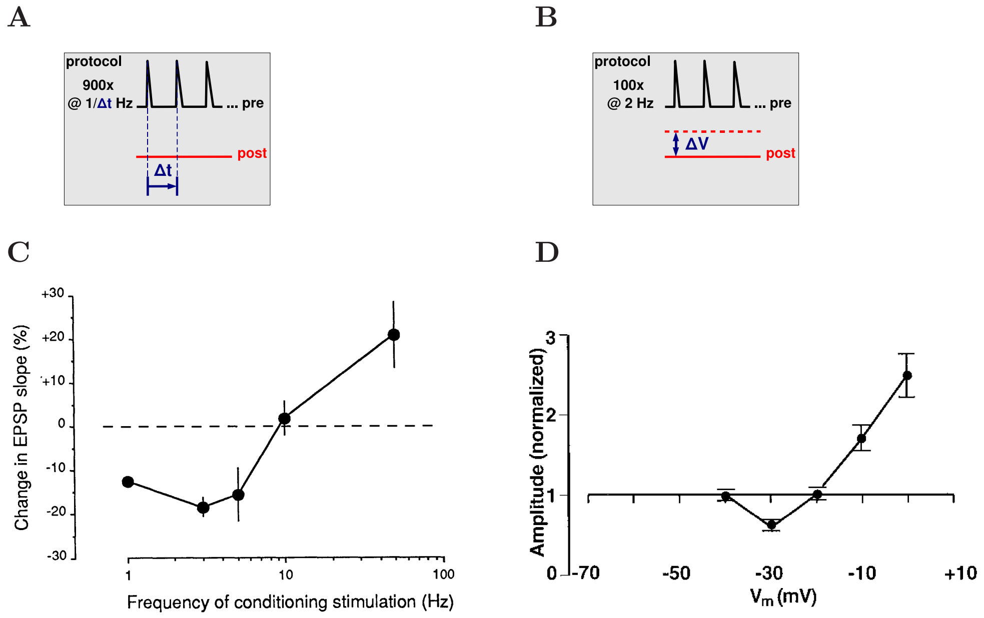

Figure 2.3: Experimental plasticity outcomes in response to presynaptic stimulation only and to presynaptic stimulation paired with postsynaptic depolarization in the hippocampus. ***A & C,*** Synaptic plasticity evoked by presynaptic stimulation only: Panel *A* depicts a sketch of the stimulation protocol involving presynaptic stimulation at frequency $f = 1/\Delta t$ for 900 times. The postsynaptic cell is not stimulated nor is postsynaptic activity blocked in these experiments (Dudek and Bear 1992). The mean change in EPSP slope ($\pm$ SEM) measured 30 min after conditioning of the CA3-CA1 pathway is shown as a function of the presynaptic stimulation frequency in panel *C* ($n \geq 5$, figure adapted from Dudek and Bear 1992). ***B & D,*** Synaptic plasticity evoked by short presynaptic stimulation paired with postsynaptic depolarization: The stimulation protocol is composed of 100 presynaptic stimuli occurring at 2 Hz paired with concurrent decrease of the postsynaptic membrane potential (V_{m}) at which the postsynaptic CA1 neuron is held during pairing (panel *B*). Panel *D* shows the EPSC amplitude relative to the baseline measured by taking the average of a $2-3$ ms window around the EPSC peak 30 min after pairing. See text for more details (figure adapted from Ngezahayo et al. 2000).

Precisely the same type of stimulation protocols are effective to evoke LTP and LTD in the neocortical layer IV neurons providing evidence that common principles may govern plasticity in the neocortex and the hippocampus (Kirkwood et al. 1993). It is important to mention that these presynaptic stimulation protocols at different frequencies include a whole bundle of afferents and thereby ensure sufficient synaptic input to induce action potentials post-synaptically backpropagating into the dendritic tree. This fact is an expression of the associativity of long-term modifications. In accordance with the requirement for postsynaptic activity, a block of postsynaptic spiking prevents the induction of LTD at low stimulation frequencies (3 Hz) in Schaffer collateral - CA1 neuron synapses (Christie et al. 1996). It is however unclear whether hippocampal neurons *in vivo* fire at 100 Hz for one second (compare (Bliss and Lømo 1973)) or continuously at low frequency for hundreds of seconds (Dunwiddie and Lynch 1978; Dudek and Bear 1992). Pyramidal cells in the CA1 region commonly fire short ($30-40$ ms) bursts of three to four spikes (frequency of these spikes ~ 100 Hz) (Kandel and Spencer 1961; Ranck 1973). These bursts are repeated at the Θ-frequency (Green et al. 1960), which are electroencephalographic waves in the range of $5-12$ Hz that occur when animals are engaged in exploratory, attentive behavior (Grastyan et al. 1959; Vanderwolf 1969; Bland 1986). Indeed, it has been shown *in vitro* that bursts at ~ 100 Hz most effectively evoke LTP in hippocampal slices if presented at the Θ-frequency of about 5 Hz (Larson and Lynch 1986; Larson and Lynch 1986). Θ-burst evoked LTP is stable *in vivo* for ~ 10 days and up to 3 weeks (Staubli and Lynch 1987). These experiments are performed on Schaffer collateral - CA1 neuron projections and indicate that electrical stimulations resembling *in vivo* activity patterns produces stable potentiation of postsynaptic responses.

In case of presynaptic activation only, the necessary postsynaptic activation is conveyed by the stimulation itself. However, the magnesium block of the NMDA receptor could also be expelled by depolarizing directly the postsynaptic cell. Respective experiments in the hippocampal CA1 subfield show that presynaptic stimulation paired with modest postsynaptic depolarization ($-40 < V_{\mathrm{m}} < -20$ mV and 100 stimuli delivered at 2 Hz in the experiments of Ngezahayo et al. (2000); see Fig. 2.3*B* and *D*) lead to LTD, and to LTP for stronger depolarizations ($V_{\mathrm{m}} > -20$ mV) (Artola et al. 1990; Ngezahayo et al. 2000) (Fig. 2.3*B* and *D*). Similar results can also be obtained by pairing presynaptic stimulation with postsynaptic depolarizing current pluses (Gustafsson et al. 1987).

All experiments mentioned so far confirm that long-term synaptic modifications occurs in response to the simultaneous activation of both pre- and postsynaptic neurons. Most of the induction protocols, however, require either prolonged depolarizations of the postsynaptic neuron (Artola et al. 1990; Ngezahayo et al. 2000) or strong enough input to the postsynaptic neuron (Bliss and Lømo 1973; Dunwiddie and Lynch 1978; Dudek and Bear 1992) potentially leading to a strong

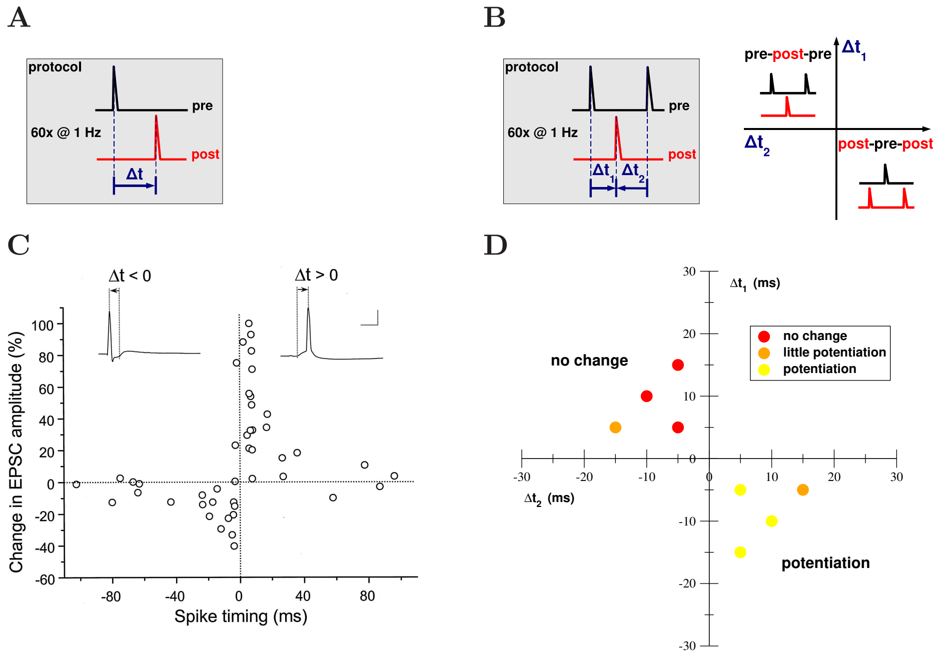

Figure 2.4: Experimental plasticity outcomes in response to STDP spike-pair and -triplet stimulation protocols. ***A & C,*** Synaptic potentiation and depression within critical time difference (Δt) windows in response to spike-pair stimulation protocols: The sketch in panel *A* illustrates the stimulation protocol, *i.e.* pre- and a postsynaptic spikes with fixed time lag Δt are presented at 1 Hz for 60 times. The percentage change in the EPSC amplitude $20-30$ min after the repetitive stimulation is depicted as a function of the time lag Δt in panel *C* (figure adapted from Bi and Poo 1998). ***B & D,*** Synaptic changes in response to STDP spike-triplet stimulation protocols: The sketch on the left hand side of panel *B* illustrates the stimulation protocol and the convention of the sign of the two time lags Δt_1 and Δt_2 specifying the triplet. A triplet consisting of a postsynaptic spike encircled by two presynaptic spikes is characterized by a positive Δt_1 and a negative Δt_2 (second quadrant in the diagram on the right hand side), while two postsynaptic spikes encompassing a presynaptic spike are defined by $\Delta t_1 < 0$ and $\Delta t_2 > 0$ (fourth quadrant in the diagram on the right hand side). Triplets with fixed Δt_1 and Δt_2 are presented 60 times at 1 Hz. The change in EPSC amplitude for 8 different triplets is indicated in panel *D* (figure adapted from Wang et al. 2005). Both experiments are done in cultured hippocampal neurons.

depolarization of the neuron. Thus, it has been debated whether or not postsynaptic action potentials are crucial for LTP/LTD induction, as originally suggested by Hebb (1949). In later experiments, intracellular techniques allow precise control over pre- and postsynaptic spiking activity, providing evidence at the single-cell level that coincidence between afferent input with postsynaptic spiking evokes long-term modifications. In general, presynaptic input (onset of the EPSP) occurring with little time difference to the postsynaptic action potential results in maximal synaptic modification, while no plasticity occurs if the temporal difference between both is large. In the hippocampus (Levy and Steward 1983; Gustafsson et al. 1987; Magee and Johnston 1997; Bi and Poo 1998), the Xenopus tectum (Zhang et al. 1998), visual cortex (Markram et al. 1997; Sjöström et al. 2001) and the somatosensory cortex (Feldman 2000) an EPSP occurring prior to the backpropagating action potential (pre-post pairing) evokes LTP, and the anti-causal order, *i.e.* the EPSP occurs after the postsynaptic neuron spiked (post-pre pairing), leads to LTD. In other words, if the input from the presynaptic neuron contributed to a subsequentially evoked postsynaptic spike, the connection is strengthened. On the other hand, in case the presynaptic input did not contribute to the postsynaptic spike and occurs after the postsynaptic spike, the connection is weakened (see an illustration of the results from Bi and Poo (1998) in Fig. 2.4*A* and *C*). Other forms of STDP have been identified. In the cerebellum-like structure of the electric fish, the pairings for which LTP and LTD occur are inversed, *i.e.* pre-post pairings lead to LTD and post-pre pairings to LTP (Bell et al. 1997). In another form of STDP, the plasticity result does not depend on the order of the pre- and the postsynaptic spike but on their relative time difference only. That is, the plasticity results are symmetric with respect to simultaneous occurrence of pre- and postsynaptic spike ($\Delta t = 0$; in spiny stellate neurons of layer IV in rat somatosensory cortex (Egger et al. 1999); in the cerebellum determined by the temporal difference between parallel fiber and climbing fiber input (Wang et al. 2000)). These cases will not be studied here, instead, we will focus on the form of plasticity observed in retinotectal connections as well as in neocortical and hippocampal pyramidal cells.

Ever since spike-timing dependent plasticity was discovered, it attracted a lot of attention, both experimentally and theoretically (see below). The original experiments on spike-timing dependent plasticity involve the repetitive presentation of pairs of pre- and postsynaptic spikes at low frequency (60 spike-pairs are presented at 1 Hz in the experiments performed on hippocampal cultures by Bi and Poo (1998), for example). Further studies investigated plasticity results in response to triplets and quadruplets of spikes. Generally speaking, whether the synapse gets potentiated or depressed in response to repetitive presentation of triplets of spikes cannot be deduced by adding linearly the changes emerging from the spike-pairs composing the triplet. In cultured hippocampal neurons for ex-

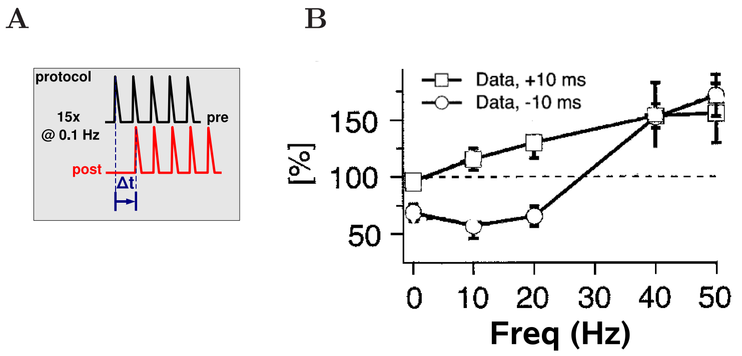

Figure 2.5: Frequency dependence of spike-timing dependent plasticity (STDP) in the visual cortex. ***A & B,*** The stimulation protocol is composed of blocks of 5 pre- and postsynaptic spike-pairs, where each pair has a time lag of either $\Delta t = +10$ ms or $\Delta t = -10$ ms. The repetition frequency (f) of the pair within the block is varied and the blocks are presented 15 times at a frequency of 0.11 Hz (see panel *A*). An exception is the stimulation protocol at $f = 0.1$ Hz consisting of 50 spike-pairs repeated at 0.1 Hz. Such stimulations evoke synaptic changes as depicted in panel *B* for $\Delta t = +10$ ms (squares) and for $\Delta t = -10$ ms (circles) as a function of the repetition frequency of the spike-pair in the block (figure adapted from Sjöström 2001).

ample, a triplet consisting of two presynaptic spikes arriving before and after a postsynaptic action potential (pre-post-pre triplet) does not evoke any changes (Bi and Wang 2002; Wang et al. 2005). This is consistent with a linear sum of plasticity results of both spike-pairs forming the triplet, in other words, potentiation and depotentiation cancel each other. Following this logic, a post-pre-post triplet (one postsynaptic spike arrives before and one after the presynaptic spike; post-pre-post triplet) would not evoke any changes. Experimental results however indicate that LTP is evoked with the post-pre-post stimulation pattern (Bi and Wang 2002; Wang et al. 2005) (see Fig. 2.4*B* and *D*). Between pyramidal neurons in layer 2/3 of the rat visual cortex, this behavior seems to be inversed, meaning that pre-post-pre triplets potentiate synapses and post-pre-post triplets depress connections (Froemke and Dan 2002). When the first spike arrives about $20 - 25$ ms before the succeeding pair of spikes, pre-post-pre patterns evoke LTD, while post-pre-post stimulations evoke LTP (Froemke and Dan 2002). It has been suggested that this difference between hippocampal and visual cortex triplet data stems from different dynamics of short-term depression (Cai et al. 2007) (see below). The nonlinearity of plasticity results in response to spike-triplet appears also for spike-quadruplets. A pre-post pair followed by a post-pre pair does not evoke any changes, while the reversed order - post-pre pair followed by a pre-post pair - yields LTP in hippocampal cell cultures (Wang et al. 2005).

Attention should be drawn to the fact that the pre-post or post-pre pairings in the doublet experiments had to be presented for 60 (Bi and Poo 1998; Wang et al. 2005) or 75 times at a fixed frequency (Markram et al. 1997; Sjöström et al. 2001). Both, LTP and LTD, attain their maximal amplitude after 60 spike-pair presentations (Froemke et al. 2006), while LTP can already be evoked after a few pairings (Gustafsson et al. 1987; Froemke et al. 2006). These results are consistent with data by Wittenberg and Wang (2006) indicating that LTP is present after a few pairings (30) and LTD emerges after longer stimulations (100 pairings). Sjöström et al. (2001) show that the plasticity outcome in the visual cortex furthermore depends on the frequency at which the spike-pairs are presented (see Fig. 2.5). Pre-post pairings evoke no change and post-pre pairings induce LTD at low presentation frequencies, while both pairings potentiate the synapse at high frequencies. We want to point out the consistency of these results with plasticity results in response to presynaptic stimulation protocols mentioned above, *i.e.* low stimulation frequencies evoke LTD and high stimulation frequencies evoke LTP (Dudek and Bear 1992). As a step towards more realistic situations potentially occurring *in vivo*, Froemke and Dan (2002) induce synaptic modifications by natural spike-train segments occurring *in vivo* in the visual cortex in response to visual stimuli. In these experiments, the segments were exposed to pairs of neurons in slices for 60 times at 0.2 Hz and the evoked synaptic modifications could be predicted by a model based on STDP results.

A common theme across the mentioned protocols seems to be the fact that low stimulation frequencies favor LTD induction while high stimulation frequencies trigger LTP. Furthermore, coincident pre- and postsynaptic spikes in causal firing order appear to be a natural pattern to associate synaptic connections, while the anti-causal order disassociates synaptic connection. It is generally assumed that neurons which take part in the same pattern of activity, *i.e.* receive correlated input, tend to reinforce their connections. Such correlation-based plasticity has been proposed as a mechanism for unsupervised experience-based development of neuronal circuitry, particularly in the cortex. This view is supported by experimental data from the perirhinal cortex indicating that experience leads to similar response preference of nearby neurons, *i.e.* nearby neurons tend to correlate (Erickson et al. 2000).

2.5 Bistable synapses in the hippocampus

In the previous section, stimulation paradigms are discussed which have been shown to change synaptic strength by stimulating presynaptic neurons (presynaptic stimulation at different frequencies, for example) or pre- and postsynaptic neurons in conjuction (STDP protocol, for example). Until now, these changes were described as increases, in case of LTP, or decreases, in case of LTD, of synap-

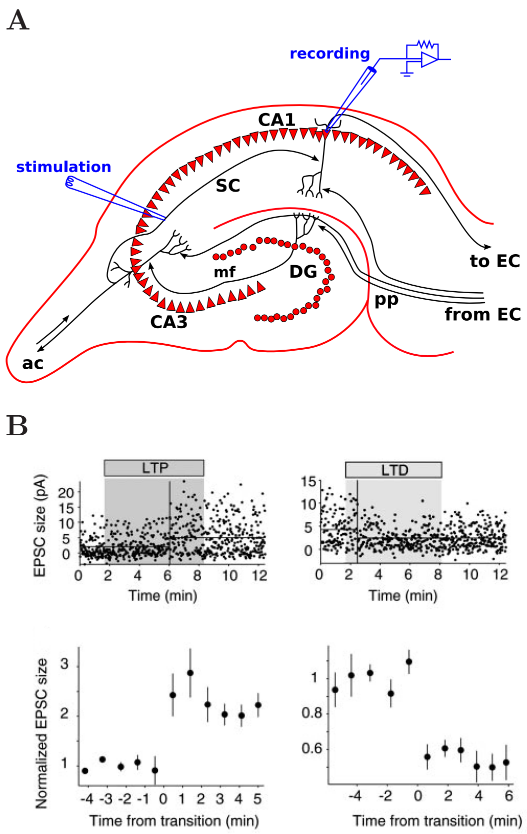

Figure 2.6: Experimentally determined all-or-none switch-like synaptic changes at the Schaffer collateral - CA1 synapse. ***A,*** Stimulation of the Schaffer collateral - CA1 pyramidal cell pathway in the hippocampus: The minimal stimulation protocol technique (see text) is applied to the Schaffer collateral projection and putative single-synaptic responses are recorded from pyramidal neurons in the CA1 subfield of the hippocampus (Petersen et al. 1998; O'Connor et al. 2005b). The configuration of such experiments in the rat hippocampus is illustrated in panel *A*. ***B,*** Unitary plasticity events take place in single steps: Putative single synapse responses recorded before, during (shaded region) and after the LTP (above, left hand side) and the LTD (above, right hand side) stimulation protocol are shown as a function of time. The depicted responses are measured in 2-ms windows at the peak of the EPSC. To illustrate the immediate step-like transitions 10-response bins were grouped and aligned with respect to the point of transition at $t = 0$ min for the LTP (below, left hand side) and the LTD (below, right hand side) event (figure adapted from O'Connor et al. 2005).

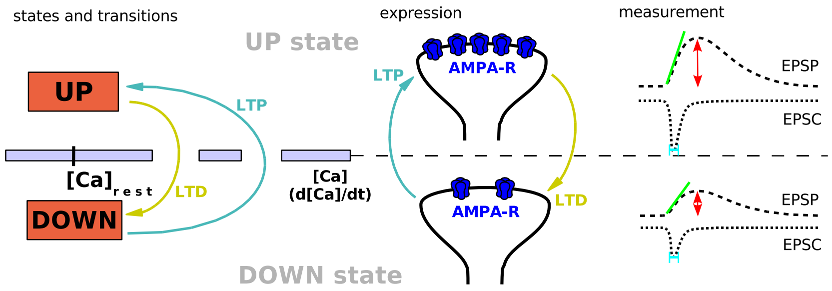

Figure 2.7: Scheme of a bistable synapse. A bistable synapse exhibits two stable states - DOWN and UP - at resting calcium levels (*i.e.* transitions between both states are not possible at resting calcium levels). Since intracellular calcium elevations are a necessary and sufficient signal to induce LTP and LTD, transitions from the DOWN to the UP state (LTP, light blue arrows) supposedly occur during fast and high calcium transients and vice versa (LTD, light green arrows) if the system is exposed to moderate calcium concentrations for a long time (left panel). The two discrete state are most likely expressed by different numbers of functional AMPA receptors in the membrane in the hippocampus (middle panel). The two states can be experimentally characterized by the amplitude (red arrows) or the slope (green bars) of the excitatory postsynaptic potential (EPSP, right panel). Furthermore, also the current around the peak of the excitatory postsynaptic current (EPSC, cyan brackets) is used to access synaptic strength. See text for more details.

tic strength. We focus on the nature of these changes in this section. Experiments showing that these changes are switch-like all-or-none transitions are discussed in more detail.

In all the experiments on long-term synaptic modifications mentioned so far, LTP (resp. LTD) refers to a long-lasting increase (resp. decrease) of synaptic strength and usual measures to quantify this change are the EPSP/EPSC amplitude, the initial EPSP slope or the current in a 2-ms window at the peak of the EPSC (see right hand panel in Fig. 2.7). This means that the changes are embodied in EPSP properties recorded at the soma of the postsynaptic neuron before and after the stimulation protocol. This implies furthermore that the recorded signal is a sum of single EPSPs occurring at all stimulated synaptic terminals and propagating towards the soma. As already mentioned above, LTP/LTD protocols typically involve the stimulation of a large number of afferents, *i.e.* the recorded signals and changes in EPSP size stem from an ensemble of synapses and reflect properties of a compound signal. For this reason, most of the plasticity experiments give no insight into the nature of synaptic changes at the single synapse level. More recent experiments on plasticity at the CA3 Schaffer collateral - CA1 synapse try to address exactly this question (Petersen et al. 1998; O'Connor et al. 2005b). In particular, they try to answer the question whether synaptic strength changes occur in an analog or a digital manner. In other words, is the size of the EPSP at the level of a single synapse changing continuously or can it take specific values only? If the latter is true, can the synapse take two, three, ... or more states? In the most simple case of two stable states, the synapse is called binary or bistable.

The experiments performed by Petersen et al. (1998) and O'Connor et al. (2005b) use a minimal stimulation technique on CA3 Schaffer collateral - CA1 connections in Sprague-Dawley rats (postnatal day $13-21$, see Fig. 2.6*A*). The following three criteria characterize for minimal stimulation: (i) the mean amplitude and failure rate of responses are insensitive to changes of stimulus intensity of at least 10 %, (ii) decreasing the stimulus strength leads to an abrupt and total failure of the postsynaptic response to occur, and (iii) response latency does not change over the course of the experiment. With such minimal stimulation, they aim to putatively evoke single-synapse responses by electrically simulating only one or a very low number of Schaffer collateral axons (Raastad 1995; Isaac et al. 1996). The underlying assumption that one projection makes on average one synaptic contact with a CA1 neuron seems to be true for young animals ($>$ 1 month old) (Bolshakov and Siegelbaum 1995; Stevens and Wang 1995). During development, however, the connectivity is increased by forming multiple synaptic contacts between single CA3-CA1 cell pairs (Hsia et al. 1998). Taken together, the minimal stimulation technique is a means to minimize the number of synapses activated in an attempt to record postsynaptic signals stemming from single synapses.

Employing the minimal stimulation technique, O'Connor et al. (2005b) evoke LTP by stimulating the Schaffer collateral axon at 1 Hz and pairing every 10th stimulus with a postsynaptic depolarization to 0 mV for 40 times (*i.e.* in total 400 presynaptic stimuli are given during the protocol). LTD induction consists in pairing every third stimulus with a depolarization to -55 mV for 130 times (390 stimulations in total). The EPSC size increases during the LTP stimulation protocol and decreases during the LTD protocol (see Fig. 2.6*B*). Applying statistical tests to this change in EPSC size leads to the conclusion that theses changes are all-or-none switch like events. They fit ramp functions to the experimentally obtained and binned EPSC sizes and to artifical data sets with known ramp times. Based on the comparison of these fits, the most likely ramp times where on the time scale of 1 min or less, and, under the stimulation conditions, these events cannot be distinguished from step transitions (O'Connor et al. 2005b). They show furthermore that these events saturate synapses to full potentiation or depression. That means that once a synapse got potentiated it cannot be potentiated a second time, but the potentiation can be reversed by a subsequent LTD induction protocol. Accordingly, a second LTD induction protocol cannot decrease EPSC size further suggesting that the investigated synapse has two stable states, *i.e.* the synapse is binary. Within the time resolution of the experiments, these changes are sudden transitions, taking place on the time scale of seconds. Results obtained by Petersen et al. (1998) on potentiation of putative single-synapses reached the same conclusion, but LTD induction has not been considered in this study. Bagal et al. (2005) use glutamate uncaging paired with brief postsynaptic depolarization and report long-lasting potentiation of single dendritic spines in hippocampal CA1 cells. This potentiation shared many features with conventional LTP such as a dependence on NMDA activation and the ability to be reversed, or depotentiated, in a NMDA-R-dependent manner by low-frequency stimulus trains. Again, potentiation was expressed in a stepwise, all-or-none manner. This step-like event occurred ≈ 38 s after the pairing pulse and when it occurred it was expressed in less than 10 s (Bagal et al. 2005). In the experiments of O'Connor et al. (2005b), step-like LTP transitions occurred on average 1.3 min after the onset of the stimulation protocol and LTD transitions after 3.1 min.

To summarize, the experimental results of LTP and LTD induction on single synapses suggest that synapses can be described as occupying two states of low or high transmission efficacy. This implies that potentiation or depression observed in experiments including the stimulation of an ensemble of synapses is composed out of many step-like events of single synapses. LTP (resp. LTD) experiments on such an ensemble start from a mixture of states and can maximally potentiate (resp. depress) all connections. Consequently, the properties of synaptic plasticity outlined above must apply to switch-like transitions in single synapses. These properties are, for example, the requirement for pre- and postsynaptic activity or the fact that the major signal driving binary changes is the dynamics of the intracellular calcium concentration (Yang et al. 1999; Mizuno et al. 2001; Ismailov et al. 2004; Nevian and Sakmann 2006). Since the main mechanism proposed for the expression of LTP seems to involve an increase in the number of functional AMPA-Rs in the plasma membrane (see reviews by Malenka and Nicoll 1999 and Malinow and Malenka 2002) or the phosphorylation state of AMPA-Rs (Benke et al. 1998; Lee et al. 2000; Lee et al. 2003; see also review by Soderling and Derkach 2000) or both, binary changes seem to imply that synaptic changes involve always a cluster of AMPA receptors all at once (see scheme in Fig. 2.7 and review by Lisman (2003)). The number of AMPA receptors in the postsynaptic density of a spine is believed to vary from none for silent synapses to around 50 (Kennedy 2000).

As a means of information storage, graded synaptic changes (Bienenstock et al. 1982; Oja 1982) seem to be more susceptible to drift in a noisy environment than all-or-none binary changes (Hopfield 1982). Thus discreteness might help to make information storage in a neural network more robust. In this framework, one synapse is able to store one bit of information imprinted by synaptic plasticity. On a longer time scale however, step-like changes of synaptic strength give way to events like altered gene-expression that may take a more continuous character.

2.6 Biochemical pathways underlying LTP/LTD

This work focuses on the molecular mechanism of LTP/LTD induction and maintenance in Schaffer collateral - CA1 neuron synapses. Although LTP in other synapses seems to rely on different induction pathways and expression mechanisms, the LTP at CA1 synapses exhibits common characteristics compared to LTP observed at glutamatergic excitatory synapses throughout the mammalian brain including the cerebral cortex (Kirkwood et al. 1993). Known biochemical pathways and proteins involved in induction and maintenance of long-term synaptic modifications are highlighted in this secion. This is done with a special emphasis on the biochemistry involved in spike-timing dependent plasticity at Schaffer collateral - CA1 neuron synapses.

2.6.1 NMDA receptor activation and calcium signaling

LTP and LTD are believed to be related to memory formation since a large body of evidence has been gathered demonstrating that both rely on similar molecular mechanisms (see review article by Lynch 2004). Whitlock et al. (2006) found, for example, that inhibitory avoidance learning in rats produced the same changes in hippocampal glutamate receptors as induction of LTP with high-frequency stimulation. They conclude that inhibitory avoidance training induces LTP in CA1 neuron synapses. Another characteristic example for such evidence is the blockade of the NMDA receptor which impairs a variety of hippocampal-dependent learning (such as impairment of forming a spatial map) and prevents the induction of LTP in such animals (Morris et al. 1986; Abraham and Mason 1988). Though the induction of LTP at the Schaffer collateral - CA1 neuron synapse necessitates activation of NMDA receptors (Collingridge et al. 1983; Bliss and Collingridge 1993), basal synaptic transmission and the expression of the potentiated state are not affected by NMDA blockade (Morris et al. 1986). The requirement of NMDA activation for LTP induction has also been identified for LTP induction between thick, tufted layer V pyramidal neurons in rat visual cortex (Artola and Singer 1987; Bear et al. 1992; Markram et al. 1997; Sjöström et al. 2001) and in layer IV to layer II/III pyramidal cell synapses in the somatosensory cortex (Castro-Alamancos et al. 1995; Feldman 2000; Nevian and Sakmann 2006). Also the segregation into eye-specific layers via an activity-dependent process in the lateral geniculate nucleus (LGN) shows LTP/LTD-specific properties and relies on NMDA-R activation (Hahm et al. 1991; Mooney et al. 1993). NMDA-mediated LTP has moreover been studied in amphibia, for example (in tectal neurons of the tectum in Xenopus tadpoles, Zhang et al. 1998). With respect to spike-timing dependent plasticity, not surprisingly, LTP induction evoked by pre-post pairings depends on the large calcium influx through NMDA-Rs in the hippocampus (Magee and Johnston 1997) and the somatosensory cortex (Nevian and Sakmann 2006). On the other hand, calcium channel antagonists (nimodipine for L-type channels; or Ni^{2+} for T-type channels) also block LTP without any effect on baseline EPSPs in hippocampal slices (Magee and Johnston 1997). Contrarily, Bi and Poo (1998) report that blocking L-type Ca^{2+} channels (by nimodipine) does not affect LTP induction by pre-post pairings but prevents LTD induction in response to post-pre pairings. Nevian and Sakmann (2006) show that VDCCs are necessary for the induction of LTD in the somatosensory cortex (see Fig. 2.9).

LTP and LTD seem to rely on calcium influx through different channels but both require necessarily postsynaptic calcium elevations (Neveu and Zucker 1996; Yang et al. 1999; Nevian and Sakmann 2006). Neveu and Zucker (1996) could even show that the release of caged-calcium by photolysis in hippocampal CA1 pyramidal cells is sufficient to evoke LTP and LTD, and that concurrent presynaptic activity is not required. The calcium sensors that trigger the long-lasting changes respond to the global, volume-averaged increase in intracellular calcium concentration and calcium microdomains around local sources of calcium influx are not important (Nevian and Sakmann 2006). They show that LTP and LTD are equally sensitive to fast (BAPTA) and slow (EGTA) Ca^{2+} buffers loaded in the postsynaptic cell.

2.6.2 Protein signaling cascades

Three of the main calcium-responsive signaling pathways that have been identified and shown to participate in LTP/LTD induction and expression as well as learning and memory are CaMKII-dependent signaling, cyclic AMP-dependent signaling and calcineurin signaling. See Fig. 2.9 for a schematic depiction of the biochemical pathways.

Calcium/calmodulin-dependent protein kinase II In its basal state, the activity of the calcium/calmodulin-dependent protein kinase II (CaMKII) is extremely low. Regulation of intracellular calcium levels allows the neuron to link activity with phosphorylation of CaMKII. The kinase functional domains (12 per holoenzyme) are attached by stalklike appendages to a gear-shaped core, grouped into two clusters of 6 subunits (see Fig. 2.8 and Kolodziej et al. (2000)). Each subunit contains a catalytic, an autoregulatory and an association domain. In the basal state, the regulatory domain interacts with the catalytic domain to block ATP and substrate sites. The autoregulatory domain binds furthermore Ca^{2+}/CaM which allows for release of autoinhibition upon binding of calcium/calmodulin. In addition to relieving autoinhibition, binding of Ca^{2+}/CaM also initiates autophosphorylation at the residue theronine-286 (Thr^{286}) in the autoregulatory domain.

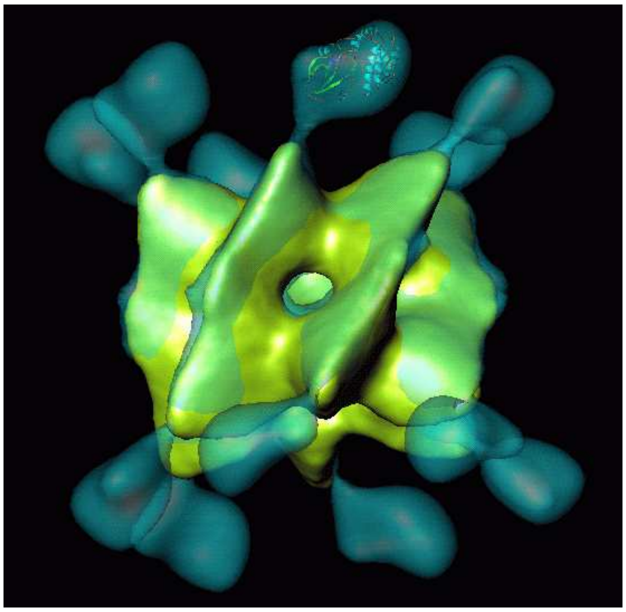

Figure 2.8: Three-dimensional reconstructions of CaMKII. Cryo-electron microscopy followed by 3-D reconstructions is used to produce data on the 3-D structure of the CaMKII holoenzyme. The recombinant form of the neuronal (α) isoform of CaMKII is a twelve-subunit complex organized in two stacked hexameric rings (above and below, colored in turquoise). The functional, catalytic domains reside in foot-like processes that extend away from a central gear-shaped core (middle, colored in green) formed by the C-terminal domains of each subunit. The association domain comprises the gear-shaped core (Kolodziej et al. (2000), with kind permission by M. Neal Waxham, http://nba.uth.tmc.edu/homepage/waxham/).

Phosphorylation of this site occurs as an inter-subunit reaction in the holoenzyme and requires Ca^{2+}/CaM binding to both the 'catalytic' and the 'substrate' subunits (Hanson et al. 1994). Autophosphorylation enables the enzyme to remain autonomously active after dissociation of Ca^{2+}/CaM (Miller and Kennedy 1986). Phosphorylation at Thr^{286} also alters the interaction of the kinase with Ca^{2+}/CaM, causing its off-rate to fall by other three orders of magnitude (Meyer et al. 1992). This phenomenon has been termed "calmodulin trapping". If calcium levels are low for long enough, Ca^{2+}/CaM will dissociate from the kinase. Dissociation renders additional autophosphorylation sites in the regulatory domain available. Thr^{305} and Thr^{306}, which are protected by bound Ca^{2+}/CaM, can now undergo autophosphorylation if the kinase is still in its active, Thr^{286} phosphorylated state. Phosphorylation of these additional sites prevents rebinding of Ca^{2+}/CaM and maximal activation of the kinase. See reviews by Hudmon and Schulman (2002) and Griffith (2004) for more details of the regulation of CaMKII activity.

In its activated state, CaMKII is reversibly translocated to a postsynaptic density-bound state where it interacts with multiple LTP related partners structurally organizing protein anchoring assemblies (Shen and Meyer 1999; Hayashi et al. 2000; Fink and Meyer 2002; Lisman et al. 2002; Colbran 2004). The direct phosphorylation of the AMPA receptor GluR1 subunit enhances AMPA channel function (Mammen et al. 1997; Derkach et al. 1999). It has furthermore been shown that phosphorylation of AMPA-Rs by active CaMKII drives AMPA receptors to synapses (Hayashi et al. 2000; see also review article by Lisman et al. 2002). Mutated mice lacking the ability of CaMKII autophosphorylation exhibit profound deficits in hippocampus-dependent learning and memory and also completely fail to exhibit LTP induction in the hippocampal CA1 subfield under standard stimulation protocols (Giese et al. 1998). The importance of CaMKII autophosphorylation in hippocampal LTP has furthermore been demonstrated during LTP induction via spike-timing stimulation protocols with spike-pair and -triplets. LTP is cancelled in the presence of KN-62, a specific blocker of CaMKII which binds to the enzyme and blocks the activation by calcium/calmodulin (Wang et al. 2005). However, the role of CaMKII beyond induction of synaptic long-term modifications remains controversial. Enzymatic activity of CaMKII decreases to baseline within ~ 15 min after LTP induction (Lengyel et al. 2004). In contrast, Sanhueza et al. (2007) show that a noncompetitive inhibitor of CaMKII can reverse LTP and they suggest that a component of synaptic memory maintenance is attributable to CaMKII in CA1 region synapses.

Protein kinase A and calcineurin The cyclic adenosine monophosphate (cAMP)-dependent protein kinase A (PKA) cascade is thought to mediate synapse to nucleus signaling and seems to initiate synthesis of proteins and RNA during the late phase of LTP induction in the hippocampal area CA1 (> 1 h) (Abel et al. 1997; Nguyen and Kandel 1997). These studies suggest that the early phase of LTP induction and basal synaptic transmission are not affected by cAMP-PKA inactivation. On hippocampus to prefrontal cortex connections however, LTP induction is accompanied by a rapid increase in PKA activity during the early phase (Jay et al. 1998). Also for the CA3-CA1 pathway, LTP induction by high-frequency stimulations can be blocked by inhibiting postsynaptic cAMP-PKA in contrast to the experimental results above (Blitzer et al. 1995; Blitzer et al. 1998). The requirement of PKA for LTP induction can be overcome by direct inhibition of postsynaptic phosphatases (Blitzer et al. 1995), suggesting that PKA gates LTP by blocking protein phosphatases (see below). The calcium-sensitivity of this pathway relies upon calcium/calmodulin-initiated conversion of adenosine triphosphate

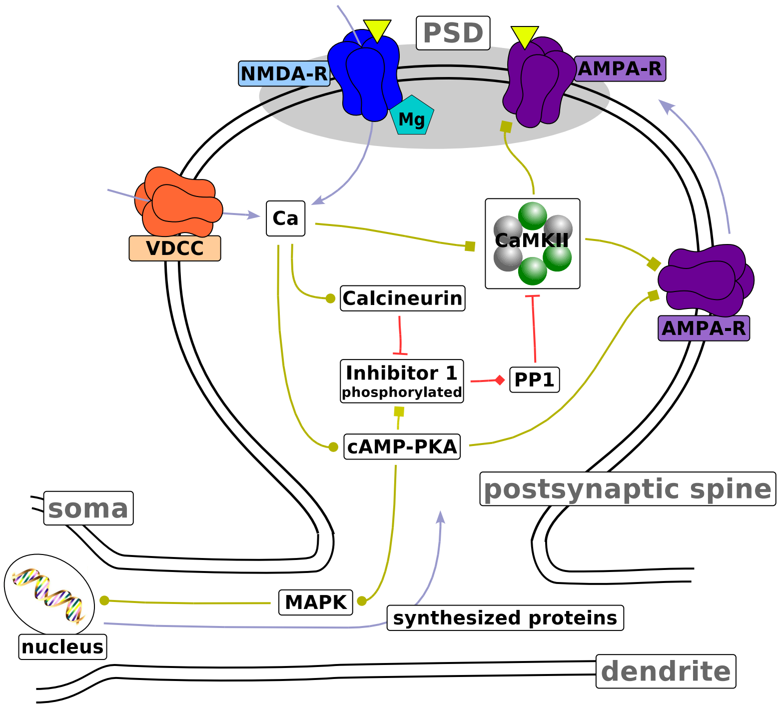

Figure 2.9: Protein signaling cascades underlying LTP/LTD. Biochemical pathways are depicted which have been identified to be involved in LTP/LTD induction and maintenance at the Schaffer collateral - CA3 neuron synapse. Light blue arrows indicate transport of the respective entities. Light green connections indicate stimulation of target activity. Squares at the end of light green connections indicate that the stimulation is due to phosphorylation of the target. Red connections depict inhibition of target activity through dephosphorylation (indicated by a bar at the end of the connection) or binding (indicated by the diamond at the of the connection). The yellow triangles show neurotransmitter binding to receptors located in the postsynaptic density (PSD). See text for more details and names of the depicted entities.

(ATP) into cAMP by adenylyl cyclase (Cooper et al. 1995). Elevation of cAMP, in turn, activates the cAMP-dependent protein kinase A (Glantz et al. 1992; Carr et al. 1992). Stimulating this pathway by increasing the adenylyl cyclase activity is shown to induce LTP in hippocampal slices without the requirement for any electrical stimulation, an effect that can be blocked with PKA inhibitors (Frey et al. 1993). Similarly, overexpression of adenylyl cyclase in transgenic mice enhances LTP and learning (Wang 2004). Though PKA directly phosphorylates the AMPA receptor GluR4 subunit, both PKA activity and CaMKII activity are necessary to incorporate AMPARs into the cell membrane (Esteban et al. 2003).

Experimental results indicate that the sign of hippocampal synaptic plasticity is regulated by the balance between protein phosphorylation and dephosphorylation mediated by PKA and calcineurin, respectively. Consistent with this idea, overexpression of calcium/calmodulin-dependent calcineurin in the forebrain of transgenic mice was found to impair an intermediate and PKA-dependent phase of LTP, as well as the transition from short- to long-term memory and memory retrieval (Mansuy et al. 1998; Winder et al. 1998). On the other hand, inhibition of calcineurin activity facilitates LTP *in vitro* and *in vivo* in a PKA-dependent manner (Malleret et al. 2001). Consistent with these findings, LTD evoked during STDP stimulation by depressing post-pre spike-pairs is blocked in the presence of calcineurin inhibitors while the same blockade unmasks potentiation for spike-triplets (Wang et al. 2005). Similar results are found for presynaptic stimulation protocols inducing LTP/LTD. A kinase inhibitor (inhibiting CaMKII and PKC) blocks LTP and reveals LTD for $1 - 100$ Hz stimulation protocols. On the other hand, a phosphatase inhibitor (blocking protein phosphatase 1 - PP1 - and protein phosphatase 2A (PP2A)) prevents LTD for intermediate stimulation frequencies ($1 - 10$ Hz) but leaves LTP induction unchanged at high stimulation frequencies. These results suggest that the kinase and the phosphatase pathways interact at one or several points in the signaling cascade. A proposed converging point of the cAMP-PKA and the calcineurin pathways is the inhibitor 1. That is, hippocampal LTD induction involves calcium/calmodulin-dependent calcineurin dephosphorylating inhibitor 1 (Mulkey et al. 1994). On the other hand, synaptic stimulation that induces cAMP-dependent LTP raises the amount of phosphorylated I1 in the CA1 region (Blitzer et al. 1998). This increase was dependent on the PKA activity since is was blocked by PKA inhibitors. Phosphorylated inhibitor 1 is a specific blocker of protein phosphatase 1 (Ingebritsen and Cohen 1983). In other words, the differential calcium-dependent activation of the calcineurin and the cAMP-PKA pathway is expressed in the phosphorylation level of inhibitor 1 which in turn inhibits PP1 in its phosphorylated state. During the induction of hippocampal LTD, the inactivation of inhibitor 1 through dephosphorylation increases PP1 activity (Mulkey et al. 1994). Disruption of PP1 binding to synaptic targeting proteins is reported to block synaptically evoked LTD but does not affect basal synaptic transmission in CA1 pyramidal cells. PP1 has no direct access to synaptic AMPARs, while PP1 is the only phosphatase able to dephosphorylate CaMKII in the PSD (Strack et al. 1997).

The signaling cascade continues towards the nucleus through the mitogen-activated protein kinase (MAPK). PKA activates this enzyme after hippocampus-dependent learning in mice. Furthermore, MAPK inhibitors block the maintenance of LTP (Waltereit and Weller 2003; Sweatt 2004). This cascade targets the cAMP-responsive element binding protein (CREB) in the nucleus and therefore governs the expression of LTP/memory effector proteins (Bozon et al. 2003; Chen et al. 2003). These results indicate that this branch of the cAMP-dependent signaling cascade plays a key role during the late phase of LTP most likely accompanied by altered gene expression (Goelet et al. 1986; Alberini et al. 1995).

Do the outlined molecular pathways also underly spike-timing dependent plasticity in other brain areas? LTP induction in the visual and the somatosensory cortex, for example, relies on the coincidence detection of pre- and postsynaptic activity by the NMDA receptor as in the hippocampus (Sjöström et al. 2003; Nevian and Sakmann 2006). Contrary to the pathways uncovered in the hippocampal CA3-CA1 system however, LTD seems to involve retrograde signaling to the presynaptic side. Postsynaptic calcium elevations mediated by VDCCs as well as the activation of metabotropic glutamate receptors (mGluRs) are necessary for LTD induction. An application of a mGluR antagonist results in a complete block of LTD but had no effect on the calcium transients (Nevian and Sakmann 2006). This block of LTD was attributable to the disruption of the G-protein coupled cascade involving retrograde endocannabinoid signaling (Sjöström et al. 2003; Sjöström et al. 2004; Piomelli 2003; Nevian and Sakmann 2006). Interestingly, Otani et al. (1998) report a mGluR pathway dependent form of LTD at the Schaffer collateral - CA1 neuron projection.

More proteins have been suggested to be important for LTP/LTD, such as protein kinase C, phosphatidylinostiol 3-kinase, Protein kinase Mζ, tyrosine kinase Src to name just a few of them (see reviews by Bliss and Collingridge (1993) and Malenka and Bear (2004)). Except for the pathway involving CaMKII and associated proteins, the signal transduction pathways required for triggering long-term synaptic changes remain elusive with many potential players but few definite answers about specific roles in induction and maintenance mechanisms.

2.7 Models of synaptic plasticity

The biological mechanisms underlying synaptic plasticity have inspired mathematical models ever since the early hypothesis that flexibility and adaptability in neural networks might be established at the connections between neurons, and long before the first experimental evidence of synaptic plasticity. It is noteworthy that Hebb (1949) and Konorski (1948) captured in their approaches many properties of long-term modifications long before the first experiments confirmed the postulated input-specificity and associativity of synaptic modifications. After a short overview over rate-based plasticity models, we will focus on the class of mathematical models trying to reproduce aspects of spike-timing dependent plasticity. Rather than presenting an exhaustive list of models, different approaches will be highlighted, together with some exemplary studies.

2.7.1 Rate-base plasticity models

Synaptic plasticity models originating from the synaptic coincidence-detection rule suggested by (Hebb 1949) describe the activity of each neuron by a single variable which normally represent the firing rate. In the simplest mathematical representation of Hebb's conjecture, the synaptic weight increases in case of simultaneous pre- and postsynaptic activity. Such a plasticity rule is called the basic Hebb rule and typically requires the imposition of an upper saturation bound to prevent synaptic weights from unbounded growth. Moreover, the basic Hebb rule fails to induce competition between synapses.

The later discovery that synapses can also depress, which is not a part of Hebb's conjecture and is not implemented in basic Hebb rules, led to so-called covariance rules. Synaptic weights are reduced if the pre- or the postsynaptic activity fall below a certain level in such rules. Covariance rules predict LTP if the pre- and the postsynaptic activities go both above or both below their corresponding thresholds. A convenient choice for such a threshold is the average value of the corresponding activity, for example. Similar to the basic Hebb rule, covariance rules are unstable, due to the positive feedback, and noncompetitive.

In covariance rules, synaptic plasticity can occur even in the absence of pre- or postsynaptic activity. To avoid this, Bienenstock et al. (1982) suggested a plasticity rule which requires pre- and postsynaptic activity to change synaptic weight, consistent with experiments. The rule, which is called BCM rule, has a threshold on the postsynaptic activity defining whether synaptic strength is increased or weakened. If this threshold is allowed to vary with the postsynaptic activity (sliding threshold), synaptic modifications can be stabilized against unbounded growth and competition between synapses is implemented.

Another more direct way to stabilize synaptic weights is to add terms that depend explicitly on the weights. This is typically done in form of weight normalizations corresponding to the idea that the postsynaptic neuron can support only a fixed total synaptic weight. Such a constraint can be implemented by limiting the sum of synaptic weights (realized in the Hebb rule with subtractive normalization, for example) or the sum of their squares (imposed dynamically in the Oja rule, Oja (1982)). Naturally, limiting the weights prevents them from growing without bound. Also, competition is introduced by normalization since the increase in one weight forces other weights to decrease.

A form of the covariance rule is used in the Hopfield model (Hopfield 1982), for example. The activity variable of one neuron (s_i) in this model is simplified to being binary, *i.e.* the neuron is either active ($s_i = +1$) or inactive ($s_i = -1$). A synapse is potentiated if both neurons are active or inactive and and depressed if both neurons occupy different states. The basic idea behind such a model is to build a system where a given set of states, the memorized pattern, are the energy minima of the network dynamics. However, these memories have to be uncorrelated. When the memories have significant overlaps between them, the performance falls drastically. A variant of the Hopfiled model is introduced by Tsodyks and Feigelman (Tsodyks and Feigel'man 1988). Their model also uses a covariance rule and is able to store sparse, biased memory patterns. Activity states of neurons are defined in terms of 0 for quiescent and 1 for firing, which is more appropriate for storage of correlated patterns.

2.7.2 Spike-timing dependent plasticity models

Models based purely on spike-timing The simulation of the spike-timing dependence of synaptic plasticity requires models describing the spike times in pre- and postsynaptic neurons, rather than just their firing rate. Remarkably, the spike-timing dependent plasticity learning rule (*i.e.* causal pairs of pre-and postsynaptic spikes get potentiated and anti-causal depressed) has been proposed in a mathematical study of the barn owl sound localization system before the first experiments revealed STDP learning (Gerstner et al. 1996). A paradox leading to the proposition was the fact that auditory and electronsensory neural systems encode relevant signals in the range of a few microseconds with neurons which are at least one order of magnitude slower. The proposed model gave rise to the first generation of models describing STDP triggered synaptic weight changes based on the occurrence times of the pre- and postsynaptic spikes. In other words, every spike-pair is evaluated, and depending on whether the presynaptic spike occurred before or after the postsynaptic one, the synaptic weight is increased or decreased, accordingly (Gerstner et al. 1996). Such spike-timing based plasticity rules can be differentiated by whether the change in synaptic weight scales with synaptic strength (multiplicative learning rule: Kistler and van Hemmen 2000; van Rossum et al. 2000; Rubin et al. 2001; Gütig et al. 2003) or not (additive learning rule: Gerstner et al. 1996; Eurich et al. 1999; Kempter et al. 1999; Roberts 1999; Song et al. 2000). Bounds have to be imposed as hard constraints in additive models to prevent synaptic weights from growing infinitely high. In contrast, multiplicative models assume attenuation of potentiating and depressing synaptic changes as the corresponding upper and lower bound is approached. This is referred to as an implementation of soft boundaries. However, adding up plasticity changes induced by pair-wise interactions of spikes cannot account for the non-linearities inherent in synaptic changes induced by spike-triplets (Bi and Wang 2002; Froemke and Dan 2002; Wang et al. 2005) and the frequency dependence of STDP (Sjöström et al. 2001), for example. To reconcile these experimental results within the framework of models purely based on spike-timing, higher-order interactions going beyond evaluation of spike-pairs have been proposed: (i) An efficacy to evoke synaptic changes is assigned to each pre- and postsynaptic spike. This efficacy depends only on the interval from the preceding spike in the same neuron (Froemke and Dan 2002). (ii) Synaptic modifications are based on triplets of spikes, that means that the update rule considers sets of three spikes (*i.e.* two pre- and one post- or one pre- and two postsynaptic spikes; Pfister and Gerstner 2006). (iii) The magnitude of LTP suggested by the STDP curve is additionally influenced by the membrane depolarization and by the instantaneous firing rate of the postsynaptic neuron. Furthermore, if spike interactions producing LTP are presumed to "win" over those producing LTD, this model can capture the frequency dependence of cortical STDP (Sjöström et al. 2001). Interestingly, Izhikevich and Desai (2003) show that the STDP spike-pair learning rule can be linked to the BCM rule if only nearest-neighbor spike-pairings are taken into account and correlations between pre- and postsynaptic activities are neglected. As illustrated above, such a STDP spike-pair rule can however not be generalized to reproduce spike-triplet data.

These approaches are useful tools to study the impact of STDP on unsupervised learning of input correlations in neural networks. In this context, the additive learning rule has been shown to retain inherently unstable dynamics while exhibiting strong competition between afferent synapses. This yields bimodal synaptic distributions and restricts its ability to generate graded representations of input features. Moreover, because of the strong competition, patterns in the synaptic distribution can emerge that do not reflect patterns of correlated activity in the input. On the other hand, multiplicative models result in stable synaptic dynamics. However, because of reduced competition, all synapses are driven to a similar equilibrium value, even at moderately strong input correlations. Gütig et al. (2003) show that an intermediate learning rule (through appropriately scaling of the weight dependence of the update) can be tuned such that it is possible to learn synaptic respresentations of input correlations while maintaining the system in a stable regime. Pfister and Gerstner (2006) show that the triplet-based model leads to input selectivity in a simple feedforward model, a necessary property for receptive field development, for example. However, by changing the synaptic weights based on spike-times only, these effective implementations tell us nothing about the biochemical mechanisms leading to synaptic changes.

Models based on calcium amplitude or dynamics In a first step towards biologically more realistic models, the pre- and postsynaptic voltage- (Abarbanel et al. 2002) or the postsynaptic calcium dynamics (Karmarkar and Buonomano 2002; Karmarkar et al. 2002; Shouval et al. 2002; Abarbanel et al. 2003) triggered by pre- and postsynaptic spikes are simulated. In models simulating calcium dynamics, a presynaptic spike evokes a NMDA receptor mediated long-lasting calcium influx which is strongly increased by the coincident occurrence of a postsynaptic spike removing further the magnesium block. Independently, a backpropagat-

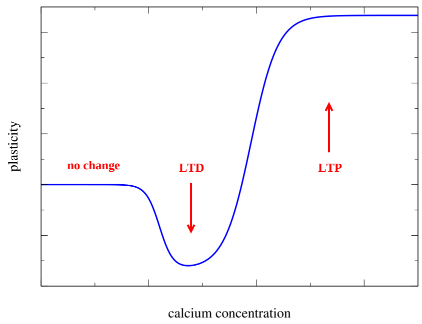

Figure 2.10: Calcium control hypothesis. The calcium control hypothesis suggested by numerous experiments and incorporated in mathematical models (see text) implies that low calcium levels do not evoke any changes, intermediate calcium levels depress the synapse (corresponding to a LTD event) and high calicum transients potentiate the synapse (corresponding to a LTP event). Note that depression and potentiation are not sudden events but occur with a respective time constant, whereas LTP induction is faster than LTD induction. See text for more details.

ing action potential opens voltage-dependent calcium channels (VDCCs) leading to a short-lasting calcium transient. The models determine the induced synaptic weight change based on the maximal amplitude (Karmarkar and Buonomano 2002) or the time course (Shouval et al. 2002; Abarbanel et al. 2003; Cai et al. 2007) of the calcium transients triggered by pre- and postsynaptic spikes during respective stimulation protocols. The magnitude and sign of resulting synaptic changes are based on the calcium control hypothesis, meaning that different calcium levels trigger different forms of synaptic plasticity (*i.e.* when the calcium level is below a threshold, no modification occurs; if calcium resides in an intermediate calcium range, the synaptic weight is decreased and if calcium increases above a certain threshold, the synaptic strength is potentiated; see Fig. 2.10 for an illustration). With respect to STDP, these models seem to commonly predict the appearance of a second LTD range for large positive time differences between the pre- and the postsynaptic spikes. Post-pre pairings evoke calcium transients which linearly superimpose and therefore yield moderate calcium elevations promoting LTD. Pre-post pairings result in supralinear superpositions of the calcium transients which attain high calcium levels required to evoke LTP. If the time-difference between the pre- and the postsynaptic spike grows larger, the calcium transients pass again through a region of moderate levels inducing LTD. STDP spike-pair experiments however have not indicated depression of pre-post pairings (but see Nishiyama et al. (2000) and Wittenberg and Wang (2006)). Shouval and Kalantzis (2005) show that stochastic properties of synaptic transmission can markedly reduce the LTD magnitude at positive time lags. Karmarkar and Buonomano (2002) hypothesize that two functionally distinct calcium pools could trigger different readout mechanisms for LTP and LTD in order to overcome this difficulty. Taking into account stochastic synaptic dynamics (short-term depression, stochastic transmitter release and back-propagating action potential depression/facilitation) allows to reproduce spike-triplet data of hippocampal and visual cortex neurons with models based on calcium dynamics (Cai et al. 2007). The nonlinearity of plasticity results between pre-post-pre and post-pre-post triplets is attributed in this model to the difference in consecutive occurrence of either two presynaptic- or two postsynaptic spikes, respectively. Depending on the recovery dynamics of neurotransmitter release, release probability and the depression/facilitation dynamics of back-propagating potentials, pre-post-pre and post-pre-post triplets can generate markedly different calcium dynamics leading to different plasticity results.

Though this class of models allows to reproduce a bulk of details with regard to spike-timing dependent plasticity, the phenomenological detector systems reading out calcium transients based on the calcium control hypothesis do not reflect the dynamics and structure of biochemical, intracellular signaling cascades. Taking such cascades into account might however lead to considerable differences in temporal dynamics and behavior of adding up synaptic changes during a stimulation protocol. With regard to unsupervised learning of input correlations in neural networks, for example, such differences seem to crucially determine input correlation sensitivity and resulting synaptic weight distributions.

Models based on calcium dynamics and complex, dynamic readout systems
Another type of models involves the description of dynamic signaling cascades. Though such an approach is motivated by realistic, biochemical pathways, known intracellular signaling pathways involved in LTP/LTD induction are not mimicked. Since calcium is believed to be the main messenger triggering intracellular signaling cascades, the activation of the pathways relies on the calcium dynamics related to the occurrence of pre- and postsynaptic spikes. Rubin et al. (2005) propose a biochemical detector system based on pathways resembling the CaMKII kinase-phosphatase system. They show that the model reproduces experimental STDP outcomes but their model does not exhibit bistability. In that model, high, short-lasting calcium levels evoke LTP, low and prolonged calcium elevations above a certain threshold evoke LTD and intermediate calcium levels act like a "Veto" preventing LTD induction. The dynamics of the "Veto" mechanism prevents in particular the appearance of LTD for large positive time lags in response to STDP stimulation. The model proposed by Rubin et al. (2005) indicates that synaptic changes combine in a highly nonlinear fashion inbetween spike-pairs and are most likely not a result of piecewise, linear additions of changes evoked by single spike-pairs. How such behavior is however realized by known calcium-dependent

signaling cascades shown to be involved in LTP/LTD induction has not been studied so far.

2.7.3 Bistable, biochemical models

Another line of modeling research addresses the issue of maintenance of the evoked synaptic state during the early phase of LTP/LTD. As outlined above, the expression of plasticity involves multiple molecular players. Molecules, however, have a short lifetime of the order of minutes to days, whereas some memories can be retained for years. Despite the fact that long-term modifications involve structural reorganization, altered gene transcription and new protein synthesis in the late phase (see review by Malenka and Bear (2004)), the question remains how the induced state can be preserved by a machinery involving a limited number of proteins in the presence of protein turnover. A plausible solution is the concept of a molecular switch. Such switches formed by a number of proteins can recruit newly synthesized proteins to adopt a particular "stored" state and thus retain state information despite molecular turnover. Experimental and theoretical studies suggest positive feedback loops to be at the origin of such switches which express in the simplest form two stable states.

The problem of synaptic stability was first noted by Francis Crick in 1984 who suggested that cooperative interactions among proteins can overcome the problem of molecular turnover for long-term memory (Crick 1984). The idea of a molecular switch storing information beyond protein lifetime was further developed by Lisman (1985). He showed in a simple mathematical model by using known enzymatic reactions that a kinase can exist in two stable states: a unphosphorylated "off" state and a phosphorylated "on" state. Transitions from "off" to "on" can be induced by another phosphorylating kinase and the evoked state acts autocatalytically to sustain the phosphorylation level and to phosphorylate downstream kinases. Reverse transitions could be induced by phosphatase activity. The first candidate protein proposed to be a the origin for such a switch is the calcium/calmodulin-dependent protein kinase II. Theoretical studies in the late 1980's showed that the complex holoenzyme composed of 12 subunits can exhibit a switch-like behavior due to calcium-independent autophosphorylation (Lisman and Goldring 1988). Binding of calcium/calmodulin to a CaMKII subunit activates phosphorylation of exogenous substrates. Activation of adjacent subunits in the holoenzyme stimulates intersubunit autophosphorlation, decreasing the calcium/calmodulin dissociation rate and preventing inactivation when calmodulin dissociates. This autonomous activity prolongs CaMKIIs enzymatic activity beyond fast-decaying calcium transients (see details of CaMKII function reviewed in Hudmon and Schulman (2002)). Based on experimental results from Miller and Kennedy (1986), Lisman and Goldring (1988) showed mathematically that even in the presence of phosphatase activity and of protein turnover (described by replacing phosphorylated proteins with newly synthesized dephosphorylated proteins in their model) the CaMKII system is capable of storing graded information in a stable manner. Numerous studies have investigated in detail the dynamics of CaMKII autophosphorylation in response to the intracellular calcium concentrations (Michelson and Schulman 1994; Matsushita et al. 1995; Dosemeci and Albers 1996; Coomber 1998; Kubota and Bower 1999; Holmes 2000; Kubota and Bower 2001; Dupont et al. 2003). The phosphorylation level of CaMKII subunits does however not exhibit a bistable behavior in these models. The CaMKII system has received this remarkable attention since it is known that the phosphorylated CaMKII enzyme can directly phosphorylate AMPA receptors (Mammen et al. 1997) and therewith enhance channel function (Derkach et al. 1999) or drive AMPA-R into synapses (Hayashi et al. 2000) (see above).

We want to highlight two mathematical models of CaMKII autophosphorylation/dephosphorylation behavior published in 2000. Both show that the CaMKII protein can exhibit a bistable phosphorylation behavior in a range of calcium concentrations, *i.e.* a highly- and and weakly phosphorylated state coexist in this range (Zhabotinsky 2000; Okamoto and Ichikawa 2000). Both models include biochemical details of calcium-triggered autophosphorylation and dephosphorylation of the CaMKII protein: (i) the calcium/calmodulin-dependence of the initiation and subsequent phosphorylation steps is taken into account; (ii) subsequent phosphorylation steps are facilitated due to the increase in calcium/calmodulin affinity of a phosphorylated subunit and the fact that a phosphorylated subunit stays active as catalyst for the autophosphorylation reaction (see details below and Hudmon and Schulman (2002)); and (iii) the dephosphorylation of CaMKII subunits by protein phosphatase 1 is implemented according to the Michaelis-Menten scheme (Michaelis and Menten 1913). With these components implemented in the model, both studies show that the CaMKII phosphorylation level has three steady-states in a range of calcium concentrations: a stable weakly-phosphorylated steady-state, a stable highly-phosphorylated state and an intermediate unstable fixed-point. This unstable steady-state separates the bassins of attraction of the two stable steady-states. The range of bistability goes from 0.094 to 0.67 μM intracellular calcium in Zhabotinsky (2000) (see Fig. 2.11*A*) and from 0.73 to 0.85 μM calcium in Okamoto and Ichikawa (2000). The difference in extent and location of the bistable range can be explained by the differing implementations of the dephosphorylation activity in both models. While Okamoto and Ichikawa (2000) describe the phosphatase activity as a constant independent of calcium, Zhabotinsky (2000) takes into account that the protein phosphatase 1 activity is itself governed by calcium. That is, PP1 is inhibited by phosphorylated inhibitor 1 and inhibitor 1 is in turn dephosphorylated by calcium-dependent calcineurin and phosphorylated by the cAMP-PKA pathway (see above). The consideration

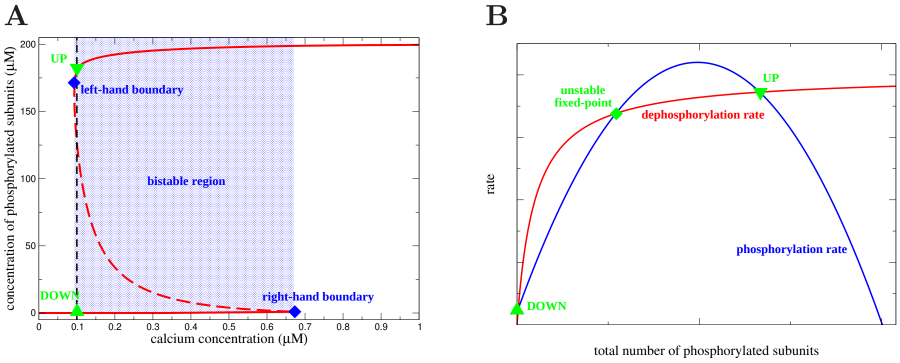

Figure 2.11: Bistability of the CaMKII phosphorylation level in modeling studies. ***A,*** Concentration of phosphorylated CaMKII subunits as a function of calcium: Zhabotinsky (2000) and Okamoto and Ichikawa (2000) showed that the phosphorylation level of CaMKII can exhibit a bistable behavior. That is, two stable phosphorylation states - a weakly- and a highly-phosphorylated state - exist is a range of calicum (reaching from $Ca = 0.094\ \mu$M to $Ca = 0.67\ \mu$M in the shown case, taken from Zhabotinsky 2000). Stable steady-states are depicted by full red lines and unstable fix-points by the dashed line. UP to DOWN transitions occur below the left-hand boundary of this bistable region and DOWN to UP transition are evoked if the system is exposed sufficiently long to calcium concentrations higher than the right-hand boundary of the bistable region. Zhabotinsky furthermore showed that the bistable region can include the calcium resting concentration $Ca_0 = 0.1\ \mu$M. Panel *A* is a reproduction of the model results proposed by Zhabotinsky (2000). ***B,*** Total phosphorylation (blue line) and dephosphorylation rates (red line) illustarting the steady-states of the system in the bistable region: The overall phosphorylation and dephosphorylation rates are shown as functions of the total number of phosphorylated subunits of all CaMKII holoenzymes. The intersection points of both rates characterize balanced phosphorylation and dephosphorylation and mark the steady-states of the system. Two of the steady-states are stable (marked UP and DOWN) and the intermediate steady-state is unstable. Hence, the situation shown corresponds to the relative postion of both rates in the bistable region exhibiting three stable-state (shaded region in *A*). Note that the dephosphorylation rate saturates and the phosphorylation rate vanishes at high total phosphorylation levels. See more details in text.

of this protein signaling cascade yields a Hill function like behavior of the PP1 activity as a function of calcium, *i.e.* the PP1 activity is inhibited at low calcium concentrations and increases with increasing calcium. This explains to a large extent the wide bistability range including the calcium resting concentration (at $Ca_0 = 0.1\ \mu$M) in the Zhabotinsky model. Note however that the level of phosphorylated inhibitor 1 is unrealistically high at low calcium concentrations in this study ($\sim 100\ \mu$M at $Ca_0 = 0.1\ \mu$M).

Where does the bistability in the phosphorylation behavior of CaMKII subunits come from? This question can be answered by inspecting the total rates of autophosphorylation and dephosphorylation of CaMKII subunits. Fig. 2.11*B* shows schematically how both rates vary as a function of the total number of phosphorylated subunits. The intersection points, the points where the total autophosphorylation rate balances the total dephosphorylation rate, mark the three steady-states of the system. The left- and the right hand steady-states are stable and the middle one is unstable. Two criteria are necessary for these three intersection points, essential for bistability, to emerge: (i) The total dephosphorylation rate has to saturate at high phosphorylation levels (see red line in Fig. 2.11*B*). Describing dephosphorylation according to the Michaelis-Menten scheme, which is valid if the enzyme (PP1) is present in small amounts compared to the substrate (phosphorylated subunits), gives rise to this saturation. (ii) The cooperativity of autophosphorylation is at the origin of the bump-like behavior of the total autophosphorylation rate. Subsequent phosphorylation in the ring is faster than the initial autophosphorylation rate since only a single calcium/calmodulin complex is required as compared to two for the initiation step (see Hudmon and Schulman (2002)). Without this facilitation of autophosphorylation, the total rate would stay constant with increasing number of phosphorylated CaMKII subunits and the three intersection points with the dephosphorylation rate could not be realized. In summary, the saturation of the phosphatase activity dephosphorylating CaMKII combined with the cooperativity of the autophosphorylation rate yields the bistability of the CaMKII phosphorylation level.

Miller et al. (2005) investigated the stability of the CaMKII switch with respect to stochastic fluctuations since under realistic conditions such a switch is composed of a few molecules only. Experimental estimates of the total CaMKII concentration and the volume of the postsynaptic density suggest that the number of CaMKII proteins in this structure is of the order $50-100$ holoenzymes (Hanson and Schulman 1992; McNeill and Colbran 1995; Harris and Stevens 1989; Doi et al. 2005). The average lifetime of a single CaMKII protein is about 30 h independently of its phosphorylation state (Ehlers 2003). Using the model of Zhabotinsky (2000), Miller et al. (2005) show that the CaMKII switch composed of a realistic number of CaMKII protein is stable for years and up to a human lifetime even in the presence of protein turnover, phosphatase as well as free calcium fluctuations. However, the localization of CaMKII is not restricted to the PSD, but translocation and diffusive exchange between the PSD and the cytosol create an ongoing flux (Shen and Meyer 1999; Shen et al. 2000; Sharma et al. 2006). Hayer and Bhalla (2005) investigate the stability of the CaMKII switch and the insertion of AMPA receptors in the presence of protein trafficking and turnover. Besides the bistability of the CaMKII phosphorylation level, they identify an independent AMPA receptor switch based on self-recruitment of receptors into the synapse (Ehlers 2000; Esteban et al. 2003). Depending on whether both switches function completely independently, or tightly coupled determines if three or two stable states exist in such a system. The average lifetime of such switches depends on the coupling and ranges from 24 h to more than a year (Hayer and Bhalla 2005). The existence of a second switch besides CaMKII ensuring the maintenance of AMPA receptors in the membrane could be a means to maintain the evoked synaptic state on longer time scales. Especially, since CaMKII enzymatic activity decreases to baseline within ~ 15 min after LTP induction (Lengyel et al. 2004) (see above).

Compared to the detailed models of CaMKII protein function, the study by Hayer and Bhalla (2005) belongs to a different class of models since in contrast to the studies outlined above, the intrinsic activation and the intrinsic enzymatic properties of single proteins are not resolved (the intersubunit autophosphorylation of CaMKII is not described at length, for example). Instead, extensive protein signaling networks based on known interactions are investigated. Two types of signal transmission mechanisms are implemented in such approaches: (i) protein-protein interactions and enzymatic reactions such as protein phosphorylation and dephosphorylation; (ii) and protein degradation or production of intracellular messengers. Positive feedback loops in these protein networks involving several proteins such as protein kinase C and mitogen-activated protein kinase, for example, have been shown to lead to bistability (Bhalla and Iyengar 1999).

Another possibility for bistability to arise that has been suggested is the modulation of trafficking rates due to local clustering of receptors in the synaptic membrane. This leads to metastable states that can outlast the lifetime of individual receptors, thus providing a mechanism for long-term maintenance of bidirectional synaptic changes (Shouval 2005).

Furthermore, ongoing neural activity has been shown to potentially form a positive feedback loop with synaptic weight increase (Smolen 2007). This gives rise to bistability which is dependent on the frequency of calcium elevations, *i.e.* longer inactive periods would return the synapse to the low weight state.

Besides the shown existence of bistability in all these approaches, the question whether experimental stimulation protocols known to induced LTP/LTD evoke transitions between the stable steady-states in these models has not been tested. In particular, detailed studies on the CaMKII autophosphorylation switch did not elaborate realistic conditions for which the system switches from the highly- to the weakly phosphorylated state (Zhabotinsky 2000; Okamoto and Ichikawa 2000). In these models, this transition would occur if the intracellular calcium concentration drops persistently below resting levels which does not seem to be consistent with experimentally measured calcium levels during LTD induction protocols (Yang et al. 1999; Zucker 1999; Mizuno et al. 2001; Ismailov et al. 2004; Nevian and Sakmann 2006). On the contrary, the transition from the weakly- to the highly phosphorylated steady-state occurs if the system is repetitively exposed to high calcium levels, consistent with experimental data.

2.7.4 Outline of the approach chosen here

The approach presented in this thesis is highlighted in this section. Using current knowledge about biochemical pathways involved in synaptic long-term modifications, we propose a model which combines induction and maintenance of synaptic changes. Here, we especially highlight the motivation of the proposed model in light of previous experimental and mathematical work.

The above mentioned, experimentally inspired calcium control hypothesis (see Fig. 2.10) implies no synaptic changes for resting and low calcium levels, LTD at intermediate calcium levels and LTP induction at high calcium elevations. These three functionally different calcium regions translate for a bistable system into the following three criteria: (i) Two stable steady-states, UP and DOWN, exist at resting and low levels of calcium. This requirement assures the stability of the evoke synaptic state under resting conditions and activity which does not lead to considerable calcium accumulations. (ii) Prolonged, intermediate calcium elevations move the system from the UP to the DOWN state (up-to-down transition). Such up-to-down transitions would take place in the range of calcium levels typically present in response to LTD stimulation protocols and would therefore correspond to a LTD event. Starting from the DOWN state, no transition occurs. (iii) Repetitive exposures to high calcium levels would transfer the system from the DOWN to the UP state (down-to-up transition). Such a transition conforms to a LTP event occurring in response to fast and high calcium transients. In contrast, no transition occurs for the same type of calcium dynamics if the system resides initially in the UP state. Regarding existing propositions for possible bistable systems, the realization of these three criteria has not been addressed so far by modeling studies.

We use the models showing that the CaMKII kinase - phosphatase system can exhibit a bistable phosphorylation behavior (Okamoto and Ichikawa 2000; Zhabotinsky 2000) as a starting point for our investigations. In the CaMKII system, the DOWN and the UP state correspond to a weakly- and a highly phosphorylated state of the ensemble of CaMKII proteins. Zhabotinsky (2000) shows that both states can coexist at resting calcium levels ($Ca_0 = 0.1$ μM in this study) corresponding to criterion (i) above. Note however that the phosphorylated inhibitor 1 concentration inhibiting PP1 reaches unrealistic high levels at low calcium concentrations in Zhabotinsky's model. We elaborate in detail under which realistic conditions the CaMKII system exhibits bistability at resting calcium. Furthermore, it has been shown by Okamoto and Ichikawa (2000) and Zhabotinsky (2000) that high calcium elevations move CaMKII from the weakly- to the highly-phosphorylated state due to the increase in calcium/calmodulin-dependent autophosphorylation (criterion (iii) above). A region at intermediate calcium concentrations within which the CaMKII moves from the UP to the DOWN state is however missing in the existing studies. We propose that such a region, which we call 'LTD-window', emerges from the protein signaling cascade governing the PP1 activity in a calcium-dependent manner. As Zhabotinsky (2000), we incorporate the calcium-dependent activation of calcineurin but unlike his approach, we furthermore consider the separate activation of the cAMP-PKA pathway by calcium (see above). We elaborate conditions for which this cascade yields an elevated PP1 activity at intermediate calcium concentrations and therefore gives rise to the 'LTD-window' in this range.

The CaMKII system consistent with the three criteria described above is exposed to realistic calcium dynamics generated by pre- and postsynaptic activity patterns. These considerations of the CaMKII dynamics are similar to the investigations by Rubin et al. (2005) but rely on existing proteins and known protein-protein interactions, unlike the phenomenological signaling cascade used in this study. In particular, we investigate conditions for which the CaMKII system reproduces plasticity results in response to the STDP protocol; and which transitions occur in response to purely presynaptic- and purely postsynaptic stimulation with repetitive single-spikes or pairs of spikes. During exposure to the STDP protocol, different parts of the protein signaling cascade are blocked and the resulting plasticity results are compared with experimental assays blocking respective phosphatases or kinases.

Similar investigations as with the six-subunit model of the CaMKII protein are performed with a simplified model based on CaMKII with two-subunits only. This simplified model reduces the number of equations accounting for the model dynamics to two and therefore gives some insights in the CaMKII phosphorylation behavior. The steady-states and the dynamic properties in response to different experimental stimulation protocols known to induce LTP/LTD are studied.

Starting from the extensive description of CaMKII autophosphorylation and dephosphorylation in the CaMKII holoenzyme, key-elements of the model are elaborated in the last part of the thesis. We propose a reduced model of the CaMKII phosphorylation level description. In other words, we identify the crucial components of the CaMKII system which give rise to the bistability and allow to reproduce experimentally suggested transition behaviors. The steady-state behavior of this reduced model is motivated by the phosphorylation description in the simplified two-subunit CaMKII model. CaMKII phosphorylation and dephosphorylation are two calcium-dependent processes. The reduced model preserves therefore biological meaningful components. Simultaneously, the simplicity of the model allows to study thoroughly how the model parameters influence the CaMKII phosphorylation behavior. In particular, we examine which properties of the model influence the exact shape of the STDP curve in response to spike-pair stimulation protocols. The reduced model allows to pin down the contribution of specific biochemical signaling cascades to observed plasticity results in response to known

LTP/LTD induction protocols.

Italic style symbols in this thesis refer to concentrations of the respective element or protein. The extensive use of plural, active formulations such as “we present” or “we investigate” is an effort to improve the readability of this thesis.

3

LTP and LTD in a model of a bistable synapse based on CaMKII

In this chapter, we present a realistic model for the protein network of the post-synaptic density, focusing on the pathways affecting the phosphorylation and dephosphorylation dynamics of calcium/calmodulin-dependent protein kinase II (CaMKII). The steady-states of the CaMKII phosphorylation level and its dynamics in response to realistic calcium transients are investigated in a detailed model of the 12-subunit CaMKII holoenzyme. Parts of the results presented in this chapter have been published recently (Graupner and Brunel 2007).

We start with investigating the steady-states of the phosphorylated CaMKII subunit concentration as a function of calcium. The total calcium/calmodulin-triggered autophosphorylation and the protein phosphatase 1 (PP1)-mediated dephosphorylation balance each other at low and high CaMKII phosphorylation levels at resting calcium concentrations. This gives rise to two stable steady-states at resting conditions. The calcium-dependent activation of calcineurin at intermediate calcium levels increases PP1 activity through dephosphorylation of inhibitor 1 (I1). This increase in dephosphorylation activity destroys the stability of the highly-phosphorylated steady-state, while leaving the weakly-phosphorylated steady-state. At high calcium concentrations, PP1 activity is inhibited via the activation of the cyclic AMP protein kinase A pathway, which in turn phosphorylates I1 inhibiting PP1. Together with the strong calcium/calmodulin-triggered autophosphorylation, the highly-phosphorylated state is the only steady-state of the CaMKII system. See Fig. 3.1*A* for an illustration of the steady-state behavior of the CaMKII phosphorylation level.

In the second part of the chapter, the CaMKII system is exposed to calcium transients evoked by stimulation protocols known to induce synaptic long-term modifications. Calcium influx is mediated by NMDA receptors in response

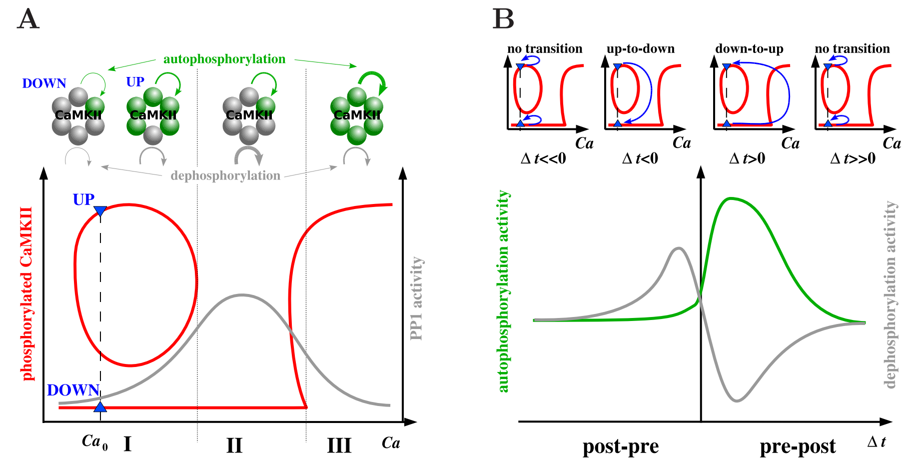

Figure 3.1: Schematic presentation of steady-states and dynamics of the CaMKII phosphorylation level.. ***A,*** Steady-states of the phosphorylated CaMKII subunit concentration and the autophosphorylation - dephosphorylation balance as functions of calcium: The upper row shows rings of six functionally coupled subunits of the CaMKII holoenzyme. A gray subunit stands for dephosphorylated and a green one for phosphorylated. The green and the gray curved lines indicate calcium-dependent autophosphorylation and PP1-mediated dephosphorylation, respectively. Their width corresponds to the strength of the respective process in the three different calcium regions (I, II and III). At low calcium levels, including the calcium resting level (region I), autophosphorylation and dephosphorylation balance each other at two different CaMKII phosphorylation levels, giving rise to bistability at resting calcium (Ca_0), *i.e.* a weakly- (DOWN) and a highly-phosphorylated (UP) stable state coexist. The PP1 activity dephosphorylating CaMKII (gray line in lower panel) has a peak at intermediate calcium levels. As a result, the UP state loses stability, leaving the weakly-phosphorylated state as the only stable steady-state in region II. The PP1 dephosphorylation activity is suppressed and autophosphorylation is strong at high calcium levels (region III). In consequence, the highly-phosphorylated state is the only stable state of the CaMKII system in region III. ***B,*** CaMKII transition behavior in response to the STDP stimulation protocol: Bidirectional transitions between the DOWN and the UP state in response to calcium transients evoked by the STDP stimulation protocol are illustrated in the upper row. Changing the time difference between pre- and postsynaptic spike (Δt) yields different activation levels of CaMKII autophosphorylation (green line) and dephosphorylation (gray line in lower panel): Autophosphorylation and dephosphorylation reach moderate levels, outweigh each other and evoke no transitions when $\Delta t \ll 0$ or $\Delta t \gg 0$; Ca^{2+} transients reach intermediate levels which maximize PP1 build-up and therefore CaMKII dephosphorylation activity when $\Delta t < 0$ (gray line in lower panel). Up-to-down transitions occur in response to such stimulation protocols. $\Delta t > 0$ yields large calcium elevations which strongly activate autophosphorylation and suppress PP1 activity evoking down-to-up transitions (see also panel *A*).

to presynaptic activation and through voltage-dependent calcium channels activated by back-propagating action potentials, which furthermore increase the current through activated NMDA-Rs. Transitions between the weakly- and the highly-phosphorylated state are a result of differential activation of the calcium-dependent autophosphorylation and dephosphorylation processes. In response to the spike-timing dependent plasticity stimulation protocol, for example, post-pre pairings (negative time lag between pre- and postsynaptic spike) favor dephosphorylation leading to transitions from the highly- to the weakly-phosphorylated state. Pre-post pairings suppress dephosphorylation activity instead and simultaneously evoke strong autophosphorylation of CaMKII. In conjuction, this evokes transitions from the weakly- to the highly-phosphorylated steady-state. In summary, we can show that the CaMKII system reproduces experimentally observed transition behavior in response to the STDP stimulation protocol. See Fig. 3.1*B* for an illustration of the transition dynamics of the CaMKII system in response to STDP protocols.

3.1 The calcium/calmodulin-dependent protein kinase II system

The model describing the calcium/calmodulin-dependent autophosphorylation and dephosphorylation mediated by protein kinase 1 of CaMKII is introduced in this section. Phosphorylation of a CaMKII subunit by its neighboring subunit requires calcium/calmodulin to bind to the substrate subunit. The catalytic subunit is active if bound to Ca^{2+}/calmodulin, or phosphorylated. Dephosphorylation of phosphorylated CaMKII subunits by PP1 in the PSD is implemented according to the Michaelis-Menten scheme. We also take into account how calcium/calmodulin influences PP1 activity via a protein signaling cascade. Finally, we model postsynaptic calcium and postsynaptic membrane potential dynamics induced by pre- and postsynaptic spikes in order to investigate the effects of spike-induced calcium transients on the dynamics of the CaMKII system.

3.1.1 CaMKII auto- and dephosphorylation

Calcium binding to calmodulin Calmodulin contains four calcium binding sites, two at the C- and two at the N-terminal domain. Calcium binding happens in a cooperative manner in each one of these pairs (Chin and Means 2000). The following scheme describes the macroscopic binding of calcium to calmodulin, *i.e.* we take into account the number of bound calcium ions only, regardless of the occupied microscopic binding sites:

$$\mathrm{M} \underset{-\mathrm{Ca}^{2+}}{\overset{\substack{K_1 \\ +\mathrm{Ca}^{2+}}}{\rightleftharpoons}} \mathrm{C}_1 \underset{-\mathrm{Ca}^{2+}}{\overset{\substack{K_2 \\ +\mathrm{Ca}^{2+}}}{\rightleftharpoons}} \mathrm{C}_2 \underset{-\mathrm{Ca}^{2+}}{\overset{\substack{K_3 \\ +\mathrm{Ca}^{2+}}}{\rightleftharpoons}} \mathrm{C}_3 \underset{-\mathrm{Ca}^{2+}}{\overset{\substack{K_4 \\ +\mathrm{Ca}^{2+}}}{\rightleftharpoons}} \mathrm{C}. \tag{3.1}$$

Here M is free intracellular calmodulin and C_i $(i = 1, 2, 3, 4)$ with $\mathrm{C}_4 \equiv \mathrm{C}$ denotes the calcium/calmodulin complex with i bound calcium ions. Calmodulin target proteins including CaMKII are partially activated by calmodulin with two, three or four calcium ions bound. However, CaMKII autophosphorylation rates induced by calmodulin bound with two or three calcium ions are much smaller than with calmodulin bound with four calcium ions (Shifman et al. 2006). Hence, we consider for simplicity that only calmodulin bound with four calcium ions is able to phosphorylate CaMKII. Since the binding of calcium by calmodulin is fast (with binding rates of the order $\sim 1000\ (\mu M \cdot s)^{-1}$ (Linse et al. 1991; Klee 1988)) we assume reaction (3.1) to be in equilibrium with the calcium concentration. The macroscopic dissociation constants of successive calcium binding are taken from Linse *et al.* (see Tab. 3.1A for parameters; Linse et al. 1991). The total concentration of calmodulin is $CaM_0 = M + C_1 + C_2 + C_3 + C$. Experimental studies suggest that the total available level of calmodulin in neurons is $CaM_0 \approx 10\ \mu\mathrm{M}$ (Meyer et al. 1992; Persechini et al. 1996; Chin and Means 2000). Here, we use a smaller value due to the vast number of target proteins of calmodulin besides CaMKII, and the sequestration of calmodulin by neurogranin in spines under resting conditions (see Tab. 3.1 and Meyer et al. 1992; Persechini and Stemmer 2002). For simplicity, we do not consider the dynamics of calmodulin sequestration by neurogranin, which has been suggested to provide calmodulin during LTP protocols (Zhabotinsky et al. 2006). Assuming a calmodulin bath is an effective way to implement dissociation of calmodulin-neurogranin complexes, which provides calmodulin to the PSD during autophosphorylation and phosphatase/kinase activation.

Autophosphorylation of CaMKII The calcium/calmodulin-dependent protein kinase II (CaMKII) holoenzyme has 12 domains, grouped into two clusters each with six functionally coupled subunits (Bradshaw et al. 2002; Hudmon and Schulman 2002). CaMKII is activated by Ca^{2+}/calmodulin binding to its subunits. Ca^{2+}/calmodulin binding to adjacent subunits in the subunit ring stimulates intersubunit autophosphorylation at the residue theronine-286 in the autoregulatory domain (Thr^{286}). Autophosphorylation increases CaMKII affinity for Ca^{2+}/calmodulin and prolongs activation beyond dissociation of Ca^{2+}/calmodulin. In turn, as long as CaMKII stays activated it can bind to the NMDA-R and phosphorylate exogenous substrates (Hanson and Schulman 1992; Hudmon and Schulman 2002). For simplicity, some aspects of CaMKII function

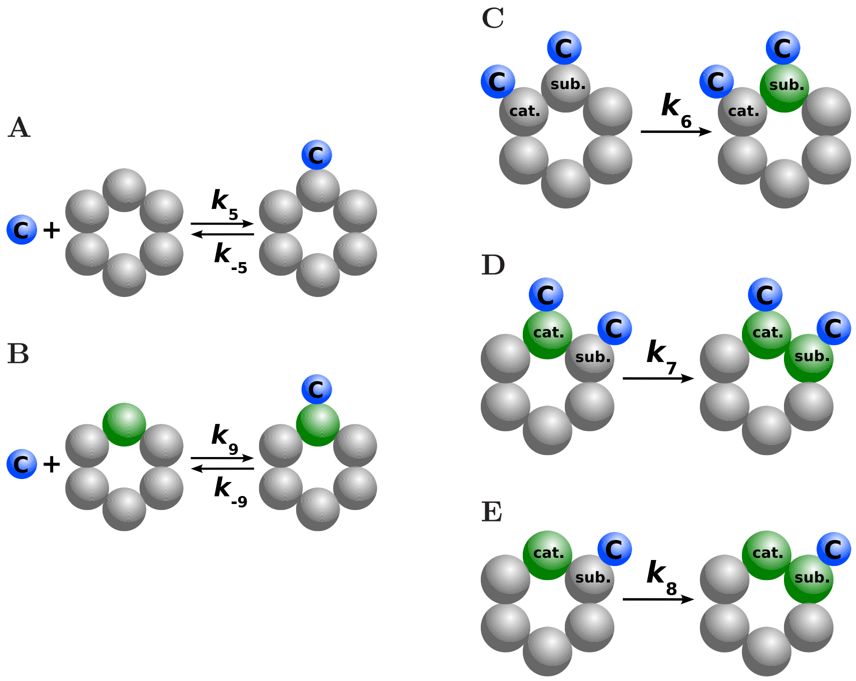

Figure 3.2: Schematic representation of calcium/calmodulin binding to a CaMKII subunit and the intersubunit phosphorylation steps. Calcium/calmodulin binding and phosphorylation reactions of a ring of six functionally coupled subunits of the CaMKII holoenzyme: A gray subunit stands for dephosphorylated and a green subunit for phosphorylated. ***A,B,*** The calcium/calmodulin complex (C, blue circle) can bind to a dephosphorylated (*A*) or a phosphorylated subunit (*B*) with dissociation constants $K_5 = k_{-5}/k_5$ or $K_9 = k_{-9}/k_9$, respectively. Note that the calmodulin binding (*A* and *B*) and the autophosphorylation steps (shown in panel *C*-*E*) are assumed to take place independently of the phosphorylation state of other subunits in the ring (here depicted as dephosphorylated, *i.e.* in gray). ***C,D,E,*** The three possible intersubunit phosphorylation steps: In all three cases, the catalytic subunit and the substrate subunit are labeled with **cat.** and **sub.**, respectively. Unlabeled subunits are depicted as dephosphorylated but the three phosphorylation steps are assumed to proceed independently of their phosphorylation state. (*C*) Initiation step: calmodulin has to bind to the two interacting subunits, *i.e.* to the substrate and the catalyst, in order to phosphorylate the substrate subunit at Thr^{286} (shown in green). (*D*) Calmodulin is bound to the phosphorylated catalyst and the subunit to be phosphorylated. (*E*) The phosphorylated subunit stays active as catalyst after calmodulin dissociation and phosphorylates the substrate subunit bound with calmodulin. k_6, k_7 and k_8 denote the respective autophosphorylation rates of the three steps described above.

are not accounted for in the model. Any differences between the CaMKIIα and -β isoforms are not considered. The binding of calcium/calmodulin and protein phosphatase 1 to a subunit is assumed to be independent of the state of neighboring subunits. The autophosphorylation at Thr^{305} and Thr^{306} is not considered.

CaMKII autophosphorylation is an intersubunit process during which one subunit acts as substrate and the neighboring subunit as catalyst. For autophosphorylation to take place, calmodulin has to be bound to the substrate subunit (Hudmon and Schulman 2002). Autophosphorylation at Thr^{286} or binding of calmodulin each disable the autoinhibitory domain, therefore the catalytic subunit can be in one of the following states: (i) bound with calmodulin, (ii) phosphorylated and bound with calmodulin or (iii) phosphorylated only (for an illustration see Fig. 3.2*C*-*E*; Lisman et al. 2002).

The chemical reaction schemes in Fig. 3.2*A*-*E* show schematically how binding of calmodulin and autophosphorylation is represented in the model. Reactions in panel *A* and *B* show calcium/calmodulin complex binding to dephosphorylated- or phosphorylated subunits, respectively. Autophosphorylation steps where the catalytic subunit is bound with calcium/calmodulin, phosphorylated and bound with calcium/calmodulin or phosphorylated only are illustrated in Fig. 3.2*C*, *D* and *E*, respectively. The intersubunit autophosphorylation is likely to be a directed interaction in the ring and is here assumed to proceed in the clockwise direction (Lisman et al. 2002).

For the autophosphorylation steps depicted in Fig. 3.2*C*, *D* and *E* to occur, the substrate subunit must bind the calcium/calmodulin complex C. Let γ be the probability that a dephosphorylated subunit S binds with C, *i.e.* $\gamma = SC/(S+SC)$ (SC stands for an dephosphorylated subunit bound with C); and γ^* the probability that a subunit phosphorylated at Thr^{286}, S*, binds with C, *i.e.* $\gamma^* = S^*C/(S^* + S^*C)$ (S*C stands for a phosphorylated subunit bound with C). Assuming reactions in Fig. 3.2*A* and *B* to be in equilibrium and using the Law of Mass Action yields $SC = S \cdot C/K_5$ and $S^*C = S^* \cdot C/K_9$, respectively, where $K_5 = k_{-5}/k_5$ and $K_9 = k_{-9}/k_9$ are the dissociation constants of the reactions shown in Fig. 3.2*A* and *B*, respectively. These assumptions lead to:

$$\gamma = \frac{SC}{S+SC} = \frac{C}{K_5 + C}, \tag{3.2}$$

$$\gamma^* = \frac{S^*C}{S^* + S^*C} = \frac{C}{K_9 + C}. \tag{3.3}$$

The probability that reaction in Fig. 3.2*C* takes place in a unit time between two subunits in the single direction is $k_6\gamma^2$. Correspondingly, the probability for reaction in Fig. 3.2*D* to occur in a unit time is $k_7\gamma\gamma^*$ and for reaction in Fig. 3.2*E* to occur is $k_8\gamma(1-\gamma^*)$. This probabilistic description of autophosphorylation allows us to describe a given subunit by 2 possible states only, *i.e.* whether or not a subunit is phosphorylated at Thr^{286}. Note that with a 6 subunit ring this yields 14 macroscopic distinguishable activation states (see appendix A.1 on page 176). This ansatz does not account for calmodulin consumption during the process of autophosphorylation, *i.e.* a bath of calmodulin is assumed. Similar approaches have been used in previous investigations of CaMKII phosphorylation dynamics (Okamoto and Ichikawa 2000; Zhabotinsky 2000; Coomber 1998; Holmes 2000; Kubota and Bower 2001; Dupont et al. 2003).

Dephosphorylation of CaMKII PP1 is the only protein phosphatase that dephosphorylates CaMKII associated with the postsynaptic densities (Strack et al. 1997). The dephosphorylation of a free, phosphorylated subunit (S^*) and a phosphorylated subunit bound with the calcium/calmodulin complex (S^*C) are described according to the Michaelis-Menten scheme:

$$\mathrm{S^* + D \underset{k_{-11}}{\overset{k_{11}}{\rightleftharpoons}} S^*{\cdot}D \overset{k_{12}}{\rightarrow} S + D}, \tag{3.4}$$

$$\mathrm{S^*C + D \underset{k_{-11}}{\overset{k_{11}}{\rightleftharpoons}} S^*C{\cdot}D \overset{k_{12}}{\rightarrow} SC + D}, \tag{3.5}$$

where D denotes the concentration of active PP1. Note that dephosphorylation happens independently if a subunit is bound with the calcium/calmodulin complex or not. Assuming the (S*·D) and (S*C·D) formations are at equilibrium, *i.e.* $\frac{d}{dt}(\mathrm{S^*{\cdot}D}) \approx \frac{\mathrm{d}}{\mathrm{dt}}(\mathrm{S^*C{\cdot}D}) \approx 0$, we can use the standard Michaelis-Menten equation (Michaelis and Menten 1913) to obtain the per-subunit rate of dephosphorylation, k_{10},

$$k_{10} = \frac{k_{12} D}{K_\mathrm{M} + S_\mathrm{active}}, \tag{3.6}$$

where the Michaelis constant K_M is given by $K_\mathrm{M} = (k_{-11} + k_{12})/k_{11}$ and S_active is the total concentration of phosphorylated CaMKII subunits, $S_\mathrm{active} = \sum_{i=0}^{n=13} m_i \cdot S_i$, where m_i is the number of phosphorylated subunits of the macroscopic activation state i (see appendix A.1 on page 176 for more details). The per-subunit rate of dephosphorylation, k_{10}, is proportional to the amount of available phosphatase, D. Furthermore, the dephosphorylation rate *per* subunit declines if a lot of subunits are phosphorylated and the phosphatase activity remains constant, *i.e.* if S_active is high and D constant. This saturation of k_{10} leads to the bistable behavior of the CaMKII phosphorylation level (see section 3.2.1 on page 55).

3.1.2 Ca^{2+}-dependent PP1 activity via protein signaling cascade including PKA and calcineurin

The dephosphorylation activity of PP1 is indirectly governed by calcium/calmodulin via inhibitor 1 (I1), *i.e.* phosphorylated inhibitor 1 inhibits PP1

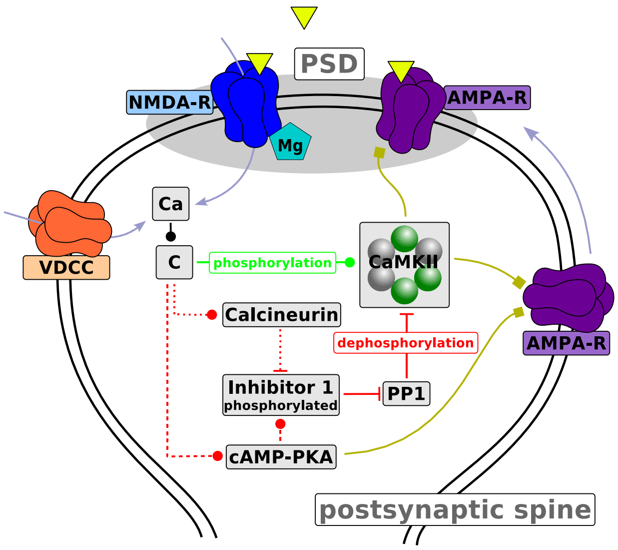

Figure 3.3: Protein signaling cascade governing CaMKII autophosphorylation and PP1 activity. Interactions shown with a circle at the end of a line indicate stimulation - whereas lines ending with a bar stand for inhibition of target activity. Calcium enters the postsynaptic spine through NMDA receptors and VDCCs (light blue lines). Calcium/calmodulin (C) directly phosphorylates CaMKII (green line). Furthermore, the dephosphorylation of CaMKII by protein phosphatase 1 (PP1) is indirectly controlled by calcium/calmodulin via a protein signaling cascade (red lines). Calcium/calmodulin-directed phosphorylation of inhibitor 1 via cyclic-AMP and PKA increases CaMKII activity by inhibiting PP1. This CaMKII stimulating pathway is depicted in red dotted lines. On the contrary, activation of calcineurin activates PP1 by dephosphorylating inhibitor 1, which in turn leads to increased CaMKII dephosphorylation. This pathway, shown in red dashed lines, decreases CaMKII activity. Active CaMKII and PKA phosphorylate AMPA receptors (light green lines with square) and therefore increases AMPA-R channel function or potentially delivers AMPA-R to the PSD. The model of the protein signaling cascade presented in this section describes the part of the signaling pathway which is shown with gray shaded background.

(Oliver and Shenolikar 1998; Munton et al. 2004). Inhibitor 1 (I1) itself is phosphorylated by calcium-activated cyclic AMP-dependent protein kinase A (PKA) and protein kinase G and dephosphorylated by protein phosphatase 2A and the calcium-dependent phosphatase calcineurin (Cohen and Cohen 1989; Shenolikar 1994; Mulkey et al. 1994; Blitzer et al. 1998; Malleret et al. 2001; Svenningsson et al. 2004). See Fig. 3.3 for a scheme of this protein signaling cascade. A simple realization of the protein signaling cascade is given by

$$\mathrm{I_G} \underset{v_{\mathrm{CaN}}(C)}{\overset{v_{\mathrm{PKA}}(C)}{\rightleftharpoons}} \mathrm{I}, \tag{3.7}$$

$$\mathrm{I} + \mathrm{D} \underset{k_{-13}}{\overset{k_{13}}{\rightleftharpoons}} \mathrm{D_I}, \tag{3.8}$$

where $\mathrm{I_G}$ refers to dephosphorylated I1, I denotes phosphorylated inhibitor 1 (I1P), D is free PP1 and $\mathrm{D_I}$ stands for inhibited PP1, *i.e.* PP1 bound with phosphorylated inhibitor 1. See Fig. 3.3 for a scheme of the protein signaling cascade.

The balance between inhibitor 1 phosphorylation (v_{PKA})- and dephosphorylation rate (v_{CaN}) is calcium/calmodulin-dependent. The enzymatic activity of calcineurin can be described by a Hill equation (Stemmer and Klee 1994). The PKA activity is also known to be calcium/calmodulin-dependent via cyclic AMP (Cooper et al. 1995) but there is no data characterizing this dependency. We chose to describe both by a Hill equation

$$v_{\mathrm{x}}(C) = k_{\mathrm{x}}^0 + \frac{k_{\mathrm{x}}}{1 + (\frac{K_{\mathrm{x}}}{C})^{n_{\mathrm{x}}}}, \qquad \mathrm{x} = \mathrm{CaN,\ PKA} \tag{3.9}$$

with a calcium/calmodulin-independent base activity (k_{x}^0) which also accounts for protein kinase G phosphorylation (x=PKA) and protein phosphatase 2A dephosphorylation (x=CaN). k_{x} is the maximal, calcium/calmodulin-dependent activity, K_{x} the half activity concentration and n_{x} denotes the Hill coefficient.

Applying the Law of Mass Action and taking into account protein phosphatase 1 conservation yields

$$\frac{dI}{dt} = -k_{13}ID + k_{-13}(D_0 - D) - v_{\mathrm{CaN}}(C)I + v_{\mathrm{PKA}}(C)I_0, \tag{3.10}$$

$$\frac{dD}{dt} = -k_{13}ID + k_{-13}(D_0 - D), \tag{3.11}$$

where I_0 and $D_0 = D + D_{\mathrm{I}}$ refer to the total I1 and PP1 concentration, respectively. The concentration of dephosphorylated, free inhibitor 1, I_0, is treated like a bath, assuming a rapid exchange between the PSD with the spine volume and between the spine and the parent dendrite, as in (Zhabotinsky 2000; Miller et al. 2005). Therefore, inhibitor 1 is not conserved in Eq. (3.10) due to this bath assumption.

Applying the Law of Mass Action and taking into account the geometry of the CaMKII six-subunit ring, its autophosphorylation and dephosphorylation by PP1 can be described by a system of coupled, ordinary differential equations for concentrations of CaMKII with different numbers of phosphorylated subunits (see Eq. (A.1) - (A.14) in appendix A.1).

A, Parameters determined by experiments

Parameter	Definition	Value	Reference
K_1		$0.1\ \mu$M	
K_2	dissociation constants of	$0.025\ \mu$M	(Linse et al. 1991)
K_3	calcium binding to calmodulin	$0.32\ \mu$M	
K_4		$0.4\ \mu$M	
$CaMKII_0$	total CaMKII concentration	8.33, 16.67 μM	(Strack et al. 1997)
K_5	diss. const. of dephosph. subunit and C	$0.1\ \mu$M	(Meyer et al. 1992)
K_9	diss. const. of phosph. subunit and C	$1 \cdot 10^{-4}\ \mu$M	(Koninck and Schulman 1998)
k_{13}	I1P, PP1 association rate	500 (s μM)$^{-1}$	(Bhalla and Iyengar 2002; Endo et al. 1996)
k_{-13}	I1P, PP1 dissociation rate	0.1 s^{-1}	
K_{CaN}	calcineurin half activity concentration	$0.053\ \mu$M	(Stemmer and Klee 1994)
n_{CaN}	calcineurin Hill coefficient	3	

B, Parameters determined by constraints imposed by the model

Parameter	Definition	Value and Range : [X−Y]	Comment
k^0_{PKA}	PKA base activity	0.00359 [0.0031 − 0.0041] s^{-1}	constrain the
k_{PKA}	max. Ca^{2+}/CaM-dep. PKA act.	100 [2 − 804] s^{-1}	location of the
K_{PKA}	PKA half activity concentration	0.11 [0.085 − 0.189] μM	'LTD' and 'LTP' windows
n_{PKA}	PKA Hill coefficient	8 [6.8 − 14.9]	in the steady-state scenario
k_{CaN}	max. Ca2+/CaM-dep. calcineurin act.	18, 20 [16.6 − 18.1] s^{-1}	changes the PP1 level during stim.
k_{12}	maximal dephos. rate	6000 s^{-1} see text	change velocity of the PP1 dynamics
D_0	total PP1 concentration	$0.2\ \mu$M	by scaling with R (and Q for k_{12})
k_6	prob. of phos. step shown in Fig. 3.2C	6 s^{-1}	change the velocity
k_7	prob. of phos. step shown in Fig. 3.2D	6 s^{-1} see text	of autophosphorylation
k_8	prob. of phos. step shown in Fig. 3.2E	6 s^{-1}	by scaling with Q

C, Other parameters

Parameter	Definition	Value	Comment
CaM_0	total calmodulin concentration	$0.1\ \mu$M	see text
K_{M}	Michaelis constant of dephosphorylation	$0.4\ \mu$M	as in (Zhabotinsky 2000)
k^0_{CaN}	calcineurin base activity	0.1 s^{-1}	arbitrarily chosen, changing these values
I_0	total I1 concentration	$1\ \mu$M	does not affect the steady-state results

Table 3.1: Parameters of the detailed six-subunit model

3.1.3 Parameters of the six-subunit model

The model describing the interactions between proteins contains a large number of parameters (25). In some cases, we used experimentally determined values (see Tab. 3.1*A* for a list of those parameters). Other parameters are not (or poorly) determined experimentally. These parameters were varied systematically or were determined by the constraints we impose on the model (see Tab. 3.1*B*). Finally, a few parameters were set on the basis of previous modeling studies or set to an arbitrary value, in cases in which changing this value does not alter the results of the model (see Tab. 3.1*C*).

The calcium-dependent steady-state concentration of phosphorylated CaMKII subunits depends heavily on the choice of the parameters defining the PKA pathway (k^0_{PKA}, k_{PKA}, K_{PKA}, n_{PKA}). These parameters are adjusted in order to obtain the 'LTD' and the 'LTP window' at specific intervals of calcium concentrations (see section 3.2.2 on page 58). The maximal calcineurin activity k_{CaN} is used to adjust the PP1 level evoked during the STDP stimulation protocol (see section 3.3.2 on 64).

The total calmodulin concentration (CaM_0) is smaller than the value found in experimental studies, due to the reasons given above (see "Calcium binding to calmodulin" paragraph on page 48). K_{M} is taken from the modeling study of Zhabotinsky (2000). Eq. (3.10) and (3.11) give the steady-state PP1 concentration, $D_{\mathrm{steady-state}} = D_0/(1 + (I_0 k_{13} v_{\mathrm{PKA}})/(k_{-13} v_{\mathrm{CaN}}))$. Hence, $D_{\mathrm{steady-state}}$ depends on I_0, v_{PKA} and v_{CaN} through the single variable $I_0 \frac{v_{\mathrm{PKA}}}{v_{\mathrm{CaN}}}$. This means that out of the 5 parameters I_0, k^0_{CaN}, k_{CaN}, k^0_{PKA} and k_{PKA}, the steady-state PP1 concentration depends on three independent combinations of those parameters, *e.g.* $I_0 \frac{k^0_{\mathrm{PKA}}}{k^0_{\mathrm{CaN}}}$, $k_{\mathrm{PKA}}/k^0_{\mathrm{PKA}}$ and $k_{\mathrm{CaN}}/k^0_{\mathrm{CaN}}$. Thereby two out of these five parameters can be set arbitrarily. The total I1 concentration and the calcineurin base activity, I_0 and k^0_{CaN}, are set to the values given in Tab. 3.1*C* and are kept constant throughout all investigations, while the remaining three parameters k_{CaN}, k^0_{PKA} and k_{PKA} are obtained by constraints imposed on the model (see Tab. 3.1*B*). On the other hand, the dynamics of the protein signaling cascade depends on all 5 parameters. We address this issue via the scaling parameter R which influences the PP1 response dynamics (see section 3.3.6 on page 88).

3.2 Steady-state phosphorylation behavior of the CaMKII system

We investigate how the *steady-state* values of the total concentration of phosphorylated CaMKII subunits, S_{active}, depend on the concentration of calcium and the dephosphorylation activity in this section. We furthermore study how the steady-state behavior changes with the number of interacting subunits in the cluster.

3.2.1 Bistability of the CaMKII system with constant PP1 activity

Here, we start by exploring Ca^{2+}/calmodulin-stimulated autophosphorylation of CaMKII at a fixed dephosphorylation activity. This will allow us later to better understand how the parameters of the signaling cascade controlling dephosphorylation activity affect the phosphorylation behavior of CaMKII. To do this, we set the PP1 dephosphorylation activity to a constant, independent of the calcium concentration (this is equivalent to removing the red lines in Fig. 3.3 except for the interaction between CaMKII and PP1). The PP1 dephosphorylation activity is the product of k_{12}, the maximal dephosphorylation rate, and D, the free PP1 concentration (see Eq. 3.6).

Fig. 3.4*A* shows the steady-state concentration of phosphorylated CaMKII subunits as a function of the calcium concentration for 2, 4, 6 and 8 functionally connected subunits in the CaMKII cluster. The graphs show that in all cases there exists a range of calcium concentration for which the system is bistable (region between the diamond and the circle in case of the six subunit model). In the bistable region, three steady-states are present. The top and the bottom

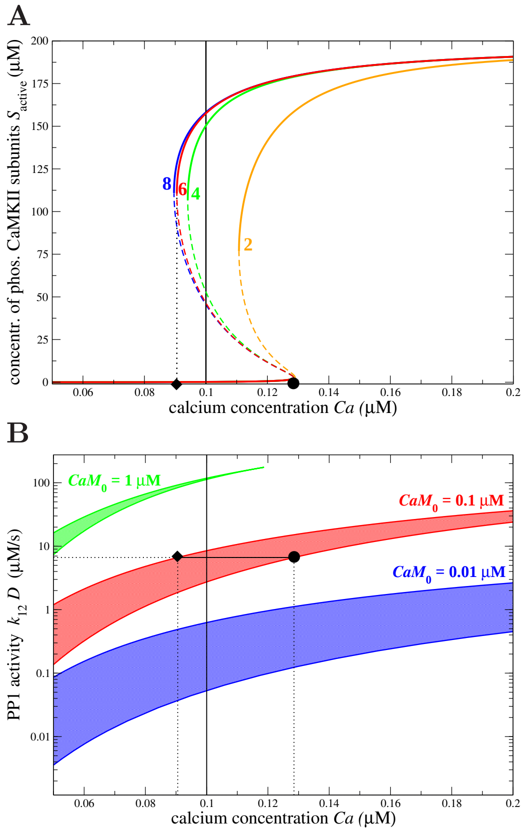

Figure 3.4: CaMKII bistability properties with constant PP1 activity. ***A,*** Bistability of the steady-state concentration of phosphorylated CaMKII subunits as a function of calcium concentration, for various numbers of subunits: The steady-state concentration of phosphorylated CaMKII subunits, S_{active}, is shown for different numbers of subunits in an interacting cluster (subunit number indicated in the panel). Dashed thin lines characterize unstable steady-states and full lines show stable steady-states. The left-hand calcium boundary of the bistable region for the six subunit model is indicated by the diamond and the right-hand boundary by the circle. In all cases, the total concentration of subunits is 200 μM, *i.e.* $CaMKII_0 = 50$ μM for the two subunit, $CaMKII_0 = 25$ μM for the four subunit, $CaMKII_0 = 16.67$ μM for the six subunit and $CaMKII_0 = 12.5$ μM for the eight subunit case. The total level of calmodulin, CaM_0, is 0.1 μM for all cases. The vertical full line shows the position of the calcium resting concentration in both panels. The PP1 activity is kept constant at $k_{12} \cdot D = 6.648$ μM/s. ***B,*** Boundaries of the bistable region in the PP1 activity - calcium concentration plane for different levels of calmodulin with the six subunit model: Lines of any given color depict the location of the left-hand (upper line) and the right-hand (lower line) boundaries of the bistable region with respect to the PP1 activity. Shaded areas between both boundaries mark the regions of bistability in the PP1 activity - calcium plane. Different colors correspond to different levels of calmodulin as indicated in the panel. The diamond illustrates the position with respect to calcium of the left-hand ($Ca = 0.091$ μM) and the circle of the right-hand boundary ($Ca = 0.129$ μM) of the bistable region for parameters as for the six subunit case in A ($CaM_0 = 0.1$ μM, $k_{12} \cdot D = 6.648$ μM/s). See Table 3.1 for other parameters.

steady-states (depicted by the thick full lines) are stable, whereas the intermediate one (dashed thin lines) is unstable. The branch of unstable steady-states separates the basins of attraction of the highly- and the weakly-phosphorylated stable steady-states. This means that the system will converge to the UP state if it is initially above this line, while it will converge to the DOWN state if it is below this line. As in other studies on CaMKII bistability, the bistable phosphorylation behavior emerges from the combination of strong cooperativity of CaMKII autophosphorylation and the saturation of the per-subunit dephosphorylation rate, k_{10} (see Eq. (3.6)), at high phosphorylation levels (Lisman 1985; Zhabotinsky 2000; Okamoto and Ichikawa 2000) (see also Fig. 2.11*B* on page 39). This saturation arises from the Michaelis-Menten approach employed to describe dephosphorylation, which is valid if the enzyme (PP1) is present in small amounts compared to the substrate (phosphorylated subunits). This is plausible since the CaMKII protein is localized at high concentrations in the PSD (Hanson and Schulman 1992; McNeill and Colbran 1995; Lisman et al. 2002).

Fig. 3.4*A* demonstrates that the increasing saturation of the per-subunit dephosphorylation rate with increasing number of interacting subunits in the holoenzyme ring plays a crucial role in the extent of the bistable region. Whereas the difference between the two and the four subunit model is very pronounced, increasing further the number of subunits has less and less impact on the size of the bistable region – it still increases substantially when this number goes from four to six, but there is almost no noticeable difference between the six and the eight subunit model. The effect of the number of subunits on the extent of the bistable region is mainly due to an increase in the range of stability of the UP state with increasing subunit number, since the stronger saturation of the per-subunit dephosphorylation rate becomes apparent in the highly-phosphorylated state only (see Eq. (3.6)). On the other hand, the range of stability of the DOWN state is essentially unaffected by the number of subunits, since it is mostly controlled by the balance between the dephosphorylation rate and the probability of the initiation step to occur. Interestingly, experimental data indicate that the number of functionally coupled subunits in a CaMKII holoenzyme ring is six (Bradshaw et al. 2002; Hudmon and Schulman 2002; Rosenberg et al. 2005), which could be a good compromise between having both a relatively small number of subunits and a large bistability range. In the following, we consider a model with six subunits.

How the location and the extent of the bistable region changes with respect to the PP1 dephosphorylation activity is shown in Fig. 3.4*B*. The curves depict the boundaries of the bistable region for the six subunit model in the PP1 activity - calcium concentration plane, for three values of the total calmodulin concentration, CaM_0 (indicated by the three different colors). For each value of CaM_0, the colored area shows the bistable region in which the UP and the DOWN state coexist. Above the colored area, only the DOWN state is present, while below that area, only the UP state is present. The resting calcium concentration can be included in the bistable region, provided the PP1 activity is chosen accordingly (e.g. $(k_{12} \cdot D) = 6.648$ μM/s for $CaM_0 = 0.1$ μM in Fig. 3.4*B*). Note that the bistable range vanishes at the PP1 activity level of 175.236 μM/s, regardless of the calmodulin level (only shown for the $CaM_0 = 1$ μM case). This is due so the fact that the calcium concentration Ca is related to the active calmodulin concentration, $C(Ca)$, by a nonlinear relationship $C(Ca) = CaM_0/(1 + K_4/Ca + K_3K_4/Ca^2 + K_2K_3K_4/Ca^3 + K_1K_2K_3K_4/Ca^4)$ which is independent of PP1 activity. Furthermore, the active calmodulin concentration is linearly dependent on the total calmodulin level (CaM_0). Consequently, the curves shown in Fig. 3.4*B* can be horizontally transfered into each other by accounting for the nonlinear relationship between calcium and active calmodulin and the linear relation between total calmodulin and active calmodulin. Such a transformation preserves the point at which the bistability vanishes as indicated by the data.

3.2.2 'LTD window' in a model with Ca^{2+}-dependent PP1 activity via protein signaling cascade including PKA and calcineurin

The right-hand boundary of the bistable region in Fig. 3.4*A* corresponds to an down-to-up switching threshold: If the calcium concentration increases persistently above this level, the CaMKII will converge from a weakly-phosphorylated to a highly-phosphorylated state (down-to-up switching). Hence, we define the range above this right-hand bifurcation point 'LTP window'. It corresponds to high calcium concentrations, consistent with experimental data on the range of calcium concentrations leading to LTP.

The available experimental data also suggest that (i) at resting calcium concentrations, no transitions should occur (both UP and DOWN states should be stable) (ii) for intermediate calcium concentrations (higher than resting concentration, but lower than the down-to-up switching threshold), LTD transitions should occur. This would happen if the UP state was no longer stable in an intermediate range of calcium concentrations - in such a scenario, the UP state would be stable in two disconnected regions, one around resting calcium concentration, and the other one at high calcium concentrations. The region where the UP state would not be stable could be called 'LTD window' since the system would exhibit LTD (up-to-down switching) whenever the calcium concentration stays in that region for a sufficiently long time, *i.e.* the CaMKII would converge from a highly-phosphorylated state to a weakly-phosphorylated state in this range of calcium. The scenario depicted in Fig. 3.4 seems however at odds with this picture.

How can the steady-state picture of Fig. 3.4*A* be modified to obtain such a LTD window? A possible scenario is to take into account the protein signaling cascade governing PP1 dephosphorylation activity in a calcium/calmodulin-dependent manner (see Fig. 3.3). In this way, the active concentration of PP1, D, changes with calcium and the region of bistability is not any more defined by a horizontal line in Fig. 3.4B. Rather, the location and extent of the LTD and the LTP windows are given by the intersections of the curve describing how the steady-state PP1 activity changes with calcium concentration with the curves specifying the location of the left- and the right-hand boundary of the bistable region in the PP1 activity - calcium concentration plane.

Fig. 3.5B shows an example in which the steady-state PP1 activity ($k_{12} \cdot D$) vs calcium concentration curve (purple line) intersects the bifurcation lines (red lines) four times, such that a LTD window emerges in a range of intermediate calcium concentrations. As the figure shows, this can be obtained whenever the PP1 activity has a sufficiently large peak at some intermediate calcium concentrations. This peak has to be such that in a range of calcium concentrations, PP1 activity is above both bifurcation lines (region between intersection points **2** and **3** in Fig. 3.5B). As discussed above, only the DOWN state is stable in this region. This PP1 peak is in turn obtained due to PKA activating at higher calcium concentration than calcineurin, since the balance between calcineurin and PKA activity determines the level of PP1 inhibition via inhibitor 1 (see Fig. 3.3 and 3.5A). Hence, the peak in steady-state PP1 concentration at intermediate calcium concentrations is due to a relative increase in calcineurin activity with respect to PKA activity in this range (compare Fig. 3.5A and B). To include the calcium resting concentration, Ca_0 (marked by the vertical thin line in Fig. 3.5), in a region of bistability, PP1 activity at Ca_0 has to reside in-between both bifurcation lines. The fourth intersection point defines the down-to-up switching threshold, *i.e.* the left-hand boundary of the LTP window (see point **4** in Fig 3.5B and C). The range of bistability between points marked **3** and **4** in Fig. 3.5C emerges from the declining PP1 activity (purple line in Fig. 3.5B) crossing the ascending range of bistability (red shaded area in Fig. 3.5B). These opposing trends lead to a narrow range of bistability at high calcium concentrations in the example presented here since the intersections of both define the borders of the bistable region.

In practice, the location of these four intersection points can be chosen by adjusting parameters describing the calcium/calmodulin-dependent activation of PKA and calcineurin activity (see section 3.1.2 on page 51). We can obtain four such parameters (PKA base and maximal activity k^0_{PKA} and k_{PKA}, respectively, the PKA half activity concentration K_{PKA} and the PKA Hill coefficient n_{PKA}, see Eq. (3.9)) by simultaneously solving four equations, *i.e.* one for each of the four intersection points **1, 2, 3** and **4** at $Ca = 0.09$, 0.22, 0.36 and 0.37 μM (see Fig. 3.5B). Fig. 3.5A displays the resulting instantaneous calcium/calmodulin-dependent phosphorylation, v_{PKA}, and dephosphorylation, v_{CaN}, rates of inhibitor 1 (see Eq. (3.9)) leading to the steady-state PP1 concentration scenario shown in

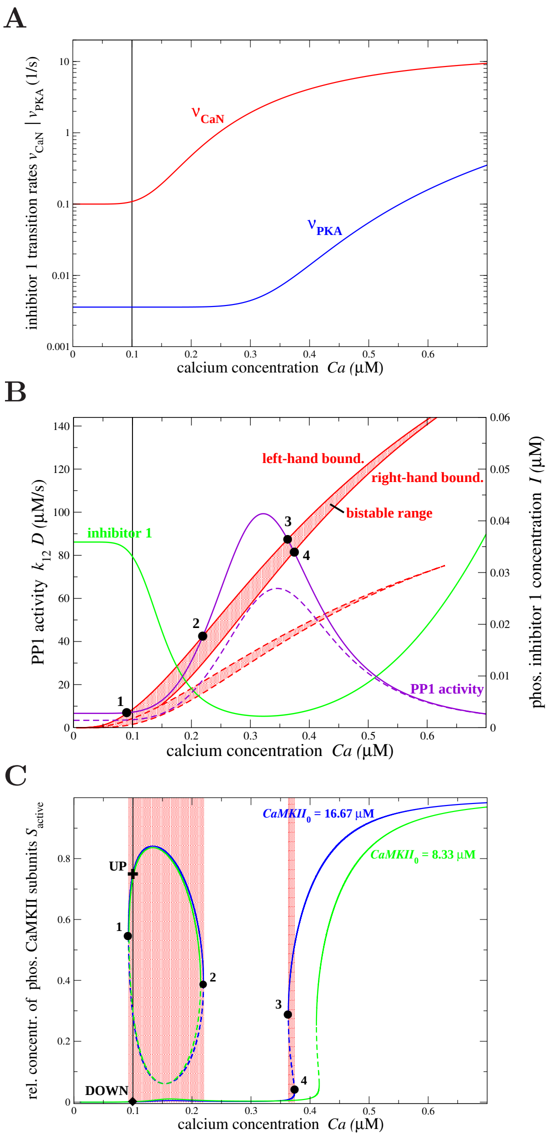

Figure 3.5: Ca^{2+}-dependent PP1 activity via protein signaling cascade and phosphorylated CaMKII subunit concentration steady-states. ***A,*** Phosphorylation and dephosphorylation rate of inhibitor 1 as functions of the calcium concentration: The red line shows the calcineurin activity dephosphorylating inhibitor 1, $v_{\mathrm{CaN}}(C)$, as a function of calcium and the blue line shows the PKA activity leading to phosphorylation of I1, $v_{\mathrm{PKA}}(C)$. Both rates are given by Eq. (3.9). The calcium/calmodulin complex concentration, C, is in equilibrium with the present calcium concentration. The total calmodulin concentration is $CaM_0 = 0.1$ μM. The vertical thin full line depicts the position of the calcium resting concentration in all panels. ↗ *See continuation on next page.*

Fig. 3.5B by the full purple line. The parameters obtained through this procedure can be found in Tab. 3.1B. Tab. 3.1B also shows the ranges of values of each parameter for which the above described behavior is qualitatively observed. These ranges are obtained varying each parameter while keeping the remaining three constant. This shows that the system is relatively robust to parameter changes. It reacts most sensitively to changes in k^0_{PKA}, whose value can be varied by about 14 % in both directions, while the other parameters can be varied over a range of about 100 % and even $\sim$ 800 % for k_{PKA}. Note that the choice of the maximal calcineurin activity, k_{CaN}, which basically controls the height of the PP1 peak shown in Tab. 3.1B, depends also on constraints discussed in the section 3.3.6 on page 84.

The system is also robust to changes in the total CaMKII concentration, as shown in Fig. 3.5C where we compare the bifurcation diagrams for $CaMKII_0 =$ 16.67 μM (blue line) and 8.33 μM (green line) provided the PP1 activity is rescaled accordingly by using $k^0_{\mathrm{PKA}} = 0.007$ 1/s in the latter case (other parameters remain unchanged). Note that both values of $CaMKII_0$ cover a range of CaMKII concentration that encompasses experimental estimates ($\sim$ 10 μM) for the PSD (Hanson and Schulman 1992; McNeill and Colbran 1995; Lisman et al. 2002). The dashed lines in Fig. 3.5B show the position of the bistable region (dashed red lines) and the steady-state PP1 activity (dashed purple line) in the PP1 activity - calcium plane for $CaMKII_0 = 8.33$ μM and $k^0_{\mathrm{PKA}} = 0.007$ (see Tab. 3.1 for other parameters).

To summarize the results so far, the model behavior is such that: (i) The calcium

Figure 3.5: ***B,*** Bistable region, PP1 activity and I1P steady-state concentration in the PP1 - Ca^{2+} plane: The full lines correspond to a total CaMKII concentration of $CaMKII_0 = 16.67$ μM, whereas dashed lines correspond to $CaMKII_0 = 8.33$ μM . The full red lines mark the positions of the left-hand (line above) and right-hand (line below) boundaries of the bistable region (red shaded region between both lines) with respect to the PP1 activity for $CaM_0 = 0.1$ μM. The purple and the green full lines show the calcium-dependent steady-state of the PP1 activity, $k_{12} \cdot D$, and I1P concentration, I, respectively, given by the rates shown in panel A. The numbered points 1, 2, 3 and 4 at the intersections of the PP1 steady-state with the full red lines give the locations of the boundaries (saddle-node bifurcation points) of the bistable regions. The dashed red and purple lines depict the boundaries of the bistable region and the steady-state PP1 activity, respectively, for the case $CaMKII_0 = 8.33$ μM (see text). ***C,*** Steady-states of the phosphorylated CaMKII subunit concentration (S_{active}) as a function of calcium: Full lines characterize stable steady-states whereas dashed lines mark unstable steady-states. Steady-states for $CaMKII_0 = 16.67$ μM are shown in blue and for $CaMKII_0 = 8.33$ μM in green. Red shaded areas depict regions of bistability for the $CaMKII_0 = 16.67$ μM case, *i.e.* three steady-states (two stable and one unstable steady-state) exist for a given calcium concentration. Bifurcation points are numbered as in B. The cross (diamond) marks the position of the UP (DOWN) state at resting calcium concentration for the $CaMKII_0 = 16.67$ μM case (see Tab. 3.1 and text for parameters, $k_{\mathrm{CaN}} = 18$ s^{-1}).

resting concentration is included in a region of bistability, giving rise to two stable steady-states - DOWN and UP - at resting conditions (marked by the diamond and the cross in Fig. 3.5*C*, respectively); (ii) In a region of intermediate calcium concentrations, only a weakly-phosphorylated steady-state exists (the LTD window, between filled circles marked **2** and **3**); (iii) Conversely, at high calcium concentrations, only the highly-phosphorylated steady-state is stable (the LTP window, beyond filled circle marked **4** in Fig. 3.5*C*). This scenario is now qualitatively consistent with experimental data. Note that, in contrast with Zhabotinsky (2000), our model does not require an unrealistic high phosphorylated inhibitor 1 concentration at resting calcium concentration ($I \approx 100\ \mu$M in his model) to have a stable highly-phosphorylated CaMKII state (compare green line in Fig. 3.5*B* and Zhabotinsky 2000 at this concentration).

3.3 The CaMKII system exposed to various stimulation protocols

Up to this point, we have investigated the steady-states of the CaMKII kinase-phosphatase system as a function of the intracellular calcium concentration. In experimental conditions, however, synaptic modifications are evoked by calcium transients resulting from experimental stimulation protocols inducing synaptic plasticity. Hence, the occurrence of transitions between weakly- and highly-phosphorylated states in the model needs to be examined in response to such calcium dynamics. Here, we explore in which conditions the spike-timing dependent plasticity (STDP) protocol as well as various purely pre- or purely postsynaptic stimulation protocols induce such transitions. Exposed to the STDP stimulation protocol, we furthermore investigate the CaMKII transition behavior if different proteins in the signaling cascade are blocked. The effect of spike-triplets (see e.g. Wang et al. (2005)) and the dependence of STDP on the spike-pair repetition frequency (see e.g. Sjöström et al. (2001)) is discussed in chapter 5.

3.3.1 Synaptic activity and postsynaptic calcium signaling

To investigate how the model behaves when realistic calcium transients are applied to it, we use the following model for postsynaptic calcium and postsynaptic membrane potential dynamics. We focus on a single spine compartment, and do not simulate the backpropagation of the action potential from its initiation site to the spine. Instead, we model the action potential dynamics directly at the spine.

Postsynaptic membrane potential The postsynaptic membrane potential is modeled using the Hodgkin-Huxley formalism in a single compartment. The reference volume for the membrane potential and the calcium dynamics model is taken to be a postsynaptic spine ($V_{\rm spine} \approx 1\ \mu{\rm m}^3$, $r_{\rm spine} \approx 0.5\ \mu{\rm m}$). The dynamics of the membrane potential V follows the differential equation

$$C_{\rm m}\frac{dV}{dt} = -I_{\rm L} - I_{\rm Na} - I_{\rm K} - I_{\rm NMDA} - I_{\rm CaL} - I_{\rm AMPA} + I_{\rm stim}, \tag{3.12}$$

where $C_{\rm m}$ is the whole cell capacitance of 0.1 nF, $I_{\rm x}$ (x = L, Na, K, NMDA, CaL, AMPA) are the ionic currents listed in appendix A.2 on page 177. An action potential is evoked by a 1 ms depolarizing pulse current $I_{\rm stim}$ of 3 nA.

Postsynaptic calcium dynamics The model of the calcium dynamics involves the two main sources of postsynaptic calcium influx in the spine: NMDA receptors (NMDA-R) and voltage-dependent calcium channels (VDCC) (Bollmann et al. 1998). Extrusion, diffusion and slow buffering is accounted for by a single exponential decay, yielding the following equation for the time course of the intracellular calcium concentration

$$\tau_{\rm Ca}\frac{dCa}{dt} = -(Ca - Ca_0) + \tau_{\rm Ca}\zeta(\beta_{\rm NMDA}I_{\rm NMDA} + \beta_{\rm CaL}I_{\rm CaL}), \tag{3.13}$$

where Ca is the free, intracellular calcium concentration, $\tau_{\rm Ca} = 12$ ms refers to the single exponential time constant of the passive decay process (Sabatini et al. 2002), Ca_0 is the calcium resting concentration and $\zeta = 5182.15\ \mu$M/C converts the ion currents into concentration changes per time for a spine of volume $\approx 1\ \mu{\rm m}^3$ (see appendix A.2 on page 177). $I_{\rm x}$ (x = NMDA, CaL) are the ionic currents in appendix A.2 on page 177. Scaling parameters $\beta_{\rm NMDA} = 1/1000$ and $\beta_{\rm CaL} = 1/100$ take into account both the immediate uptake of calcium by intracellular buffers ($\sim$ 99 %, Helmchen et al. (1996)) and the fact that only about $\sim$ 10 % of the NMDA-mediated current is carried by calcium ions (see Burnashev et al. (1995), Schneggenburger (1996) and appendix A.2 on page 177).

Noisy calcium transients To investigate stochastic effects, we add two possible noise sources to the model: (i) NMDA receptor maximum conductance drawn at random at each presynaptic spike and (ii) maximum conductance of the voltage-dependent calcium channel drawn at random at each postsynaptic spike.

The maximum conductances of the NMDA receptor and the voltage-dependent calcium channel mediated calcium influx are both drawn from binomial distributions characterized by the total number of channels $N_{\rm tot}$ and the opening probability per channel $p_{\rm o}$. Each pre- or postsynaptic spike gives rise to an integer number, $n_{\rm o}$, of NMDA or CaL channel openings, respectively. We assume that the channels open independently of each other. The single channel conductance

g_{single} is chosen so that the mean calcium amplitudes are as stated below. To account for the stochasticity of calcium ions influx, Gaussian noise with zero mean and a variance scaled with n_o is added to $(n_o \cdot g_{\text{single}})$. The parameters of the NMDA and CaL maximum conductance distributions are adjusted such that they fit the experimental findings of single spine measurements by Mainen *et al.* and Sabatini & Svoboda, respectively (Mainen et al. 1999; Sabatini and Svoboda 2000) (see Tab. A.1 for parameters).

The parameters describing postsynaptic calcium and postsynaptic membrane potential dynamics are taken from previous modeling studies (Destexhe et al. 1998; Wang 1999; Sabatini and Svoboda 2000; Poirazi et al. 2003; Purvis and Butera 2005). We systematically vary the calcium amplitudes evoked by a pre- (ΔCa_{pre}) and a postsynaptic spike (ΔCa_{post}), keeping their ratio constant, $\Delta Ca_{\text{post}} = 2 \cdot \Delta Ca_{\text{pre}}$ (see section 3.3.2 on 64 and appendix A.2 on page 177).

3.3.2 STDP simulation protocol

For the STDP protocol, we use a standard repetitive stimulation protocol (60 pairs at 1 Hz, see experiments by Bi and Poo 1998). Each stimulation pair consists of a presynaptic spike at time t_{pre} and a back-propagating postsynaptic action potential occurring at time $t_{\text{post}} = t_{\text{pre}} + \Delta t$. In experimental conditions, LTD is evoked for short negative Δts, while LTP is evoked for short positive Δts (Bell et al. 1997; Markram et al. 1997; Magee and Johnston 1997; Bi and Poo 1998; Debanne et al. 1998).

Deterministic calcium dynamics Fig. 3.6A shows the time course of calcium concentration transients evoked by one pair of a pre-synaptic spike and a back-propagating action potential (BPAP) at different Δts. An isolated postsynaptic spike generates a calcium transient of amplitude ΔCa_{post}, due to opening of calcium channels induced by the depolarization caused by the BPAP. Likewise, an isolated pre-synaptic spike generates another calcium transient of amplitude ΔCa_{pre}, due to NMDA channel opening. Below, we will vary systematically the size of ΔCa_{pre}, keeping the ratio constant, $\Delta Ca_{\text{post}}/\Delta Ca_{\text{pre}} = 2$ (Sabatini et al. 2002). See section 3.3.1 on page 62 for details of the model.

What happens when pre and postsynaptic spikes are sufficiently close together so that their respective calcium transients overlap?

For short negative time differences, $\Delta t < 0$ *ms (post before pre):* The decaying phase of the fast BPAP-evoked calcium signal overlaps in time with the long-lasting calcium transient mediated by NMDA receptors (see Fig. 3.6A for the $\Delta t = -10$ ms case). Though this temporal overlap has only a weak effect on the integral (shown in Fig. 3.6B by the cyan line) and no impact on the maximal amplitude (shown in Fig. 3.6B by the red line) of the calcium transient induced by the pair

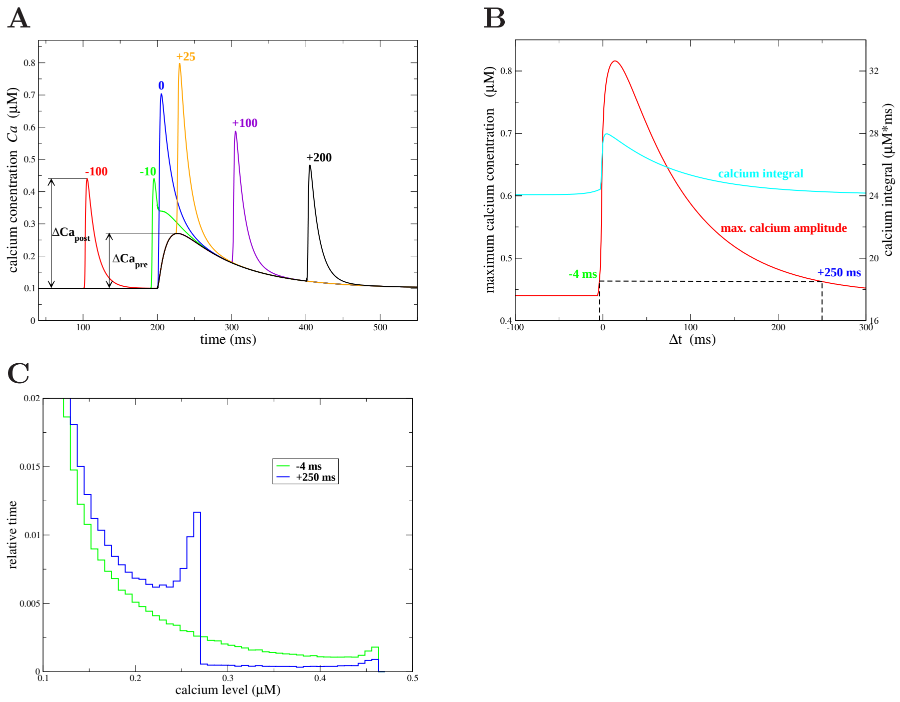

Figure 3.6: Calcium dynamics and statistics evoked by a pair of a pre- and a postsynaptic spike occurring at different time lags, Δt. ***A***, Temporal evolution of the intracellular calcium concentration generated by the model in response to a presynaptic spike at $t_{\mathrm{pre}} = 200$ ms and an additional postsynaptic spike at $t_{\mathrm{post}} = t_{\mathrm{pre}} + \Delta t$: The time lag between both spikes, Δt, is indicated at the corresponding curve in ms. The calcium amplitudes of the isolated pre- ($\Delta Ca_{\mathrm{pre}} = 0.17$ μM) and postsynaptic ($\Delta Ca_{\mathrm{post}} = 0.34$ μM) responses are indicated in panel *A*. ***B***, Maximal amplitude and integral of the calcium transients evoked by a pre- and postsynaptic spike-pair: The maximal amplitude (red line) attained during spike-pair stimulation is shown as a function of the time lag, Δt (left hand scale). The fact that calcium transients evoked by the $\Delta t = -4$ ms and the $\Delta t = 250$ ms protocols reach the same max. amplitude ($Ca = 0.463$ μM) is indicated by the dashed, black lines. The calcium integral of one spike-pair is obtained according to $\int (Ca(t) - Ca_0)dt$ and depicted as a function of Δt (full, cyan line). ***C***, Time spent at different calcium levels: The calcium transients evoked by $\Delta t = -4$ ms (green line) and $\Delta t = 250$ ms (blue line) protocols which evoke the same maximal amplitudes (see panel *B*) are compared with respect to the time they spent at different calcium levels. Note that the large peak around $Ca_0 = 0.1$ μM is not shown. See Tab. A.1 for parameters.

of spikes compared to a case in which both transients do not interact at all (large positive and large negative Δt), the time spent by the system in different intervals of calcium concentrations does change significantly with Δt. This is illustrated in Fig. 3.6*B* and *C* for $\Delta = -4$ ms and $\Delta = 250$ ms, both calcium transients exhibit the same maximal calcium amplitude (see horizontal black dashed line in Fig. 3.6*B*) but they differ considerably in the times spent at different calcium levels (see Fig. 3.6*C*). This feature largely contributes to the fact that LTD can potentially be observed at short negative Δts only (see below).

For positive time differences, $\Delta t > 0$ ms (pre before post): The strong depolarization by the BPAP increases drastically the voltage-dependent NMDA-R mediated calcium current, I_{NMDA}, leading to a supra-linear superposition of the two contributions. Fig. 3.6*B* shows that the maximal calcium amplitude attained at $\Delta t = 14$ ms reaches a level of $Ca = 0.816$ μM. The ratio between the calcium peak amplitude at $\Delta t = 14$ ms and the linear sum of individual pre- and postsynaptically evoked calcium transients ($0.17 + 0.34$ μM) is about 1.4, consistent with experimental data (Nevian and Sakmann 2006) (note that Nevian and Sakmann (2006) pair the presynaptic spike with *three* postsynaptic action potentials to assess the non-linearity factor in their Fig. 5*D*). The large amplitude at short positive Δt explains to a large extent the occurrence of LTP at short positive Δt and also prevents LTD transitions at large positive Δt protocols (see discussion below). The repetitive presentation (60 times at 1 Hz) of the pre- and postsynaptic spike-pair produces repetitively the calcium transient shown in Fig. 3.6*A* for a few examples of Δt.

LTP and LTD-like transitions as a function of Δt. When the parameters of the model are chosen accordingly, the model reproduces qualitatively the experimental results in response to the STDP stimulation protocol: (i) Short positive Δt stimulation protocols move CaMKII from the weakly-phosphorylated state to the highly-phosphorylated state. Starting from the UP state, no transition occurs. (ii) A system being at rest at the UP state is switched to the DOWN state by short negative Δt protocols whereas the same protocol does not evoke transitions from the DOWN to the UP state. (iii) Large positive and negative Δts do not evoke transitions between the DOWN and the UP states. We show in Fig. 3.7, 3.8, 3.9 and 3.12 (red lines) the behavior of the model for parameters shown in Tables 3.1, with $k_{\mathrm{CaN}} = 18$ s^{-1} and $\Delta Ca_{\mathrm{pre}} = 0.17$ μM.

Fig. 3.7 shows the dynamics of the system for the whole stimulation protocol and until the system has reached the final steady-state except for panel *A* and *B*, which depict the time course of the calcium concentration and the postsynaptic voltage for the presentation of one spike-pair only. Fig. 3.7*C, D* show the time course of active PP1, while *E, F* show the dynamics of phosphorylated CaMKII

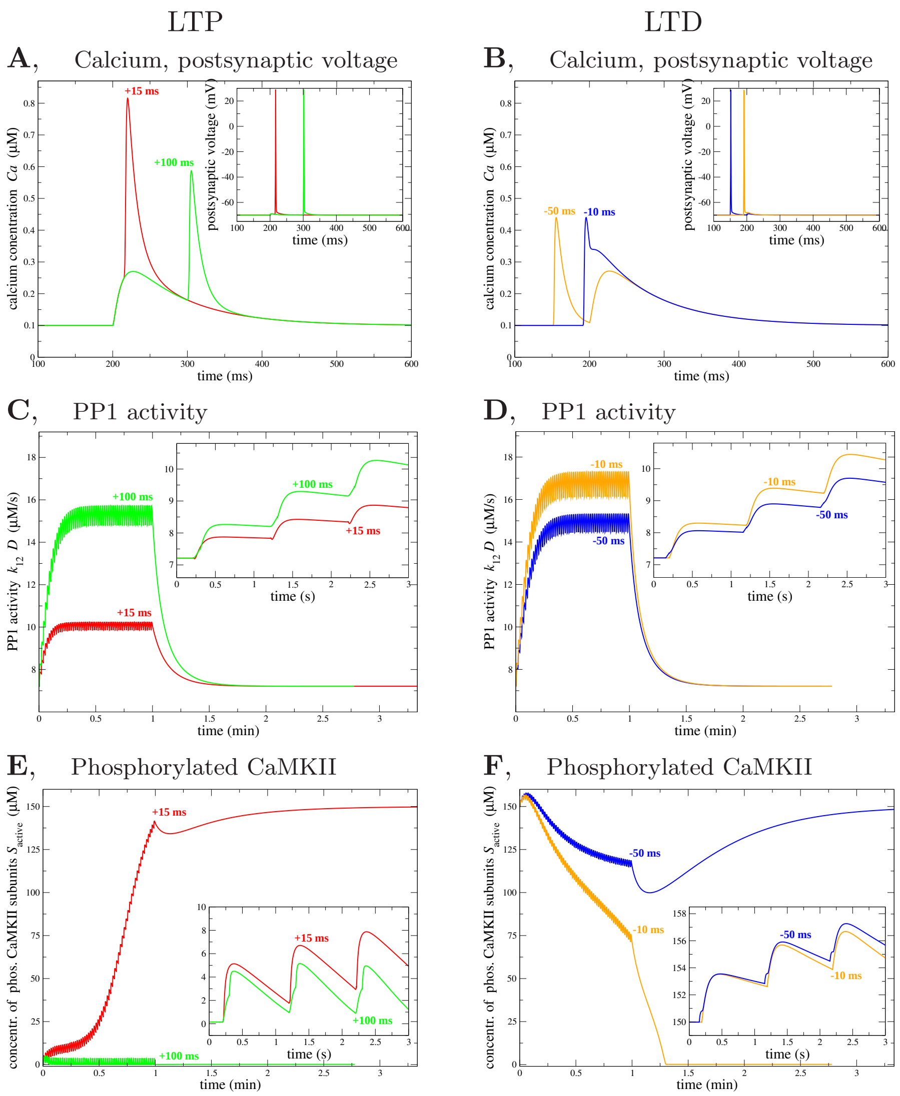

Figure 3.7: Time course of calcium, postsynaptic voltage, PP1 activity and phosphorylated CaMKII subunit concentration during STDP stimulation protocols with $\Delta t = -50$, -10, 15 and 100 ms. The left panels, *A*, *C* and *E* show the dynamics during STDP stimulation protocols with $\Delta t = 15$ ms (red lines) and $\Delta t = 100$ ms (green lines), with the system initially in the DOWN state. In the right panels *B*, *D* and *F* the CaMKII system is initially in the UP state and is subjected to stimulation protocols with $\Delta t = -50$ ms (blue lines) and $\Delta t = -10$ ms (orange lines). Note that the time course of calcium and the postsynaptic voltage (insets) in panel *A* and *B* are shown for one spike pair presentation only. The PP1 and S_{active} time course (*C*, *D*, *E* and *F*) is shown for the full stimulation protocol with 60 spike-pair presentations at 1 Hz and until the system converges to the final steady-state. The insets in panel *C*, *D*, *E* and *F* display the dynamics on a shorter time scale (first three spike-pairs in the stimulation protocol). In this figure: $k_{\text{CaN}} = 18$ s^{-1}, $\Delta Ca_{\text{pre}} = 0.17$ μM. The PP1 steady-state activity is 7.21 μM/s at $Ca_0 = 0.1$ μM (compare Fig. 3.5*B*).

subunit concentration. The left column shows the dynamics of the system when it is initially in the DOWN state (low concentration of phosphorylated CaMKII subunits) for two representative time lags ($\Delta t = 15$ ms and 100 ms), while the right column shows the dynamics when it is initially in the UP state, again for two representative time lags ($\Delta t = -50$ and -10 ms).

To understand why the system exhibits transitions in specific ranges of Δt, is it first crucial to examine how PP1 activation depends on Δt. For the value of ΔCa_{pre} chosen here, PP1 activation is the largest at short negative time differences, since such values of Δt maximize the time spent by the system in the range of calcium concentrations close to PP1 peak activation (see Fig. 3.5*B*). On the other hand, PP1 activation is minimal for short positive time lags since Ca goes transiently to high concentrations and spends a short time at intermediate values. Let us now focus on the situation in which the system is initially in the DOWN state. During the stimulation protocol two situations can arise. For short positive time differences (as e.g. the 15 ms case shown in the Fig. 3.7), the increase in PP1 activity is low and insufficient to counterbalance the large increase in the concentration of phosphorylated CaMKII subunits, since high calcium transients strongly favor the autophosphorylation process which outweighs the low dephosphorylation activity. Hence, the system reaches a high phosphorylation level during the stimulation protocol and converges gradually towards its equilibrium value in the UP state thereafter. On the other hand, for negative and large positive time lags, the increase in PP1 activity is large enough to counterbalance the calcium/calmodulin triggered autophosphorylation, *i.e.* CaMKII stays dephosphorylated and remains in the DOWN state (see e.g. the 100 ms case in Fig. 3.7).

When the system is initially in the UP state, the concentration of phosphorylated CaMKII subunits again depends on the competition between dephosphorylation by PP1 and autophosphorylation progress during the protocol. Again, we have two possible outcomes of the protocol: either the PP1 concentration becomes large enough such that the system gets sufficiently dephosphorylated and moves in the basin of attraction of the DOWN state during the stimulation protocol (this occurs e.g. for the -10 ms case shown in Fig. 3.7); or it is not large enough and autophosphorylation prevails, *i.e.* the system remains in the basin of attraction of the UP state. For the parameter set used in Fig. 3.7, this happens for large negative and positive time lags.

Another way of visualizing the dynamics during and after the STDP protocol consists in plotting the trajectory of the system in the PP1 activity - concentration of phosphorylated CaMKII subunits, S_{active}, plane. This is done for several values of Δt in Fig. 3.8*A* and *B*. The DOWN and the UP stable steady-states of the CaMKII phosphorylation level are shown by the diamond and the cross, respectively (located at the intersections of the S_{active} and $(k_{12}D)$ nullclines). In Fig. 3.8*A* the system is initially in the DOWN state, whereas it is initially in the

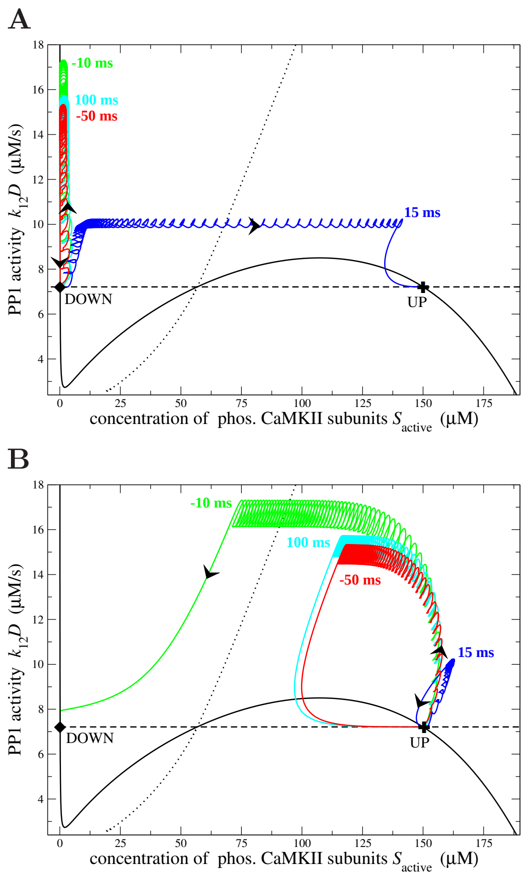

Figure 3.8: Dynamics of the system in the PP1 activity - phosphorylated CaMKII subunit concentration phase-plane. Panels A and B show the $k_{12}D$ - S_{active} trajectories during STDP protocols with $\Delta t = -50$ ms (red), $\Delta t = -10$ ms (green), $\Delta t = 15$ ms (blue) and $\Delta t = 100$ ms (cyan) and until the system reaches the final steady-state. ***A,*** System initially in the DOWN state (diamond); ***B,*** System initially in the UP state (cross). The black arrows indicate the direction of motion of the system along the trajectory for some examples. The full and the dashed black line depict the S_{active} and the $k_{12} \cdot D$ nullclines at resting conditions ($Ca_0 = 0.1$ μM), respectively. Therefore, the intersections of both nullclines mark the positions of the steady-states of the system: two stable - the DOWN (diamond) and the UP (cross) state - and one unstable at $S_{\text{active}} \approx 56.8$ μM. Note that the PP1 activity nullcline (dashed black line) is independent of S_{active} (see Eqs. (3.10) and (3.11)) whereas the S_{active} nullcline (full black line) is dependent on ($k_{12}D$) and S_{active} (see Eqs. (A.1)-(A.14)). The separatrix, separating the basins of attraction of the two stable steady-states is shown as a dotted black line (see Tab. 3.1 for parameters, $k_{\text{CaN}} = 18$ s^{-1}, $\Delta Ca_{\text{pre}} = 0.17$ μM).

UP state in Fig. 3.8*B*. In both figures the end of the stimulation protocol corresponds to the point at which PP1 and S_{active} stop to oscillate, and there is a sharp turn of the trajectories in the plane. In this plane, the separatrix (dotted black line) marks the boundary between the basins of attraction of both stable steady-states. Depending on the position of the system at the end of the stimulation protocol relative to this separatrix, the system relaxes either to the UP or the DOWN state. The separatrix is obtained by adjusting numerically Δt to be at the boundary between the regions in which a transition to the UP (resp. DOWN) state occurs or not.

The outcomes of the deterministic STDP protocols for Δt values from -100 to 150 ms are summarized in Fig. 3.9 (red line). We consider a large population of independent synapses submitted to the same protocol, in which initially half of the synapses are in the DOWN state and the other half in the UP state. The figure shows the relative change in the fraction of synapses in the UP state as a function of Δt ($+1$ means all synapses initially in DOWN where switched to UP; 0 means no change; -1 means all synapses in UP have switched to DOWN). There is a range of values of Δt (from 10 to 16 ms) for which all synapses initially in the DOWN state switch to the UP state (LTP). LTD, or up-to-down transitions of the synapses initially in the UP state, is observed in a range of Δt values from -14 to -2 ms (see red line in Fig. 3.9).

STDP protocol stimulation with stochastic calcium dynamics The CaMKII kinase-phosphatase system in the PSD is composed of a few molecules only (~ 30 CaMKII holoenzymes, Petersen et al. 2003) hence stochastic fluctuations potentially play an important role (see Miller et al. 2005). The CaMKII system is also exposed to fluctuating calcium transients stemming from stochastic neurotransmitter release, stochastic channel opening and the stochastic nature of neurotransmitter as well as calcium diffusion (Mainen et al. 1999; Sabatini et al. 2002). It is therefore necessary to investigate the dynamic behavior of the CaMKII system in the presence of noise. Here we choose for simplicity to introduce fluctuations in calcium transients exclusively.

Two sources of noise are introduced in the calcium dynamics simulations: (i) the NMDA receptor maximum conductance is drawn at random at the occurrence of each presynaptic spike and (ii) the maximum conductance of the voltage-dependent calcium channel is drawn at random at the occurrence of each postsynaptic spike. Both conductances are drawn from binomial distributions similar to those measured in experiments (Mainen et al. 1999; Sabatini and Svoboda 2000) (see section 3.3.1 on page 62 for more details). Some examples of noisy calcium transients are shown in the inset of Fig. 3.9 (dashed lines; the full line depicts the average transient corresponding to the traces shown in Fig. 3.6*A*).

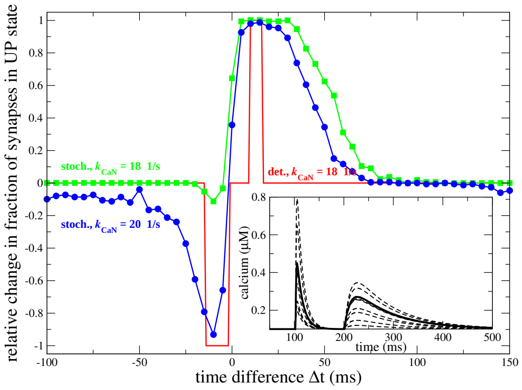

Figure 3.9: Synaptic transitions in response to STDP. The relative change in the fraction of synapses in the UP state in response to deterministic (red line) and stochastic (green and blue lines with symbols) STDP stimulation protocols is shown as a function of Δt. 0 means no net change in the number of synapses in the UP state, positive relative change means a net increase of synapses in the UP state and a negative relative change means a net increase of synapses in the DOWN state. Stochastic stimulation results are shown for $k_{\text{CaN}} = 18$ 1/s (green line with squares, same value as in deterministic case) and $k_{\text{CaN}} = 20$ 1/s (blue line with circles). ($\Delta Ca_{\text{pre}} = 0.17$ μM). The inset shows some example calcium transients (dashed lines) of the stochastic stimulation protocol evoked by a spike-pair with $\Delta t = -100$ ms and $t_{\text{pre}} = 200$ ms. The avergage calcium transient is shown by the full line and is the same as the red curve in Fig. 3.6, *i.e.* this is the calcium transient utilized for the deterministic stimulation protocol. The stochastic stimulation results are averaged over $N = 300$ synapses.

Again, we consider a large population of independent synapses exposed to stochastic stimulation protocols. $N = 300$ independent synapses are simulated, 150 initially in the DOWN and 150 in the UP state. Applying the stimulation protocol leads to stochastic transitions between UP and DOWN states. Fig. 3.9 shows the relative change in the fraction of synapses in the UP state as a function of Δt, for $k_{\text{CaN}} = 18$ s^{-1} and 20 s^{-1}. For example, a relative change of -0.8 for $\Delta t = -15$ ms ($k_{\text{CaN}} = 20$ s^{-1} case) means that 120 of the synapses in the UP state (out of the 150) switched to the DOWN state in response to this protocol, while none of the 150 synapses in the DOWN state experienced a down-to-up transition during the $\Delta t = -15$ ms stimulation.

The variability in maximum NMDA and CaL current conductances results in a variability of calcium transients around the mean transients. The consequence of this variability in calcium transients is that, while the shape of the PP1 level vs Δt (as shown in Fig. 3.15*C*) is qualitatively unchanged, the PP1 level reached during stimulation protocols is significantly reduced. This is due to the fact that the variability in calcium transients decreases the time spent by the system at calcium concentrations which maximize PP1 build-up. Hence, the probability that the PP1 level is high enough to make the system switch to the DOWN state becomes small for $k_{\text{CaN}} = 18\ \text{s}^{-1}$ (the value used in deterministic simulations). Consequently, the up-to-down transition probability at short negative time lags is low and LTD is effectively absent in this case (see green line with squares in Fig. 3.9). However, the LTD probability becomes larger as k_{CaN} is increased. Fig. 3.9 shows an up-to-down switching probability of about -0.93 for short negative time lags with $k_{\text{CaN}} = 20\ \text{s}^{-1}$ (at $\Delta t = -10$ ms). The range of k_{CaN} values for which a considerable amount of LTD can be observed goes from $k_{\text{CaN}} \approx 19\ \text{s}^{-1}$ (relative change of at the least -0.5 at short negative Δt) to $k_{\text{CaN}} \approx 21\ \text{s}^{-1}$ (relative change less than -0.5 for large positive and large negative Δt). Fig. 3.9 also shows that with $k_{\text{CaN}} = 20\ \text{s}^{-1}$ there exists already a small but finite probability of eliciting LTD transitions for large positive and large negative time lags, due to variability in calcium transients. To summarize, down-to-up transitions occur robustly for a large range of parameters at short positive time lags. On the contrary, the range of short negative values of Δt for which up-to-down switches are observed is less robust to noise (see discussion in section 6.1.3 on page 159).

3.3.3 STDP stimulation protocol and protein inhibitors

With the objective of revealing the role of single proteins or entire sub-paths of signaling cascades in synaptic long-term modifications, experimental assays combine stimulation protocols with drug perfusion inhibiting protein kinases or protein phosphatases. Since the elements in the implemented protein signaling cascade correspond to realistic counterparts, we can check easily the effect of specific protein inhibitors in the model.

Broadband phosphatase inhibitors A typical experiment to investigate the role of protein phosphatases in synaptic plasticity is the application of phosphatase inhibitors during the presenation of stimulation protocols inducing synaptic changes (Mulkey et al. 1994; Malleret et al. 2001; O'Connor et al. 2005b; Wang et al. 2005). The general observation is that phosphatase inhibitors prevent LTD while sparing LTP. We investigate the effect of phosphatase inhibitors in our model by gradually reducing the dephosphorylation activity of PP1. We study the changes in the steady-states of the phosphorylated CaMKII subunit concentration and in the transition behavior.

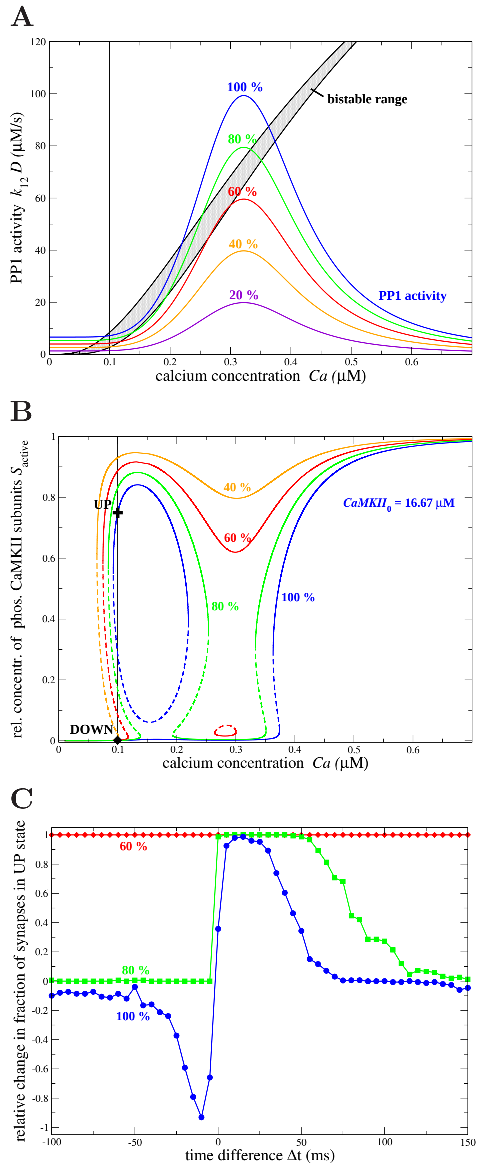

Figure 3.10: Scaling PP1 activity: phosphorylated CaMKII subunit concentration steady-states and transition outcomes. ***A*,** The same scenario as in Fig. 3.5*B* is depicted. The gray shaded area shows the position of the bistable range in the PP1 activity - calcium concentration plane. The steady-state PP1 activity is shown for different total PP1 concentrations, D_0. For example, in the 80 % case, the total PP1 concentration is $0.8D_0$, *i.e.* 0.16 μM (see Tab. 3.1). The vertical black line marks the position of the calcium resting concentration at $Ca_0 = 0.1$ μM. ↗ *See continuation on next page.*

Since the steady-state PP1 concentration is given by $D_{\text{steady}-\text{state}} = D_0/(1 + (I_0 k_{13} v_{\text{PKA}})/(k_{-13} v_{\text{CaN}}))$ (see section 3.1.3 on 54), scaling down D_0 corresponds to a reduction of the steady-state PP1 activity given by the purple line in Fig. 3.5*B*. Consequently, the intersections between the boundaries of the bistable region (given by the red lines in Fig. 3.5*B*) and the PP1 activity change, *i.e.* the locations and the ranges of the LTD and the LTD window change. Moreover, the position of the PP1 activity with respect to the bistable region in the PP1 activity - calcium concentration plane defines whether the UP or the DOWN or both states are stable (see above). Scaling down the total PP1 concentration leads to a diminution in extent of the LTD window and to the emergence of a second LTP window at low calcium concentrations (see the 80 % case shown by the green line in Fig. 3.10*A* and *B*). Decreasing further protein phosphatase strength makes the LTD window disappear and a large LTP window emerges starting at low calcium concentrations (see 60 and 40 % cases in Fig. 3.10*A* and *B*). Finally, reducing the PP1 concentration below $\sim$ 40 % results in a loss of the stability of the DOWN state at resting calcium concentrations, leaving the UP state as the only stable steady-state for all calcium concentrations.

Fig. 3.10*C* shows the transition results in case the model with reduced total PP1 concentration is exposed to the STDP stimulation protocol evoking noisy calcium transients. Consistent with experiments, reducing the PP1 concentration by 20 % leads to a loss of LTD transitions (see green line in Fig. 3.10*C*), while increasing the range and the probability to see LTP transitions. Due to the increase in extent of the LTP window in the model, STDP protocols paired with a PP1 concentration reduction to 60 % and more result in up-to-down transitions for all time differences Δt (see red line in Fig.3.10*C*).

Protein kinase A and calcineurin inhibitors Inhibiting increasingly PP1 activity corresponds to a successive elimination of the entire protein signaling cascade governing CaMKII dephosphorylation (see Fig. 3.3). Here, we inhibit PKA and calcineurin activity specifically and examine the CaMKII transition behavior in response to this partial impairment. Furthermore, it is shown that a constant,

Figure 3.10: ***B,*** The steady-states of the phosphorylated CaMKII subunit concentration are depicted for the different total PP1 concentration cases shown in panel *A* in the same color. Full lines mark stable steady-states and dashed lines depict unstable steady-states. The positions of the UP and the DOWN states at calcium resting conditions are shown for the 100 % PP1 concentration case by the cross and the diamond, respectively ($CaMKII_0 = 16.67$ μM, $k_{\text{CaN}} = 18$ s^{-1}, see Tab. 3.1 for parameters). ***C,*** The average relative changes in the fraction of synapses in the UP state for three different total PP1 concentrations are shown (cases marked in the panel and colors correspond to the cases shown in panel *A* and *B*). The blue line with circles shows the same results as the blue line in Fig. 3.9 for $D_0 = 0.2$ μM as given in Tab. 3.1, *i.e.* the 100 % case ($N = 300$, see Tab. 3.1 for other parameters).

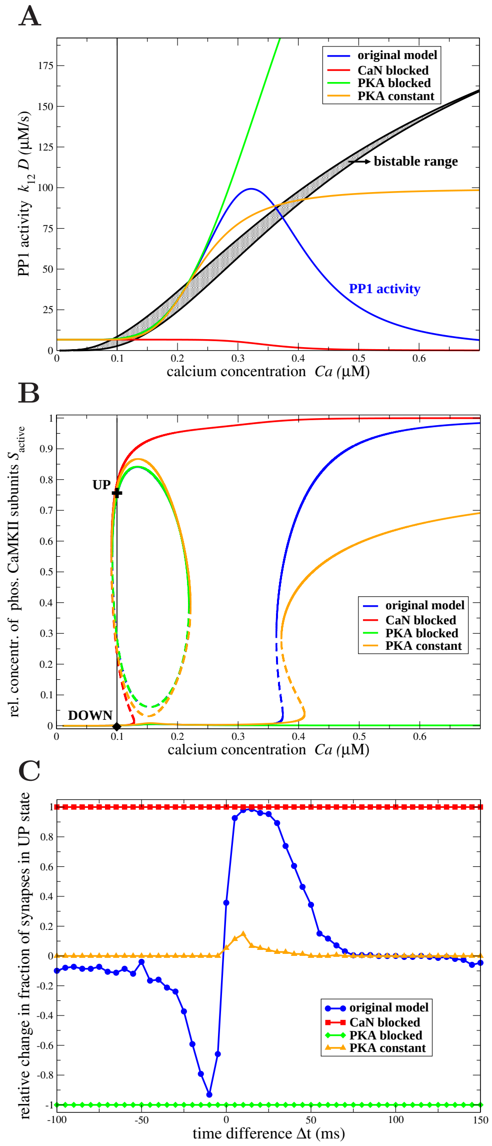

Figure 3.11: Blocking calcineurin and PKA as well as constant PKA activity: phosphorylated CaMKII subunit concentration steady-states and transition outcomes. ***A*,** The steady-state scenario as in Fig. 3.5*B* is depicted. The gray shaded area shows the position of the bistable range in the PP1 activity - calcium concentration plane. The steady-state PP1 activity is shown for different realizations of the protein signaling cascade: with intact protein signaling cascade (blue line, reproduction of the full purple line in Fig. 3.5*B*), with calcium-dependent calcineurin activity blocked ($k_{\mathrm{CaN}} = 0$, red line), with calcium-dependent PKA activity blocked ($k_{\mathrm{PKA}} = 0$, green line) and with constant PKA activity (orange line, $k^0_{\mathrm{PKA}} = 0.00359$ s^{-1} and $k_{\mathrm{PKA}} = 0$, see text for other parameters). The vertical black line marks the position of the calcium resting concentration at $Ca_0 = 0.1$ μM. ↗ *See continuation on next page.*

calcium-independent PKA activity can lead to a similar steady-state behavior of the CaMKII phosphorylation level as shown above for the case with calcium-dependent PKA activity.

Calcineurin is not the only phosphatase dephosphorylating inhibitor 1, also the calcium-independent protein phosphatase 2A dephosphorylates I1 (Nishi et al. 1999; Svenningsson et al. 2004). Consequently, the targeted inhibition of calcium-activated calcineurin (as done by Wang et al. (2005)) does not fully impair inhibitor 1 dephosphorylation and can be implemented in the model by setting the calcium-dependent part of the calcineurin pathway to zero, *i.e.* $k_{\mathrm{CaN}} = 0$ (see Eq. 3.9). This results in a constant, calcium-independent activity dephosphorylating inhibitor 1 given by k^0_{CaN}. Fig. 3.11*A* shows the steady-state PP1 activity as a function of calcium with $k_{\mathrm{CaN}} = 0$ (red line). While bistability at calcium resting conditions is preserved, the PP1 activity is strongly suppressed for increasing calcium concentrations since the PKA-pathway activation inhibiting PP1 is not counterbalanced by calcineurin activation. As a result in the steady-state picture of phosphorylated CaMKII subunits, the 'LTD window', emerging from an elevated PP1 activity at moderate calcium levels, disappears and the 'LTP window' is extended to low calcium levels (see red line in Fig. 3.11*B*).

On the other hand, phosphorylation of inhibitor 1 is mediated by cAMP-PKA and by protein kinase G (Sahin et al. 2006) hence the same argumentation as for the calcineurin pathway can be applied to the PKA pathway. That is, blocking the calcium-stimulated cAMP-PKA signaling can be implemented in the model by setting k_{PKA} to zero. Therefore, the constant, calcium-independent activity phosphorylating inhibitor 1 is given by k^0_{PKA}. Fig. 3.11*A* (green line) shows that the steady-state PP1 activity reaches high values at high calcium concentrations in this case since calcineurin activation is not counterbalanced by PKA activation. Again, bistability at $Ca_0 = 0.1\ \mu$M is preserved with $k_{\mathrm{PKA}} = 0$ but the 'LTD window' is expanded to high calcium levels. The 'LTP window' disappears in this case (see green lines Fig. 3.11*B*). Fig. 3.11*C* shows that in both cases ($k_{\mathrm{CaN}} = 0$ and $k_{\mathrm{PKA}} = 0$) the dependence of the transition result on Δt in response to the STDP spike-pair stimulation protocol is lost. Down-to-up transitions are evoked

Figure 3.11: ***B,*** The steady-states of the phosphorylated CaMKII subunit concentration are depicted for the different realizations of the protein signaling cascade shown in panel *A* in the same color. Full lines mark stable steady-states and dashed lines depict unstable steady-states. The positions of the UP and the DOWN states at resting calcium conditions are shown for the intact protein signaling cascade case by the cross and the diamond, respectively ($CaMKII_0 = 16.67\ \mu$M, $k_{\mathrm{CaN}} = 18\ \mathrm{s}^{-1}$, see Tab. 3.1 and text for parameters). ***C,*** The average relative changes in the fraction of synapses in the UP state for the four different realizations of the protein signaling cascade are shown (colors correspond to the cases shown in panel *A* and *B*). The blue line with circles shows the same results as the blue line in Fig. 3.9 for the intact protein signaling cascade ($N = 300$, see Tab. 3.1 for other parameters).

for all Δt if calcineurin is blocked ($k_{\mathrm{CaN}} = 0$) and up-to-down transitons occur for all time lags if PKA is blocked ($k_{\mathrm{PKA}} = 0$).

We have included a calcium-stimulable adenylate cyclase in the model resulting in a calcium-activated PKA activity (see Fig. 3.3). There exist, however, types of adenylate cyclase which are not calcium-stimulable (Cooper et al. 1995; Zhabotinsky 2000 uses a constant PKA activity, for example). Fig. 3.11*A* and *B* (orange lines) show that even with a constant PKA activity, a steady-state scenario of phosphorylated CaMKII subunits similar to the one shown in Fig. 3.5*C* (reproduced in Fig. 3.11*B* by the blue lines) can still be obtained. This behavior can be understood by inspecting the steady-state PP1 activity (orange line in Fig. 3.11*A*) which exhibits a Hill function-like behavior in case of constant PKA activity. If the slope of the Hill function is steeper than the slope of the lines indicating the boundaries of the bistable region (black lines and grey shaded area in Fig. 3.11*A*), the three criteria necessary for a CaMKII steady-state scenario consistent with experiments can still be met: (i) The PP1 activity has to reside inbetween both lines indicating the boundaries of the bistable region at Ca_0 to yield two stable states at resting calcium. (ii) At intermediate calcium levels, the PP1 activity has to lie above the bistable region. This gives rise to the 'LTD window' where the DOWN state is the only steady-state of the system. (iii) At high calcium concentrations, the PP1 activity should drop below the bistable region for the 'LTP window' to emerge. Fig. 3.11*A* shows that a bump-like (blue line, calcium-dependent PKA activity) and a Hill function-like behavior (orange line, calcium-independent, constant PKA activity) fulfill the above outlined criteria (see also section 3.2.2 on page 58). Whether both exhibit potentially the same transition behavior in response to the STDP stimulation protocol remains to be investigated. Exposing the constant PKA activity case to 60 spike-pair stimulations at 1 Hz shows a low down-to-up transition probability for short, positive Δt only (see orange line in Fig. 3.11*C*). The parameters used to describe the protein signaling cascade in the constant PKA activity case are: $K_{\mathrm{CaN}} = 0.0195\ \mu\mathrm{M}$, $k^0_{\mathrm{CaN}} = 0.1\ \mathrm{s}^{-1}$, $k_{\mathrm{CaN}} = 1.53\ \mathrm{s}^{-1}$, $n_{\mathrm{CaN}} = 4$ and $k^0_{\mathrm{PKA}} = 0.00359\ \mathrm{s}^{-1}$. Note that in comparison with the values given in Tab. 3.1, K_{CaN}, k_{CaN} and n_{CaN} are changed. The procedure to obtain those parameters is the same as describe above for the case with calcium-dependent PKA activity. We fix the four intersection points of the steady-state PP1 activity with the bifurcation lines which allows us to fix four parameters. The location of the most leftward intersection point is determined by k^0_{CaN} and k^0_{PKA} which remain unchanged since this point is the same as in the original model (see Fig. 3.11*A*). The remaining three intersection points yield K_{CaN}, k_{CaN} and n_{CaN}.

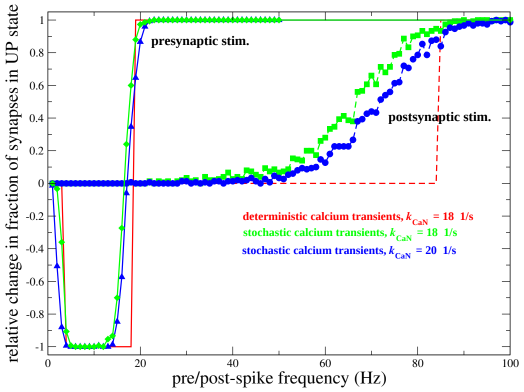

Figure 3.12: Synaptic transitions in response to purely presynaptic, or purely postsynaptic stimulation protocols. Relative change in fraction of synapses in the UP state after purely pre-, or purely postsynaptic stimulation protocols, as a function of frequency: The stimulation protocol consists of 60 pre- (full lines) or postsynaptic spikes (dashed lines) at a given frequency. Red lines: deterministic stimulation, $k_{\text{CaN}} = 18$ 1/s. Green lines with diamonds or squares: stochastic pre- or postsynaptic stimulations, respectively, with $k_{\text{CaN}} = 18$ 1/s. Blue line with triangles or circles: stochastic pre- or postsynaptic stimulations, respectively, with $k_{\text{CaN}} = 20$ 1/s. The stochastic stimulation results are averaged over $N = 300$ synapses.

3.3.4 Purely pre- or purely postsynaptic stimulation protocols

The early coincidence detection rule of synaptic plasticity formulated by Hebb (1949) required concurrent pre- and postsynaptic activity for synaptic changes to occur. This postulate has been verified by numerous experiments. Since transitions in the CaMKII system presented here depend on postsynaptic calcium elevations only, one could imagine that purely pre- or postsynaptic activity can induce such transitions without concurrent activation of the post- or the presynaptic neuron, respectively. We show in this section that this is indeed the case and that presynaptic spike-pairs evoke up-to-down transition and postsynaptic spike-pairs down-to-up transitions.

Pre- or postsynaptic stimulation at different frequencies Experiments on STDP show that pre- or postsynaptic spikes alone at the same stimulation frequency (1 Hz) do not evoke any plasticity (see for example Nevian and Sakmann 2006). To check the behavior of the model in this situation, we expose the CaMKII system to either 60 pre- or postsynaptic spikes at different frequencies and show the transitions results for the deterministic calcium transient case in Fig. 3.12 by red lines. 60 presynaptic spikes alone do not evoke any transitions at low frequencies (1-3 Hz). For presynaptic stimulations in the range 4-18 Hz up-to-down transitions occur and for frequencies equal and larger than 19 Hz the CaMKII system is switched from the DOWN to the UP state (see full red line in Fig. 3.12). The transition outcomes change dramatically if stimulation occurs exclusively with postsynaptic spikes. 60 postsynaptic spikes do not evoke transitions up until a stimulation frequency of 84 Hz (see dashed red line in Fig. 3.12). Above 85 Hz, transitions from DOWN to UP occur. Note that the spike-pairs during the STDP spike-pair stimulation protocol employed above are presented at a frequency of 1 Hz only, *i.e.* pre- or postsynaptic spikes alone at this frequency do not evoke transitions, consistent with experiments (Nevian and Sakmann 2006). Note also that the model does not incorporate frequency-dependent attenuation of EPSPs and BPAPs. Attenuation of BPAPs at high frequencies would prohibit down-to-up transitions in the purely postsynaptic protocol at any frequency.

We also expose the CaMKII system to fluctuating calcium transients evoked by pre- or postsynaptic frequency stimulations. The implementation of calcium transient noise is exactly as for STDP spike-pair protocols above. The average relative changes in the fraction of synapses in the UP state for these stimulations are shown for varying frequencies in Fig. 3.12 for $k_{\mathrm{CaN}} = 18$ and 20 1/s ($N = 300$ synapses). Presynaptic stimulations at frequencies between $\sim$ 2 and $\sim$ 16 Hz evoke a net increase of synapses in the DOWN state, while stimulation above $\sim$ 16 Hz lead to LTP transitions. Again, no up-to-down transitions are observed with postsynaptic stimulation alone, while stimulation frequencies above $\sim$ 50 Hz yield a net increase of the number of synapses in the UP state.

Pre- or postsynaptic spike-pair stimulation at different time differences In addition to known experimental stimulation protocols, we expose the CaMKII system to purely presynaptic spike-pairs or purely postsynaptic spike-pairs. Pairs of spikes with the same time difference are presented 60 times at different frequencies. We investigate the transition behavior of the model for varying time differences between the spikes in the pair and for different presentation frequencies. Note that the response of the CaMKII system to fluctuating calcium transients only is studied in this section.

The average relative changes in the number of synapses in the UP state for stimulations with purely pre- or purely postsynaptic spike-pairs are explored as a function of the time difference between the two spikes. The transition results are depicted in Fig. 3.13. Presynaptic spike-pairs lead to up-to-down transitions in a Δt range from 0 to about 500 ms for $f = 1$ Hz, while purely postsynaptic spike pairs evoke down-to-up transitions in the CaMKII system in a Δt range from 3 to 8 ms for $f = 1$ Hz. The spike-pairs have to be presented at a sufficient high frequency such that the phosphorylation changes can sum up and eventually switch the basin of attraction, *i.e.* converge to the opposite stable steady-state. Spike-pairs presented at 0.1 Hz do not lead to any transitions in the purely presy-

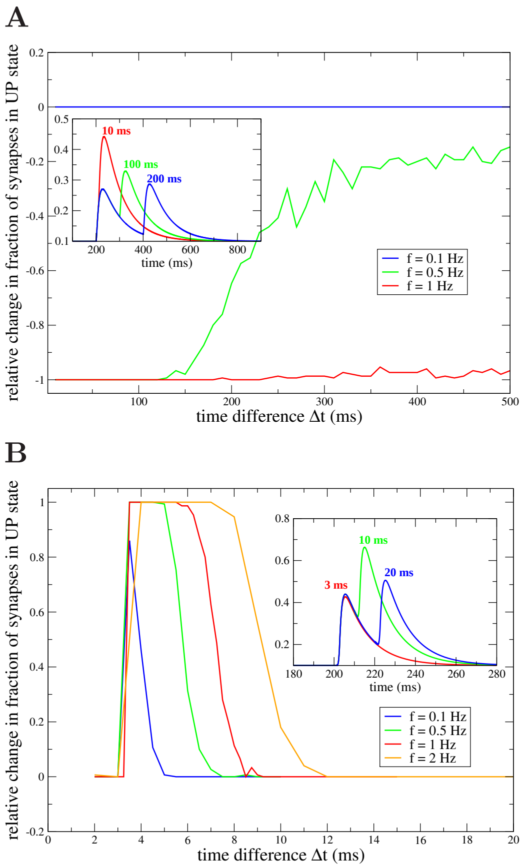

Figure 3.13: Synaptic transitions in response to purely pre-, or purely postsynaptic spike-pairs. ***A,*** The average, relative change in the fraction of synapses in the UP state in response to presynaptic spike-pairs is shown as a function of the time difference between the spikes, *i.e.* the first presynaptic spike is occurring at $t_{\text{pre}\,1}$ and the second presynaptic spike at $t_{\text{pre}\,2} = t_{\text{pre}\,1} + \Delta t$. The pre-synaptic spike-pair is presented for 60 times at three different frequencies, f: blue line: $f = 0.1$ Hz, green line: $f = 0.5$ Hz and red line: $f = 1$ Hz. The inset shows the time course of the average calcium transient for one spike-pair for three example Δts (marked in the inset). ***B,*** The average, relative change in the fraction of synapses in the UP state in response to postsynaptic spike-pairs is shown as a function of the time difference between the spikes, *i.e.* the first postsynaptic spike is occurring at $t_{\text{post}\,1}$ and the second postsynaptic spike at $t_{\text{post}\,2} = t_{\text{post}\,1} + \Delta t$. The protocol is the same as used in panel *A* except that pairs of postsynaptic spikes are presented, again at different frequencies, f: blue line: $f = 0.1$ Hz, green line: $f = 0.5$ Hz, red line: $f = 1$ Hz and orange line: $f = 2$ Hz. The inset shows three example average calcium transients evoked by one spike-pair for three different Δts (marked in the inset; $\Delta Ca_{\text{pre}} = 0.17$ μM, $k_{\text{CaN}} = 20$ 1/s, $N = 300$, see Tab. 3.1 for other parameters).

naptic stimulation protocol and yield a small down-to-up transition probability for postsynaptic spike-pairs (see blue lines in Fig. 3.13*A* and *B*). On the other hand, increasing the presentation frequency of the spike-pairs enlarges the range of Δt within which transitions occur (see Fig. 3.13*B*).

The difference in transition outcomes between presynaptic and postsynaptic spike-pair stimulation can be explained by inspecting the calcium transients evoked by both stimulation protocols. Example average calcium transients provoked by two consecutive presynaptic spikes or two consecutive postsynaptic spikes are shown in the insets of Fig. 3.13*A* and *B*, respectively. The maximum calcium amplitude attained by pairs of postsynaptic spikes is much larger than the calcium amplitude evoked by presynaptic spikes (maximum amplitude for $\Delta t = 10$ ms is ~ 0.7 μM for presynaptic spike pairs and ~ 0.45 μM for postsynaptic spike-pairs with the parameters given in Tab. 3.1). On the other hand, pairs of presynaptic spikes evoke calcium transients which last much longer than postsynaptic pairs of spikes (compare the different time scales of the insets in Fig. 3.13*A* and *B*). With respect to the calcium ranges which lead to different build-up levels of PP1 activity, the high calcium transients evoked by postsynaptic spike-pairs strongly activate the cAMP-PKA pathway and therefore suppress PP1 activity. Paired with the strong CaMKII autophosphorylation due to high calcium concentrations, this leads to down-to-up transitions in response to closely spaced postsynaptic spike-pairs. Even single postsynaptically evoked calcium transients reach calcium levels sufficiently high to activate the cAMP-PKA pathway which is the reason why continuous postsynaptic stimulation at varying frequencies does not pass through a LTD range (see Fig. 3.12 and compare the small PP1 build-up in the inset in Fig. 3.7*D* in response to the postsynaptically evoked calcium transient in the $\Delta t = -50$ ms protocol). In contrast, the long-lasting calcium transients evoked by purely presynaptic spike-pairs spend a lot of time in calcium ranges maximizing PP1 build-up. This leads to strong dephosphorylation of CaMKII by PP1 which cannot be counterbalanced by moderate autophosphorylation evoked by intermediate calcium levels, hence up-to-down transitions are evoked for closely spaced postsynaptic spike-pairs. Again, this explains also why ongoing presynaptic stimulation at different frequencies evokes LTD at low presentation frequencies before the calcium transients are adding up sufficiently at higher frequencies to activate the cAMP-PKA pathway and evoke strong autophosphorylation (this happens above $f \approx 16$ Hz in Fig. 3.12).

3.3.5 Changing individually calcium influx through NMDA-Rs and VDCCs

We want to disentangle how much the calcium influx mediated by voltage-dependent calcium channels and by NMDA receptors contribute individually to

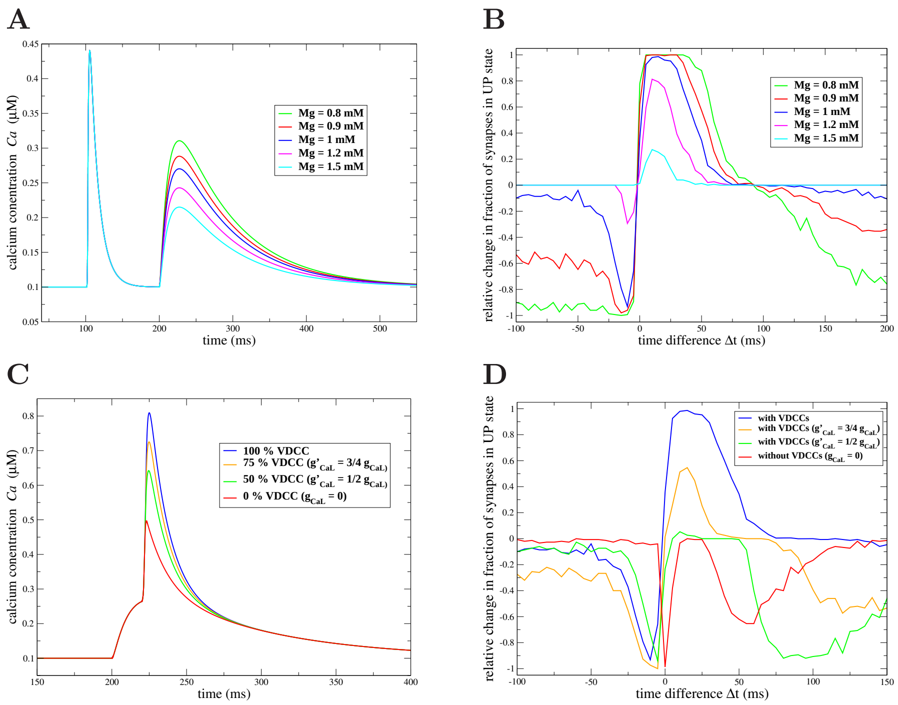

Figure 3.14: STDP transition results for varying external $[\mathrm{Mg}]^{2+}$ concentrations and different levels of VDCC inhibition. ***A,*** Average calcium transients in response to a pre- and postsynaptic spike-pair with $\Delta t = -100$ ms and different external magnesium levels: The presynaptic spike occurs at $t_{\mathrm{pre}} = 200$ ms and the postsynaptic one at $t_{\mathrm{post}} = 100$ ms. Changing the external magnesium concentration (as marked in the panel) changes the magnitude of the calcium influxes evoked by NMDA-Rs only. ***B,*** Transition results in response to stochastic STDP stimulation protocols and different external magnesium levels: The average relative change in the number of synapses in the UP state is shown as a function of Δt and for different external $[\mathrm{Mg}]^{2+}$ concentrations (as marked in the panel). ***C,*** Average calcium transients in response to a pre- and postsynaptic spike-pair with $\Delta t = 20$ ms and different inhibition levels of VDCCs: The presynaptic spike occurs at $t_{\mathrm{pre}} = 200$ ms and the postsynaptic one at $t_{\mathrm{post}} = 220$ ms. Reducing the maximal conductance of the VDCCs (as marked in the panel) decreases their contribution to the joint calcium transient at the occurrence of the postsynaptic spike. ***D,*** Transition results in response to stochastic STDP stimulation protocols and varying inhibition levels of VDCCs: The average, relative change in the number of synapses in the UP state is shown as a function of Δt for different levels of voltage-dependent calcium channel inhibition: no inhibition (blue line, same result as shown by the blue line in Fig. 3.9), 75 % inhibition (orange line), 50 % inhibition (green line) and with VDCCs completely blocked (red line, *i.e.* $g_{\mathrm{CaL}} = 0$) (see Tab. A.1). Note that all other parameters are left unchanged ($\Delta Ca_{\mathrm{pre}} = 0.17$ μM, $k_{\mathrm{CaN}} = 20$ 1/s, $N = 300$, see Tab. 3.1 for parameters).

the final transition results in response to STDP spike-pair stimulations in this section. For this purpose, the calcium current mediated by VDCCs is increasingly blocked. To allow an easier reproducibility by experiments, we change the NMDA contribution by modifying the external magnesium concentration.

Changing external magnesium concentration The external magnesium concentration governs the strength of the voltage-dependent magnesium block of the NMDA receptor. That means, the higher the external magnesium concentration, the stronger the NMDA-mediated ion current is impaired at highly depolarized membrane potentials, while in magnesium free solution the $[\mathrm{Mg}]^{2+}$ block is relieved and the NMDA-mediated current increases drastically (see Sabatini et al. (2002) investigating single spine calcium transients with and without external magnesium). The magnesium concentration under realistic conditions is ~ 1 mM (Jahr and Stevens 1990) as used so far in the model (see Eq. (A.33)). Fig. 3.14*A* shows how the calcium transient evoked by a spike-pair with $\Delta t = -100$ ms changes if the magnesium concentration is varied between 0.8 and 1.5 mM. Note that the VDCC-mediated calcium transient occurring at $t = 100$ ms is not affected by the external magnesium concentration. Fig. 3.14*B* depicts the average transition results of the CaMKII system in response to stochastic STDP stimulation protocols for different levels of external $[\mathrm{Mg}]^{2+}$. Reducing the calcium influx by augmenting $[\mathrm{Mg}]^{2+}$ decreases the LTP and the LTD amplitudes while making the LTD part of the STDP curve disappear first (compare blue, magenta and cyan lines in Fig. 3.14*B*). Increasing the NMDA-mediated calcium current leaves the LTP part at short positive Δt relatively unaffected but induces LTD transitions for all other Δt values (compare green and red lines in Fig. 3.14*B*). The latter is due to the long-lasting calcium elevation mediated by NMDA-Rs which spends a large amount of time in calcium ranges maximizing PP1 build-up and therefore evoking up-to-down transitions.

Changing the VDCC-mediated calcium current We chose to reduce progressively the maximal conductance of the voltage-dependent calcium channel (g_{CaL}, see Tab. A.1) to get an insight in its contribution to STDP outcomes in response to spike-pair stimulations. The amplitude of the VDCC-mediated calcium transient scales linearly with g_{CaL} which implies for $g_{\mathrm{CaL}} = 0$ that back-propagating action potentials do not contribute to the calcium signal any more in the absence of presynaptic activity. As long as the NMDA receptor is, however, activated by glutamate in response to a presynaptic spike (which is the case for positive Δt), the back-propagating action potential increases the NMDA-mediated current by expelling the voltage-dependent magnesium block (see Eq. (A.33)). This behavior is illustrated in Fig. 3.14*C* for three different levels of VDCC inhibition in response to spike-pairs with a time lag of $\Delta t = 20$ ms. Note the contribution of the back-propagating action potential to the NMDA-mediated component even with full impairment of VDCCs (shown by the red line).

Fig. 3.14*D* illustrates the average transition results of the CaMKII system in response to stochastic STDP stimulation protocols for different levels of VDCC inhibition. The LTP part of the STDP curve is most sensitive to the reduction in VDCC-mediated calcium influx, *i.e.* LTP transitions disappear first while the LTD range moves to positive Δt values and a second LTD range appears at large positive Δt. For $g_{\mathrm{CaL}} = 0$, down-to-up transitions have completely disappeared and up-to-down transitions occur in two distinct time lag regions: for Δt values around zero time lag and for large positive Δt values (see red line in Fig. 3.14*D*).

3.3.6 Effect of parameter changes on the behavior of the model

The model with the parameter set discussed until this point reproduces qualitatively experimentally observed transition outcomes of the STDP protocol. To get an insight in the dynamic behavior of the model, we now discuss how changing parameters affect the transition behavior. Numerical investigations of the model show that two characteristics of the CaMKII system dynamics are crucial: (i) How the level of PP1 activity at the end of the stimulation protocol depends on Δt; (ii) The time course of CaMKII autophosphorylation and dephosphorylation, and of PP1 build-up influences the number of spike pairs during the stimulation protocol necessary to evoke down-to-up- or up-to-down transitions. For simplicity, the following considerations use deterministic calcium transients, *i.e.* no noise is added.

Effect of the amplitude of calcium transients and of the calcineurin activity on the PP1 activity level. We have shown above that a peak in steady-state PP1 activity at moderate calcium concentrations occurs if the cAMP-PKA pathway activates at higher calcium concentrations than the calcineurin pathway (see Fig. 3.5*A*). Here, we address the question of how the dynamics of the PP1 activity during the stimulation protocol changes as a function of the balance between the activation of both pathways. Changing the NMDA-R mediated calcium amplitude ΔCa_{pre} and the BPAP evoked calcium response, keeping their ratio constant ($\Delta Ca_{\mathrm{post}} = 2 \cdot \Delta Ca_{\mathrm{pre}}$), and also keeping the parameters of the protein signaling cascade constant, allows us to change the balance between the activation of both pathways and to get an insight into what controls the dependence of the PP1 activity level on Δt. Fig. 3.15*A* and *C* show the PP1 activity level immediately after the presentation of *one* and *60* spike-pairs, respectively, as a function of Δt, for different values of ΔCa_{pre}. Note that the dependence of PP1 activity with respect to

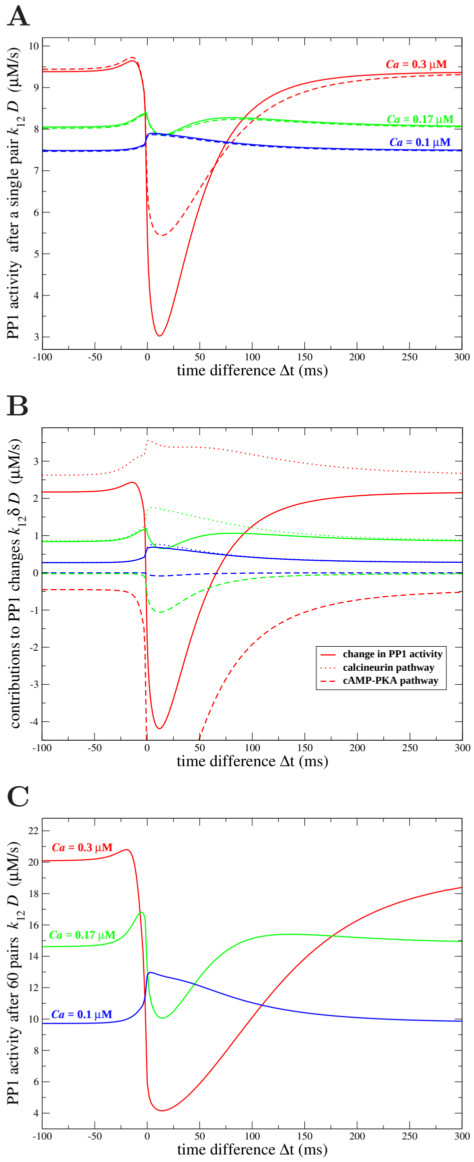

Figure 3.15: PP1 activity level after the presentation of one or 60 spike pairs as a function of Δt and the amplitude of calcium transients. ***A*,** PP1 level after the presentation of one spike pair as a function of Δt: Dashed lines: numerical integration of Eqs. (3.10) and (3.11). Full lines: approximate solution $(k_{12}(D^* + \delta D(t)))$ from numerical integration of Eq. (A.44). The three different colors correspond to three different calcium amplitudes ΔCa_{pre} as marked in the panel. ↗ *See continuation on next page.*

Δt after the presentation of one spike-pair (Fig. 3.15*A*) is qualitatively preserved after the entire stimulation protocol of 60 spike-pair presentations (Fig. 3.15*C*).

Fig. 3.15*B* represents the change in PP1 activity induced by a single spike-pair, computed from Eq. (A.44), as well as contributions of the PKA and calcineurin pathways to this change. The dashed lines in Fig. 3.15*B* show the contribution of the cAMP-PKA pathway to the change in PP1 activity (second term in the integral of Eq. (A.44)). This contribution is negative, since this pathway decreases PP1 activity. Due to the high half activation calcium concentration of $v_{\mathrm{PKA}}(C)$ (see blue line in Fig. 3.5*A*), the cAMP-PKA pathway is sensitive to high calcium elevations only. The negative contribution of this pathway increases drastically when the calcium amplitude ΔCa_{pre} increases, since the calcium transients spend more time in the range of cAMP-PKA activation. In response to the supra-linear superposition of the NMDA-R and the BPAP evoked currents at short positive time differences, this pathway ensures a low level of PP1 activity in this range.

The dotted lines in Fig. 3.15*B* show the contribution of the calcineurin pathway to the change in PP1 activity. This contribution is positive, since this pathway increases PP1 activity. The calcineurin pathway activates at lower calcium concentrations than the PKA pathway (see red line in Fig. 3.5*A*; integral of the first part of Eq. (A.44)), and therefore this pathway is sensitive to the time spent by the system at intermediate and high calcium levels. This calcineurin contribution starts to increase at negative time differences (when calcium transients induced by pre- and postsynaptic-spikes start to interact), reaches a peak close to $\Delta t = 0$, and then decreases slowly with Δt.

The sum of the two contributions yields the net change in PP1 activity (full lines of Fig. 3.15*B*). For $\Delta Ca_{pre} = 0.17$, the value chosen in the rest of the investigations on the detailed CaMKII model, the PP1 change vs Δt curve shows first a peak at negative Δt (due to increase in calcineurin activity in this range), followed by a trough at positive Δt (due to the strong increase in PKA activity in this range). There is a secondary peak of PP1 change at larger values of Δt (~ 100 ms) because calcineurin activity decays more slowly with Δt than PKA activity. However, this

Figure 3.15: ***B,*** The increase or decrease of PP1 activity induced by a single spike-pair (full lines) as well as the contributions from the calcineurin pathway (dotted lines) and the cAMP-PKA pathway (dashed lines) to this change in PP1 activity as a function of Δt: The three colors correspond to the same three different calcium amplitudes ΔCa_{pre} as marked in panel *A*. The dotted and dashed lines are obtained from numerical integration of the first and the second term in Eq. (A.44), respectively. The full lines depict the sum of both contributions and represents $k_{12} \cdot \delta D(t)$ after the presentation of the first pair of spikes (see appendix A.3 on page 181). ***C,*** Total level of PP1 activity after the *whole* stimulation protocol as a function of Δt: The depicted PP1 level is obtained from numerical integration of Eqs. (3.10) and (3.11) during stimulation protocols. The different colors correspond again to the three different calcium amplitudes as in *A* and *B* (see Tab. 3.1 for parameters, $k_{\mathrm{CaN}} = 18\ \mathrm{s}^{-1}$).

peak is smaller than the peak at negative Δt, which explains why LTD is observed at short negative Δt but not large positive ones.

Changing the size of the calcium transients potentially changes qualitatively the shape of this curve because it affects the time spent by the system in different calcium concentration ranges. For example, decreasing the size of the calcium transients weakens considerably the PKA pathway, leading to increase in PP1 activity for negative as well as positive values of Δt. On the other hand, increasing the calcium transients leads to a strengthening of the PKA pathway relative to the calcineurin pathway, leading to a much smaller peak in the PP1 change curve at short negative Δt. This peak eventually vanishes for $\Delta Ca_{\text{pre}} \geq 0.4\ \mu$M (not shown).

Since transitions are a result of an unbalance between autophosphorylation and dephosphorylation mediated by PP1, the Δt range for which transitions are evoked or prevented can therefore be controlled by means of the calcium amplitude. If the calcium amplitude is decreased in the model, no transitions are observed any more (e.g. for $\Delta Ca_{\text{pre}} = 0.15\ \mu$M). On the other hand, increasing the calcium amplitude extends the Δt range for which up-to-down and down-to-up transitions are evoked ($Ca_{\text{pre}} = 0.18\ \mu$M, LTD range: $[-21... -3]$ ms and LTP range: $[3...33]$ ms; results not shown). These predictions could be checked experimentally by changing the external calcium concentration and therefore changing the calcium influx evoked by pre- and postsynaptic spikes.

To summarize, there exists a range of ΔCa_{pre} for which the PP1 level at the end of the stimulation protocol as a function of Δt exhibits a maximum for short negative Δts and is low enough to be outweighed by autophosphorylation for short positive Δts. This is a requirement for the CaMKII system to exhibit LTD-like transitions at short negative time intervals only, *and* LTP-like transitions at short positive time intervals only. However, these qualitative features of the PP1 activation vs Δt curve are not sufficient to ensure that STDP protocol stimulations with short negative time lags lead to transitions from the UP to the DOWN state only. In addition, (i) the absolute level of PP1 activity for short negative Δt stimulations must be high enough to evoke up-to-down transitions; (ii) at the same time, the total PP1 level has to be low enough such that for large negative and large positive time lag stimulations the system remains in the UP state and that for short positive Δt protocols autophosphorylation prevails over dephosphorylation leading to down-to-up transitions. These two criteria can be met by changing the maximal calcium/calmodulin-dependent calcineurin activity k_{CaN}, which changes the amplitude of the peak of the PP1 vs Ca^{2+} steady-state curve at moderate calcium concentrations (purple lines in Fig. 3.5*B*). Consequently, this parameter allows us to control the PP1 level attained during the stimulation protocol for all Δts. In particular, the range $16.6\ \text{s}^{-1} \leq k_{\text{CaN}} \leq 18.1\ \text{s}^{-1}$ fulfills the two requirements above for simulations with deterministic calcium transients (Figs. 3.7, 3.8

and the red as well as the green lines in Fig. 3.9 and 3.12 use $k_{\mathrm{CaN}} = 18\ \mathrm{s}^{-1}$). The same arguments apply for simulations with stochastic calcium transients. The range of values of k_{CaN} for which the LTD probability for short negative Δt is larger than 0.5 and the LTD probability for large negative and large positive Δt is smaller than 0.5 is $19\ \mathrm{s}^{-1} < k_{\mathrm{CaN}} < 21\ \mathrm{s}^{-1}$ ($k_{\mathrm{CaN}} = 20\ \mathrm{s}^{-1}$ is used in all stochastic STDP stimulations presented here).

Effect of kinetics of autophosphorylation and dephosphorylation on the number of spike-pair presentations needed for transitions. The autophosphorylation rates k_6, k_7, k_8, the maximal dephosphorylation rate k_{12} and the total PP1 concentration D_0 determine the velocity of autophosphorylation as well as dephosphorylation dynamics of CaMKII and the dynamics of the PP1 response during exposure to the STDP protocol. We introduce scaling parameters R and Q such that varying R and Q does not change the steady-state behavior of the CaMKII system (see Fig. 3.5*B* and *C*) nor the maximum PP1 activity reached during the stimulation but only the dynamics of the system. Both scaling parameters are varied extensively in order to investigate their impact on the transition behavior of the model, *i.e.* $0.002 \leq R \leq 2$ and $0.083 \leq Q \leq 1.67$.

R is chosen such as to control the dephosphorylation kinetics, while leaving the PP1 activity, given by the product $k_{12} \cdot D$, constant. This leaves the steady-state behavior intact since it depends on this product only. Hence, in the following simulations, k_{12} and D_0 are replaced by $k'_{12} = k_{12} \cdot R$ and $D'_0 = D_0/R$, where k_{12} and D_0 are the 'control' parameters listed in Tab. 3.1*B*. R controls how fast the dephosphorylation dynamics responds to calcium transients, since the PP1 build-up during the presentation of the stimulation protocol and the decay dynamics thereafter depends on the value of D but not on k_{12} (see Eq. (A.41) in appendix A.3 on page 181). Fig. 3.16*A* shows the PP1 activity time course for three different values of R during and after the STDP stimulation protocol with $\Delta t = 15$ ms, *i.e.* for $R = 0.002$, 0.078 and 1.

Q scales the autophosphorylation rates k_6, k_7 and k_8 together with the maximal dephosphorylation rate k_{12} as $k'_{\mathrm{x}} = Q \cdot k_{\mathrm{x}}$ (with x= $6, 7, 8$ and 12), where all the rates k_{x} take the values listed in Tab. 3.1*B*. This corresponds to a rescaling of the y-axis in Fig. 3.5*B*, *i.e.* the points of intersection between the bistable range (red shaded areas) and the PP1 activity (purple lines) are kept fixed and therefore the steady-state concentration of phosphorylated CaMKII subunits (Fig. 3.5*C*) is left unchanged. We illustrate the impact of changes in Q on the dynamics of S_{active} in Fig. 3.16*B* for three different Qs and $R = 1$ as well as three different Rs and $Q = 1$. Since the temporal evolution of S_{active} is a result of the competing autophosphorylation and dephosphorylation progress, the choice of *both* scaling parameters influences S_{active} dynamics (see Fig. 3.16*B*). Note that $R = 1$ and

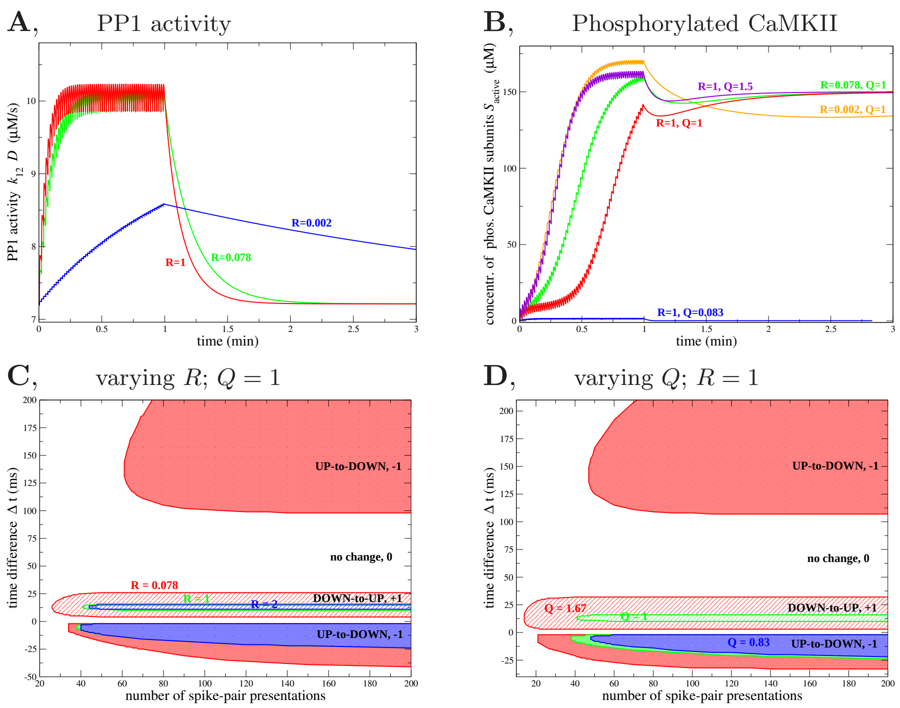

Figure 3.16: Impact of the kinetics of PP1 activity and CaMKII phosphorylation on the number of spike-pair presentations leading to transitions. ***A & B,*** Time course of PP1 activity ($k_{12}D$) (A) and phosphorylated CaMKII subunit concentration (B) during and after the STDP stimulation protocol for different values of R and Q (deterministic stimulation protocol, 60 spike pairs with $\Delta t = 15$ ms). The build-up of PP1 activity ($k_{12} \cdot D$) is shown in panel A for $R = 0.002$ (blue line), $R = 0.078$ (green line) and $R = 1$ (red line; same curve as in Fig. 3.7*C*). Q has no impact on PP1 dynamics. The time course of phosphorylated CaMKII subunit concentration is depicted in B for five sets of values of R and Q (indicated close to the corresponding curves). ***C & D,*** The impact of the number of spike-pair presentations and of R and Q on the Δt ranges for which transitions occur is depicted for deterministic stimulation protocols. White region: no change (relative change in fraction of synapses in the UP state is 0); diagonally striped regions: down-to-up transitions (relative change in fraction of synapses in the UP state is +1); shaded regions: up-to-down transitions (relative change in fraction of synapses in the UP state is −1). In each case, down-to-up - and up-to-down transition regions in the same color correspond to the same choice of R (panel *C*) or Q (panel *D*). All the cases in panel C use $Q = 1$ paired with: red regions: $R = 0.078$; green regions: $R = 1$; and blue regions: $R = 2$. In panel D: blue regions: $Q = 0.83$ (no down-to-up transitions); green regions: $Q = 1$; and red regions: $Q = 1.67$. $R = 1$ is utilized in all cases in panel D, *i.e.* the green regions in panel C and D are identical (see Tab. 3.1 for parameters, $\Delta Ca_{\mathrm{pre}} = 0.17$ μM, $k_{\mathrm{CaN}} = 18$ s^{-1}).

$Q = 1$ is used everywhere in the investigations on the extensive CaMKII model, except for the results discussed in this section and shown in Fig. 3.16.

Increasing R accelerates the convergence of PP1 towards a steady-state oscillation. In Fig. 3.16*A*, this happens after ~ 20 and ~ 30 spike-pair presentations for $R = 1$ and $R = 0.078$, respectively. This constant value is not attained during the 60 s stimulation protocol with $R = 0.002$ at all. Reaching such a steady-state behavior is needed for the system to be robust to changes in the number of spike-pair presentations. Indeed, if the PP1 activity is still in the raising phase at the end of the stimulation protocol (as in the case $R = 0.002$, see blue line in Fig. 3.16*A*), then more spike-pair presentations would lead to a higher PP1 level and therefore to up-to-down transitions for a drastically wider range of Δt values if the system is initially in the UP state. On the other hand, less spike-pair presentations would not give rise to any transitions at all. Fig. 3.16*C* and *D* give an insight in how the Δt ranges for which transitions occur depend on R, Q and the number of spike-pair presentations. For $R = 1$ and $Q = 1$ ($k_{\mathrm{CaN}} = 18\ \mathrm{s}^{-1}$, $\Delta Ca_{\mathrm{pre}} = 0.17$), the range of Δt values evoking down-to-up transitions saturates beyond 50 spike-pair presentations, whereas the range resulting in up-to-down transitions becomes essentially insensitive to the number of spike pair presentations beyond ~ 150 spike-pairs (see green regions in Fig. 3.16*C* or *D*; both depict the same results). Increasing R further does not lead to any significant changes in the ranges of transitions compared to the case $R = 1$ (compare green and blue regions in Fig. 3.16*C* for $R = 1$ and $R = 2$, respectively, and see appendix A.3 on page 181). Decreasing R slows down the convergence towards a stable range of time lags evoking down-to-up or up-to-down transitions (compare $R = 1$ - green regions - and $R = 0.078$ - red regions - cases in Fig. 3.16*C*). This is due to the slower convergence of PP1 activity to its oscillatory behavior around a constant value during the stimulation protocol (see Fig. 3.16*A*). The examples in Fig. 3.16*A* show furthermore that the smaller R, the slower the decay of PP1 activity after the stimulation protocol. When $R = 0.078$ the PP1 dephosphorylation activity decay after the stimulation protocol is so slow that large positive time lag stimulations evoke transitions from UP to DOWN (see upper red shaded region in Fig. 3.16*C*, $Q = 1$, $k_{\mathrm{CaN}} = 18\ \mathrm{s}^{-1}$, $\Delta Ca_{\mathrm{pre}} = 0.17\ \mu\mathrm{M}$). Up-to-down transitions at large positive time lags appear in the range up until 200 spike-pair presentations for $R \lesssim 0.202$.

Similar arguments hold for the scaling parameter Q that controls CaMKII autophosphorylation and dephosphorylation dynamics. Indeed, the degree of CaMKII subunit phosphorylation should also reach a steady oscillation around a constant value during the presentation of spike pairs, for the system to exhibit robust behavior (see the ($R = 1, Q = 1.5$) and the ($R = 1, Q = 0.083$) cases in Fig. 3.16*B*). The larger the Q, the faster autophosphorylation (through an increase of k_6, k_7 and k_8; Fig. 3.2*C*, *D* and *E*) and dephosphorylation (through an increase of k_{12}, Eq. (3.6)) proceed. Therefore, less spike-pair presentations are required to evoke transitions and the Δt ranges leading to down-to-up- or up-to-down transitions saturate at smaller numbers of spike-pair presentations (see Fig. 3.16*D*). For $Q = 0.083$, no transitions are observed at all in the range from 1 to 200 spike pair presentations (see blue line in Fig. 3.16*B*). Down-to-up transitions appear after 60 spike-pair presentations for $Q \gtrsim 1$ ($k_{\mathrm{CaN}} = 18\ \mathrm{s}^{-1}$, $R = 1$) whereas up-to-down transitions occur at lower Q values (see $(R = 1, Q = 0.83)$ case in Fig. 3.16*D*). For $Q \gtrsim 1.25$ dephosphorylation progress wins over autophosphorylation and leads to up-to-down transitions for large positive time lags (see red regions for $(R = 1, Q = 1.67)$ in Fig. 3.16*D*).

4

The two-subunit CaMKII system

The number of functionally interacting subunits in a CaMKII holoenzyme cluster is most likely six and one CaMKII holoenzyme combines two such clusters (Bradshaw et al. 2002; Hudmon and Schulman 2002; Rosenberg et al. 2005). This is why we have been focusing on the six subunit model until this point. In this chapter, a two subunit model is investigated. The two subunit model allows for some simplifications which are not possible in the more realistic case with six subunits. The two subunit model possesses the minimal number of subunits required to account for the cooperativity of autophosphorylation and the saturation of dephosphorylation. Hence, the two subunit model shares basic characteristics with the six subunit model. Despite the fact that two subunits are accounted for only, the consideration of this simplified model gives some insights which apply in return for more realistic models.

The steady-state investigations of the CaMKII model with two functionally subunits follow the lines of the six subunit case presented in the previous chapter. However, the elevated PP1 activity at moderate calcium concentrations is not described by taking into account the entire protein signaling cascade. Its bump-like behavior with respect to calcium is phenomenologically reproduced. Together with the cooperative autophosphorylation of CaMKII this assures: bistability at resting calcium concentration, a 'LTD window' at intermediate calcium levels and a 'LTP window' at high calcium concentrations.

The model generating calcium transients in response to pre- and postsynaptic spikes is drastically simplified. Only the ionic currents mediating calcium ions are accounted for. We show that experimental plasticity results can be reproduced in response to STDP stimulation protocols (Magee and Johnston 1997; Markram et al. 1997; Bi and Poo 1998), presynaptic stimulation at different frequencies (Dudek and Bear 1992) and presynaptic stimulation paired with postsynaptic holding potentials (Artola et al. 1990; Ngezahayo et al. 2000). With the same parameter set across different protocols, we can show that experimental protocols which evoke LTD in experiments maximize PP1 build-up in the model. This in turn switches the CaMKII system from the UP to the DOWN state. Protocols shown to evoke experimentally LTP suppress PP1 activity and favor calcium-triggered autophosphorylation in the model which results in down-to-up transitions.

4.1 The simplified model of the two-subunit CaMKII system

Since the transition behavior of the CaMKII system is a result of an unbalance between CaMKII autophosphorylation and dephosphorylation mediated by PP1, we seek to describe the dynamics of the system by two differential equations only: one accounting for the CaMKII phosphorylation level and one accounting for the PP1 activity.

4.1.1 The CaMKII protein phosphorylation level

We start from the model equations describing CaMKII autophosphorylation and dephosphorylation in the two subunit ring. The descriptions of intersubunit autophosphorylation and dephosphorylation of subunits is implemented in the same way as for the six subunit case, *i.e.* the equations below are the equivalent to Eqs. (A.1)-(A.14) but for two subunits. The time course of phosphorylation and dephosphorylation in the two-subunit ring is given by

$$\dot{S}_0 = -2k_6\gamma^2 S_0 + k_{10}S_1, \tag{4.1}$$

$$\dot{S}_1 = 2k_6\gamma^2 S_0 - k_7\gamma S_1 - k_{10}S_1 + 2k_{10}S_2, \tag{4.2}$$

$$\dot{S}_2 = k_7\gamma S_1 - 2k_{10}S_2. \tag{4.3}$$

S_i refers to the concentration of the three ($i = 0, 1, 2$) macroscopic distinguishable activation states of the two-subunit CaMKII ring. The subscript i gives furthermore the number of phosphorylated subunits, *i.e.* S_1 refers to the concentration of CaMKII rings with one phosphorylated subunit. k_6 and k_7 are the autophosphorylation rates of the initiation step and subsequent phosphorylation steps, respectively (see Fig. 3.2*C*, *D* and *E*). γ is the probability that a dephosphorylated subunit is bound to the calcium/calmodulin complex. k_{10} is the PP1-dependent dephosphorylation rate given by $k_{10} = k_{12}D/(K_{\mathrm{M}} + \rho)$, where k_{12} is the maximal dephosphorylation rate and K_{M} is the Michaelis constant (see Eq. (3.6)). Note that dephosphorylation of CaMKII by PP1 is described according to the Michaelis-Menten scheme. Since the total concentration of phosphorylated subunits, ρ, in k_{10} is given by $\rho = S_1 + 2S_2$, the system of differential equations

(Eqs. (4.1)-(4.3)) is not linear. Note that, as in the six subunit model $k_7 = k_8$ is used, which simplifies $k_7\gamma\gamma^* + k_8\gamma(1-\gamma^*) = k_7\gamma$.

The total concentration of phosphorylated subunits is given by $\rho = S_1 + 2S_2$, which yields together with with Eq. (4.2) and (4.3)

$$\dot{\rho} = 2k_6\gamma^2 S_0 + k_7\gamma(2(Z - S_0) - \rho) - k_{10}\rho. \tag{4.4}$$

$2CaMKII_0 = Z$ is the total concentration of 2 subunit rings and is introduced by the protein mass conservation $Z = S_0 + S_1 + S_2$. Note that each CaMKII holoenzyme comprises two subunit clusters, *i.e.* the subunit cluster concentration is twice the total CaMKII concentration.

We seek for a simplification which allows to describe the dynamics of the concentration of phosphorylated subunits, $\rho(t)$, by a single differential equation. This can be done by assuming that S_2 reaches its steady-state immediately in response to calcium transients, *i.e.* $\dot{S}_2 = 0$. Due to the strong cooperativity of autophosphorylation, *i.e.* once a subunit is phosphorylated subsequent phosphorylation steps happen much faster, it is reasonable to assume that the second phosphorylation step (from S_1 to S_2) is fast compared to the initiation step (from S_0 to S_1). Assuming $\dot{S}_2 = 0$ yields the following expression for S_0 from Eq. (4.3) using $\rho = S_1 + 2S_2$ and $Z = S_0 + S_1 + S_2$

$$S_0 = \frac{(k_7\gamma + k_{10})(2Z - \rho) - k_{10}\rho}{2k_7\gamma + 2k_{10}}. \tag{4.5}$$

Plugging this expression in Eq. (4.4) yields

$$\dot{\rho} = 2k_6\gamma^2 Z - \frac{(k_{10}^2 + 2k_6k_{10}\gamma^2 + k_6k_7\gamma^3)\rho}{k_7\gamma + k_{10}}. \tag{4.6}$$

S_2 being in equilibrium ($\dot{S}_2 = 0$) is the only assumption made to get this single differential equation describing the time course of the phosphorylated CaMKII subunit level in the two subunit model (Eq. (4.6)). This assumption does not affect the steady-state properties of ρ with respect to calcium, *i.e.* the steady-states of Eq. (4.6) reproduce exactly the steady-states of the full two subunit model given by setting Eqs. (4.1)-(4.3) to zero, *i.e.* $\dot{S}_0 = \dot{S}_1 = \dot{S}_2 = 0$. Setting Eq. (4.6) to zero yields the steady-state value of ρ given by a cubic equation

$$\begin{aligned} 0 = \quad & \rho^3 + \rho^2 2\left(\tfrac{k_{12}D}{k_7\gamma} + K_{\mathrm{M}} - Z\right) \\ & +\rho\left(\tfrac{(k_{12}D)^2}{k_6k_7\gamma^3} + 2K_{\mathrm{M}}\tfrac{k_{12}D}{k_7\gamma} + {K_{\mathrm{M}}}^2 - 2Z(\tfrac{k_{12}D}{k_7\gamma} - 2K_{\mathrm{M}})\right) \\ & -2K_{\mathrm{M}}Z\left(\tfrac{k_{12}D}{k_7\gamma} + K_{\mathrm{M}}\right), \end{aligned} \tag{4.7}$$

in which γ and also the active PP1 concentration, D, are calcium-dependent. However, we treat the PP1 activity ($k_{12} \cdot D$) like a calcium-independent, constant parameter in this section.

Bifurcation points Here, we investigate the steady-states of the phosphorylated CaMKII concentration (ρ) in the two subunit model in more detail. Considering the limit of high phosphorylated subunit concentrations, *i.e.* $K_M \ll \rho$ ($K_M = 0.4$ μM and $\rho_{max} = 200$ μM with $CaMKII_0 = 50$ μM), simplifies the dephosphorylation rate as follows

$$k_{10} = \frac{k_{12}D}{K_M + \rho} \approx \frac{k_{12}D}{\rho}. \tag{4.8}$$

Therefore, the cubic equation describing the steady-states of ρ (Eq. (4.7)) simplifies to

$$0 = \rho^3 + \rho^2 2\left(\frac{k_{12}D}{k_7\gamma} - Z\right) + \rho\left(\frac{k_{12}D}{k_7\gamma}\left(\frac{k_{12}D}{k_6\gamma^2} - 2Z\right)\right), \tag{4.9}$$

where one solution for the steady-states of ρ becomes $\rho_1 = 0$ μM and the two remaining solutions are given by the quadratic equation

$$\rho_{2/3} = Z - \frac{k_{12}D}{k_7\gamma} \pm \sqrt{\left(Z - \frac{k_{12}D}{k_7\gamma}\right)^2 - \frac{k_{12}D}{k_7\gamma}\left(\frac{k_{12}D}{k_6\gamma^2} - 2Z\right)}. \tag{4.10}$$

At the left-hand boundary of the bistable region the simplification is valid since the concentration of phosphorylated subunits ρ is high. This point is given by $\rho_2 = \rho_3$, which yields the following expression

$$\left(Z - \frac{k_{12}D}{k_7\gamma}\right)^2 = \frac{k_{12}D}{k_7\gamma}\left(\frac{k_{12}D}{k_6\gamma^2} - 2Z\right). \tag{4.11}$$

In the PP1 activity - calcium concentration plane, the left-hand boundary of the bistable region is therefore given by

$$D = \frac{\gamma Z}{k_{12}\sqrt{\frac{1}{k_6 k_7 \gamma} - \frac{1}{k_7{}^2}}}. \tag{4.12}$$

On the other hand, the right-hand boundary of the bistable region can be approximated by the intersection of ρ_3 with the steady-state $\rho_1 = 0$, *i.e.* by setting ρ_3 to zero. In the PP1 activity - calcium concentration plane this gives

$$D = \frac{2k_6\gamma^2 Z}{k_{12}}. \tag{4.13}$$

It is easy to see that the right-hand boundary of the bistable region is determined by the probability of the initiation step to occur, expressed by $k_6\gamma^2$. The higher the probability of the initiation step to occur, the more the right-hand boundary moves to lower calcium concentrations for the same PP1 activity level. Attention should be drawn to the fact that the simplified expression for the right-hand boundary is likely to deviate from the right-hand boundary in the two subunit model (given by the exact solution of Eq. (4.7)) since the assumption $K_{\mathrm{M}} \ll \rho$, used to derive Eq. (4.13), does not hold at low ρ concentration levels. The bifurcation points as given by Eq. (4.7) are compared with the approximative expressions for the left-hand (Eq. (4.12)) and the right-hand bifurcation point (Eq. (4.13)) in Fig. 4.1*A*.

4.1.2 PP1 dephosphorylation activity

The description of the time course of CaMKII subunit phosphorylation could be simplified to one differential equation (Eq. (4.6)) in the previous section. It has been shown in the detailed six-subunit model that the overall dynamics of the CaMKII phosphorylation level is the result of the interplay between CaMKII phosphorylation and dephosphorylation mediated by PP1, the latter showing a time course with approximately the same time constant as the phosphorylation level of CaMKII subunits. In the full model, the PP1 dynamics is given by two differential equations describing the PP1 and the inhibitor 1 dynamics (Eqs. (3.10) and (3.11)). Again, we seek to simplify the PP1 dynamics description to one differential equation capturing the basic features of the full CaMKII model with six subunits.

Starting from the estimation of PP1 build-up (Eq. (A.43)) during the stimulation protocol we have

$$\delta D(t) = A_2 e^{\lambda_{\mathrm{fast}} t} \int_0^t e^{-\lambda_{\mathrm{fast}} \tau} S(\tau) d\tau + B_2 e^{\lambda_{\mathrm{slow}} t} \int_0^t e^{-\lambda_{\mathrm{slow}} \tau} S(\tau) d\tau, \qquad (4.14)$$

with $A_2 = -k_{13} D^* / (\lambda_{\mathrm{fast}} - \lambda_{\mathrm{slow}})$, $B_2 = k_{13} D^* / (\lambda_{\mathrm{fast}} - \lambda_{\mathrm{slow}})$ and $S(\tau) = (-\delta v_{\mathrm{CaN}}(\tau) I^* + \delta v_{\mathrm{PKA}}(\tau) I_0)$. See appendix A.3 on page 181 for more details. The time constants are given by

$$\begin{aligned} \lambda_{\mathrm{fast}} &= -(k_{13}(D^* + I^*) + k_{-13}), && (4.15) \\ \lambda_{\mathrm{slow}} &= -\frac{(k_{13} I^* + k_{-13}) v_{\mathrm{CaN}}}{k_{13}(D^* + I^*) + k_{-13}}. && (4.16) \end{aligned}$$

Since the first term in Eq. (4.14) decays fast, we neglect its contribution to PP1 build-up and can write

$$\dot{D} = \lambda_{\mathrm{slow}} D + B_2 S(t), \qquad (4.17)$$

from the right-hand term in Eq. (4.14).

Using the steady-state expression for inhibitor 1 concentration $I^* = I_0 v_{\mathrm{PKA}} / v_{\mathrm{CaN}}$ and $\delta v_{\mathrm{CaN}} = v_{\mathrm{CaN}} - k^0_{\mathrm{CaN}}$, Eq. (4.17) becomes

$$\dot{D} = \lambda_{\mathrm{slow}} D + \frac{k_{13} D^*}{\lambda_{\mathrm{fast}} - \lambda_{\mathrm{slow}}} I_0 v_{\mathrm{PKA}} \left(\frac{k^0_{\mathrm{CaN}}}{v_{\mathrm{CaN}}} - \frac{k^0_{\mathrm{PKA}}}{v_{\mathrm{PKA}}} \right). \qquad (4.18)$$

If we furthermore take into account that $\lambda_{\text{fast}} \gg \lambda_{\text{slow}}$ and make the simplifications

$$C_1 = \left|\frac{k_{13} D^* I_0}{\lambda_{\text{fast}}}\right| = \text{const.}, \tag{4.19}$$

$$\lambda_{\text{slow}} = -\frac{(k_{13} I^* + k_{-13}) v_{\text{CaN}}}{k_{13}(D^* + I^*) + k_{-13}} \approx -C_2 v_{\text{CaN}} = -\text{const.} v_{\text{CaN}}, \tag{4.20}$$

we get

$$\dot{D} = -C_2 v_{\text{CaN}} D + C_1 v_{\text{PKA}} \left(\frac{k^0_{\text{PKA}}}{v_{\text{PKA}}} - \frac{k^0_{\text{CaN}}}{v_{\text{CaN}}}\right), \tag{4.21}$$

with the steady-state for D given by

$$D_{\text{steady-state}} = \frac{C_1}{C_2} \frac{v_{\text{PKA}}}{v_{\text{CaN}}} \left(\frac{k^0_{\text{PKA}}}{v_{\text{PKA}}} - \frac{k^0_{\text{CaN}}}{v_{\text{CaN}}}\right). \tag{4.22}$$

v_{CaN} and v_{PKA} are characterized by

$$v_{\text{x}}(C) = k^0_{\text{x}} + \frac{k_{\text{x}}}{1 + (\frac{K_{\text{x}}}{C})^{n_{\text{x}}}}, \tag{4.23}$$

with x=CaN,PKA (see Eq. (3.9)). C denotes the active, calcium-dependent calmodulin concentration.

The characteristics of the PP1 dynamics and steady-state do not change considerably if the calcium/calmodulin dependence of the PKA activity is neglected, *i.e.* $v_{\text{PKA}}(Ca) \equiv k^0_{\text{PKA}}$ (see below). If furthermore C_1 and k^0_{PKA} are combined, *i.e.* $C_1 \to C_1 k^0_{\text{PKA}}$, and a calcium-independent steady-state activity D_0 is introduced, the temporal evolution of PP1 becomes

$$\dot{D} = -C_2 v_{\text{CaN}}(D - D_0) + C_1 \left(1 - \frac{k^0_{\text{CaN}}}{v_{\text{CaN}}}\right), \tag{4.24}$$

with the steady-state given by

$$D_{\text{steady-state}} = D_0 + \frac{C_1}{v_{\text{CaN}} C_2} \left(1 - \frac{k^0_{\text{CaN}}}{v_{\text{CaN}}}\right). \tag{4.25}$$

Provided that v_{CaN} has a positive derivative with respect to calcium, which is the case since it is described by a Hill equation (Eq. 4.23), Eq. (4.25) has a maximum at $v_{\text{CaN}} = 2k^0_{\text{CaN}}$ leading to the bump of PP1 activity at intermediate calcium concentrations. This bump of PP1 activity ensures that calcium elevations to intermediate levels enhance PP1 activity and eventually lead to up-to-down transitions, *i.e.* LTD.

Note, the fact that the calcium/calmodulin dependence of the PKA activity (v_{PKA}) becomes redundant is a result of the simplification procedure. The detailed model requires this dependence in order to produce elevated PP1 activity at intermediate calcium concentrations. This can be seen by inspecting the derivative of the PP1 steady-state concentration ($D_{\mathrm{steady-state}}$) with respect to calcium in the detailed model. If $v_{\mathrm{PKA}} = v^0_{\mathrm{PKA}}$ is assumed, this expression is given by

$$\frac{d(D_{\mathrm{steady-state}})}{d(Ca)} = \frac{D_0}{1 + I_0 \frac{k_{13}}{k_{-13}} \frac{v^0_{\mathrm{PKA}}}{v_{\mathrm{CaN}}}} I_0 \frac{k_{13}}{k_{-13}} \frac{v^0_{\mathrm{PKA}}}{v^2_{\mathrm{CaN}}} \frac{d(v_{\mathrm{CaN}})}{d(Ca)}, \tag{4.26}$$

which has no null if the derivative of v_{CaN} with respect to calcium is always positive. As pointed out above, this is the case if v_{CaN} is given by Eq. (4.23).

To summarize, the temporal dynamics of the CaMKII phosphorylation level of a two-subunit holoenzyme and the PP1 activity dephosphorylating CaMKII could be reduced to a differential equation system with two equations, *i.e.* Eq. (4.6) and (4.24), respectively. In comparison, the description of the de- and phosphorylation progress in the model of the six-subunit CaMKII ring requires 13 differential equations (Eqs. (A.1)-(A.14)) and the PP1 activity is determined by two differential equations (Eqs. (3.10) and (3.11)). S_2 has been assumed to be in quasi steady-state to derive a single equation describing the phosphorylation level dynamics in the two-subunit model (Eq. (4.6)). The PP1 activity description has been simplified in an effective way, while preserving the bump-like steady-state behavior and approximately the dynamics of PP1.

Parameters of the simplified two-subunit model The parameters of the simplified two-subunit model listed in Tab. 4.1A directly correspond to parameters used in the six-subunit model. Their values are left unchanged and are determined either by experiments (K_1, K_2, K_3, K_4, CaM_0, $CaMKII_0$, K_5, K_{CaN}, n_{CaN}) or take the values used in the six-subunit model (k_6, k_{12}). Note that $CaMKII_0$ has been increased in order to keep the total concentration of subunits constant, *i.e.* $\rho_{\max} = S_{\mathrm{active\ max}} = 200\ \mu$M.

Not all the parameters of the six-subunit model are directly assigned to parameters of the simplified two-subunit model (see parameters in Tab. 4.1B). Fig. 3.4A shows that the bistable range has a smaller extent in the case of two-subunit as compared to the six-subunit case. k_7 is increased with respect to k_6 in order to compensate for this and expand the bistable range in the simplified two-subunit model (see Fig. 4.1A). Since the derivation of the PP1 dynamics involves many simplifications, we do not strive to map directly the parameters of the six-subunit model describing PP1 behavior to the simplified model parameters. C_2, D_0, k^0_{CaN} and k_{CaN} are adjusted in order to obtain the 'LTD' and the 'LTP' windows at specific intervals of calcium concentrations (see Fig. 4.1A). Choosing the four intersection points of the PP1 activity with the boundaries of the bistable region (see Fig. 4.1A) allows to determine these four parameters. C_1 is used to adjust the PP1 level attained during the exposure to stimulation protocols (see Fig. 4.3 and

A, Parameters taken without changes from references and the six-subunit model

Parameter	Definition	Value	Reference
K_1	dissociation constants of calcium binding to calmodulin	0.1 μM	(Linse et al. 1991)
K_2		0.025 μM	
K_3		0.32 μM	
K_4		0.4 μM	
CaM_0	total calmodulin concentration	0.1 μM	see text
$CaMKII_0$	total CaMKII concentration	50 μM	(Strack et al. 1997)
K_5	diss. const. of dephosph. subunit and C	0.1 μM	(Meyer et al. 1992)
k_6	probability of phos. step 1, Fig. 3.2C	6 s^{-1}	six-subunit model
K_{M}	Michaelis constant of dephosphorylation	0.4 μM	(Zhabotinsky 2000)
k_{12}	maximal dephos. rate	6000 s^{-1}	six-subunit model
K_{CaN}	calcineurin half activity concentration	0.05 μM	(Stemmer and Klee 1994)
n_{CaN}	calcineurin Hill coefficient	4	

B, Parameters determined by the simplified two-subunit model

Parameter	Definition	Value	Comment
k_7	probability of phos. step 2 and 3, Fig. 3.2D, E	9.6 s^{-1}	used to increase bistable range
C_1	constant 1	0.119, 0.123 μM/s	changes PP1 level during stim.
C_2	constant 2	10	constrain the
D_0	PP1 base activity	$7.4 \cdot 10^{-4}$ μM	location of the
k^0_{CaN}	calcineurin activity	0.4 s^{-1}	'LTP' and 'LTD' windows
k_{CaN}	max. Ca^{2+}/CaM-dep. calcineurin activity	20 s^{-1}	in the steady-state scenario

Table 4.1: CaMKII phosphorylation - PP1 activity parameters for the simplified two-subunit model

4.4). It has a similar role as k_{CaN} in the detailed CaMKII model and is therefore adjusted in the same way (see above).

Scaling parameters R and Q To change the dynamics of the de- and autophosphorylation progress as well as the PP1 response to calcium transients, we introduce scaling parameters R and Q. The effect of both scaling parameters is equivalent to the effect of their counterparts introduced in the six-subunit model (see 3.3.6 on page 88 for more details). As in the six-subunit model, changes of these two parameters do not change the steady-state picture. R is chosen to keep the product of k_{12} and D constant but to rescale k_{12}, D_0 and C_2 as $k'_{12} = k_{12} \cdot R$, $D'_0 = D_0/R$ and $C'_2 = C_2 \cdot R$. Note that C_2 has to be rescaled as well in order to scale uniformly the steady-states of the PP1 activity (see Eq. (4.25)). Q scales the autophosphorylation rates k_6 and k_7 as well as the dephosphorylation rate k_{12} as $k'_{\mathrm{x}} = k_{\mathrm{x}} \cdot Q$ (with x $= 6, 7, 12$). All the rates and constants take the values given in Tab. 4.1. $R = 1$ and $Q = 1$ is used for the steady-state investigations (section below), whereas $R = 0.2$ and $Q = 8.3$ are employed to reproduce experimental plasticity results (described from section 4.3.2 on).

Note that Q is larger compared to the detailed six-subunit model where $Q = 1$. Since we use smaller calcium amplitudes in response to pre- and postsynaptic stimulation in the simplified model ($\Delta Ca_{\mathrm{pre}} = 0.17$ μM in the detailed six-subunit model, $\Delta Ca_{\mathrm{pre}} = 0.12$ μM in the simplified two-subunit model), autophosphorylation progresses more slowly. Q is used to compensate for this.

4.2 Steady-states of the two-subunit model

A similar approach as for the six-subunit model is chosen to investigate the behavior of the simplified two-subunit model. This allows to directly compare the steady-states and the dynamics of both models. At first, the steady-state behavior of the simplified two-subunit model is studied. In other words, the steady-states of the CaMKII phosphorylation level (Eq. (4.6)) and of the PP1 activity (Eq. (4.24)) are explored with respect to the calcium concentration and the dephosphorylation activity.

It has been shown in the previous chapter that the extent of the bistable range with respect to calcium becomes smaller with decreasing number of subunits in the cluster of interacting subunits (see Fig. 3.4*A*). Naturally, the two-subunit model of CaMKII has a smaller range of bistability since the saturation of the per-subunit dephosphorylation rate is reduced in comparison with the six-subunit model. However, increasing the rates of the autophosphorylation steps shown in Fig. 3.2*D* and *E* (given by k_7 and k_8) allows to increase the bistable range of the two-subunit model such that the range matches approximately the range of bistability in the six-subunit model. Both ranges are depicted in the PP1 activity - calcium concentration plane in Fig. 4.1*A* (simplified two-subunit model: green shaded region; six-subunit model: red lines). Fig. 4.1*A* depicts furthermore the boundaries of the bistable region as given by the approximative Eqs. (4.12) and (4.13) (shown by the black lines). As discussed above, the left-hand boundary with respect to calcium is well approximated by Eq. (4.12) since the simplification used to derive both analytical expressions ($K_\mathrm{M} \ll \rho$) is met for the left-hand boundary. In contrast, the right-hand boundary is overestimated with respect to calcium by Eq. (4.13). This is the case since the right-hand boundary is located at very low ρ concentrations (see Fig. 3.4*A*), where the above stated assumption does not hold anymore.

The steady-state PP1 activity is aligned relative to the bistable region of CaMKII phosphorylation in the simplified two-subunit model following the criteria outlined for the six-subunit model: (i) For the model to exhibit bistability at calcium resting conditions, the PP1 activity has to reside in the bistable region (green shaded region in Fig. 4.1*A*) at Ca_0. (ii) The 'LTD window' emerges if the PP1 activity lies above the bistable region at intermediate calcium concentrations. (iii) Finally, for the 'LTP window' to emerge, the PP1 activity has to drop below both lines marking the boundaries of the bistable region for high calcium concentrations. This scenario can be achieved if the steady-state PP1 activity exhibits a Hill function like behavior as a function of calcium (see Fig. 3.11 on page 75). However, another possibility is that the PP1 activity shows a bump at intermediate calcium concentrations (see Fig. 3.5 on page 60). The latter possibility is chosen here. The steady-state PP1 activity is given by Eq. (4.25) and is adjusted

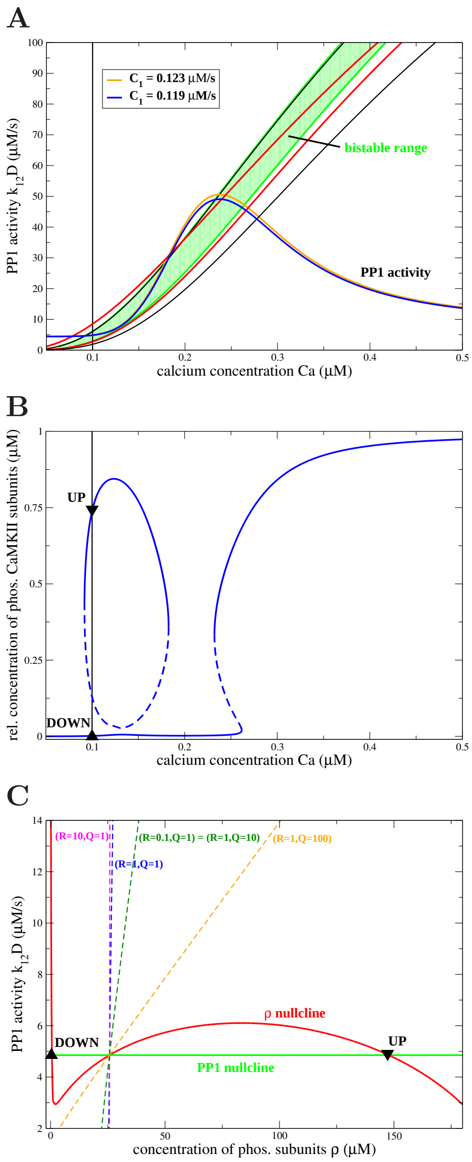

Figure 4.1: Steady-states of the CaMKII phosphorylation level and the PP1 activity in the simplified two-subunit model.
A**,** The boundaries of the bistable region of the six- and the two-subunit model in the PP1 activity - calcium concentration plane. The upper and the lower red line show the left- and the right-hand boundary of the bistable region for the six-subunit model, respectively (same results as shown by the full red lines in Fig. 3.5). The bistable region is shown for the two-subunit model as given by Eq. (4.6) (green shaded area) and by the approximate solutions for the left-hand boundary (black line above, Eq. (4.12)) and the right-hand boundary (black line below, Eq. (4.13)). ↗ *See continuation on next page.*

such that the above stated criteria are met and such that the PP1 activity exhibits a bump at intermediate calcium concentrations (see blue and orange lines in Fig. 4.1*A*). In practice, the locations of the four intersection points of the PP1 activity (blue and orange lines in Fig. 4.1*A*) with the boundaries of the bistable region (green shaded area in Fig. 4.1*A*) are used to determine four parameters describing the PP1 activity (C_2, D_0, k^0_{CaN} and k_{CaN}). See previous section and section 3.2.2 on page 59 for more details of the parameter determination.

The steady-states of the phosphorylated CaMKII subunit concentration of the simplified two-subunit model are shown in Fig. 4.1*B*. The shown steady-state picture arises from the bistable region (green shaded area) and PP1 activity (blue line) alignment as shown in Fig. 4.1*A* ($C_1 = 0.119\ \mu$M/s). Again, the CaMKII phosphorylation level has two stable states at resting calcium concentrations, *i.e.* a highly- and a weakly-phosphorylated state - the UP and the DOWN state (indicated by the downward and the upward triangle, respectively). The highly-phosphorylated state loses stability at intermediate calcium concentrations leaving the weakly-phosphorylated state as only steady-state and the highly-phosphorylated state is the only stable state at high calcium concentrations. As discussed in the previous chapter, such a scenario is consistent with experimental data (see section 3.2.2 on page 58).

We introduced the PP1 activity - phosphorylated CaMKII subunit concentration phase-plane with the six-subunit model and show trajectories of the six-subunit model exposed to STDP stimulation protocols in this plane (see Fig. 3.8). The intersections of the nullclines in this plane mark the steady-states of the system (stable or unstable depending on the Eigenvalues of the Jacobian matrix at the equilibrium point). The separatrix separates the basins of attraction of the stable steady-states, *i.e* depending on which side of the separatrix the system is initially located, it will converge to the stable steady-state corresponding to this basin of attraction. However, the nullcline of the phosphorylated CaMKII subunit concentration (S_{active}, full black lines in Fig. 3.8) and the separatrix (dotted lines in Fig. 3.8) are projections in the two-dimensional plane. Both exist in a $(13+1)$-dimensional space since S_{active} is a sum of 13 different CaMKII activation states plus the PP1 activity. Due to this projection, they are approximations of

Figure 4.1: ***B,*** Steady-state values of the CaMKII phosphorylation level (ρ) as a function of calcium. Full lines mark stable steady-states and dashed lines mark unstable steady-states ($C_1 = 0.119\ \mu$M/s). The vertical line shows the position of the resting calcium concentration ($Ca_0 = 0.1\ \mu$M) in panel *A* and *B*. ***C***, The nullclines and separatrix in the PP1 activity - CaMKII phosphorylation level phase-plane. The nullclines of the two-variable system, ρ (red line, Eq. (4.6)) and $k_{12} \cdot D$ (green line, Eq. (4.24)) are shown in the $(k_{12} \cdot D)$ - ρ phase-plane. The separatrixes for different choices of the scaling parameters R and Q (as marked in the panel) are depicted in dashed lines. The UP and the DOWN states are marked by a downward and an upward triangle in panel *B* and *C*. See Tab. 4.1 for further parameters.

the multi-dimensional nullcline and separatrix in the two-dimensional phase-plane. For example, the trajectories should normally cross the S_{active} nullcline vertically since at the nullcline $\dot{S}_{\text{active}} = 0$. This is not the case in Fig. 3.8*A* for the $\Delta t = 15$ ms case (blue line) and in *B* for the $\Delta t = 100$ and -50 ms cases, for example (cyan and red lines). The simplified two-subunit model reduces the description of the CaMKII system dynamics to a two-dimensional problem, *i.e.* one equation for the CaMKII phosphorylation level dynamics (Eq. (4.6)) and one equation for the PP1 activity dynamics (Eq. (4.24)). This allows to calculate the exact positions of the nullclines and the separatrix in the PP1 activity - CaMKII phosphorylation concentration phase-plane. Fig. 4.1*C* shows the nullclines of ρ and $(k_{12} \cdot D)$ as well as the separatrix for resting calcium conditions, *i.e.* $Ca = Ca_0 = 0.1$ μM. Note that the concentration of phosphorylated CaMKII subunits is referred to as S_{active} in the six-subunit model and as ρ in the simplified two-subunit model.

Since the separatrix and the nullclines can be calculated exactly for the simplified two-subunit model, we choose to highlight the effect of the scaling parameters R and Q in the phase-plane for this case. It is shown in Fig. 4.1*C* how the position of the separatrix changes under changes of the scaling parameters Q and R for some examples. Increasing R speeds up the PP1 activity response to calcium transients, *i.e.* the separatrix approaches the vertical since the system will move quicker in the vertical direction. On the other hand, accelerating the progress of de- and phosphorylation implies that the system will move quicker in the horizontal direction in the PP1 activity - phosphorylated CaMKII subunit concentration phase-plane. Hence, increasing Q makes the separatrix approach the vertical in the plane. Interestingly, scaling R and Q by the same factor, does not change the relative location of nullclines and separatrix at all (see cases ($R = 0.1$, $Q = 1$) and ($R = 1$, $Q = 10$), which yield exactly the same separatrix). A separation in time scales between both variables ρ and D is possible if the dynamics of one of them would be very fast compared to the other. Such a scenario would be embodied by the separatrix being very close to the vertical (in case of fast D dynamics) or the horizontal (in case of fast ρ dynamics). However, in the cases studied here and if R and Q take similar values, this separation of time scales is not possible. Note, while changes in R do not affect the picture in the phase-plane shown in Fig. 4.1*C*, changing Q results in a congruent scaling of the y-axis. In cases in which $Q \neq 1$, the nullclines and the separatrix have been scaled back in order to compare the relative positions of the separatrixes for different Rs and Qs.

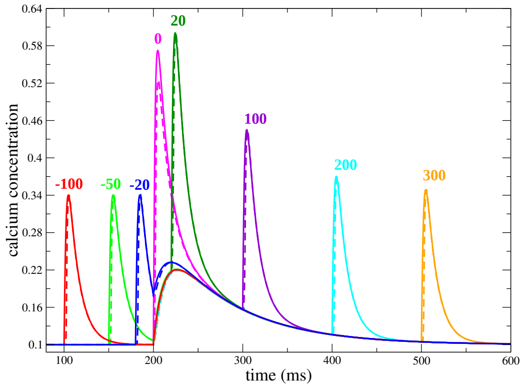

Figure 4.2: Calcium time course in response to STDP stimulation protocols: simplified and Hodgkin-Huxley based model. The time course of the intracellular calcium concentration is shown in response to STDP stimulation protocols with different time lags Δt between the pre- and the postsynaptic spikes (marked in the panel in ms), *i.e.* $\Delta t = t_{\mathrm{post}} - t_{\mathrm{pre}}$. The presynaptic spike arrives at $t_{\mathrm{pre}} = 200$ ms in all cases. The dashed lines depict the calcium dynamics simulated with the full model based on the Hodgkin-Huxley formalism (see previous chapter). The full lines are generated as described in section 4.3.1 on page 105. $B(V)$ in the simplified model is adjusted such that the amplitudes of the full model for cases with $\Delta t > 0$ ms are reproduced (see text). $\Delta Ca_{\mathrm{pre}} = 0.12$ μM and $\Delta Ca_{\mathrm{post}} = 0.24$ μM, see Tab. 4.2 for other parameters.

4.3 The two-subunit CaMKII system exposed to various stimulation protocols

The model describing the temporal dynamics of the CaMKII phosphorylation level for the simplified two-subunit case is exposed to calcium transients evoked by pre- and postsynaptic spikes as well as by postsynaptic membrane depolarizations. The transition results in response to such stimulation protocols are studied in this section.

4.3.1 Simplified synaptic activity and postsynaptic calcium signaling

The simplified model describing the postsynaptic membrane potential and the postsynaptic calcium concentration dynamics is presented here. The synaptic activity description has been reduced with the objective to simulate realistic calcium transients with little computational cost.

Postsynaptic membrane potential The membrane potential, V, of the postsynaptic neuron accounts for backpropagating action potentials (BPAPs) only. The depolarization induced by a presynaptic spike ($\Delta V \sim 1$ mV) is neglected. Therefore, the dynamics of the postsynaptic membrane potential follows

$$\frac{dV}{dt} = (V_{\mathrm{rest}} - V)/\tau_{\mathrm{m}} + V_{\mathrm{AP}} \sum_{l} \delta(t - t_l), \tag{4.27}$$

where τ_{m} denotes the single exponential decay time constant of the backpropagating action potential. V_{rest} is the resting potential and V_{AP} refers to the amplitude of the action potential. At each occurrence of a postsynaptic spike at times t_l, the membrane potential V is increased by V_{AP} (the sum on the right-hand side of Eq. (4.27) goes over all postsynaptic spikes occurring at times t_l).

Postsynaptic calcium dynamics The calcium dynamics model implements the two main sources of postsynaptic calcium influx: NMDA receptors (NMDA-Rs) and voltage-directed calcium channels (VDCCs). Extrusion and slow buffering of calcium is accounted for by a single exponential decay. The time course of the intracellular calcium concentration is described by

$$\frac{dCa}{dt} = (Ca_0 - Ca)/\tau_{\mathrm{Ca}} + \zeta(I_{\mathrm{NMDA}} + I_{\mathrm{VDCC}}), \tag{4.28}$$

where τ_{Ca} refers to the single exponential time constant of the passive decay process. Ca_0 is the calcium resting concentration, ζ converts the ion currents into concentration changes per time and is for the spine volume ($\sim 1\ \mu\mathrm{m}^3$) $\zeta = 5182.15$ μM/C (see appendix A.2 on page 177). I_{NMDA} and I_{VDCC} are the influx calcium currents mediated by NMDA-Rs and by VDCCs, respectively. Both are given by

$$I_{\mathrm{NMDA}} = g_{\mathrm{NMDA}} r_{\mathrm{NMDA}} B(V(t) - E_{\mathrm{Ca}}) \text{ and } I_{\mathrm{VDCC}} = g_{\mathrm{VDCC}} r_{\mathrm{VDCC}}(V(t) - E_{\mathrm{Ca}}). \tag{4.29}$$

g_{x} (with x=NMDA, VDCC) refers to the maximum conductance of the respective current. The time course of the dimensionless opening variable, r_{x}, of both currents is modeled by an instantaneous rise followed by a single exponential decay given by

$$\frac{dr_{\mathrm{x}}}{dt} = r_{\mathrm{x}}/\tau_{\mathrm{x}} + \sum_{\mathrm{k/l}} \delta(t - t_{\mathrm{k/l}}). \tag{4.30}$$

τ_{x} refers to the single exponential decay time constant of the NMDA (x=NMDA) and the VDCC opening variable (x=VDCC), respectively. At the occurrence of a presynaptic spike at time t_k or of a postsynaptic spike at time t_l, r_{x} is increased by one. The sum on the right-hand side of Eq. (4.30) goes over all presynaptic spikes occurring at times t_k for x=NMDA and over all postsynaptic spikes at times t_l for x=VDCC. B accounts for the voltage dependence of the NMDA current due to the magnesium block. We choose to keep the half activation voltage constant at the value given by Jahr and Stevens ($V_{1/2} = -20.525$ mV) and adjust the gain

Parameter	Definition	Value	Reference
V_{rest}	resting potential	-70 mV	
τ_{AP}	action potential decay time constant	2 ms	
V_{AP}	action potential amplitude	100 mV	
Ca_0	calcium resting concentration	0.1 μM	
τ_{Ca}	passive decay constant of calcium	12 ms	(Sabatini et al. 2002)
E_{Ca}	calcium reversal potential	140 mV	(Poirazi et al. 2003)
τ_{NMDA}	NMDA current inactivation time constant	80 ms	
τ_{VDCC}	VDCC current inactivation time constant	2 ms	
ΔCa_{pre}	presynaptically evoked calcium amplitude	0.12 μM	see text
ΔCa_{post}	postsynaptically evoked calcium amplitude	$2\Delta Ca_{\text{pre}}$	(Sabatini et al. 2002)

Table 4.2: Postsynaptic membrane potential and calcium concentration parameters

of B to yield the same calcium amplitudes as in the Hodgkin-Huxley based model (compare Eq. (A.33) on page 179; Jahr and Stevens 1990). The resulting function of B is given by

$$B(v) = \frac{B_{\text{scal}}}{1 + \exp\left(-0.056V\right) \cdot \frac{1}{3.156}}. \tag{4.31}$$

B_{scal} is introduced to scale B to 1 at $V = -70$ mV. Note the changes in parameters compared to the representation of B in the Hodgkin-Huxley formalism (see Eq. (A.33)). E_{Ca} is the calcium reversal potential. See Tab. 4.2 for other parameters characterizing the synaptic activity model. Their values are set to realistic values (V_{rest}, τ_{AP}, V_{AP}, Ca_0, E_{Ca}), taken from experiments (τ_{Ca}, ΔCa_{post}) and adjusted to reproduce calcium transients of the more realistic model (τ_{NMDA}, τ_{VDCC}; see Fig. 4.2). $\Delta Ca_{\text{post}}/\Delta Ca_{\text{pre}} = 2$ is taken from Sabatini et al. (2002). $\Delta Ca = 0.12$ μM is chosen such that for the choice of the LTD and the LTP window locations experimental plasticity data can be reproduced. Changing ΔCa would require a change in the LTD/LTP window locations (see section 3.3.6 on page 84). The implementation of fluctuating calcium transients is equivalent to its description in connection with the six-subunit model (see section 3.3.1 on page 63 for details and Tab. A.1 for parameters).

Some example calcium transients in response to STDP stimulation protocols with different time lags between the pre- and the postsynaptic spikes are shown in Fig. 4.2. Note that apart for the calcium transient evoked by the $\Delta t = 0$ ms protocol, the simplified model presented here reproduces both qualitatively and quantitatively calcium transients generated with the more realistic model of synaptic activity.

4.3.2 Transition results for the simplified two-subunit model

Here, we study the transition behavior of the simplified two-subunit model exposed to calcium transients elicited by spike-timing dependent plasticity protocols with spike-pairs and spike-triplet (Bell et al. 1997; Markram et al. 1997; Magee and Johnston 1997; Bi and Poo 1998; Froemke and Dan 2002; Wang et al. 2005).

Furthermore, as in the six-subunit model, the CaMKII system describing a two-subunit cluster is subjected to a purely presynaptic stimulation protocol with different presynaptic simulation frequencies (Dudek and Bear 1992). Additionally, the transition behavior between the two stable steady-states is investigated if exposed to calcium transients generated by presynaptic stimulation paired with postsynaptic depolarization (Artola et al. 1990; Ngezahayo et al. 2000). In the latter case, Ngezahayo et al. (2000) briefly stimulate afferents at 2 Hz for 50 seconds while holding the postsynaptic CA1 neuron at different potentials V_{m} in hippocampal slices of adult mice. If the short simulation is paired with holding potentials between -40 and -20 mV, LTD is induced while holding potentials above -20 mV lead to LTP.

Generally speaking, the simplified two-subunit model reproduces qualitatively the plasticity outcomes in response to the considered experimental stimulation protocols. The transition results are summarized in Fig. 4.3 for STDP spike-pair, presynaptic stimulation and pairing stimulation protocols and in Fig. 4.4 for STDP spike-triplet stimulation protocols. Transition results are shown in response to deterministic calcium transients and fluctuating calcium transients evoked by the respective stimulation protocols. In the simplified two-subunit model, C_1 is the parameter which controls the height of the bump of PP1 activity at intermediate calcium concentrations (see Fig. 4.1*A*). Therefore, C_1 in the simplified model is equivalent to k_{CaN} in the six-subunit model. Both parameters also influence the level of PP1 build-up attained during the exposure to stimulation protocols. As it is shown for the six-subunit model (see Fig. 3.9), fluctuating calcium transients require an increase in the PP1 bump amplitude in order to compensate for the decrease in PP1 level attained during the stimulation protocol, *i.e.* $C_1 = 0.119$ is used for simulations with deterministic calcium transients and $C_1 = 0.123$ for stochastic calcium dynamics (compare section 3.3.2 on page 70).

STDP spike-pair protocol The STDP spike-pair protocols consits of stimulation with 60 pairs of spikes at 1 Hz with different time difference between the pre- and postsynaptic spikes. Exposed to the STDP spike-pair stimulation protocol, up-to-down transitions are evoked for short negative time differences and down-to-up transitions for short positive Δt (see 4.3*A*). The range of time lags evoking LTD is smaller than the range leading to LTP which is equivalent to results of the six-subunit model while experiments seem to indicate the opposite trend (Markram et al. 1997; Bi and Poo 1998; Bell et al. 1997; Magee and Johnston 1997).

Purely presynaptic stimulation protocols The simplified two-subunit model is exposed to calcium transients evoked by 900 presynaptic spikes occurring at different frequencies. The transition behavior reproduces quantitatively experimental

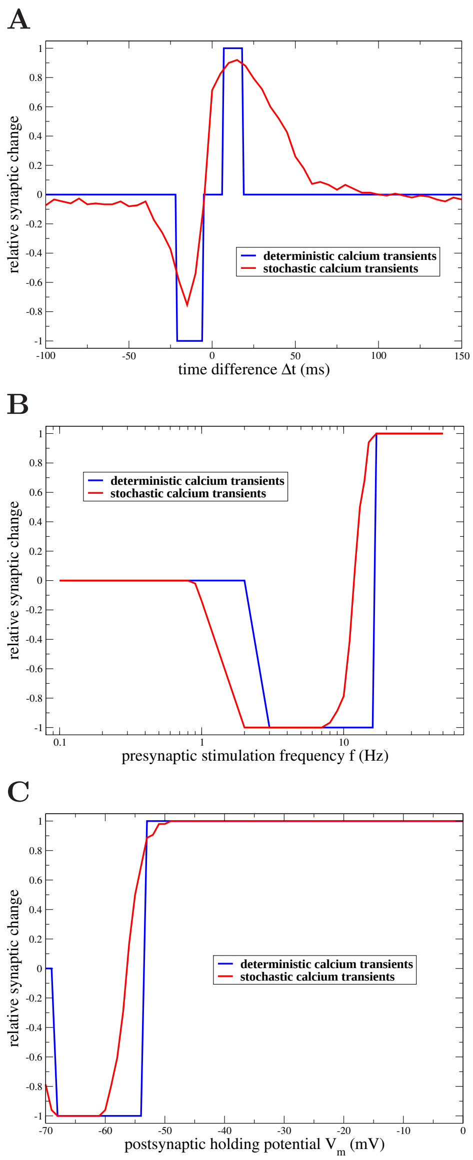

Figure 4.3: Transition outcomes of the simplified two-subunit model of CaMKII in response to experimental stimulation protocols evoking LTP/LTD. ***A, B & C,*** Changes in the number of synapses in the UP state are shown for three different experimental stimulation protocols evoking deterministic calcium transients (results shown by blue lines, $C_1 = 0.119$ μM) and fluctuating calcium transients (results shown by red lines, $C_1 = 0.123$ μM, $N = 300$). $\Delta Ca_{\mathrm{pre}} = 0.12$ μM is used in all simulations. ΔCa_{pre} determines the average pre- and postsynaptically evoked ($\Delta Ca_{\mathrm{post}} = 2\Delta Ca_{\mathrm{pre}}$) calcium amplitudes for fluctuating calcium transients. ↗ *See continuation on next page.*

synaptic plasticity results. For stimulation frequencies in the range $1 < f < 10$ Hz LTD is observed and for frequencies above 10 Hz LTP is induced (Fig. 4.3*B*; compare Dudek and Bear (1992)).

Pairing protocols As outlined above, the pairing protocol refers to presynaptic stimulation at 2 Hz for 50 s (*i.e.* 100 presynaptic spikes) combined with holding the postsynaptic cell at different membrane potentials, V_m (see Artola et al. (1990), Ngezahayo et al. (2000)). Starting at the resting membrane potential ($V_\mathrm{m} = -70$ mV), presynaptic stimulation at 2 Hz evokes up-to-down transitions in the simplified two-subunit CaMKII system. This is the same stimulation as for the purely presynaptic stimulation protocol discussed in the previous paragraph except that 100 presynaptic spikes are evoked instead of 900 in the case above (compare results in Fig. 4.3*B* at 2 Hz with Fig. 4.3*C* at $V_\mathrm{m} = -70$ mV). The pairing protocol evokes LTD up until a holding potential of ~ -56 mV and LTP for holding potentials at more depolarized levels (see Fig. 4.3*C*). The fact that LTD is seen for much lower holding potentials as suggested by experimental data could be due to short-term depression (STD). Once neurotransmitters have been released in the synaptic cleft after vesicle fusion triggered by an arriving presynaptic spike, the vesicle is not ready for subsequent release within a time range of $\tau \sim 1$ s in the hippocampus (Stevens and Wang 1995; Dobrunz and Stevens 1997; Murthy and Stevens 1999; Pyott and Rosenmund 2002). Hence, presynaptic spikes occurring at 2 Hz do not always lead to synaptic transmission while in the simulation results presented here every presynaptic spikes evokes a postsynaptic calcium transient. The failure of neurotransmitter release could explain why much higher holding potentials are required to evoke LTD and LTP in experiments (see discussion concerning short-term depression in the following chapter).

STDP spike-triplets STDP spike-triplet protocols use the same occurrence frequency and number of stimulation patterns than spike-pair protocols except that three spikes are presented instead of pairs of pre- and postsynaptic spikes only. Triplets are formed by either two presynaptic spikes enclosing a postsynaptic spike (pre-post-pre triplet) or by two postsynaptic spikes encircling a presynaptic spike (post-pre-post triplet) (see section 2.4 on page 18 for more details). Experimental data from hippocampal slices suggest that pre-post-pre triplets do not lead to synaptic changes while post-pre-post triplets evoke LTP (Wang et al. 2005). Inconsistent with these data, the simplified two-subunit model (see Fig. 4.4) as well

Figure 4.3: The stimulation protocols are: STDP spike-pair stimulation with different time differences, Δt, between pre- and postsynaptic spikes (panel *A*), purely presynaptic stimulation at different frequencies, f (panel *B*), and presynaptic stimulation paired with different postsynaptic holding potentials, V_m (panel *C*). See Tab. 4.1 and 4.2 for further parameters.

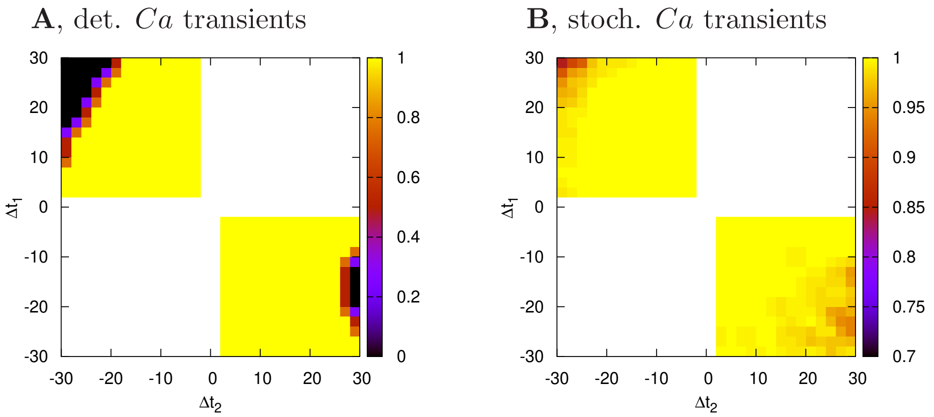

Figure 4.4: Transition outcomes of the simplified two-subunit model of CaMKII in response to STDP spike-triplet protocols. ***A & B*** Transition results of the CaMKII system in response to spike-triplet stimulation protocols (60 triplets presented at 1 Hz) with deterministic (panel A) and stochastic (panel B) calcium transients are shown ($\Delta Ca_{\mathrm{pre}} = 0.12\ \mu$M; $C_1 = 0.119\ \mu$M/s in A and $C_1 = 0.123$ in B). The color of each point at a respective (Δt_1, Δt_2) position indicates the relative change in the number of synapses in the UP state (see color scale). Note that the relative changes for all simulations shown are positive, *i.e.* only down-to-up transitions occurred ($N = 100$ in the stochastic case).

as the full six-subunit model (results shown in Fig. 5.10B) show down-to-up transitions for post-pre-post and pre-post-pre triplets. In both models, the triplet of three spikes evokes a large calcium transient which reaches calcium ranges minimizing PP1 activity and triggering strong CaMKII autophosphorylation. Together, this moves the CaMKII system from the DOWN to the UP state. Again, short-term depression of synaptic transmission could potentially change the transition behavior since pre-post-pre triplets include two consecutive presynaptic spikes in contrast to post-pre-post triplets (see Cai et al. (2007) and the discussion on short-term depression in the following chapter).

To summarize, the derivation of the simplified two-subunit model describing CaMKII autophosphorylation and dephosphorylation reduced the six-subunit model characterized by 13 + 2 differential equations to a two-dimensional model, *i.e.* one variable describing the phosphorylation level of CaMKII (ρ, Eq. (4.6)) and another one for the dynamics of the PP1 activity (D, Eq. (4.24)). However, the steady-state properties and the transition behavior of the simplified two-subunit model reproduces the features shown by the more detailed six-subunit model. The two-subunit model can be seen as a realistic but simulation time-saving way to describe CaMKII behavior. On the other hand, the amount of parameters required to characterize the simplified two-subunit model is not substantially reduced compared to the six-subunit model (CaMKII de- and phosphorylation system: six-subunit model → 25 parameters in Tab. 3.1, simplified two-subunit model → 18 par. in Tab. 4.1; synaptic activity: six-subunit model $\rightarrow$ 21 par. in Tab. A.1 and text, simplified two-subunit model $\rightarrow$ 15 par. in Tab. 4.2 and Tab. A.1). This fact makes a thorough study of the model behavior with respect to the parameter space impossible. Therefore, the simplified two-subunit model does not seem suitable to get further insights into which conditions have to be met in order to observe transitions in the model which are consistent with experiments.

5

LTP/LTD in a reduced model of a bistable synapse

In this chapter, we present a reduced model of the complex biochemical models describing the CaMKII kinase - phosphatase system. The reduced model is used to understand the CaMKII phosphorylation dynamics in more detail. It can be seen an idealization of the extensive model, discarding most of the details while keeping the minimal ingredients that give rise to a plastic, bistable synapse, with similar phenomenology of transitions as in the detailed models. Since the features of the reduced model can be related to their biochemical counterparts in the more detailed two-subunit and six-subunit CaMKII models, we can develop a qualitative understanding of the underlying biological mechanisms by means of the easier-to-study reduced model.

The reduced model implements bistability of the CaMKII phosphorylation level at resting calcium conditions. Furthermore, competing de- and phosphorylation processes activate above specific calcium concentrations and decrease and increase the phosphorylation level, respectively. We show that the transition results obtained in response to STDP spike-pair stimulation protocols are crucially determined by the relative choice of these activation thresholds. Transition results in response to STDP spike-pair stimulations of previously proposed models can be accounted for in the more general framework of the reduced model. More specifically, we identify a range of parameters for which a second LTD range at positive time differences emerges as in some models based on calcium dynamics (Karmarkar et al. 2002; Shouval et al. 2002; Abarbanel et al. 2003; Cai et al. 2007). More importantly, we show that this second LTD range can be avoided within the same model framework by changing the levels of phosphorylation and dephosphorylation activation. We suggest furthermore possible mechanisms underlying different plasticity outcomes across different brain regions such as the hippocampus and the visual cortex.

5.1 From the detailed CaMKII system to the reduced model

In the previous two chapters, we build on the idea that the CaMKII kinase - phosphatases system provides a core mechanism being at the origin of a bistable synapse. Experimental plasticity results can be reproduced in the framework of CaMKII autophosphorylation and dephosphorylation by PP1 which is in turn governed by a protein signaling cascade. Moreover, the evoked state can be stably maintained on long time scales due to bistability at resting calcium conditions. However, the complexity of the six- and the two-subunit models presented above makes it difficult to identify which details of the model give rise to which aspects of the dynamic behavior. In particular, the high number of parameters renders a systematic investigation of the model behavior across the parameter space extremely difficult.

The reduced model describes the phosphorylation level of calcium/calmodulin-dependent protein kinase II (CaMKII) subunits in the post-synaptic density (PSD) in a simplified way. Bistability and the ability to reproduce experimental plasticity results are the key elements of the detailed models of the CaMKII system presented above. Hence, the reduced model should recover both properties.

Bistability allows to maintain the evoked phosphorylation state in the absence of synaptic activity. It emerges from the interplay of the overall autophosphorylation rate and the overall dephosphorylation rate which balance each other at three points (giving rise to two stable and one unstable steady-state, see Fig. 2.11*B*). Mathematically, a system with three steady-states can be described in a simple way by an equation of the type $\dot{x} = -F(x)$, where $F(x)$ is a cubic function. Interestingly, the steady-states of the two-subunit model are given by a cubic equation in the phosphorylation level ρ (Eq. (4.7)), that has three zeros in some calcium range. This is due to the fact that the right-hand side of the differential equation characterizing the time course of the phosphorylation level ρ (Eq. (4.6)) contains a cubic function, multiplied by another function of ρ (which drops out during the derivation of the steady-state). We therefore account for bistability by a simple cubic function in the equation describing the temporal dynamics of the reduced model.

Enzymatic reactions change the phosphorylation state of CaMKII subunits, namely CaMKII autophosphorylation and dephosphorylation by PP1. Their differential activation and inhibition by calcium/calmodulin provides the basis for the reproduction of experimentally suggested plasticity results. We can in particular show with the help of the detailed six-subunit model that the activation of the calcineurin pathway at lower calcium concentrations compared to the PKA pathway yields the crucial PP1 activity profile in response to STDP spike-pair stimulation protocols. That is, PP1 activity shows a peak at negative time differences evoking LTD and a trough at positive time lags which induces LTP in conjuction with the strong autophosphorylation (see section 3.3.6 on page 84). The impact of the PP1 activity level on the transition outcome stresses the importance of two competing processes activating at distinct calcium levels. We account for this by implementing a phosphorylation and a dephosphorylation process. Both activate at different calcium concentrations in the reduced model.

5.1.1 CaMKII phosphorylation level

The dynamics of the phosphorylated CaMKII subunit concentration (ρ) is given by

$$\dot{\rho} = \alpha(c)(\rho_{\rm up} - \rho) - \beta(c)\rho - \rho(\rho_{\rm up} - \rho)(\rho_{\rm m} - \rho)/\tau, \tag{5.1}$$

where c is the concentration of free, intracellular calcium, and $\alpha(c)$ as well as $\beta(c)$ are calcium-dependent phosphorylation and dephosphorylation rates, respectively. Both are zero at resting conditions, *i.e.* at $Ca_0 \equiv c_0 = 0.1\ \mu$M ($\alpha(c_0) = \beta(c_0) = 0$). τ is the calcium-independent time constant of the CaMKII phosphorylation level.

Since $\alpha(c)$ and $\beta(c)$ are zero at c_0, $\rho = 0$ and $\rho = \rho_{\rm up}$ are stable steady-states, while $\rho = \rho_{\rm m}$ is the unstable steady-state at resting conditions. The unstable steady-state separates the basins of attraction of both stable states. For illustration purposes, we treat Eq. (5.1) as a conservative force 'driving' the phosphorylation level. It can then be represented by a potential energy function which satisfies $\partial E/\partial\rho = -\dot{\rho}$. The depiction of the potential energy landscape (with $E = -\alpha\rho_{\rm up}\rho + \rho^2(\alpha+\beta+\rho_{\rm up}\rho_{\rm m}/\tau)/2 - \rho^3(\rho_{\rm up}+\rho_{\rm m})/(3\tau) + \rho^4/(4\tau) + A$, where A is the integration constant) of Eq. (5.1) illustrates the location of the steady-states (see Fig. 5.1*I*, *II* and *III*). At resting conditions, the energy function exhibits a double well potential stemming from the cubic term in Eq. (5.1) (see Fig. 5.1*I*). For simplicity, we choose the total CaMKII subunit concentration to be $\rho_{\rm up} = 1$ μM, *i.e.* the stable steady-states at resting calcium are at $\rho = 0$ and $\rho = 1\ \mu$M. The unstable steady-state is chosen to be at $\rho_{\rm m} = \rho_{\rm up}/2 = 0.5\ \mu$M in most parts of this chapter except for the results shown in Fig. 5.9*A* and *B*. The results presented here apply to any other choice of the total CaMKII subunit concentration (ρ') provided the time constant τ is rescaled accordingly as $\tau' = \tau \cdot (\rho'_{\rm up}/\rho_{\rm up})^2$ (for $\rho_{\rm m} = \rho_{\rm up}/2$).

In case phosphorylation and dephosphorylation are not activated (that is $\alpha = \beta = 0$) and $\rho_{\rm m} = \rho_{up}/2$, Eq. 5.1 can be integrated and the expression for the time

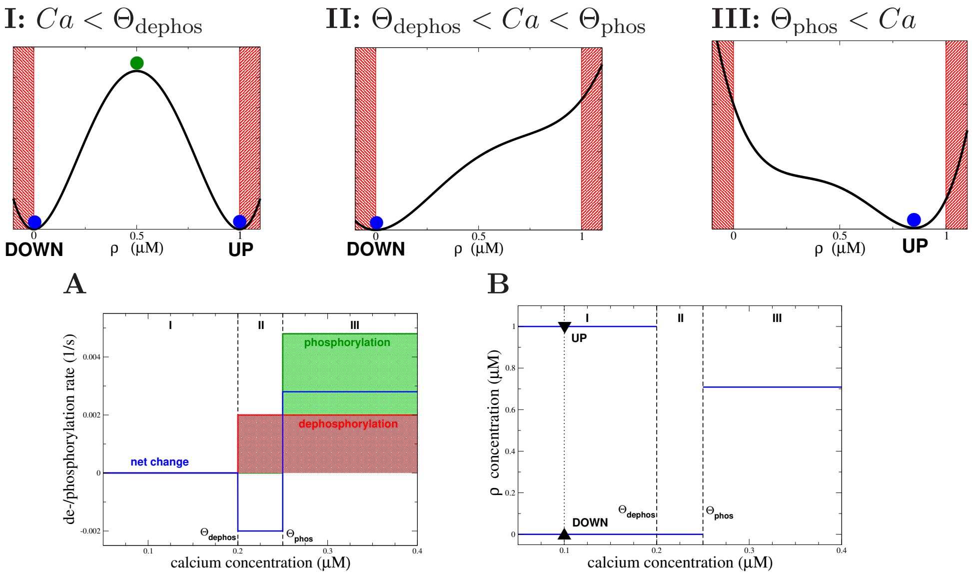

Figure 5.1: Schematic representation of the CaMKII phosphorylation level in the reduced model. ***I, II*** and ***III*** show schematically the potential energy landscape of Eq. (5.1) (energy function E given in text) for three calcium ranges: *I*: $Ca_0 \leq Ca < \Theta_{\text{dephos}}$, *II*: $\Theta_{\text{dephos}} < Ca < \Theta_{\text{phos}}$ and *III*: $\Theta_{\text{phos}} < Ca$, respectively. The stable steady-states in each of the three cases is marked by the blue circle, while the position of the unstable steady-state is indicated by the dark green circle in panel *I* ($\rho_{\text{up}} = 1\ \mu$M and $\rho_{\text{m}} = \rho_{\text{up}}/2$). ***A***, The step functions representing dephosphorylation, phosphorylation and net change in phosphorylation level of CaMKII: The dephosphorylation (red line, Eq. (5.4)) and phosphorylation rates (green line, Eq. (5.3)) are shown with respect to the calcium concentration. The net change in CaMKII phosphorylation level is the difference between phosphorylation and dephosphorylation and is characterized by the blue line. The choice of $\Theta_{\text{phos}} > \Theta_{\text{dephos}}$ divides the calcium range into three different regions: I, II and III characterized by zero, negative and positive net changes, respectively (see panels I, II and III). ***B***, The steady-states of the CaMKII phosphorylation level: The blue lines mark stable steady-states of the CaMKII phosphorylation level (Eq. 5.1) as functions of calcium. Full lines indicate stable steady-states and the dashed line marks unstable steady-states. Again, the steady-states are divided in three distinct regions with respect to calcium: in I a highly- and a weakly-phosphorylated stable steady-state coexist together with the unstable steady-state at ρ_{m}; in II (inbetween Θ_{dephos} and Θ_{phos}) only the weakly-phosphorylated state is stable; while in III (above Θ_{phos}) the highly-phosphorylated is stable only. The two stable steady-states at resting calcium conditions ($c_0 = 0.1\ \mu$M), DOWN and UP for the weakly- and the highly-phosphorylated steady-state, are illustrated by the upward and the downward triangle, respectively.

course of the CaMKII phosphorylation level is given by

$$\rho_{1/2}(t) = \frac{\rho_{up}\chi_0 + \frac{\rho_{\text{up}}}{2}e^{-t/\tau'}}{2(\chi_0 + e^{-t/\tau'})} \pm \sqrt{\left(\frac{\rho_{up}\chi_0 + \frac{\rho_{\text{up}}}{2}e^{-t/\tau'}}{2(\chi_0 + \exp^{-t/\tau'}}\right)^2 - \frac{\frac{\rho_{\text{up}}^2}{4}e^{-t/\tau'}}{\chi_0 + e^{-t/\tau}}}, \quad (5.2)$$

with $\chi_0 = (\rho_{\text{up}}/2 - \rho_0)^2/(\rho_0(\rho_{\text{up}} - \rho_0))$ and $\tau' = 2\tau/\rho_{\text{up}}^2$. ρ_0 refers to the phosphorylation level at $t = 0$, *i.e.* $\rho_0 = \rho(t = 0)$. If, for example, the initial value is one of the two stable steady-states, $\rho_0 = 0$ or $\rho_0 = \rho_{\text{up}}$, the time course is given by $\rho_2(t) = 0$ or $\rho_1(t) = \rho_{\text{up}}$ for all times. In case the initial state is at the unstable steady-state $\rho_0 = \rho_{\text{up}}/2$, the solution is $\rho_{1/2}(t) = \rho_{\text{up}}/2$. In reality, however, the system will never stay at the unstable steady-state since small perturbations will make the phosphorylation level converge to one of the two stable steady-states. In general, solution $\rho_2(t)$ is valid if $0 \leq \rho_0 < \rho_{\text{up}}/2$ and $\rho_1(t)$ if $\rho_{\text{up}}/2 < \rho_0 \leq \rho_{\text{up}}$.

De- and phosphorylation of CaMKII De- and phosphorylation of CaMKII is implemented in a calcium-dependent manner. For simplicity, the typically Hill-function like activation of such processes is described here by step functions and the binding of calcium to calmodulin before activation of downstream targets is not accounted for. Every time the calcium transient crosses a given threshold (Θ_{phos}), and as long as $c(t)$ stays above this threshold, the phosphorylation rate takes a constant value, a. The same applies for dephosphorylation and is described by

$$\alpha = aH[c(t) - \Theta_{\text{phos}}], \quad (5.3)$$

$$\beta = bH[c(t) - \Theta_{\text{dephos}}], \quad (5.4)$$

where Θ_{phos} and Θ_{dephos} are the thresholds for phosphorylation and dephosphorylation, respectively. Below the respective thresholds, the functions are zero. Above the respective thresholds, phosphorylation and dephosphorylation take the constant rates a and b, respectively. H refers to the Heaviside step function with $H[c - \Theta] = 0$ for $c < \Theta$ and $H[c - \Theta] = 1$ for $c \geq \Theta$. $\alpha(c)$ and $\beta(c)$ are shown in Fig. 5.1*A* as functions of calcium.

In the following we assume that the phosphorylation threshold is larger than the dephosphorylation threshold, *i.e.* $\Theta_{\text{dephos}} < \Theta_{\text{phos}}$. In other words, phosphorylation of CaMKII activates at higher calcium concentrations than dephosphorylation (compare Lisman (1989) and Zhabotinsky (2000)). In such a case, the model exhibits a range of calcium, above Θ_{dephos} and below Θ_{phos}, within which only the weakly-phosphorylated state is stable since dephosphorylation is active but not phosphorylation (see region II in Fig. 5.1). If the phosphorylation rate is larger than the dephosphorylation rate (*i.e.* $a > b$), only the highly-phosphorylated state is stable above Θ_{phos} since the net change in phosphorylation (defined as the difference between phosphorylation- and dephosphorylation rate, *i.e.* $a - b$) is positive (Fig. 5.1*A*). See the illustration of the potential energy landscape for the three conceptually different calcium regions in Fig. 5.1*I* - *III* and the steady-states of the model as a function of calcium in Fig. 5.1*B*. Note that the net change curve (shown by the blue line in Fig. 5.1*A*) is consistent with the calcium control hypothesis (depicted in Fig. 2.10). The reduced model yields such a behavior based on two assumptions, $\Theta_{\mathrm{dephos}} < \Theta_{\mathrm{phos}}$ and $a > b$.

5.1.2 Postsynaptic calcium dynamics

Presynaptic spikes evoke postsynaptic calcium transients mediated by NMDA-Rs. Postsynaptic spikes activate voltage-dependent calcium channels (VDCCs) through back-propagating action potentials leading to calcium influx. For simplicity, we do not model postsynaptic membrane potential dynamics. We therefore disregard the voltage-dependence of NMDA-Rs. The activation of VDCCs in response to the BPAP is implemented in an effective way.

The calcium contributions from pre- ($c_{\mathrm{pre}}(t)$) and postsynaptic spikes ($c_{\mathrm{post}}(t)$) are added up to yield the total intracellular calcium concentration

$$c(t) = c_0 + c_{\mathrm{pre}}(t) + c_{\mathrm{post}}(t), \tag{5.5}$$

where c_0 is the resting calcium concentration ($c_0 = 0.1$ μM).

A presynaptic spike activates NMDA receptors mediating a calcium concentration elevation characterized by $c_{\mathrm{pre}}(t)$. The time course of this calcium transient is described by

$$\dot{c}_{\mathrm{pre}} = -c_{\mathrm{pre}}/\tau_{\mathrm{pre}} + \omega r(t), \tag{5.6}$$

$$\dot{r} = -r/\tau'_{\mathrm{pre}} + D_{\mathrm{pre}} \sum_k \delta(t - t_k), \tag{5.7}$$

where ω is chosen such that D_{pre} gives the maximum amplitude of the elevation,

$$\omega = -\frac{1}{\tau'_{\mathrm{pre}}} \left(\frac{\tau_{\mathrm{pre}}}{\tau'_{\mathrm{pre}}}\right)^{\tau'_{\mathrm{pre}}/(\tau_{\mathrm{pre}} - \tau'_{\mathrm{pre}})} \omega_0. \tag{5.8}$$

τ'_{pre} refers to the finite rise time of the NMDA-mediated contribution and τ_{pre} is the decay time. We use $\tau_{\mathrm{pre}} = 45$ ms and $\tau'_{\mathrm{pre}} = 15$ ms in this study to yield a realistic time course of NMDA-R mediated calcium elevations (Sabatini et al. 2002). At each occurrence of a presynaptic spike at time t_k, the variable r is increased by D_{pre} (the sum on the right side and Eq. (5.7) goes over all presynaptic spikes occurring at times t_k). ω_0 is 1 and has the unit μM, *i.e.* $\omega_0 = 1$ μM.

A back-propagating action potential activates VDCCs. Due to their fast activation dynamics compared to NMDA-Rs (see Sabatini et al. (2002)) we describe the VDCC-mediated calcium transient as a sum of two single exponentially decaying functions with different decay times but immediate rise times, *i.e.* $c_{\text{post}} = (1-r)c_{\text{post}}^{(fast)} + rc_{\text{post}}^{(slow)}$ where

$$\dot{c}_{\text{post}}^{(fast)} = -c_{\text{post}}/\tau_{\text{post}}^{f} + D_{\text{post}} \sum_{l} \delta(t-t_l), \tag{5.9}$$

$$\dot{c}_{\text{post}}^{(slow)} = -c_{\text{post}}/\tau_{\text{post}}^{s} + D_{\text{post}} \sum_{l} \delta(t-t_l). \tag{5.10}$$

τ_{post}^{f} and τ_{post}^{s} are the single exponential decay time constants of the fast and the slow decaying contributions, respectively. r is used to change the balance between the fast and the slow decaying elevation, *i.e.* only the fast decaying contribution is present when $r = 0$, while only the slow contribution is present when $r = 1$. D_{post} refers to the total amplitude of the VDCC-mediated transient. Sabatini et al. (2002) measured back-propagating action potential evoked calcium transients in single spines and found a decay time constant of 15 ms, which is taken to be the fast decay time constant here, *i.e.* $\tau_{\text{post}}^{f} = 15$. The slow decay time constant is varied to investigate the effect of a slowly decaying VDCC-mediated calcium component. The slow calcium component could stem from slow release of calcium from calcium sequestration systems or from a slowly decaying tail of the backpropagating action potential, a so-called "after-depolarizing potential" (Magee and Johnston 1997; Larkum et al. 2001) (see also Shouval et al. (2002)). We choose $r = 0$ in most of the following investigations. Only the results shown in Fig. 5.6 use $r \neq 0$. The finite rise time of the NMDA-R-mediated calcium transient and the different decay time constants of the NMDA-R- the VDCC-mediated contributions are motivated by calcium measurement in dendritic spines (Sabatini et al. 2002). However, in section 5.2 on page 122 we will consider the simpler case of calcium transients with immediate rise times and identical decay time constants for c_{pre} and c_{post}, *i.e.* $\tau_{\text{pre}} = \tau_{\text{post}}^{f}$ $(r = 0)$.

5.1.3 Stochasticity in the model

CaMKII holoenzymes and proteins associated with CaMKII phosphorylation and dephosphorylation are present in small quantities in the PSD (e.g. ~ 30 CaMKII holoenzymes according to Kennedy (2000) and Petersen et al. (2003)). Consequently, stochastic fluctuations play an important role. Moreover, the system is exposed to fluctuating calcium transients stemming from stochastic neurotransmitter release, stochastic channel opening and the stochastic nature of neurotransmitter as well as calcium ion diffusion (Mainen et al. 1999; Sabatini et al. 2002). In the model presented here, we describe stochastic neurotransmitter release (short-term depression, STD) and introduce fluctuations in the calcium transients.

In the following sections, we investigate the CaMKII phosphorylation level dynamics in two cases: exposed to (i) deterministic calcium transients and (ii) stochastic calcium transients. For deterministic calcium transients (i), every presynaptic spike evokes a postsynaptic calcium transient and the pre- and postsynaptically evoked transients have always the same calcium amplitude (*i.e.* D_{pre} and D_{post}, respectively). In other words, short-term depression and fluctuations in the calcium transients are *not* implemented in this case. On the other hand, stochastic calcium transients (ii) account for short-term depression *and* the fluctuations of calcium transients. Note that we vary the amount of noise in the calcium transients and the parameters of the neurotransmitter release during the investigations but both are always implemented in conjunction.

Fluctuating calcium transients To account for noise in the calcium elevations mediated by NMDA-Rs and VDCCs, we draw the maximum amplitudes of both calcium transients at the occurrence of pre- and postsynaptic spikes randomly. The NMDA-R-mediated maximum amplitude, D_{pre}, is drawn at random from a binomial distribution with mean $\bar{D}_{\mathrm{pre}} = q_{\mathrm{pre}} N_{\mathrm{pre}} \cdot p_{\mathrm{pre}}$ and variance $\sigma^2_{\mathrm{pre}} + q^2_{\mathrm{pre}}(1-p_{\mathrm{pre}})$ at the occurrence of each presynaptic spike. The maximum amplitude mediated by VDCCs, D_{post}, is drawn at random from a binomial distribution with mean $\bar{D}_{\mathrm{post}} = q_{\mathrm{post}} N_{\mathrm{post}} p_{\mathrm{post}}$ and variance $\sigma^2_{\mathrm{post}} + q^2_{\mathrm{post}}(1 - p_{\mathrm{post}})$ at each postsynaptic spike. q_{x} refers to the quantal size and is given by $q_{\mathrm{x}} = \bar{D}_{\mathrm{x}}/p_{\mathrm{x}} N_{\mathrm{x}}$. p_{x} is the opening probability of a single receptor/channel and N_{x} is the total number of available receptors/channels (x = pre, post). σ_{x} is the variance of the gaussian noise with zero mean which is added to the value of D_{x} drawn from the binomial distribution. σ_{x} scales with the number of open receptors at each occurrence of a spike (x = pre, post). The parameters of the binomial distributions are taken from calcium transient distributions recorded at single spines by Mainen et al. (1999) for NMDA-R and by Sabatini and Svoboda (2000) for VDCC stimulations (see Tab. 5.1).

Short-term depression We choose the following model to account for the stochastic nature of presynaptic neurotransmitter release. The presynaptic pool contains N_{v} vesicles and each vesicle is released and refilled independently at the occurrence of a presynaptic spike with probability p_{r0}. The probability that a vesicle is available at the site of release, p_{r}, is zero immediately after a vesicle discharge and recovers according to a Poisson process with time constant τ_{rec}, *i.e.* at any time step (step size dt) the site of release will be re-occupied with probability dt/τ_{rec}. We chose $p_{\mathrm{r0}} = 0.19$, $\tau_{\mathrm{rec}} = 1000$ ms and $N_{\mathrm{v}} = 2$ to describe hippocampal STD

A, Parameters characterizing CaMKII phosphorylation level dynamics

Parameter	Definition	Value Parameter set used in Fig. 5.3	 Figs. 5.6, 5.7, 5.8 & 5.10	 Fig. 5.9 (i, ii, iii)
ρ_{up}	total CaMKII concentration		1 μM	
ρ_{m}	unstable steady-state	0.5 μM	0.5 μM	0.5, 0.5, 0.555 μM
τ	phosphorylation level time constant	-	5 s	5 s
a	phosphorylation rate	-	0.0245 1/s	0.019, 0.0047, 0.0245 1/s
b	dephosphorylation rate	-	0.005 1/s	0.005, 0.0022, 0,005 1/s
a/b	ratio of a and b	2.4, 2.489	4.9	3.8, 2.12, 4.9
Θ_{phos}	phosphorylation threshold	0.25 μM	0.35 μM	0.35 μM
Θ_{dephos}	dephosphorylation threshold	0.2 μM	0.25 μM	0.25 μM

B, Parameters characterizing synaptic activity

Parameter	Definition	Value intermediate noise	 realistic noise	Reference
D_{pre}	NMDA-mediated transient amplitude	0.1 μM		free parameters,
$\bar{D}_{\mathrm{post}}$	VDCC-mediated transient amplitude	0.2 μM		ratio changed
τ_{pre}	NMDA-mediated transient decay time	45 ms		
τ'_{pre}	NMDA-mediated transient rise time	10 ms		(Sabatini et al. 2002)
τ^{f}_{post}	VDCC-mediated transient decay time	15 ms		
N_{pre}	total number of NMDA receptors	20		(Kennedy 2000)
p_{pre}	single channel opening probability	0.5		(Nimchinsky et al. 2004)
σ_{pre}	SD of the Gaussian noise added	1 % of $\bar{D}_{\mathrm{pre}}$	3.3 % of $\bar{D}_{\mathrm{pre}}$	(Mainen et al. 1999)
N_{post}	total number of CaL channels	20	5	
p_{post}	single channel opening probability	0.52		(Sabatini and Svoboda 2000)
σ_{post}	SD of the Gaussian noise added	10 % of $\bar{D}_{\mathrm{post}}$		
shot-term depression		hippocampus	visual cortex	
p_{r0}	vesicle release probability	0.19	0.3	see references
τ_{rec}	vesicle recovery time constant	1000 ms	141 ms	to experiments in text,
N_{v}	number of vesicles	2		and (Cai et al. 2007)

Table 5.1: Parameters of the reduced model. Unless otherwise stated, the parameters given in this table are employed in the reduced model investigations.

(Stevens and Wang 1995; Dobrunz and Stevens 1997; Murthy and Stevens 1999; Pyott and Rosenmund 2002) and $p_{\mathrm{r0}} = 0.3$, $\tau_{\mathrm{rec}} = 141$ ms and $N_{\mathrm{v}} = 2$ for STD in the visual cortex (Philpot et al. 2001). These parameters were also used by Cai et al. (2007). For simplicity, we assume that the release of a single vesicle saturates all postsynaptic binding sites, *i.e.* independently whether one or two vesicles are released, the NMDA-R mediated calcium current has the amplitude D_{pre}.

5.1.4 Parameters of the model

As stated above, we chose ρ_{up} to be 1 μM but the results apply to any other choice of ρ_{up} provided τ is rescaled accordingly ($\tau' = \tau \cdot (\rho'_{\mathrm{up}}/\rho_{\mathrm{up}})^2$, if $\rho_{\mathrm{m}} = \rho_{\mathrm{up}}/2$). For most of the results, $\rho_{\mathrm{m}} = \rho_{\mathrm{up}}/2$ is used except in Fig. 5.9*A* and *B*, where we investigate the impact of varying the location of the unstable steady-state on the CaMKII transition behavior. The ratio of the phosphorylation and dephosphorylation rate (a/b) is fixed by the requirement that STDP spike-pair stimulation protocols with large time differences between pre- and postsynaptic spike should not evoke any phosphorylation changes. a and τ are treated as free parameters and varied extensively in the model. We show that their choice determines whether or not transitions can be observed. Increasing a (and through the fixed ratio (a/b) also b) or decreasing τ augments the transition probability for a given stimulation protocol and vice versa. Θ_{phos} and Θ_{dephos} are treated as free parameters in the model. The qualitative transition behavior depends on their choice relative to the maximal calcium amplitudes $\bar{D}_{\mathrm{pre}}$ and $\bar{D}_{\mathrm{post}}$. We therefore systematically vary Θ_{phos} and Θ_{dephos} in order to explore the range of possible transition outcomes in the presence of different levels of noise. See Tab. 5.1A for parameters.

In most of the following, we chose $\bar{D}_{\mathrm{pre}}$ and $\bar{D}_{\mathrm{post}}$ to be fixed at 0.1 and 0.2 μM ($\bar{D}_{\mathrm{post}}/\bar{D}_{\mathrm{pre}} = 2$, consistent with Sabatini et al. (2002)). We also discuss how the behavior of the model changes when the ratio between $\bar{D}_{\mathrm{post}}$ and $\bar{D}_{\mathrm{pre}}$ is varied. Changing their absolute values while keeping their ratio constant does not change the behavior of the model, as long as Θ_{phos} and Θ_{dephos} are adjusted accordingly. The time constants of the NMDA-R and the VDCC mediated calcium contributions are chosen to yield realistic time courses of intracellular calcium transients (Destexhe et al. 1998; Sabatini et al. 2002). The parameters for the distributions of maximum amplitudes of the NMDA- and VDCC-mediated calcium transients are adjusted such that they fit experimental data recorded from single spines (Mainen et al. 1999; Sabatini and Svoboda 2000). Note that the parameters taken from experiments are used as the 'realistic noise' parameter set (see Tab. 5.1B). The parameters in the 'intermediate noise' set are chosen by hand such that less noisy calcium transients are obtained. The parameters describing STD in the hippocampus (Stevens and Wang 1995; Dobrunz and Stevens 1997; Murthy and Stevens 1999; Pyott and Rosenmund 2002) and the visual cortex (Philpot et al. 2001) are taken from experiments.

5.2 Calculation of evoked phosphorylation changes

The simplicity of the reduced model allows to calculate how the CaMKII phosphorylation level changes in response to stimulation protocols. These phosphorylation changes allow in turn to determine qualitative transition outcomes of the CaMKII switch in response to such protocols. We demonstrate the calculation of the transition outcomes for the STDP spike-pair stimulation protocol in this section.

Time spent above threshold for pre- and postsynaptically evoked calcium transients with immediate rise times Let us first consider the simplest case with immediate rise times of the NMDA-R- and the VDCC-mediated calcium transients and the same single exponential decay time constants for both contributions, *i.e.* $\tau'_{\mathrm{pre}} = 0$ and $\tau_{\mathrm{pre}} = \tau^{f}_{\mathrm{post}} = \tau$ $(r = 1)$. Under these conditions, the time the calcium transient spends above a given threshold (Θ_{T}) can be calculated analytically as a function of Δt. For large time differences between the pre- and the postsynaptic spike, three qualitatively different cases are distinguished: (i) the threshold is higher than both calcium transients ($D_{\text{post}} < \Theta_{\text{T}}$); (ii) the threshold lies in between the two amplitudes ($D_{\text{pre}} < \Theta_{\text{T}} < D_{\text{post}}$); (iii) and the threshold is below both calcium amplitudes ($\Theta_{\text{T}} < D_{\text{pre}}$, see Fig. 5.2*A*). In case (i), the time spent above threshold is zero for large time differences and the threshold is crossed only if both calcium transients superimpose and the threshold is smaller than the sum of both calcium amplitudes (*i.e.* $\Theta_{\text{T}} < D_{\text{pre}} + D_{\text{post}}$). The analytical expression for the times spent above threshold in the different cases can be found in appendix B.1 on page 183. Note that we choose $D_{\text{post}} > D_{\text{pre}}$ here. The times spent above threshold for the case $D_{\text{post}} < D_{\text{pre}}$ can be easily obtained by interchanging D_{pre} and D_{post} (*i.e.* $D'_{\text{pre}} \rightarrow D_{\text{post}}$ and $D'_{\text{post}} \rightarrow D_{\text{pre}}$) and inverting the sign of Δt (*i.e.* $\Delta' t \rightarrow -\Delta t$).

For special parameter values it is possible to compute analytically the times spent above threshold in the more realistic scenario when the NMDA-R- and the VDCC-mediated calcium transients have different decay time constants. Dendritic calcium measurements suggest that the decay time constant of the NMDA-mediated component is longer than the decay time constant of the VDCC mediated calcium contribution (Sabatini et al. 2002). We express this by $\tau_{\text{post}}/\eta = \tau_{\text{pre}} = \tau$ with $\eta < 1$. The times spent above threshold can be calculated if $\eta = 1/2$ or $\eta = 1/3$ since in those cases the time the calcium transient spends above Θ_{T} is given by quadratic or cubic equations, respectively. The basic equations for $\eta = 1/2$ and $\eta = 1/3$ from which the times spent above threshold can be calculated are given in appendix B.1 on page 183 (Eqs. (B.17) and (B.18)).

Net change curve To understand the transition behavior, we now need to compute the net change of the phosphorylation level induced by the two competing processes, phosphorylation and dephosphorylation. In the reduced model described by Eq. (5.1), dephosphorylation ($\beta(c)$)) and phosphorylation ($\alpha(c)$) activate above the thresholds Θ_{dephos} and Θ_{phos}, respectively. The amount of phosphorylation and dephosphorylation evoked is proportional to the time spent above each one of the two thresholds and the de- and phosphorylation rates a and b, respectively.

With respect to the STDP spike-pair protocol, it seems reasonable to impose that largely spaced spike-pairs should not evoke any changes in phosphorylation. In other words, the amount of phosphorylation and dephosphorylation induced by these pairs, if the thresholds are crossed for $|\Delta t| \gg 0$, should compensate each other. We impose this criterion since STDP plasticity results for the hippocampus and the visual cortex do not indicate long-term modifications for large time differences. Using the analytical expressions for the time spent above threshold derived above and imposing zero net change for $|\Delta t| \rightarrow \infty$ allows to calculate

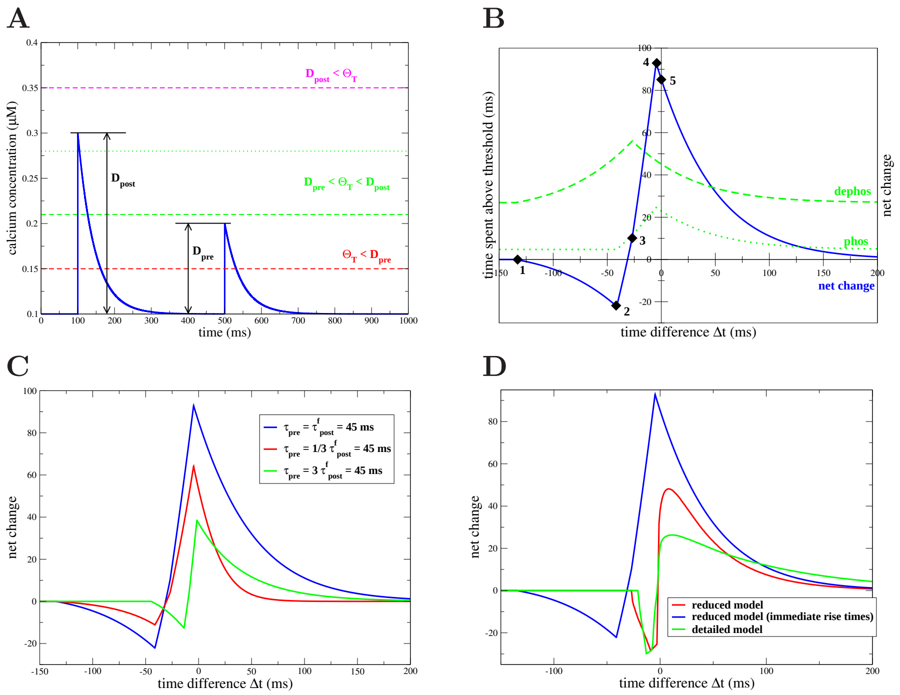

Figure 5.2: Analytically calculated and numerically determined net change curves. ***A,*** Calcium transients and locations of de/phosphorylation threshold: The depicted calcium transient is evoked by a spike-pair with $\Delta t = -400$ ms ($D_{\text{post}} = 0.2$ μM, $D_{\text{pre}} = 0.1$ μM). The post- and presynaptically evoked calcium elevations have immediate rise times and decay exponentially with the same time constant ($\eta = 1$, $\tau = 45$ ms). The three qualitatively different locations of the thresholds with respect to the calcium transients are shown by the horizontal lines in three different colors (locations marked in the panel, see appendix B.1 on page 183). ***B,*** Times spent above de- and phosphorylation thresholds and net change curve: The green lines show the times spent above the thresholds $\Theta_{\text{phos}} = 0.28$ μM (dotted green line) and $\Theta_{\text{dephos}} = 0.21$ μM (dashed green line) as functions of Δt (the respective thresholds are indicated in panel *A* in green and in the same style; $D_{\text{post}} = 0.2$ μM, $D_{\text{pre}} = 0.1$ μM). The blue line, which is referred to as net change curve, depicts the weighted difference between both times ($a/b = 5.674$, see text for more details). 5 prominent points are highlighted and numbered. Their location with respect to Δt and the net change values at these points are given by Eqs. (5.12)-(5.16). ***C,*** Net change curves for different decay time constant combinations: The three curves depict net changes in phosphorylation for the same parameter set as used in panel *C* but for three different combinations of decay time constants. The chosen time constants of the pre- and the postsynaptically calcium transients are marked in the panel. ***D,*** Net change curves for calcium transients with finite rise time of the NMDA-R-mediated component: The underlying calcium transients evoking the phosphorylation changes exhibit finite rise times of the NMDA-R-mediated calcium transient. The synaptic activity description of the reduced model (Eq. (5.5), red line) and the synaptic activity description of the detailed model (Eq. (3.13), green line) are used to generate the calcium transients (see text). For comparison, the blue line shown in panel *B* and *C* is reproduced in panel *D*.

the net change curve. We refer to the net change as to the overall change in phosphorylation after the exposure of the reduced CaMKII model (Eq. (5.1)) to a calcium transient. It is calculated accordingly: time spent above Θ_{phos} weighted by a reduced by the time spent above Θ_{dephos} weighted by b. The net change curve describes the overall phosphorylation changes as a function of Δt.

Here, we focus on the net change curve for the case of immediate rise times and equal decay time constants for the pre- and postsynaptically evoked calcium transients (*i.e.* $\eta = 1$). We furthermore choose $D_{\text{pre}} \leq \Theta_{\text{phos}} \leq D_{\text{post}}$, $D_{\text{pre}} \leq \Theta_{\text{dephos}} \leq D_{\text{post}}$ (case II in appendix B.1 on page 183) and $\Theta_{\text{dephos}} < \Theta_{\text{phos}}$. If $\eta = 1/2$ or $1/3$ and for any other choice of the de- and phosphorylation thresholds as well as the pre- and postsynaptically evoked calcium amplitudes, the net change curve can be calculated in the exact same manner. The values of the times spent above the dephosphorylation and the phosphorylation thresholds for large Δt ($|\Delta t| \to \infty$) are given by $I_{\text{D}}^{\infty} = \tau \ln(D_{\text{post}}/\Theta_{\text{D}})$ and $I_{\text{P}}^{\infty} = \tau \ln(D_{\text{post}}/\Theta_{\text{P}})$, respectively. Since de- and phosphorylation are opposing effects, zero net change for $|\Delta t| \to \infty$ implies

$$aI_{\text{P}}^{\infty} - bI_{\text{D}}^{\infty} = a\tau \ln(D_{\text{post}}/\Theta_{\text{P}}) - b\tau \ln(D_{\text{post}}/\Theta_{\text{D}}) = 0, \tag{5.11}$$

where a and b specify the phosphorylation and the dephosphorylation rate, respectively. With $a = \ln(D_{\text{post}}/\Theta_{\text{D}})$ and $b = \ln(D_{\text{post}}/\Theta_{\text{P}})$, for example, Eq. (5.11) is satisfied. Note however that Eq. (5.11) determines the ratio of a and b only, both can be multiplied by the same arbitrary constant and Eq. (5.11) is still fulfilled.

The above defined ratio of a and b assures zero net change for large Δt and allows to give analytical expressions for the net change in CaMKII phosphorylation level for all Δt (see appendix B.2 on page 186). Fig. 5.2*B* shows the net change in phosphorylation as a function of Δt for the example chosen here. Five prominent points of the net change curve are labeled in Fig. 5.2*B* and their values are given by the following analytical expressions

$$
\begin{aligned}
1 : \Delta t &= -\tau \ln \left(D_{\text{post}} / (\Theta_{\text{dephos}} - D_{\text{pre}}) \right), \\
N_1 &= 0, \qquad (5.12) \\
2 : \Delta t &= -\tau \ln \left(D_{\text{post}} / (\Theta_{\text{phos}} - D_{\text{pre}}) \right), \\
N_2 &= -\tau \ln \left[\frac{\Theta_{\text{phos}}}{\Theta_{\text{dephos}}} \right] \ln \left[\frac{D_{\text{post}}}{\Theta_{\text{phos}}} \right], \qquad (5.13) \\
3 : \Delta t &= -\tau \ln(D_{\text{post}} / \Theta_{\text{dephos}}), \\
N_3 &= \tau \ln \left[\frac{\Theta_{\text{phos}}}{\Theta_{\text{dephos}}} \right] \ln \left[\frac{D_{\text{pre}} + \Theta_{\text{dephos}}}{D_{\text{post}}} \right], \qquad (5.14) \\
4 : \Delta t &= -\tau \ln(D_{\text{post}} / \Theta_{\text{phos}}), \\
N_4 &= \tau \ln \left[\frac{\Theta_{\text{phos}}}{\Theta_{\text{dephos}}} \right] \ln \left[\frac{D_{\text{pre}} + \Theta_{\text{phos}}}{\Theta_{\text{phos}}} \right], \qquad (5.15) \\
5 : \Delta t &= 0, \\
N_5 &= \tau \ln \left[\frac{\Theta_{\text{phos}}}{\Theta_{\text{dephos}}} \right] \ln \left[\frac{D_{\text{pre}} + D_{\text{post}}}{D_{\text{post}}} \right]. \qquad (5.16)
\end{aligned}
$$

Δt specifies the x-location and N_{x} (with x = 1...5) gives the net change value for the respective location (see Fig. 5.2*B*).

We want to draw the attention to three properties of the calculated net change curve (shown in Fig. 5.2*B*): (i) The amplitude of the positive peak of the net change curve (point 4) is proportional to $\sim \ln((D_{\text{pre}} + \Theta_{\text{phos}})/\Theta_{\text{phos}})$ while the amplitude of the negative peak (point 2) scales with $\sim \ln(D_{\text{post}}/\Theta_{\text{phos}})$. Hence, the amplitude of the positive peak is larger than the amplitude of the negative peak if $(D_{\text{pre}} + \Theta_{\text{phos}}) > D_{\text{post}}$ (which is the case for the example shown in Fig. 5.2*B*). (ii) The positive peak (point 4) and the transition from positive to negative net phosphorylation changes (between point 2 and 3) are at negative time differences. (iii) The net phosphorylation change decays exponentially with time constant $1/\tau$ back to zero net change for positive Δt. In contrast, the net change at negative Δts vanishes at a finite negative Δt (point 1). It decays exponentially back to zero if $\Theta_{\text{dephos}} = D_{\text{pre}}$.

Fig. 5.2*C* and *D* show net change curves if the properties of the calcium transients are changed. The net change curve discussed so far assumes equal decay time constants ($\eta = 1$, $r = 0$) and immediate rise times of pre- and postsynaptically evoked calcium transients. Fig. 5.2*C* shows analytically calculated net change curves if the decay time constant of the NMDA-R-mediated calcium transient is one third (red line) and three times (green line) the decay time constant of the VDCC-mediated transient. Despite the changes in extent of positive and negative net phosphorylation ranges with respect to Δt, the three properties outlined in the previous paragraph remain valid for changes in the ratio of the two decay time constants. In a step towards more realistic calcium transients, we account for the finite rise time of the NMDA-R-mediated calcium current and show the resulting net change curves in Fig. 5.2*D*. The net changes in phosphorylation cannot be calculated analytically anymore under this condition and the shown results are obtained numerically. The underlying calcium transients evoking the net changes are generated by using the synaptic activity model described in this chapter (with $\tau'_{\mathrm{pre}} = 10$ ms, red line in Fig. 5.2*D*) and the one introduced with the six-subunit model in chapter 3 (green line in Fig. 5.2*D*, see section 3.3.1 on page 62). The finite rise time of the calcium transient through NMDA-Rs shifts the positive peak of net phosphorylation changes to positive values of Δt. It furthermore broadens the positive part of the net change curve with respect to Δt while the extent in range of negative net changes is considerably reduced. Interestingly, the negative amplitude of the net change curve becomes larger than the positive amplitude.

We show below that short-term depression and fluctuating calcium transients change considerably the shape of the net change curves. However, the analytical approach presented in this section gives insights into how parameters of the calcium transients control the specific shape of experimentally observed plasticity results in response to STDP stimulation. Furthermore, the analytical considerations are the basis for the calculation of the net change curves in the presence of noise below.

5.3 Spike-pair and -triplet stimulation protocols

We discuss the transition behavior of the reduced model in response to spike-timing dependent plasticity (STDP) stimulation protocols in this section.

5.3.1 Spike-pair stimulation, net changes in phosphorylation and transitions

The model is exposed to calcium transients evoked by repetitive presentations of pairs of pre- and postsynaptic spikes occurring at t_{pre} and $t_{\mathrm{post}} = t_{\mathrm{pre}} + \Delta t$, respectively. The resulting calcium elevation is the linear sum of the calcium transients mediated by NMDA-Rs and VDCCs. In contrast to the detailed model (Eq. (3.13)), both contributions also sum linearly for sufficiently short Δts (e.g. for $\Delta t = -10$, 10 and 100 ms in Fig. 5.3*A*). Note that the detailed model yields supralinear superpositions of the calcium transients for such Δt values due to the voltage dependence of the NMDA-R-mediated calcium transient. We use here the synaptic activity model as described above (Eq. (5.5), section 5.1.2 on page 118) without the simplification of immediate rise time for the NMDA-R-mediated calcium transient.

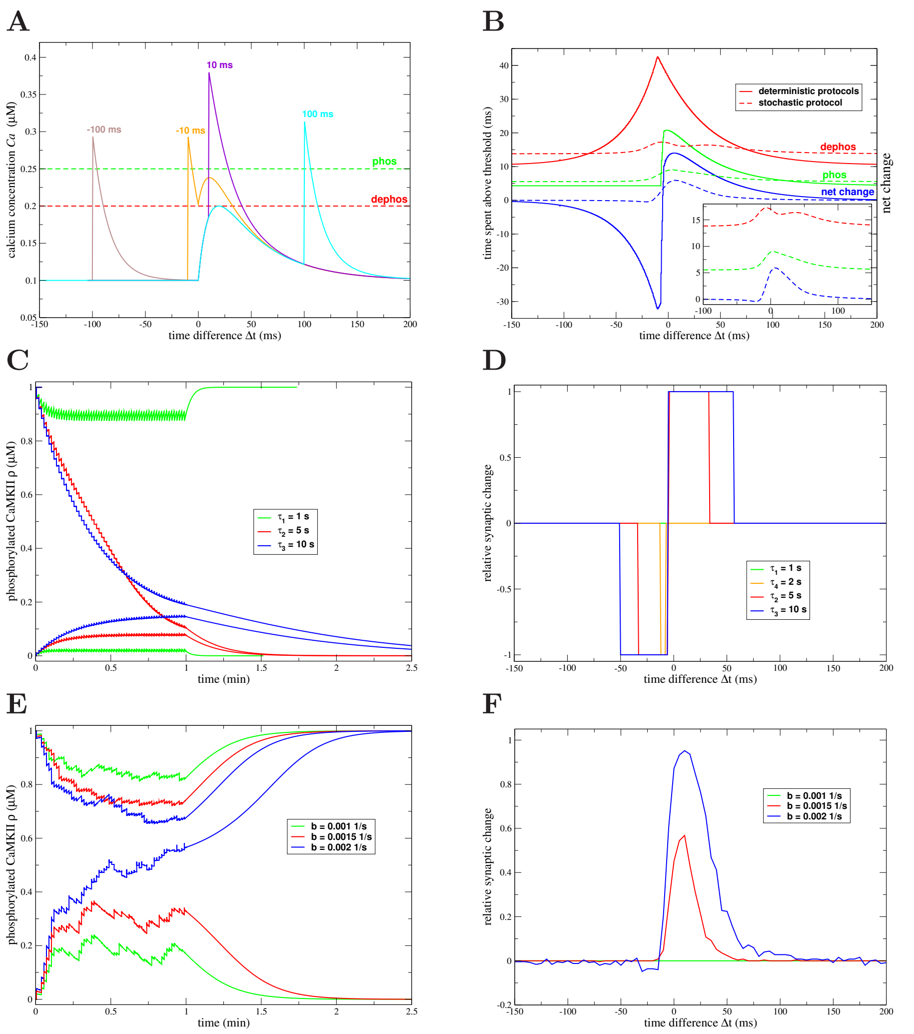

Figure 5.3: Calcium transients, net changes in phosphorylation, CaMKII phosphorylation level dynamics and transition outcomes in response to STDP spike-pair stimulation protocols. ***A***, Calcium transients evoked by single spike-pairs occurring at different Δt's (as marked in the panel): The horizontal dashed lines depict the phosphorylation (in green) and the dephosphorylation thresholds (in red) at $\Theta_{\mathrm{phos}} = 0.25$ μM and $\Theta_{\mathrm{dephos}} = 0.2$ μM, respectively. ***B***, Time spent above the phosphorylation threshold (green lines) and above the dephosphorylation threshold (red lines) as a function of Δt: Full lines represent the times in the absence of noise and STD while the dashed lines show the results with fluctuating calcium transients and STD. The blue lines refer to the net change in phosphorylation formed by the weighted difference between de- and phosphorylation, *i.e.* (net change) = $a\cdot$(phosphorylation) - $b\cdot$(dephosphorylation) (see text for more details). $a/b = 2.4$ for the noiseless case and $a/b = 2.489$ for the noisy case. The inset shows separately the results for fluctuating calcium transients and STD. ↗ *See continuation on next page.*

CaMKII gets dephosphorylated as soon as the calcium transients crosses the dephosphorylation threshold (Θ_{dephos}). Similarly, phosphorylation is activated as soon as Ca crosses the phosphorylation threshold (Θ_{phos}; see illustration in Fig. 5.3*A*). Given the calcium elevations in the absence of fluctuating calcium transients and STD, we can evaluate how much time the calcium trace spends above both thresholds as a function of Δt. The time spent above the dephosphorylation threshold is shown by the full red line in Fig. 5.3*B*, and above the phosphorylation threshold by the full green line. Since the dephosphorylation threshold is lower, the calcium trace spends more time in the range within which dephosphorylation is activated. In the example in Fig. 5.3*A*, the dephosphorylation threshold is chosen to be similar to the maximum amplitude of a calcium transient evoked by a single presynaptic spike ($\Theta_{\text{dephos}} = \bar{D}_{\text{pre}}$). For this choice of the dephosphorylation threshold, the time spent above the dephosphorylation threshold gives a measure for which range of negative values of Δt the pre- (c_{pre}) and postsynaptically (c_{post}) evoked calcium transients start to interact. In other words, as soon as the decaying tail of c_{post} starts to superimpose with c_{pre} for short negative Δt, the time spent above Θ_{dephos} starts to rise above its value for an independent postsynaptic calcium transient only (for $\Delta t < 150$ ms in Fig. 5.3).

The difference between the times spent above phosphorylation and dephosphorylation thresholds give a measure of how the phosphorylation level changes after the presentation of one spike-pair. As introduced in the previous section, we refer to this as the net change in phosphorylation level or just net change. We furthermore introduced in the previous section the constraint that pairs with large Δt should not evoke any changes in phosphorylation, *i.e.* phosphorylation and dephosphorylation should compensate each other. In Fig. 5.3*B*, multiplying the time spent above the phosphorylation threshold with 2.4 and subtracting the time spent about the dephosphorylation threshold yields the full blue line which converges to zero as $\Delta t \rightarrow \pm\infty$. This criterion of no net change outside the range of interactions of pre-and postsynaptically evoked calcium transients determines the ratio

Figure 5.3: ***C & E***, Dynamics of ρ in the absence and presence of noise: The time course of ρ (Eq. (5.1)) is shown during the stimulation protocol with $\Delta t = -10$ ms and until the system reached the final steady-state for three different choices of τ (as marked in the panel, $b = 0.001$ 1/s) in the absence of noise and STD in panel *D*. Noise and STD are present in panel *E* and three example time courses are shown for stimulation protocols with $\Delta t = 10$ ms and for three different choices of b (marked in panel, $a/b = 2.489$ is kept constant, $\tau = 5$ ms). ***D & F***, Relative change in the number of synapses in the UP state as functions of Δt in response to deterministic stimulation protocols (panel *D*) and to stochastic protocols (panel *F*): Same colors are used as in panels *C* and *E*. In the deterministic case, the relative synaptic change can only take three values: -1, 0 and $+1$ for up-to-down transition, no change and down-to-up transition, while due to the averaging in the stochastic case this change can take intermediate values ($N = 500$). See Tab. 3.1 for further parameters.

between the phosphorylation- and dephosphorylation rate, a/b (see Eq. (5.11)). For the choice of Θ_{phos} and Θ_{dephos} used in Fig 5.3, the net change in phosphorylation in response to a spike-pair as a function of Δt exhibits a behavior corresponding to experimental plasticity outcomes in response to the STDP protocol, *i.e.* short negative time lags evoke LTD and short positive time lags evoke LTP.

The net change in phosphorylation of the example discussed above shows a STDP-like behavior. But how does the net change in CaMKII phosphorylation level translate into transitions between the two stable phosphorylation states if the CaMKII model is repetitively exposed to spike pairs with fixed Δt? Spike-pairs evoke repetitively the same net change in phosphorylation given by the full blue line in Fig. 5.3*B*. The size of these sudden changes in phosphorylation level and the decay thereafter depends on the absolute values of b and the time constant τ (the ratio a/b is fixed due to the imposed requirement of zero net change for $|\Delta t| \to \infty$, see Eq. (5.11)). The larger b or τ, the more likely transitions between the UP and the DOWN state can be evoked during the stimulation protocol consisting of 60 spike-pair presentations at 1 Hz (Bi and Poo 1998; Wang et al. 2005). The effect of increasing b or τ on the dynamics of ρ is however different. Large b values result in large jumps in the phosphorylation level after each spike-pair. On the other hand, the larger τ the slower the decay of the phosphorylation level back to the UP or the DOWN state depending on whether the phosphorylation level is above or below the unstable steady-state at $\rho = \rho_{\mathrm{m}}$, respectively. If b or τ are chosen large enough such that the phosphorylation level (ρ) can cross the unstable state-state during the stimulation protocol, three scenarios can arise: (i) In the case of negative net changes (for short negative Δt in the scenario shown in Fig. 5.3*A* and *B*), the system gets repetitively dephosphorylated during the presentation of each spike-pair. If the system is initially in the UP state, the phosphorylation level will cross the unstable steady-state and move in the bassin of attraction of the DOWN state, *i.e.* an up-to-down transition occurs. If the system resides initially in the DOWN state, no transition is evoked. (ii) The situation is inverted for positive net changes (the case for short positive Δt in Fig. 5.3*A* and *B*). The repetitive phosphorylation would move the system from the DOWN to the UP state if it starts initially in the DOWN state. Starting from the UP state would not lead to a transition. (iii) For large negative and positive time lags the net change in phosphorylation is zero. Therefore, independently whether the CaMKII resides initially in the UP or the DOWN state, no transitions will occur. Similarly, if b or τ are too small, the change in phosphorylation level is not sufficient to cross the unstable steady-state for any Δt, *i.e.* no transitions would occur.

Fig. 5.3*C* and *E* show the time course of the phosphorylation level of CaMKII (ρ) during the stimulation protocol consisting of 60 spike-pairs at 1 Hz and until the system converges to the final steady-state. In *C*, every presynaptic spike evokes a postsynaptic response and no noise is added to the calcium transients (deterministic calcium transients), while in *E* fluctuating calcium transients and synaptic short-term depression are taken into account (stochastic calcium transients, see section 5.1.3 on page 119). $\Delta t = -10$ ms in all the cases shown in panel *C* and $+10$ ms in panel *E*. To illustrate the behavior described in the previous paragraph, the dynamics is shown for three different τs in *C* and b is kept constant ($b = 0.001$ 1/s) while τ is kept constant in *E* and b takes three different values ($\tau = 5$ s). For each combination of τ and b, the system is simulated being initially in the UP *and* in the DOWN state (therefore two lines of the same color are shown in Fig. 5.3*C* and *E*). As described above, increasing τ or b leads the CaMKII to switch from the UP to the DOWN state for $\Delta t = -10$ ms if it is initially in the UP state (which is the case for $\tau_2 = 5$ and 10 s in Fig. 5.3*C*, compare negative net phosphorylation change for $\Delta t = -10$ ms in *B*), or to switch from the DOWN to the UP state if the CaMKII starts in the DOWN state (for $b = 0.002$ 1/s in Fig. 5.3*E*).

Fig. 5.3*D* and *F* summarize the transition behavior of the CaMKII phosphorylation level as a function of Δt for deterministic and stochastic calcium transients, respectively. The relative synaptic change shown in these panels refers to the change in the number of synapses in the UP state. If initially half of the synapses are in the DOWN state, and the remaining half are in the UP state, a positive synaptic change implies an increase in the number of synapses in the UP state, *i.e.* the stimulation protocol evokes down-to-up transitions. On the opposite, a negative synaptic change represents an increase in the number of synapses in the DOWN state, *i.e.* up-to-down transitions occur. With deterministic stimulation protocols, the relative synaptic change can only take three values: 0, $+1$ and -1, meaning no transitions at all, all synapses initially in the DOWN state switched to the UP state and all synapses switched from the UP to the DOWN state, respectively. With stochastic stimulation protocols the relative synaptic change is an average over many trials ($N = 500$ in Fig. 5.3*F*) and can therefore take intermediate values. We want to draw the attention to the fact that the net phosphorylation change curves in Fig. 5.3*B* provide information for which ranges of Δt transitions can occur, and if they occur in which direction. In this respect, the net change curve can be seen as a window of possibility for transitions. Whether or not transitions occur in response to a stimulation protocol is determined by the choice of the the de- and phosphorylation rates, b and a, and the choice of τ. A negative net change indicates up-to-down transitions and a positive net change indicates down-to-up transitions for a given Δt. Moreover, the amplitude in net change indicates the probability of transition. For example, negative Δts evoke up-to-down transitions but no down-to-up transitions occur at positive Δts in *D* for $\tau_4 = 2$ s. This is the case since the net change curve has a larger peak a short negative time lags compared to short positive time lags (compare Figs. 5.3*B* and *D*). Note also the match between the net change curve in the presence of noise for the same de- and phosphorylation thresholds as in the noiseless case (dashed blue line in Fig. 5.3*B*) with the corresponding transition outcomes in Fig. 5.3*F* (see discussion below).

In summary, the net change curves provide information about possible transition outcomes: (i) The amplitude of the net change in phosphorylation can be seen as the probability of transition for a given Δt. (ii) The shape of the net change curve shows how the transition outcomes with respect to Δt can look like provided τ and b are chosen sufficiently large. It gives the window of opportunity of transitions for the given choice of calcium amplitudes together with the de- and phosphorylation thresholds.

Net change curves for varying de/phosphorylation thresholds The choice of the thresholds above which phosphorylation and dephosphorylation activate (Θ_{phos} and Θ_{dephos}) defines the qualitative transition outcome in the model, *i.e.* the net change in phosphorylation. We will explore the space of possible net phosphorylation change curves by varying extensively both parameters in this section. We furthermore investigate how adding noise to the calcium transients, together with stochastic vesicle release and short-term depression (STD) affects the net change curves and therefore possible transition outcomes. Note that for the STDP spike-pair protocol considered here, the slow recovery of vesicles has only a small impact on consecutive spikes since presynaptic spikes are presented at 1 Hz and the recovery time constant of released vesicles is $\tau_{\text{rec}} = 1000$ ms for the hippocampus (see Tab. 5.1). The low release probability per vesicle yields however a failure rate of 65.6 %.

If the CaMKII is exposed to fluctuating calcium transients and stochastic release as well as short-term depression is considered, two aspects have to be taken into account in the calculation of the net change curve: (i) Due to the stochastic vesicle release, not every presynaptic spike evokes a postsynaptic response (e.g. with a release probability of $p_{\text{r0}} = 0.19$ and 2 independent vesicles, the failure rate is 0.66). (ii) Since the maximal amplitude of the calcium transients evoked by pre- and postsynaptic spikes is drawn from a binomial distribution, the average time spent above a given threshold is the integral over all possible calcium amplitudes occurring with a probability given by this binomial distribution. We can calculate the net change curves in the presence of noise, stochastic release and STD in the following way. We get the time spent above the threshold Θ for a given pair of D_{pre} and D_{post}, $\kappa(\Theta, D_{\text{pre}}, D_{\text{post}})$, by simulating numerically the calcium dynamics and integrating the time the calcium trace spends above Θ. Note that the time spent above the threshold Θ cannot be calculated analytically anymore due to the finite rise time of the NMDA-R-mediated calcium transient. This is done for a discretized subset of pairs of calcium amplitudes (D_{pre}, D_{post}). Finally, we

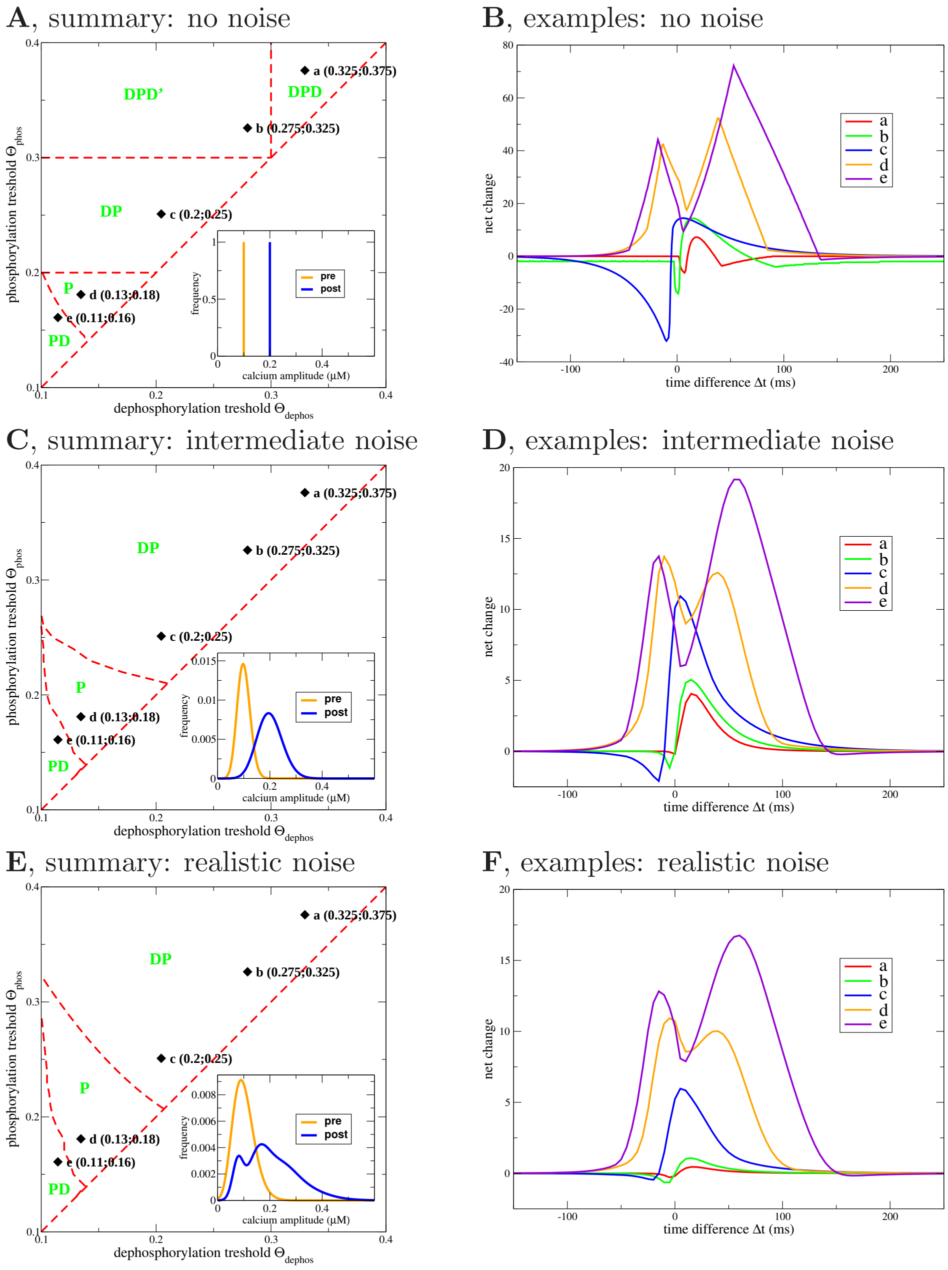

Figure 5.4: Net change curves in response to spike-pairs as a function of $\Theta_{\rm dephos}$ and $\Theta_{\rm phos}$. The $\Theta_{\rm dephos}$ and $\Theta_{\rm phos}$ plane is explored for qualitatively different shapes of net change curves as a function of Δt for three different levels of noise: *A*: no noise; *C*: intermediate noise; and *E*: realistic noise (see 5.1.3 on page 119 for more details). ↗ *See continuation on next page.*

integrate over D_{pre} and D_{post} as

$$\begin{aligned}\kappa(\Theta) &= p_r \int_0^\infty \int_0^\infty dD_{\mathrm{pre}} dD_{\mathrm{post}} \kappa(\Theta, D_{\mathrm{pre}}, D_{\mathrm{post}}) A(D_{\mathrm{pre}}) A(D_{\mathrm{post}}) \\ &\quad + (1-p_r) \int_0^\infty dD_{\mathrm{post}} \kappa(\Theta, D_{\mathrm{pre}} = 0, D_{\mathrm{post}}) A(D_{\mathrm{post}}). \end{aligned} \tag{5.17}$$

$A(D_{\mathrm{pre}})$ and $A(D_{\mathrm{post}})$ are the binomial distributions of maximal amplitudes evoked by pre- and postsynaptic spikes, respectively (see Tab. A.1). p_r is the release probability of one *or* two vesicles at the occurrence of a presynaptic spike. The green and the red dashed lines in Fig. 5.3*B* show $\kappa(\Theta_{\mathrm{phos}} = 0.25\ \mu\mathrm{M}, D_{\mathrm{pre}} = 0.1\ \mu\mathrm{M}, D_{\mathrm{post}} = 0.2\ \mu\mathrm{M})$ and $\kappa(\Theta_{\mathrm{dephos}} = 0.2\ \mu\mathrm{M}, D_{\mathrm{pre}} = 0.1\ \mu\mathrm{M}, D_{\mathrm{post}} = 0.2\ \mu\mathrm{M})$, respectively. Compared to the noiseless case, the times spent above both thresholds is increased in the presence of noise for large Δts. In the specific example shown in Fig. 5.3, presynaptically evoked calcium transients do not cross Θ_{dephos} for large Δt in the absence of noise, since $\Theta_{\mathrm{dephos}} = D_{\mathrm{pre}} + c_0$. Due to calcium transient fluctuations, presynaptically evoked calcium elevations also contribute to the time spent above Θ_{dephos} and Θ_{phos} in the noisy case. However, in the range of Δts for which $c_{\mathrm{pre}}(t)$ and $c_{\mathrm{post}}(t)$ interact, the times spent above Θ_{phos} and Θ_{dephos} are reduced due to the failure rate, *i.e.* the probability that $c_{\mathrm{pre}} = 0$.

At first, we explore the Θ_{dephos} - Θ_{phos} plane with respect to the net phosphorylation change in the absence of noise. Here, we explore the upper triangle of the Θ_{dephos} - Θ_{phos} plane only, the region where $\Theta_{\mathrm{dephos}} < \Theta_{\mathrm{phos}}$. It should be noted that the net change curves in the lower triangle are just the inverse of the net change curves in the upper triangle, *i.e.* the net change curve for (Θ_{dephos}, Θ_{phos}) equals to the net change curve with ($\Theta'_{\mathrm{dephos}} = \Theta_{\mathrm{phos}}$, $\Theta'_{\mathrm{phos}} = \Theta_{\mathrm{dephos}}$) multiplied by -1. In this upper triangle, five regions with qualitatively different net phosphorylation curves exist (see Fig. 5.4*A*).

Figure 5.4: The different distributions from which D_{pre} and D_{post} are drawn at the occurrence of each pre- and postsynaptic spike are shown in the insets in panels *A*, *C* and *E*. Boundaries at which the net change curves change qualitatively are approximated by red dashed lines in panels *A*, *C* and *E*. For each of the five different regions in *A*, an example net change curve is shown in panel *B*. These five examples are also shown for the intermediate and the realistic noise cases in panel *D* and *F*, respectively, for the same pairs of (Θ_{dephos}, Θ_{phos}) (marked in panels *A*, *C* and *E*). Note that the examples **a**, **b** and **c** belong to the region exhibiting STDP-like net change curves (**DP** area) in both noise scenarios. See Tab. 5.1 for parameters. Abbreviations **P** and **D** refer to phosphorylation and dephosphorylation, respectively, and are used to specify the qualitative shape of the net change curves for increasing Δt in the respective area. **DPD'** refers to a case where the net change curve does not converge to zero but remains negative for large negative and positive Δt (see text for more details).

Dephosphorylation-phosphorylation (DP) region: The thresholds considered in Fig. 5.3 and discussed in the previous section are part of a region in which the net change curves show a STDP-like behavior (see point **c** in Fig. 5.4): Short negative time lags provoke a negative net change - dephosphorylation - and short positive time lags lead to a positive net change - phosphorylation of CaMKII. Such net phosphorylation change curves can potentially lead to transition outcomes consistent with experimental data (Bi and Poo 1998; Wang et al. 2005).

Dephosphorylation-phosphorylation-dephosphorylation' (DPD') region: If the phosphorylation threshold is increased above the maximal amplitude of postsynaptically calcium transients, *i.e.* $\Theta_{\text{phos}} > c_0 + \bar{D}_{\text{post}}$ ($c_0 + \bar{D}_{\text{post}} = 0.3$ μM for the parameters chosen here), calcium transients cross the phosphorylation threshold only if both calcium transients interfere with each other. Therefore, the dephosphorylation evoked by the time spent above the dephosphorylation threshold cannot be compensated for by phosphorylation for large Δts. As a result, depotentiation is observed for large positive and large negative Δts (see point **b** in Fig. 5.4*A* and *B*). This furthermore implies that the ratio between phosphorylation and dephosphorylation cannot be fixed by the criterion stated above, namely to have zero net change for $|\Delta t| \to \infty$ (Eq. (5.11)). We adjust the ratio between phosphorylation and dephosphorylation in example **b** (Fig. 5.4*B*) such that the maximum net dephosphorylation and the maximum net phosphorylation have approximately the same amplitudes (this ratio is 4 for case **b** in Fig. 5.4*B*).

Dephosphorylation-phosphorylation-dephosphorylation (DPD) region: The phosphorylation threshold is larger than the maximal amplitude of postsynaptically evoked calcium transients as in the DPD' region. If furthermore the dephosphorylation threshold exceeded the maximum amplitude of calcium transients evoked by a postsynaptic spike, *i.e.* $\Theta_{\text{dephos}} > c_0 + \bar{D}_{\text{post}}$, spike-pairs with large Δts do not activate phosphorylation nor dephosphorylation at all. This means that the net change in phosphorylation for large absolute values of Δt is zero. Again, we chose the ratio between phosphorylation and dephosphorylation such that in the range of interaction between both calcium contributions, the amplitudes of positive and negative net phosphorylation changes are approximately the same (the ratio is 7 for case **a** in Fig. 5.4*B*). Despite the STDP-like behavior of the net change curve in this region, a second net dephosphorylation region at positive Δts is present. Such a range of negative net changes would lead to LTD transitions in the model in this range of Δt values. A similar region has been observed by Shouval et al. (2002), Karmarkar et al. (2002) and Abarbanel et al. (2003). It emerges from calcium transients which are large enough to cross the dephosphorylation threshold but too small to activate phosphorylation. Such a region of net dephosphorylation appears on the left-hand and the right-hand side of the non-zero net change curve, before the calcium transients are sufficiently separated and do not cross any threshold at all for larger absolute Δt values. The choice of a and b in regions DPD' and DPD yields similar positive and negative amplitudes of the net change in phosphorylation. This choice is arbitrary and it should be noted that depending on the choice of a and b, the whole range from strong net phosphorylation only to strong net dephosphorylation only can be covered for short Δts.

Phosphorylation (P) & phosphorylation-dephosphorylation (PD) region: If both thresholds are below the maximum amplitude of the NMDA-R mediated calcium contribution ($\Theta_{\text{dephos}}, \Theta_{\text{phos}} < \bar{D}_{\text{pre}}$), phosphorylation is dominant in the range of interaction of both calcium transients. However, in the PD region a small range of negative net changes exists at large positive Δts.

When noise is added to the model, net change curves change considerably. We chose to use the same parameters for the STD realization but two different binomial distributions to simulate fluctuating calcium transients. We use binomial distributions with the same mean but two different values of the variance: intermediate noise (Fig. 5.4*C* and *D*) and realistic noise (Fig. 5.4*E* and *F*).

Adding noise makes the DPD' and DPD region disappear from the considered region in the Θ_{dephos} - Θ_{phos} plane. Regions DP, P and PD move to larger Θ_{phos} values with increasing noise level. Regions DPD' and DPD disappear since due to the distribution of calcium amplitudes there exist always a fraction of amplitudes with is large enough to cross the phosphorylation and the dephosphorylation threshold even if the mean of both distributions is below both thresholds. Recall that regions DPD' and DPD emerge since calcium transients induced by large Δts do not cross the phosphorylation and the dephosphorylation threshold, respectively. Short-term depression and the fluctuations in the calcium transients together reduce strongly the positive and the negative amplitudes of the net phosphorylation change curves. Fluctuating calcium transients diminish in particular the negative part of the net change curve since this part relies on calcium transients spending time in between Θ_{dephos} and Θ_{phos}. Fluctuations reduce the time spent in this bounded region while the range evoking positive net changes above Θ_{phos} is not bounded from above and therefore less affected by fluctuations. Since not every presynaptic spike evokes a calcium response, the time spent above both thresholds is drastically reduced. However, the qualitative shape of the net change curve remains unchanged whether or not STD is added to the model. STD corresponds therefore to a general but non-uniform down-scaling of the entire net change curve.

Fig. 5.4*D* and *F* show examples of net change curves for five different choices of (Θ_{dephos}, Θ_{phos}). Comparing the net change curves between both panels confirms that increasing the noise level decreases the amplitude of the net changes in phosphorylation. As outlined in the previous paragraph, the negative and the positive peak in the net change curve curves seem to be affected differently for different pairs of Θ_{dephos} and Θ_{phos}. For case **c**, higher noise levels reduce the net dephosphorylation part more strongly than the phosphorylation part of the net change curve (compare blue lines in Fig. 5.4*D* and *F*, see previous paragraph). In another example, the net change curve amplitudes seem to get nearly balanced in case **a** for higher noise levels (see red lines in both panels).

Let us quantify further the changes of the net change curves in the presence of noise in the region in which it shows a STDP-like behavior (DP region for intermediate and realistic noise levels in Fig. 5.4*C* and *E*). We determine the peak of the largest positive net change at short positive time lags (A_{P}) and likewise for the largest negative net change at short negative time lags (A_{D}, see Fig. 5.5*A* for an illustration). The ratio of these two net change amplitudes ($A_{\mathrm{P}}/A_{\mathrm{D}}$) is shown in Fig. 5.5*B* and *D* for the intermediate and the realistic noise case, respectively. This ratio assumes very high values at the border of DP region to low dephosphorylation thresholds for both cases of noise (border at the lower left side in the Θ_{dephos} - Θ_{phos} plane). The negative peak of the net change curve emerges at this border and has therefore a small amplitude compared to the positive peak (*i.e.* the $A_{\mathrm{P}}/A_{\mathrm{D}}$ ratio is high). The ratio is everywhere above 1 in the depicted region, *i.e.* net phosphorylation at positive Δt is always larger than net dephosphorylation at $\Delta t < 0$ ms. However, the ratio approaches the value of one if the difference between the two thresholds becomes small, *i.e.* $\Theta_{\mathrm{phos}} \rightarrow \Theta_{\mathrm{dephos}}$, which is the case at the diagonal in the phase plane. Note that the simplified considerations in the previous section (immediate rise times and same decay time constants of both calcium transients) suggest that the amplitudes of the net change curve become equal if Θ_{dephos} and Θ_{phos} are chosen close to the diagonal (for the specific parameters chosen there, see above). With increasing noise, the region of nearly equal amplitudes seems to shift to higher absolute values of Θ_{phos} and Θ_{dephos} (compare **a**, **b** and **c** in Fig. 5.4*D* and *F*).

Another measure chosen to quantify the net change curves in the STDP-like region (DP region in Fig. 5.4) in the presence of noise is the ratio of the integrals of the areas below the positive (I_{P}) and the negative (I_{D}) parts of the curve (*i.e.* the ratio is determined by $I_{\mathrm{P}}/I_{\mathrm{D}}$). Fig. 5.5*C* and *E* show the ratios between the positive area and the negative area below the net change curves for intermediate and realistic noise levels. The qualitative behavior is similar to the ratio of the peaks - close to the border at low Θ_{dephos} the ratio goes to infinitively high values since the negative part of the net change curve emerges there, *i.e.* both peak and integral are very small. Again, close to the diagonal and for high Θ_{dephos} values in the high noise case, the ratio of the integral approaches 1, meaning nearly equilibrated areas under the positive and the negative part. Note, however, that the value does not drop below one at any point in the considered range.

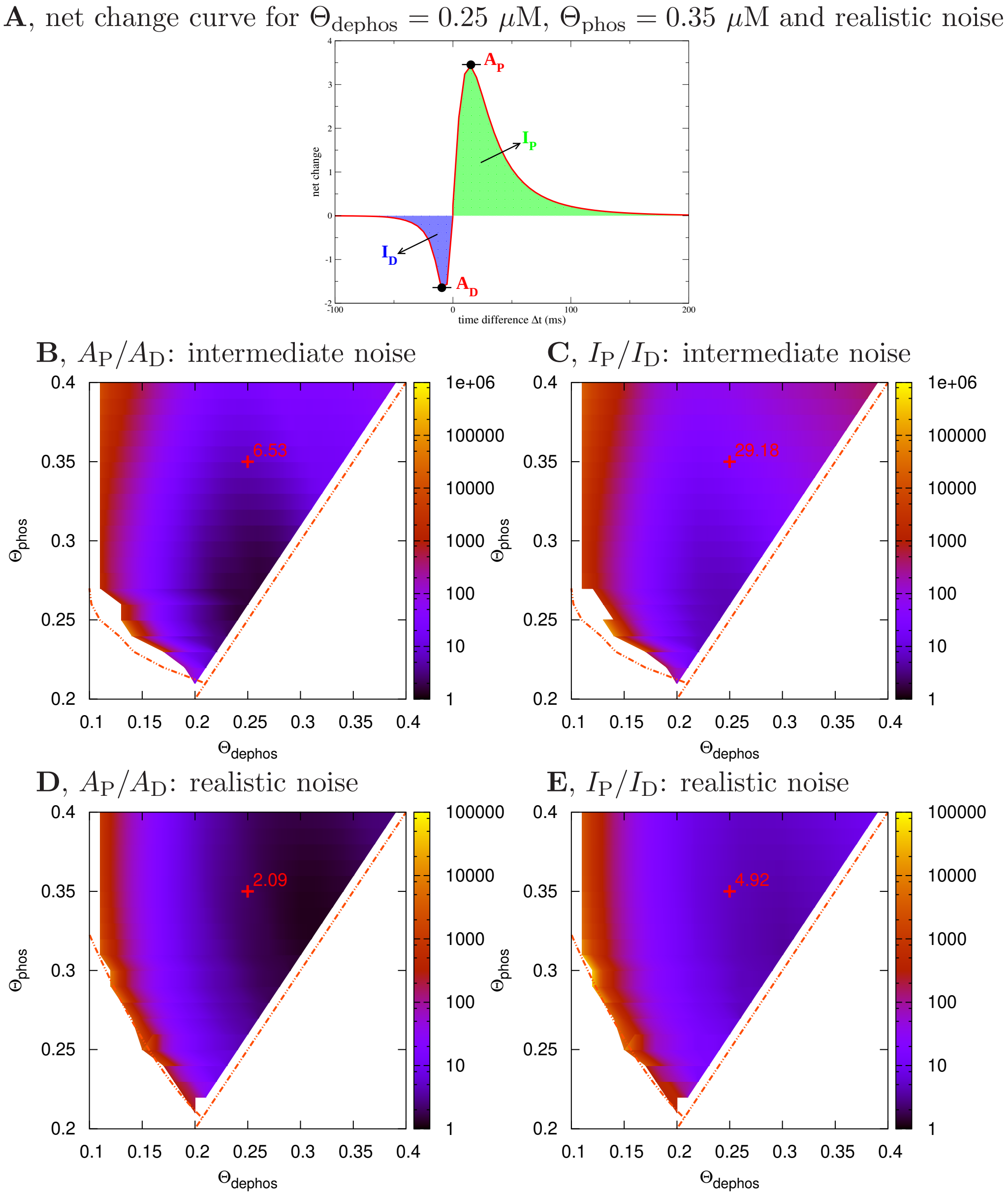

Figure 5.5: Ratios of maximal amplitudes and integrals of net change curves in the DP region. ***A***, Net change curve in CaMKII phosphorylation evoked by spike-pair stimulation for $\Theta_{\mathrm{dephos}} = 0.25\ \mu$M and $\Theta_{\mathrm{phos}} = 0.35\ \mu$M, in the presence of realistic noise: This example and all considerations in this figure refer to the **DP** ("STDP-like" net change curves) areas in Fig. 5.4*C* and *E*. The parameters analyzed in this figure are illustrated: A_{D} and A_{P}: maximal negative and positive amplitudes of the net change curve, respectively; I_{D} and I_{P}: integrals of the negative (blue shaded) and the positive part (green shaded) of the net change curve, respectively. ↗ *See continuation on next page.*

5.3.2 Spike-pair and -triplet stimulations and plasticity outcomes

After having characterized extensively how the net change curves depend on parameters, we chose a pair of de- and phosphorylation thresholds and realistic noise levels (see Tab. 5.1) in this section and expose the CaMKII model to STDP spike-pair and spike-triplet stimulation protocols. Conditions for which the plasticity outcome resembles experimental results are elaborated.

STDP spike-pair transition outcomes The net change curve for $\Theta_{\text{phos}} = 0.25$ μM and $\Theta_{\text{dephos}} = 0.2$ μM in the presence of noise is very unbalanced, *i.e.* it exhibits a small net dephosphorylation amplitude at $\Delta t < 0$ ms compared to the positive amplitude at $\Delta t > 0$ ms (see dashed blue line in Fig. 5.3*B* and transition results in *F*). As pointed out in the previous section, the ratios of the positive and negative amplitudes and of the integrals of the net change curve become more balanced, *i.e.* approaches the value of one, if the difference between Θ_{phos} and Θ_{dephos} is small and for high values of Θ_{dephos} (see Fig. 5.5*D* and *E*). However, if both thresholds are close together, the absolute values of the negative and positive net changes are small. Here we chose to examine the case $\Theta_{\text{phos}} = 0.35$ μM and $\Theta_{\text{dephos}} = 0.25$ μM. The inset in Fig. 5.6 shows the net change curve for this combination of thresholds and the main panel shows the average synaptic change after exposure to 60 pairs of spike-pairs occurring at 1 Hz as a function of Δt (see red lines).

Though the change in synaptic weights depicted by the red line in Fig. 5.6 reproduces the qualitative behavior of experimental plasticity outcomes, the quantitative match between the model results and experiments is not so good. In particular, the range of negative time lags evoking LTD is larger than the range of positive time lags evoking LTP in experiments (Magee and Johnston 1997; Bi and Poo 1998; Debanne et al. 1998; Wang et al. 2005). In the model, the extent of the LTD part is determined by the range of interaction between the postsynaptically evoked calcium transient and the presynaptically evoked one. That implies in

Figure 5.5: ***B & D***, Ratio of maximal amplitudes ($A_{\text{P}}/A_{\text{D}}$) in the Θ_{dephos} - Θ_{phos} plane for intermediate (panel *B*) and for high noise levels (panel *D*; see the two different distributions of calcium amplitudes in Fig. 5.4*C* and *E*): The ratio of amplitudes at the position ($\Theta_{\text{dephos}} =$ 0.25 μM, $\Theta_{\text{phos}} = 0.35$ μM) of the example shown in panel *A* for realistic noise is marked in panel *D*. For comparison, the ratio is also indicated for intermediate noise levels at the same point in panel *B*. ***C & E***, Ratios of the integrals below the positive and the negative part of STDP-like net change curves ($I_{\text{P}}/I_{\text{D}}$) in the Θ_{dephos} - Θ_{phos} plane for the same two levels of noise as in panel *B* and *D*: The ratio of integrals at the position ($\Theta_{\text{dephos}} = 0.25$ μM, $\Theta_{\text{phos}} = 0.35$ μM) of the example shown in panel *A* for realistic noise is marked in panel *E*. Again, the ratio is also indicated at the same point in panel *C* for intermediate noise.

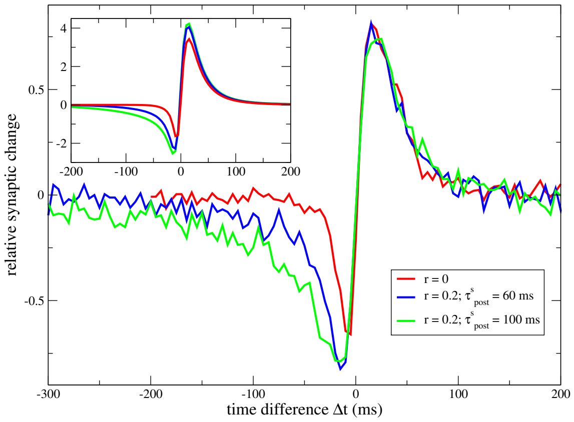

Figure 5.6: Net change and transition outcomes in response to STDP spike-pair stimulation protocols as a function of Δt. The relative change in the number of synapses in the UP state is shown for STDP spike-pair stimulation protocols as a function of Δt, for different values of the slow VDCC-mediated calcium contribution. Realistic noise levels are used to generate the calcium transients (see section 5.1.2 on page 118 for details). The three cases depicted in different colors correspond to three different combinations of fast and slow components in c_{post}: red line: $r = 0$ and $a/b = 4.9$; blue line: $r = 0.2$, $\tau^s_{\text{post}} = 60$ ms and $a/b = 5.1$; green line: $r = 0.2$, $\tau^s_{\text{post}} = 100$ ms and $a/b = 5.2$ ($b = 0.005$ 1/s in all cases). The transition outcomes show averages over $N = 500$ trials (250 synapses initially in the UP state and 250 initially in the DOWN state). The inset shows the net change curves in phosphorylation for the same combinations of parameters as for the transition outcomes, each in the same color. The ratios between phosphorylation and dephosphorylation for the net changes are: red line: $a/b = 5.05$, blue line: $a/b = 5.05$ and green line: $a/b = 5.1$ (see Tab. 5.1 for other parameters).

turn that the single exponential decay time constant of $c_{\text{post}}(t)$ governs the extent of the LTD range with respect to Δt. To test this, we split the postsynaptically evoked calcium contribution in a fast and a slow component, *i.e.* $c^{(fast)}_{\text{post}}$ and $c^{(slow)}_{\text{post}}$ decaying with τ^f_{post} and τ^s_{post}, respectively (see section 5.1.2 on page 118). r is the control parameter defining the balance between both components, *i.e.* changing r from 0 to 1 changes the composition of $c_{\text{post}}(t)$ from fast decaying component only to slow decaying component only with a weighted mixture in between (until now $r = 0$ has been employed in all simulations).

Fig. 5.6 shows what happens if the range of interaction between pre- and postsynaptic calcium transients is extended by choosing $r = 0.2$ together with $\tau^s_{\text{post}} = 60$ ms or 100 ms (see blue or green line in Fig. 5.6, respectively). The respective net phosphorylation change curves are shown in the inset. Again, the net change curves predict remarkably well the transition outcomes of the CaMKII model shown in Fig. 5.6. However, the ratios, a/b, suggested by the net change curves to yield zero net change for large absolute values of Δt *do* yield directed transitions in the simulations of the phosphorylation level dynamics for large Δt. Hence, the ratios in the simulations are chosen to take slightly different values to avoid transitions for large values of Δt (see caption of Fig. 5.6). This deviation is due to the transient of short-term depression in the beginning of the stimulation protocol. The net change curves are calculated for the case that STD reached a steady probability of evoking a postsynaptic calcium response during the stimulation protocol. p_{r} denotes the probability of release of one or two vesicles *during* the presentation of spike-pairs at 1 Hz (used in Eq. (5.17)). In the beginning of the simulations, however, there exists a transition phase from the initial conditions in which both vesicles are ready to release (since $N_{\mathrm{v}} = 2$) to the average value of vesicle release during the protocol. The initial probability to observe one or two vesicles is given by $p_{\mathrm{r0}}(2 - p_{\mathrm{r0}})$. This transition phase explains the difference in a/b ratios between the net change curve and the transition results.

In summary, the reduced model describing CaMKII phosphorylation dynamics can reproduce quantitatively experimental plasticity outcomes in response to the STDP spike-pair protocol. Depending on the choice of the activation thresholds of phosphorylation (Θ_{phos}) and dephosphorylation (Θ_{dephos}) and on the time course of the postsynaptically evoked calcium transient (*i.e.* the choice of r and τ^s_{post}), the model can even exhibit a quantitative match with experimental data.

STDP spike-triplet transition outcomes More recently, STDP stimulation protocol investigations have been extended to triplets of spikes. We expose the CaMKII model to calcium transients evoked by spike-triplets and compare the transition results to experimental plasticity data obtained in the hippocampus by Wang et al. (2005).

Each triplet consists of either two pre- and one postsynaptic spike (pre-post-pre triplet) or two post- and one presynaptic spike (post-pre-post triplet). Triplets are presented 60 times at a frequency of 1 Hz (see Wang et al. (2005)). Triplets are specified by a doublet of time differences, Δt_1 and Δt_2, where Δt_1 denotes to the time difference between the first and the second spike, and Δt_2 the time difference between second and third spike (see Fig. 2.4 for more details concerning the triplet convention). Experimentally, Wang et al. (2005) observe potentiation for post-pre-post triplets and no change for pre-post-pre triplets.

The transition results of the CaMKII model exposed to spike-triplet simulation protocols are shown in Fig. 5.7*B*. Fig. 5.7*A* shows the net change in phosphorylation obtained through numerical simulations. We use the same parameter set as in the previous section. Furthermore, Fig. 5.7 utilizes $r = 0$. The plasticity results are qualitatively unchanged when $r = 0.2$, $\tau^s_{\mathrm{post}} = 60$ ms or 100 ms (results not shown). The transition results are consistent with experimental data, *i.e.* potentiation for post-pre-post triplets (lower right quadrant) and no change

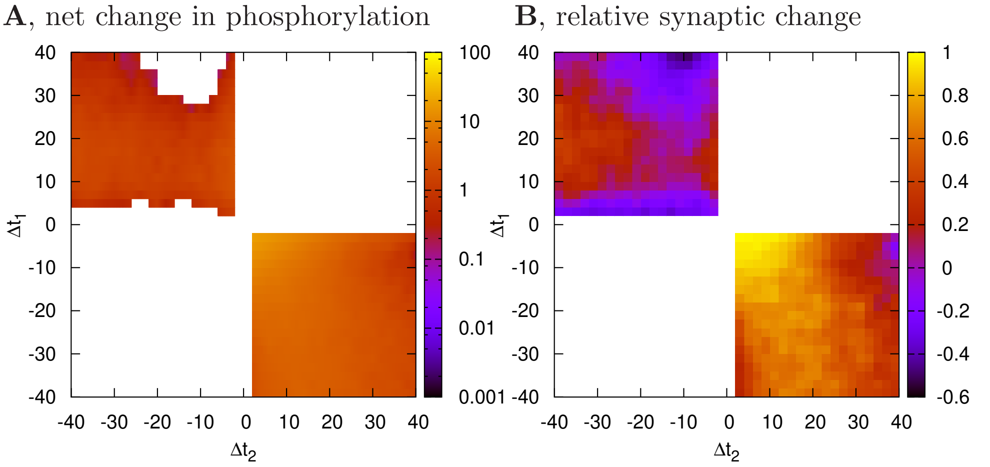

Figure 5.7: Net change and transition outcomes in response to STDP spike-triplet stimulation protocols. ***A***, Net change in CaMKII phosphorylation in response to STDP spike-triplet stimulation protocols. The net change is shown for pre-post-pre (upper left quadrant) and post-pre-post triplets (lower right quadrant). In the missing areas in the upper left quadrant, the net change assumes low negative values and cannot be depicted due to the logarithmic scaling. The same parameter set as for the case shown in Fig. 5.6 by the red line is used in panel *A* and *B* (*i.e.* $r = 0$ and $a/b = 4.9$). Both panels show averages over $N = 100$ runs (50 synapses initially in the UP and 50 in the DOWN state). ***B***, Relative synaptic change in response to STDP spike-triplet stimulation protocols. The relative change in the number in synapses in the UP state is shown (see Tab. 5.1 for more parameters).

for pre-post-pre triplets (upper left quadrant). Note that this is achieved with the same parameters as in the spike-pair simulations.

Short-term depression of synaptic transmission is at the origin of the difference between transition outcomes in response to pre-post-pre and post-pre-post triplets. Pre-post-pre triplets include two consecutive presynaptic spikes in contrast to post-pre-post triplets. Short-term depression leads on average to strongly reduced calcium elevation in response to the second spike in pre-post-pre triplets. This reduced elevation in response to the third spike in pre-post-pre triplets crosses the dephosphorylation threshold and prevents down-to-up transitions normally evoked by the first two spikes (pre-post pair) (see Cai et al. (2007)).

5.4 Frequency dependence of synaptic plasticity

Besides the relative timing between spike-pairs and -triplets, it has been shown experimentally that the frequency of synaptic stimulation determines the observed plasticity outcome (Dunwiddie and Lynch 1978; Dudek and Bear 1992). Here,

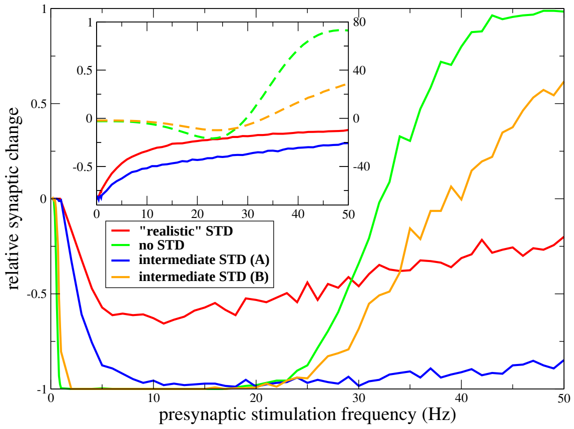

Figure 5.8: CaMKII transition results in response to presynaptic stimulations at varying frequencies. The relative change in the number of synapses in the UP state is shown for presynaptic stimulation protocols as a function of the stimulation frequency. The four depicted cases refer to different realizations of short-term depression: red line: STD with the parameters given in Tab. 5.1 for the hippocampus ("realistic" STD); green line: no STD, *i.e.* every presynaptic spike evokes a postsynaptic calcium response; blue line: case (A), $\tau_{\text{rec}} = 500$ ms and $p_{\text{r0}} = 0.19$, and orange line: case (B), $\tau_{\text{rec}} = 10$ ms and $p_{\text{r0}} = 0.5$. The inset shows the net change curves for the four different cases in the same colors as used to depict the relative synaptic change. Note that the full lines in the inset correspond to the left-hand scale of the y-axis and the dashed lines to the right-hand scale ($b = 0.005$ 1/s, $a/b = 4.9$, see Tab. 5.1 for other parameters).

we investigate the dynamics of the reduced CaMKII phosphorylation model in response to purely presynaptic stimulation protocols at different frequencies. We also vary the frequency of the spike-pair presentation of STDP protocols and study how this affects the transition outcomes.

Purely presynaptic stimulation protocols Dudek and Bear (1992) stimulate Schaffer collateral connections to the CA1 area in the Hippocampus 900 times at different frequencies, f. No changes are evoked for low stimulation frequencies ($f < 1$ Hz), intermediate stimulation frequencies lead to LTD ($1 < f < 10$ Hz) and they observe LTP for high frequencies ($f > 10$ Hz).

The reduced model of CaMKII phosphorylation is exposed to fluctuating calcium transients (realistic noise level) evoked by 900 presynaptic spikes at a fixed frequency. The transition outcomes are shown in Fig. 5.8 for different realizations of short-term depression. Let's at first focus on the case for which the same parameter set as used in Fig. 5.6 (red line) and 5.7 is utilized (shown by the red line in Fig. 5.8). No transitions are evoked for low frequencies ($f < 1$ Hz), while for $f > 1$ Hz LTD is observed up until a stimulation frequency of 50

Hz. Once a vesicle is released it is not available for release of neurotransmitter at the arrival of subsequent spikes in a time range of 1 s (see STD parameter in Tab. 5.1). Therefore for high frequencies, a large number of presynaptic spikes do not evoke postsynaptic calcium transients due to the slow recovery of released vesicles ($\tau_{\text{rec}} = 1$ s). In turn, the postsynaptic calcium elevation does not reach high enough values to activate CaMKII phosphorylation, *i.e.* dephosphorylation prevails and prevents LTP transitions for high frequencies. This behavior can also be seen by inspecting the net phosphorylation change for this stimulation protocol (shown in the inset in Fig. 5.8 by the red line). The net change curve is negative for all frequencies in the depicted range. Low frequencies, however, do not evoke LTD since the phosphorylation changes are too far apart in time from each other in order to accumulate and to lead to a crossing of the unstable steady-state, *i.e.* the phosphorylation changes decay before the next presynaptic spike evokes another dephosphorylation.

How does STD influence the transition outcome? This question is addressed by changing the parameters of the STD implementation in the model, *i.e* by changing τ_{rec} and p_{r0}. If STD is removed from the simulations, *i.e.* every presynaptic spike evokes a calcium transient, the transition outcomes qualitatively resemble experimental data (compare green line in Fig. 5.8 and Dudek and Bear (1992)): in a range of intermediate frequencies LTD transitions are evoked (for $0.6 < f < 30$ Hz) and stimulations above 30 Hz lead to LTP. The transition results with respect to f can be transferred from the realistic STD implementation (scenario described in the previous paragraph and depicted by the red line in Fig. 5.8) to the case without STD by decreasing τ_{rec} and increasing p_{r0}. In other word, by changing these two parameters (τ_{rec} and p_{r0}) transition results in between the case without STD and the case with realistic STD can be obtained. The two intermediate STD cases shown in Fig. 5.8 describe transition outcomes in between the two extreme cases for the following sets of (τ_{rec}, p_{r0}): (500 ms, 0.19) in case **A** and (10 ms, 0.5) in case **B** (see Fig. 5.8). In general, for LTP transitions to occur at high presynaptic stimulation frequencies, recovery of vesicles has to be fast and release probability high in order to allow for high postsynaptic calcium elevations.

We show here that short-term depression prevents LTP induction for high presynaptic stimulation frequencies. This results depends on the STD parameters but hippocampal STD (see Tab. 5.1) seems to rely on simultaneous postsynaptic activity in order to evoke synaptic changes. This is suggested by experimental data showing that a block of postsynaptic activity prevents the induction of LTD at low stimulation frequencies (3 Hz) in Schaffer collateral - CA1 neuron synapses (Christie et al. 1996). Note, however, that our results are valid for the specific choice of de- and phosphorylation thresholds as well as calcium amplitudes. Whether a different set of parameters can reproduce experimental STDP results and yield LTP at high presynaptic stimulation frequencies in the presence of "realistic" STD remains to be investigated. See discussion for more details.

Frequency dependence of STDP spike-pair evoked transition outcomes Until now, pairs of pre-and postsynaptic spikes are presented for 60 times at a frequency of 1 Hz. What happens if the presentation frequency is varied while the total number of spike pairings is kept constant?

Experimental data from visual cortex slices suggest that low frequency presentations of pre-post pairings ($\Delta t = 10$ ms) evoke no changes, while post-pre pairings ($\Delta t = -10$ ms) presented at low frequencies ($f = 0.1$ Hz) evoke LTD (Sjöström et al. 2001). Intermediate presentation frequencies ($f = 10$, 20 Hz) evoke LTP for pre-post pairings and LTD for post-pre pairings as it is the case in the results presented above for presentations at 1 Hz. In turn, for high presentation frequencies ($f = 40$, 50 Hz) LTP is observed for both pairings, pre-post and post-pre (Sjöström et al. 2001). The latter result can be explained by the fact that the short intervals between post-pre pairings result in accumulation of calcium in between pairs at sufficiently large frequencies. The calcium transients evoked by the pairs are not independent of preceeding and following spike-pairs as they are for $f = 1$ Hz. Therefore, phosphorylation is favored due to interactions between spike-pairs via the calcium trace. We employ the same stimulation protocol as used in experiments (see Sjöström et al. (2001)). For the low spike-pair presentation frequency of 0.1 Hz, the protocol consists of pre- and postsynaptic spike-pairs with the respective Δt (+10 ms or -10 ms) presented at a frequency of 0.1 Hz for 50 times. Induction protocols at higher frequencies (10 Hz and larger) consist of five spike-pairs at the respective frequency. These blocks of 5 pairs are repeated 15 times at 0.1 Hz. The transition between these two different stimulation patterns is done between 0.9 Hz (50 pairings at the respective f) and 1 Hz (15 times 5 pairings) protocols in our simulations.

Sjöström et al. (2001) report LTD transitions at 0.1 Hz for post-pre pairings but no changes for pre-post pairings. For the net change in phosphorylation, we impose that spike-pairs with large Δts evoke no change in phosphorylation. With this requirement and the parameters chosen so far, spike-pairs with a relative time difference of +10 ms evoke a positive net change in phosphorylation which is always larger in amplitude as the negative net change elicited by spike-pairs with $\Delta t = -10$ ms (see Figs. 5.5 and 5.6). We furthermore highlight that the net change in phosphorylation can be seen as window of opportunity to evoke transitions for specific Δt. Hence, the scenarios investigated so far suggest a higher down-to-up transition probability for $\Delta t > 0$ compared to the up-to-down transition probability for $\Delta t < 0$. This seems however at odds with the experimental results indicating that LTD induction is more likely at low presentation frequencies as LTP in the visual cortex.

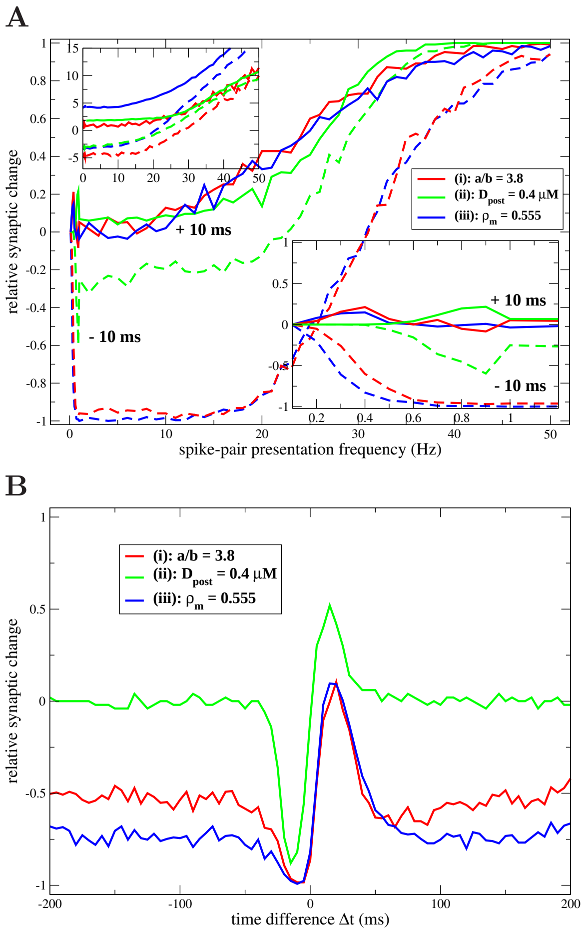

Figure 5.9: Transition outcomes in response to STDP spike-pair stimulations at varying frequencies and time differences, Δt. ***A***, Transition results in response to the STDP protocol at different presentation frequencies of spike-pairs (see experimental results from visual cortex slices in Sjöström et al. (2001) and Fig. 2.5): The relative change in the number of synapses in the UP state is shown as a function of the presentation frequency. The simulations are performed with $\Delta t = +10$ ms (full lines) and $\Delta t = -10$ ms (dashed lines). Red lines: net change curve horizontally shifted towards lower values (case (i) in text and in panel; $a/b = 3.8$, $a = 0.019$ 1/s, $\rho_{\mathrm{m}} = 0.5$ μM, $D_{\mathrm{post}} = 0.2$ μM); Green lines: higher postsynaptically evoked calcium transient amplitude (case (ii) in text and in panel; $a/b = 2.12$, $a = 0.0047$ 1/s, $\rho_{\mathrm{m}} = 0.5$ μM, $D_{\mathrm{post}} = 0.4$ μM); and blue lines: position of the unstable steady-state moved towards higher concentrations (case (iii) in text and in panel; $a/b = 4.9$, $a = 0.0245$ 1/s, $\rho_{\mathrm{m}} = 0.555$ μM, $D_{\mathrm{post}} = 0.2$ μM). The lower right inset shows the same curves in the low frequency range 0.1 – 1.2 Hz. The upper left inset shows the net change curves for the $\Delta t = +10$ ms stimulation protocol (full lines) and the $\Delta t = -10$ ms protocol (dashed lines) and for the three different realizations in the same color as in the main panel (see above).

How can we account for experimentally observed plasticity results in response to spike-pairs at different frequencies in visual cortex in the framework of the reduced model? Three different changes in the model allow to reproduce experimental data: (i) Properties of synapses in the visual cortex could be such that closely spaced pre-post pairings evoke no changes. In terms of the net change curve, this would mean that the net change in phosphorylation is zero at $\Delta t = +10$ ms or the amplitude in net change is smaller at $\Delta t = +10$ ms than at $\Delta t = -10$ ms. Adjusting this property with the parameter set used so far ($\Theta_{\text{phos}} = 0.35$ μM, $\Theta_{\text{dephos}} = 0.25$ μM) would mean that the net change for large negative and positive Δt does not converge to zero anymore. In other words, all parameters are left unchanged except for a which takes the value 0.019 1/s, *i.e.* $a/b = 3.8$ instead of $a/b = 4.9$. (ii) The criterion of zero net change for $\Delta t \rightarrow \pm\infty$ could be conserved if the amplitude of net dephosphorylation at $\Delta t = -10$ ms is larger than that of net phosphorylation at $\Delta t = +10$ ms. This implies an ratio between the maximal positive amplitude and the maximal negative amplitude of the net change curve which is smaller than 1. Such a scenario cannot be attained with the choice of $D_{\text{post}}/D_{\text{pre}} = 2$ used so far since the ratios shown in Fig. 5.5*B* and *D* never drop below 1. Also, if a slow component is added to the calcium transients evoked by BPAPs and mediated by VDCCS, the ratio seems to stay always larger than 1 (see inset in Fig. 5.6). The analytical calculations of the net change curve for calcium transients with immediate rise times suggest, however, that the negative peak of the net change curve scales with D_{post} while the positive peak scales with $D_{\text{pre}} + \Theta_{\text{phos}}$ (see section 5.2 on page 122). Hence, using a higher amplitude of the postsynaptically evoked calcium transient increases the amplitude of the negative peak and leads to a higher probability to evoke up-to-down transitions at low frequencies. (iii) Another way to reconcile zero net change for $\Delta t \rightarrow \pm\infty$ and the Sjöström data is a change in the position of the unstable steady-state which separates the basins of attraction of the UP and the DOWN state. Until now, $\rho_{\text{m}} = \rho_{\text{up}}/2$ has been used. Increasing the unstable steady-state postion extends the basin of attraction of the DOWN state and reduces that of the UP state. This means that up-to-down transitions become more likely than down-to-up transitions.

In order to reproduce the synaptic plasticity data in visual cortex, we explore the three scenarios, listed above. The respective net change curves and the transition results of the reduced model are shown in Fig. 5.9*A*. The resulting net

Figure 5.9: *B*, Transition results in response to spike-pair stimulations (60 presentations at a frequency of 1 Hz) as a function of Δt: The presentation frequency is kept constant. The results use the same parameters as in the three cases shown in panel *A* (depicted in the same colors). Short-term depression is described by parameters accounting for vesicle dynamics in the visual cortex (see Tab. 5.1). ($N = 500$, see Tab. 5.1 for other parameters).

changes in CaMKII phosphorylation for the three choices of parameters and the Sjöström stimulation protocol described above can be seen in the upper left inset in Fig. 5.9*A*. As expected for case (i), the lower amplitude in net phosphorylation for the $\Delta t = +10$ ms protocol compared to the dephosphorylation evoked by $\Delta t = -10$ ms pairings at low frequencies provokes up-to-down transitions at low frequencies only (see full and dashed red lines in the upper left inset in Fig. 5.9*A*). The same is true for case (ii), the absolute value of the negative net change for $\Delta t = -10$ ms is larger than that of the positive net change for $\Delta t = +10$ ms at low frequencies (see green lines in the upper left inset in Fig. 5.9*A*). This is due to the high $D_{\text{post}}/D_{\text{pre}}$ ratio used, *i.e.* this ratio is 4 in case (ii) instead of 2 utilized in cases (i) and (iii). This high amplitude ratio assures furthermore that the total net change converges to zero for $\Delta t \to \pm\infty$ (compare Fig. 5.9*B*). Even if the net change curves have comparable amplitudes at low presentation frequencies in case (iii) (see blue lines in the upper left inset in Fig. 5.9*A*), the higher unstable steady-state favors up-to-down transitions at low frequencies (see blue lines in Fig. 5.9*A*). High frequency stimulations however yield down-to-up switches in all cases since the calcium transients in between spike-pairs start to interact. Interestingly, whether the net change curve is horizontally shifted or the unstable steady-state is increased, the CaMKII transition results are very similar for these two cases ((i) and (iii)).

In summary, the model reproduces the frequency dependence of STDP spike-pair plasticity results in the visual cortex (Sjöström et al. 2001). We propose three different scenarios able to account for the experimental data. The three cases imply changes of different kinds on the reduced model: horizontal shift of the net change curve, larger postsynaptically evoked calcium amplitude and increase in the postion of the unstable steady-state. It would be interesting to determine a stimulation protocol which would allow to distinguish these scenarios experimentally. Exposing visual cortex neuron pairs to 60 spike-pairs at a frequency of 1 Hz, for example, does not allow to discriminate between case (i) and (iii) (see Fig. 5.9*B*).

5.5 Comparing full six-subunit and reduced model of CaMKII phosphorylation

We end this chapter by showing how the behavior of the reduced model presented in this chapter compares with the behavior of the detailed six-subunit model (see chapter III for details on the six-subunit model).

We have shown above that the level of fluctuations in the calcium transients and the implementation of short-term depression changes drastically the plasticity outcomes. In the six-subunit model, maximal conductances of the NMDA-R- and

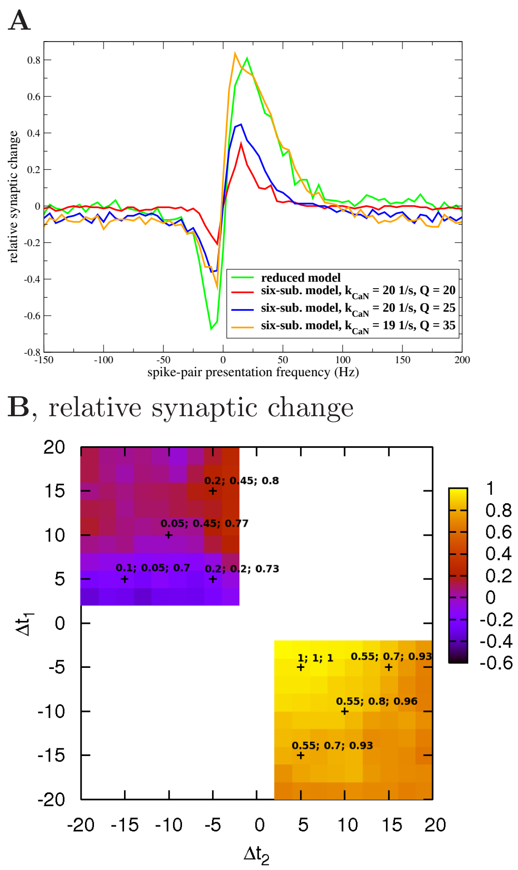

Figure 5.10: Comparison of transition outcomes between the six-subunit and the reduced model in response to STDP spike-pair and -triplet protocols. ***A***, Average transition results in response to STDP spike-pair stimulation protocols for the six-subunit and the reduced model: The green line shows the relative change in number of synapses in the UP state for the reduced model presented in this chapter (same results as shown by red line in Fig. 5.6; *i.e.* $a/b = 4.9$, $r = 0$). The transition results of the full model in response to calcium transients evoked by spike-pairs are shown for three combinations of k_{CaN} and Q: red line: $k_{\mathrm{CaN}} = 20$ 1/s and $Q = 20$, blue line: $k_{\mathrm{CaN}} = 20$ 1/s and $Q = 25$ and orange line: $k_{\mathrm{CaN}} = 19$ 1/s and $Q = 35$. $N = 500$ for the results of the reduced model (green line and background in *B*); $N = 300$ for the results of the six-subunit model. ***B*** Transition outcomes in response to spike-triplet stimulations: The transition results of the reduced model are shown in color as background (same results as in Fig. 5.7*B*). At the points of the eight combinations of Δt_1 and Δt_2 at which the full model has been examined, three relative changes in the number of synapses in the UP state are noted for three different parameter sets. The three numbers correspond to the three pairs of (k_{CaN}; Q) studied in panel *A*, which are (20 1/s; 20), (20 1/s; 25) and (19 1/s; 35) (the numbers appear in the same order). See Tabs. 3.1 and 5.1 for parameters of the six-subunit and the reduced model, respectively.

the VDCC-mediated calcium currents are drawn from the same binomial distributions as used in this study. While these conductances translate into fluctuating amplitudes of the calcium current in the six-subunit model, the drawn numbers directly yield the calcium amplitudes here. Moreover, the six-subunit model does not implement short-term depression (compare the synaptic activity implementation in section 3.3.1 on page 62 for the six-subunit model). For the comparison of both models in this section, we implement STD in the six-subunit model while leaving other parameters and model assumptions unchanged.

The transition results of the six-subunit and the reduced model presented here are shown for STDP spike-pair and -triplet stimulations in Fig. 5.10*A* and *B*, respectively. With the implementation of STD and the parameters used in chapter III ($k_{\mathrm{CaN}} = 20$ 1/s, $Q = 12$) no transitions can be observed at all in response to the spike-pair protocol for any Δt in the detailed six-subunit model (note that k_{CaN} determines the height of the steady-state PP1 activity and therefore the PP1 level attained during stimulations: see section 3.3.6 on page 84; Q is the scaling parameter changing the progress of auto- and dephosphorylation: see section 3.3.6 on page 88). Increasing the scaling parameter Q and decreasing the maximal calcineurin activity k_{CaN} allows to obtain transitions for short negative and short positive Δts without changing the steady-state properties of the full model (see Fig. 5.10*A*). The low but non-zero probability of up-to-down transitions for large negative and large positive time lags in the six-subunit model (see orange line in Fig. 5.10*A*) is not present in the reduced model since the net change curve is adjusted to zero for these values.

With respect to spike-triplet stimulation protocols, a difference in down-to-up transition probability exists between pre-post-pre (upper left quadrant) and post-pre-post triplets (lower right quadrant) in the six-subunit model for every pair of k_{CaN} and Q shown, *i.e.* post-pre-post triplets are more likely to evoke a down-to-up transition than pre-post-pre triplets as suggested by experiments (Wang et al. 2005). However, pre-post-pre triplets show a significant probability of potentiation whereas data by Wang et al. (2005) does not seem to suggest potentiation for these pairs of (Δt_1, Δt_2), *i.e.* $\Delta t_1 > 0$ ms and $\Delta t_2 < 0$ ms.

The reduced model and the more detailed six-subunit model yield in general the same qualitative transition results in response to STDP spike-pair and -triplet simulation protocols. In the presence of short-term depression, the six-subunit model does, however, not allow to capture details of the plasticity outcomes in response to spike-pair and -triplet stimulations with the *same* parameter set. More specifically, if pre-post-pre triplets yield low down-to-up transitions probabilities as suggested by experiments (Wang et al. 2005), the transition probability in response to STDP spike-pair stimulations is very low. On the other hand, increasing the transition probability in response to spike-pairs results in increasing the LTP probability for pre-post-pre triplets (compare Fig. 5.10*A* and *B*). Possible explanations for the observed transition behavior of the six-subunit model are given in the "Discussion" (see below).

6

Discussion

We investigate in this thesis how pre- and postsynaptic activity patterns are translated into changes of synaptic efficacy. We show that the molecular machinery at the synapse is capable to read out the information contained in the local calcium transients about the activity arriving at this particular synapse. And furthermore, that this information can be translated into experimentally observed plasticity results. We focus in particular on the early-phase of long-term modifications (up to 60 min) and study the induction of synaptic changes in a system forming a binary molecular switch. Such a switch can maintain the evoked synaptic state over time. The considered protein signaling network implementing know protein-protein interactions and protein properties reproduces experimental plasticity results in response to various stimulation protocols and stably maintains the evoked state. In this regard, we combine for the first time the questions of induction and maintenance of synaptic changes in a study of a biological realistic protein signaling cascade.

Whether synapses are bistable or not is a controversial issue in the neuroscience community. At first sight, it seems difficult to accept the idea of a binary system on the basis of recorded synaptic changes showing a continuous character in most of the experiments on synaptic plasticity (Dudek and Bear 1992; Bi and Poo 1998; Ngezahayo et al. 2000). Taking into account stochasticity inherent to synaptic processes and respecting the fact that stimulation protocols comprise ensemble of synapses, we show that the resulting synaptic changes exhibit a continuous behavior with respect to the stimulation parameter even if the single synapse has only two stable states. The all-or-none potentiation behavior, which one would expect from a bistable synapse, can therefore only be revealed during stimulation of single synapses (Petersen et al. 1998; Bagal et al. 2005; O'Connor et al. 2005b). The proposition that the synapse might exist in two configurations of AMPA receptor numbers only, for example, contradicts the conception one might have about the functionality of biological systems often showing a continuous behavior. However, bistability has been observed experimentally in a number of biochemical systems apart from the synapse (Degn 1968; Naparstek et al. 1974; Eschrich et al. 1980; Frenzel et al. 1995). Bistability, wherever it is present, allows to durably store information in a noisy environment in which a continuous variable would progressively deteriorate due to ongoing perturbations.

The biological realistic model of calcium/calmodulin-dependent protein kinase II (CaMKII) autophosphorylation and dephosphorylation mediated by protein phosphatase 1 exhibits bistability at resting calcium levels. This has been shown previously (Zhabotinsky 2000; Okamoto and Ichikawa 2000) and allows this molecular switch to maintain the evoked CaMKII phosphorylation level in the absence of synaptic activity. We take into account the protein signaling cascade governing PP1 activity in a calcium-dependent manner. We show that the CaMKII system allows for transitions between the highly- and the weakly-phosphorylated states at realistic calcium concentrations. Up-to-down transitions, the equivalent of an LTD event, occur at intermediate calcium concentrations due to elevated PP1 activity. Down-to-up transitions, the equivalent of an LTP event, occur at high calcium concentrations and stem from strong calcium/calmodulin-triggered autophosphorylation and the supression of PP1 activity. Therefore, the CaMKII system could provide the key element in a bistable *and* plastic switch since we show that transitions between the stable states are possible in calcium ranges associated with LTP and LTD induction protocols (Yang et al. 1999; Zucker 1999; Mizuno et al. 2001; Ismailov et al. 2004; Nevian and Sakmann 2006). To investigate this system under realistic conditions showing plasticity, we expose the CaMKII system to calcium transients evoked by spike-timing dependent stimulation protocols and purely presynaptic stimulation protocols. It is shown that the CaMKII phosphorylation level transition behavior reproduces experimentally observed plasticity results in response to such stimulation protocols. Hence, the dynamical behavior of the bistable switch allows for bidirectional changes in response to stimulation protocols known to induce corresponding transitions in experiments.

Starting from the detailed description of CaMKII autophosphorylation and dephosphorylation, we derive a reduced model of CaMKII phosphorylation featuring the main characteristics of the extensive CaMKII system. The reduced model exhibits bistability at resting calcium, the implementation of which is motivated by a simplified model of the CaMKII protein with two subunits. Intermediate calcium levels trigger CaMKII dephosphorylation as it is promoted by elevated PP1 activity in the extensive CaMKII system model. High calcium levels activate CaMKII phosphorylation which corresponds to strong calcium/calmodulin-triggered autophosphorylation and suppression of PP1 activity in this calcium range. We show that the simplicity of the reduced model allows to study the nature of transition outcomes in response to any possible stimulation protocol in detail. For the example of the STDP spike-pair stimulation protocol, we show which specific parameters of the reduced model influence which aspects of the plasticity results. Since the parameters can be related to biochemical variables, we find, for example, that the activation of phosphorylation with respect to calcium has to be higher than the individual calcium transient amplitudes in order to yield plasticity curves which exhibit balanced LTP and LTD parts. We furthermore suggest three different scenarios to be at the origin of differing plasticity outcomes in the visual cortex compared to the hippocampus. Dephosphorylation dominating phosphorylation, higher amplitudes of the calcium transients evoked by postsynaptic spikes and a higher stability of the weakly-phosphorylated CaMKII state, all the three scenarios can account for the frequency dependence of STDP recorded in visual cortex slices (Sjöström et al. 2001).

6.1 CaMKII kinase - phosphatase system

The results of the CaMKII protein model describing the progress of autophosphorylation and dephosphorylation in a six-subunit ring of the holoenzyme are discussed in this section (model introduced in chapter III). The model is referred to as six-subunit model.

6.1.1 Bistability

The model of CaMKII autophosphorylation and dephosphorylation presented in chapter III exhibits two stable steady-states of the CaMKII phosphorylation level at resting calcium conditions. This idea dates back from the pioneering paper by Crick (1984) and has since been investigated by modeling studies of increasing biochemical realism (Lisman 1985; Lisman 1989; Okamoto and Ichikawa 2000; Zhabotinsky 2000; Miller et al. 2005; Hayer and Bhalla 2005). Miller *et al.* showed that the highly-phosphorylated state in a system composed of a realistic number of CaMKII holoenzymes can remain stable on very long time scales (years) in the presence of stochastic fluctuations and protein turnover (Miller et al. 2005). Hayer & Bhalla found that CaMKII bistability is preserved in the context of translocation and localization in the PSD of the protein (Hayer and Bhalla 2005). The UP state in their study possesses a predicted lifetime of the order of tens of hours which is supported by experimental studies reporting a prolonged localization of the CaMKII at its postsynaptic site following LTP stimulation (Shen and Meyer 1999; Shen et al. 2000; Sharma et al. 2006). These studies are complementary to the work presented here. The shown existence of bistability in the presence of protein trafficking allows us to restrict our investigations to the PSD. For simplicity we furthermore do not implement stochastic fluctuations and protein turnover since they do not seem to affect the conclusions drawn here (Miller et al. 2005).

Experimentalists have reported several types of synaptic increase or decrease. For example, LTD (decrease of efficacy from 'basal' strength) and depotentiation (decrease of efficacy after potentiation) have often been considered as two distinct processes. Some of the differences between the two can be reconciled in our model by considering that a 'basal' condition is likely to be a mix of synapses in the UP and the DOWN state. O'Connor et al. (2005b) state that the initial proportion of synapses with low strength is 79 %, and 21 % with high strength at CA3-CA1 hippocampal synapses, for example. This difference in UP and DOWN state occupations gives rise to a higher probability to evoke LTP than LTD and the LTP amplitude is most likely larger than the LTD amplitude. Furthermore, a LTD protocol will decrease synaptic strength by provoking up-to-down transitions in some synapses that were initially in the UP state. On the other hand, in depotentiation protocols the initial conditions are different, because a larger fraction of the synapses are in the UP state. However, some studies indicate that depotentiation and LTD might operate through different molecular mechanisms (Zhuo et al. 1999; Lee et al. 2000; Jouvenceau et al. 2003). A more complex model than the one proposed here would be necessary to account for these experimental data.

6.1.2 LTP/LTD transitions at fixed calcium concentrations

As in previous models, the detailed six-subunit model exhibits LTP for high enough calcium concentrations. Unlike previous models however, it possesses a 'LTD window', where the system makes a transition from the highly-phosphorylated to the weakly-phosphorylated state, under plausible conditions. There are three requirements for LTP and LTD transitions to occur at realistic calcium concentrations in the six-subunit model (see Fig. 3.5*C*).

(I) The steady-state concentration of phosphorylated CaMKII subunits has to exhibit a bistable behavior, *i.e.* a highly- and a weakly-phosphorylated state should coexist in a range of calcium. This is the case if CaMKII autophosphorylation is cooperative and phosphatase activity saturates at high CaMKII phosphorylation levels. Intersubunit autophosphorlation of CaMKII is cooperative (Hudmon and Schulman 2002) and gives rise to the sensitivity of CaMKII activation to calcium oscillation frequencies, for example (Koninck and Schulman 1998; Kubota and Bower 2001). The saturation of PP1 activity is ensured if the phosphatase is present in small amounts compared to CaMKII, which itself is enriched at high concentrations in the PSD (Hanson and Schulman 1992; McNeill and Colbran 1995; Lisman et al. 2002). We show that bistability is a property of the CaMKII system which is robust to variations in the number of interacting subunits but most effectively expressed in a ring of biological size with 6 interacting subunits (see Fig. 3.4*A*).

(II) The phosphatase activity at resting conditions has to allow for two stable

CaMKII phosphorylation states. Bistability at Ca_0 is a robust property of the six-subunit model over a large range of values of most of the protein signaling cascade parameters (see Tab. 3.1*B*). However, this requirement constrains the calcium-independent activities of the calcineurin and the cAMP-PKA pathways and is the reason why the six-subunit model presented here is sensitive to changes in PKA base activity k^0_{PKA}, *i.e.* varying k^0_{PKA} more than 14 % from the value given in Tab. 3.1*B* leads to a loss of bistability at resting conditions.

(III) The 'LTD window' emerges from an elevated phosphatase activity in the range of intermediate calcium concentrations. There are two possible realizations of the cAMP-PKA pathway for such a 'LTD window' to arise: (i) If the PKA activity is assumed to be calcium-independent, the PP1 activity curve shows a Hill-function like behavior (see orange line in Fig. 3.11*A*). However, a CaMKII vs calcium bifurcation diagram qualitatively similar to Fig. 3.5*C* can be obtained (orange lines in Fig. 3.11*B*). For this scenario to show a 'LTD window', the calcineurin pathway has to activate at calcium concentrations associated with LTD induction, shown to be true for hippocampal LTD (Mulkey et al. 1994). Whether such a scenario can reproduce experimental plasticity results in response to the STDP stimulation protocols is still to be clarified in detail (see below). (ii) If the cAMP-PKA pathway is calcium/calmodulin-dependent (see also Lisman (1989)), the PP1 activity can be coupled to the calcium concentration such that a peak emerges at intermediate calcium concentrations (Fig. 3.5*B*). Several lines of experimental evidence support the inclusion of such a calcium-dependent cAMP-PKA pathway which promotes LTP by blocking phosphatases in the six-subunit model: The induction of hippocampal LTP is blocked by inhibiting cAMP-dependent protein kinase A or inhibition of postsynaptic kinases in general and is facilitated in a PKA-dependent manner by inhibiting calcineurin (Blitzer et al. 1998; Malleret et al. 2001; O'Connor et al. 2005a); a rapid increase in PKA activity accompanies the early phase of LTP in afferent fibers between hippocampus and prefrontal cortex (Jay et al. 1998); Calcium-stimulable forms of cAMP exist which indirectly control PKA activity (Cooper et al. 1995). For the CaMKII system to exhibit the 'LTD window' with a calcium/calmodulin-dependent cAMP-PKA pathway, the six-subunit model predicts that the cAMP-PKA pathway should activate at higher calcium concentrations compared to the calcineurin pathway, as this is required for the peak of PP1 activity to emerge.

Another way to assess the coupling of the protein signaling cascades to PP1 activity and to CaMKII is to check what the model predicts if we block different parts of the pathways and compare it to experimental results. We can implement the blockade of the calcineurin or the cAMP-PKA pathways in the six-subunit model by removing the calcium/calmodulin-dependence of the calcineurin or the cAMP-PKA pathways, since inhibitor 1 is also dephosphorylated by the calcium-independent protein phosphatase 2A (Cohen and Cohen 1989; Shenolikar 1994) and phosphorylated by the calcium-independent protein kinase G (Svenningsson et al. 2004). Blocking the calcium/calmodulin-dependent part of the calcineurin pathway (*i.e.* $k_{\mathrm{CaN}} = 0$) leads to facilitation of LTP, and the reverse transition (LTD) is prevented. On the contrary, blocking the calcium/calmodulin-dependent part of the PKA pathway (*i.e.* $k_{\mathrm{PKA}} = 0$) facilitates LTD and prevents LTP (see Fig. 3.11*C*). Transitions in either one of both directions can be evoked since bistability at resting conditions is preserved in both cases (Fig. 3.11*B*). All these model predictions are consistent with experimental assays inhibiting either the calcineurin (Mulkey et al. 1994; Malleret et al. 2001; Wang et al. 2005) or the cAMP-PKA pathway (Blitzer et al. 1998). If either the calcineurin or the cAMP-PKA pathways are completely abolished in the model, *i.e.* both the calcium-independent and the calcium-dependent parts are suppressed (*i.e.* $k^0_{\mathrm{CaN}} = k_{\mathrm{CaN}} = 0$ or $k^0_{\mathrm{PKA}} = k_{\mathrm{PKA}} = 0$), the system becomes locked in the UP or the DOWN state, respectively. Under these conditions bistability is not present at resting calcium concentrations and no transitions can be evoked in a stable fashion. This also means a change in basal synaptic transmission since all synapses in the system will converge to one of the two stable states. Along the lines of the argumentation above, this situation would correspond to a scenario in which all proteins de- or phosphorylating inhibitor 1 are inhibited.

Inhibiting completely protein phosphatase 1 activity, *i.e.* setting PP1 activity to zero, results in locking the system to the UP state for all calcium concentrations in our model. However, other calcium-independent phosphatases such as protein phosphatase 2A and 2C are known to dephosphorylate CaMKII (Strack et al. 1997). Adding such phosphatases to the model would lead to bistability even in the absence of PP1. Such a scenario would be consistent with experiments which have shown that LTD but not LTP requires the activation of PP1 (Mulkey et al. 1994; Morishita et al. 2001; Huang et al. 2001). To investigate a partial block of phosphatase activity by different concentrations of a broad spectrum phosphatase inhibitor, we scale down the total PP1 activity gradually (see results shown in Fig. 3.10). The six-subunit model predicts a diminution of the LTD window and an enlargement of the LTP window in this case. In terms of transitions between the stable states in response to the STDP protocol, LTD disappears first as suggested by experimental results (O'Connor et al. 2005a). Reducing the phosphatase activity further results in down-to-up transitions for all Δts before the stable DOWN state disappears if the total PP1 concentration is reduced below 40 %. The down-to-up switching threshold (right-hand border of the second bistable region in Fig. 3.10*B*) moves progressively to lower calcium concentration as a result of the partial PP1 block. When the PP1 activity is reduced to 60 %, the model predicts that LTP transitions can be evoked during exposure to calcium levels which would induce LTD in the undisturbed case. Note that interactions of the CaMKII molecule with other proteins is not accounted for in the model.

Such interactions have been shown to affect the activity of the CaMKII and could potentially manipulate the stability of the two stable phosphorylation states (see Bayer et al. (2001)).

In addition to the 'LTD window' at intermediate calcium concentrations, the six-subunit model possesses a second region of bistability between the 'LTD window' and the 'LTP window' (see region between point **3** and **4** in Fig. 3.5*C*). This region is not present in previous models and can be seen as a region of no changes. Starting from the DOWN or the UP state, calcium elevations to this range do not evoke any transition. A similar region of calcium concentrations in between LTP and LTD calcium levels leading to no plasticity is found experimentally by Cho *et al.* and discussed by Lisman as 'no man's land' (Cho et al. 2001; Lisman 2001).

6.1.3 LTP/LTD transitions in response to various stimulation protocols

We have shown that the six-subunit model can qualitatively reproduce plasticity outcomes in response to the STDP protocol. In the six-subunit model as in previous models (Kitajima and Hara 2000; Shouval et al. 2002; Karmarkar et al. 2002; Abarbanel et al. 2005) the only signal driving synaptic changes is the dynamics of the calcium concentration, consistent with current experimental data (Dudek and Bear 1992; Yang et al. 1999; Zucker 1999; Mizuno et al. 2001; Ismailov et al. 2004; Nevian and Sakmann 2006). However, previous modeling studies that use either the maximum amplitude of the calcium signal or simple readout mechanisms of the entire calcium dynamics reproduce only partially STDP results (Kitajima and Hara 2000; Shouval et al. 2002; Karmarkar et al. 2002; Abarbanel et al. 2005). In particular, it has proven difficult to prevent the appearance of a second LTD range at large positive Δts. Shouval and Kalantzis (2005) show that stochastic properties of synaptic transmission can markedly reduce the LTD magnitude in this range. Karmarkar et al. (2002) hypothesize that two functionally distinct calcium pools trigger different readout mechanisms for LTP and LTD in order to overcome this difficulty. In chapter III, we show that the compound calcium signal from VDCCs and NMDA-Rs combined with a complex readout mechanism is sufficient to account for experimental STDP data; in other words, the two calcium influxes do not have to be separated. This is due to the highly cooperative CaMKII autophosphorylation and the protein signaling cascade influencing PP1 activity, which provide a strongly nonlinear detector system, which is sensitive enough to translate differences in the time course of the calcium concentration into observed plasticity outcomes.

Finally, CaMKII phosphorylation level changes need to sum over several pairs of spikes in order to observe LTP- or LTD-like transitions, as suggested by experiments on STDP (Sjöström et al. 2001; Bi and Wang 2002; Froemke and Dan 2002;

Wang et al. 2005; Froemke et al. 2006). However, especially the difference in plasticity outcomes for pre-post-pre triplets compared to post-pre-post triplets (Wang et al. 2005) demonstrates that changes induced by successive pairs of spikes sum in a nonlinear fashion. Phosphorylation changes combine in a highly nonlinear fashion in our model going beyond simple summation of pairwise interactions. In particular, a minimal number of spike-pairs is needed to observe any plasticity, as shown in Fig. 3.16. This number depends on the kinetics of autophosphorylation and dephosphorylation dynamics in the model. Froemke et al. (2005) (visual cortex slices) and Wittenberg and Wang (2006) (hippocampal slices) showed that LTP (causal spike pairings) requires only a few spike-pair presentations whereas the appearance of LTD (anti-causal pairings) requires a longer period of stimulation ($\sim$ 100 spike pairings). Fig. 3.16*C* and *D* show the faster saturation of the time lag range evoking LTP compared to the one evoking LTD, consistent with those experimental results. Interestingly, Wittenberg and Wang (2006) see a second LTD range at large positive time differences emerging after sufficiently long stimulation ($70 - 100$ spike pairings; compare second LTD range at positive Δt emerging at high spike-pair presentation numbers in Fig. 3.16*C* and *D* for ($R = 0.078$, $Q = 1$) and ($R = 1$, $Q = 1.67$), respectively).

Rubin et al. (2005) recently proposed a model based on pathways resembling the CaMKII kinase-phosphatase system, which reproduces experimental STDP outcomes but does not exhibit bistability. In that model high, short-lasting calcium levels evoke LTP, low and prolonged calcium elevations above a certain threshold evoke LTD and intermediate calcium levels act like a “Veto” preventing LTD induction. The durations for which their detector system has to be exposed to respective calcium levels are consistent with our findings. The competition between the PP1 build-up level and the autophosphorylation progress implements naturally the concept of the veto in the six-subunit model. This balance between PP1 activity and autophosphorylation changes with Δt and defines the transition outcome: (short negative Δts) high PP1 accumulation and intermediate autophosphorylation of CaMKII evoked by linear interactions of the calcium influxes lead to LTD; (short positive Δts) low PP1 activity together with strong autophosphorylation of CaMKII as a result of supra-linear calcium summations produce LTP; (all other cases) intermediate PP1 concentrations and weak to intermediate autophosphorylation arouse no changes. In particular, the stronger cAMP-PKA pathway activation due to higher calcium elevations for large positive Δt protocols can be seen as a realistic veto preventing LTD transitions to occur in this range. The differential activation of competing pathways at different calcium levels receives further support by recent experimental studies (Gerkin et al. 2007).

We point out in the previous paragraph that the activation of the cAMP-PKA pathway at higher calcium concentrations successfully prevents LTD transitions in the six-subunit model at large positive time differences. We also show and discuss above that the steady-state picture of CaMKII subunit phosphorylation (bistability at Ca_0, 'LTD' and 'LTP window') can be reproduced with a constant cAMP-PKA activity (see Fig. 3.11*B*). Preliminary simulation results suggest, however, that such a scenario cannot prevent LTD at large Δt since PP1 activity stays elevated even for high calcium elevations (see orange line in Fig. 3.11*B*). This would lead in turn to a similar PP1 buildup level as for short negative Δt and induce LTD for both Δt ranges. Whether the higher calcium elevations at large positive Δt can induce stronger autophosphorylation sufficient to counterbalance the high PP1 activity for these protocols and prevent LTD, has to be investigated further.

We observe a larger extent of the range of Δt values evoking LTD compared to the LTP range for $R = 1$ and $Q = 1$ in the noiseless case (see Fig. 3.16*D*, green regions). In the six-subunit model, the LTD range can be either larger, or smaller, than the LTP range, depending on various parameters such as noise, R and Q. For large noise levels, the LTD range is generally smaller than the LTP range, while experimental data seems to indicate the opposite trend (compare blue line in Fig. 3.9 and Bi and Poo 1998; Sjöström et al. 2001; Froemke and Dan 2002). We investigate extensively how the parameters of the system and the noise level change the extent of the LTP and LTD ranges in chapter V (see below). In any case, the range of Δts leading to up-to-down transitions cannot be extended beyond the range of interaction between both calcium influxes. Hence, we expect the LTD range to become larger if this interaction is extended, *e.g.* due to nonlinear buffer dynamics (Rubin et al. 2005) or the recruitment of additional protein signaling cascades (Cho et al. 2001; Bender et al. 2006; Nevian and Sakmann 2006) (see discussion of the reduced model below). The six-subunit model predicts that the range of time lags evoking LTP in response to the STDP protocol can be increased by amplifying PKA activity. On the other hand, increasing the strength of the calcineurin pathway shifts down horizontally the entire STDP curve (Fig. 3.9) but does not enhance the LTD part only (results not shown).

BPAP attenuation and broadening (Stuart et al. 1997) has been shown experimentally to affect the STDP results (Froemke et al. 2005; Sjöström and Häusser 2006) and could change the balance between the ranges of time lags evoking LTP and LTD in the six-subunit model. The shape of the action potential at the spine during experimental STDP protocols most likely differs from the time course of depolarization used to mimic the BPAP in this study. Note that we elicit the action potential directly at the spine resulting in a narrow and steep voltage change. If voltage-dependent calcium channels are blocked completely, we show that LTP at positive and LTD and negative Δts disappear (see Fig. 3.14*D*). Furthermore, two separate LTD ranges emerge at positive time lags. In other words, increasing inhibition of VDCCs conveys LTP into LTD at positive Δts. Experimental data from the visual cortex show that the sign of synaptic plasticity in response to pre-post pairing stimulations is regulated by the spread of the backpropagating action potential to the synapse. Whether the progressive gradient from LTP to LTD as the distance of the synaptic contacts from the soma increases and therefore the efficacy of AP backpropagation decreases (Sjöström and Häusser 2006) corresponds to the same scenario observed for VDCC inhibition has to be investigated further. Future work has to model the divergence of the backpropagating action potential explicitely rather than just blocking VDCCs since this allows to account for the modified calcium influx through NMDA receptors as well. Bi and Poo (1998) show that the LTD part of the STDP curve is dependent on the L-type calcium channel, consistent with the results shown in Fig. 3.14*D*. In contrast to the results presented here, Bi and Poo (1998) report furthermore that the extent of potentiation is not affected by the block of L-type Ca^{2+} channels. The presence of calcium influx through other types of voltage-dependent calcium channels - such as N-type, P/Q-type or R-type - might rescue the occurrence of LTP at positive Δt in the model.

The six-subunit model also reproduces qualitatively experimental transition results evoked by a purely presynaptic stimulation protocol (Dudek and Bear 1992). Low stimulation frequencies evoke LTD and high frequencies LTP with a transition from LTD to LTP at $16-17$ Hz in our simulations (compare with Dudek and Bear 1992 where the transition happens at around 10 Hz but 900 presynaptic spikes are presented, instead of 60 here), for the same parameters that fit qualitatively experimental data on STDP. Dudek and Bear (1992) presumably stimulate many synapses simultaneously, likely leading to postsynaptic firing. Our model does not account for the excitatory postsynaptic drive resulting from strong synaptic stimulation. We conjecture that postsynaptic firing would lower the frequency at which the transition from LTD to LTP occurs in our model. The six-subunit model furthermore predicts that postsynaptic frequency stimulation evokes LTP at frequencies above 50 Hz (see Fig. 3.12). Interestingly, this type of stimulation does not evoke transitions from UP to DOWN at any frequency. However, we expect this form of plasticity to be strongly dependent on the extent and the time course of BPAP amplitude suppression. In order to bypass the problem of amplitude suppression, we expose the CaMKII system to purely pre- or postsynaptic spike-pair stimulation protocols. Regarding the purely postsynaptic protocol, it is known that high-frequency bursts of up to 5 action potentials evoke summating calcium transients throughout the dendritic tree (Waters et al. 2003). In the case of spike-pairs, the model predicts depression or up-to-down transitions for presynaptic spike-pairs independent of Δt (for $f = 1$ Hz) and potentiation, *i.e.* down-to-up transitions, for closely spaced postsynaptic spikes ($3 \leq \Delta t \leq 8$ ms for $f = 1$ Hz). Since presynaptic spikes evoke long-lasting calcium transients and postsynaptic spikes high but fast-decaying calcium elevations, the Δt ranges for which transitions can be observed in the two cases are substantially different. Nevian and Sakmann (2006) state that three postsynaptic spikes at 50 Hz without pairing with a presynaptic spike do not evoke any synaptic changes. They repeat their triplet stimulation 60 times at a frequency of 0.1 Hz at which our model does not predict any changes likewise. Note however that the transition results evoked by purely postsynaptic spike-pairs are very sensitive to the extent of summation in calcium in between spikes. If the calcium transients evoked by the back-propagating action potentials do not accumulate but the second BPAP evokes a calcium transient with the same amplitude as the first one, no down-to-up transitions are observed in the model (results not shown).

We change the external magnesium concentration and expose the model to STDP spike-pair stimulation protocols. Increasing magnesium results in a reduction of the NMDA-R mediated calcium influx. Consequently we observe a reduction in the LTP and the LTD amplitudes while LTD transitions at short negative Δt disappear first at sufficiently high magnesium levels ($[\mathrm{Mg}]^{2+} = 1.5$ mM, see Fig. 3.14*B*). Reducing external magnesium and therefore boosting the NMDA-R mediated calcium current results in an enlargement of the Δt range evoking LTP and LTD appears for large positive and negative time lags (see Fig. 3.14*B*). We also investigate the transition behavior of the CaMKII system in response to spike triplets (Wang et al. 2005), and the six-subunit model reproduces qualitatively such data provided short-term depression (STD) is added as in (Cai et al. 2007) (see Fig. 5.10*D* and discussion below).

The six-subunit model possesses two stable states of CaMKII activation, which could represent the core mechanism of binary synaptic strength maintenance. We furthermore show that it is possible to reproduce qualitatively experimental STDP results on LTP- and LTD-like transitions. These two results taken together suggest that the CaMKII associated protein network could account for storage *and* induction of synaptic changes. The model therefore predicts that the CaMKII protein also plays a major role in LTD, namely, that CaMKII gets dephosphorylated during LTD induction. Experiments addressing the role of CaMKII in LTD provide controversial results. Sajikumar et al. (2007) show on hippocampal CA1 neurons that LTD is blocked by CaMKII inhibition during induction but the application of the CaMKII inhibitor (KN-62) after the induction had no impact on LTD. In other experiments, LTD has been shown to occur in the presence of CaMKII inhibitors during LTD induction in hippocampal cultures and slices (Wang et al. 2005; O'Connor et al. 2005b). Such inhibitors bind to CaMKII and block its activation by calmodulin (inhibitor KN-62, which is known not to inhibit the autophosphorylated kinase; used in Wang et al. 2005) or interact with the ATP-binding site of CaMKII (K252a used in O'Connor et al. 2005b) (Hanson and Schulman 1992). In the presence of each of both inhibitors, CaMKII can still get dephosphorylated by PP1 and we predict a prevention of LTD to occur if the CaMKII - phosphatase interaction is disrupted. However, LTD experiments on the hippocampus, the somatosensory cortex as well as the perirhinal cortex of rats suggest that the metabotropic glutamate receptor (mGluR) pathway is also involved in LTD (Normann et al. 2000; Cho et al. 2001; Nevian and Sakmann 2006; Bender et al. 2006). The biochemical cascades emerging from mGluR activation could in principle make the occurrence of LTD transitions more robust. The negative coupling of group II mGluRs with the cAMP-PKA pathway (Watkins and Collingridge 1994; Nicoletti et al. 1996; Kemp and Bashir 2001) is consistent with the idea presented here, that LTD requires a shift in kinase - phosphatase balance in favor of phosphatases. Overall, we suggest the dynamics of the global calcium time course to play a crucial role for the sign of synaptic changes alongside with the crosstalk between signaling cascades that include the one considered here.

6.2 Reduced model of CaMKII phosphorylation

The insights obtained through the investigations of the reduced CaMKII model accounting for bistability, dephosphorylation at intermediate calcium levels and phosphorylation at high calcium are presented here.

6.2.1 Net change in phosphorylation

The equation describing CaMKII phosphorylation level dynamics (Eq. (5.1)) can be separated in two parts. The term on the right-hand side of the equation generates the two stable states at resting calcium conditions (see Fig. 5.1*I* and *B*). We can draw a connection between this cubic term and the phosphorylation description in a realistic CaMKII subunit ring through the two-subunit model. The simplified equation accounting for the phosphorylation dynamics in the two-subunit model (Eq. (4.6)) has an underlying cubic form generating three steady-states at resting calcium conditions (see cubic steady-state equation, Eq. (4.7)). A somehow different implementation of bistability is proposed in Fusi et al. (2000). As in the reduced model here, the constant drift term - or refresh term - changes its sign at the unstable steady-state in this study (ρ_{m} corresponds to the synaptic threshold θ_X in Fusi et al. (2000)). As a result, depending on whether the synaptic variable (phosphorylation level here) is below or above this threshold, it decays to the DOWN or the UP state with constant rates in Fusi et al. (2000). In contrast, the phosphorylation level in the reduced model proposed here shows an exponential decay back to the UP or the DOWN state. There is therefore no need to implement reflecting boundaries in order to prevent growing above the UP or below the DOWN state. Note furthermore that the changes of the synaptic variable in the Fusi model are induced by presynaptic spikes and that the sign of the changes depends on the postsynaptic membrane potential (Fusi et al. 2000). Synaptic calcium dynamics are not simulated. The model reproduces plasticity outcomes in response to presynaptic stimulation protocols (Dunwiddie and Lynch 1978; Dudek and Bear 1992). Fusi et al. (2000) state that the model could potentially reproduce STDP spike-pair plasticity results but additional modifications are required in order to avoid a second LTD range at large positive Δt (see discussion below).

The first two terms in Eq. (5.1) describe how phosphorylation and dephosphorylation change the CaMKII phosphorylation level. The calcium dependences of these two processes are taken to be simple step-like functions. Dephosphorylation in the reduced model reproduces schematically the activation of the calcineurin pathway in the detailed biochemical model, *i.e.* both activate predominantly during stimulation protocols evoking LTD and promote up-to-down transitions. The phosphorylation process in the reduced model corresponds to the cAMP-PKA pathway activation *and* the direct, calcium/calmodulin-triggered autophosphorylation. The activation of phosphorylation in the reduced model reflects therefore the recruitment of multiple biochemical pathways leading in combination to phosphorylation of CaMKII. These pathways activate at high calcium levels and induce down-to-up transitions. Our model provides therefore a link between the biochemical level and the calcium control hypothesis shown in Fig. 2.10 and used in several studies (Shouval et al. 2002; Karmarkar and Buonomano 2002; Abarbanel et al. 2003; Cai et al. 2007) (compare blue line Fig. 5.1*A*). As previous studies have pointed out (Lisman 1989), the reduced model confirms that dephosphorylation has to activate at lower calcium concentrations than phosphorylation ($\Theta_{\text{dephos}} < \Theta_{\text{phos}}$) in order to reproduce the qualitative shape of the calcium control hypothesis and to account for experimental plasticity results in response to the STDP protocol, for example (see Fig. 5.4). On the other hand, it is straight forward to show that a scenario with $\Theta_{\text{dephos}} > \Theta_{\text{phos}}$ and $b > a$ can account for plasticity results observed in the cerebellum, *i.e.* intermediate calcium levels evoke LTP and high calcium levels LTD (Coesmans et al. 2004; Jörntell and Hansel 2006). The respective calcium control hypothesis can be obtained by multiplying the blue line in Fig. 5.1*A* by -1.

We show that due to the step-like activation of de- and phosphorylation, it is possible to calculate analytically the net change in phosphorylation of CaMKII in response to arbitrary stimulation protocols. The analytical approach assumes pre- and postsynaptically evoked calcium transients with immediate rise times and same decay time constants or decay time constants differing by a factor of 2 or 3. Despite this simplification of the calcium dynamics, the calculation of the net change in phosphorylation provides a powerful tool to assess possible transition outcomes in response to any stimulation protocol. How stochasticity of synaptic transmission affects the net changes in phosphorylation can be calculated, provided the parameters characterizing STD and the distribution of calcium current amplitudes are known. By means of the net change curve, we can point out important features of the reduced model: (i) STDP-like transition outcomes in response to spike-pairs are a prominent behavior in a large range of de- and phosphorylation activation levels (see Fig. 5.4), while dephosphorylation has to activate at lower calcium concentrations than phosphorylation in order to reproduce reported plasticity results (Bi and Poo 1998; Wang et al. 2005). (ii) The balance between the probabilities and the Δt ranges to evoke LTP and LTD is determined by the specific relation between the activation levels of de- and phosphorylation and the amplitude distributions of the evoked calcium transients (Fig. 5.5). In particular, the positive amplitude scales with the calcium amplitude evoked by a presynaptic spike plus the activation level of phosphorylation, while the negative peak scales with the calcium amplitude evoked by a postsynaptic spike (see Eqs. (5.15) and (5.13)). These analytical expressions have been obtained by assuming calcium transients with immediate rise times and identical decay time constants for the pre- and postsynaptic calcium transients. However, the general behavior holds beyond these restrictions on the calcium transients, the considered area of activation thresholds and in the presence of noise. The amplitude of LTD transitions at short negative Δts is increased by augmenting the postsynaptically evoked calcium amplitude, for example (see Eq. (5.13) and Fig. 5.9*B*). However, other influences shape the net change curve in the more realistic cases with noise, finite rise times and different decay times of the calcium transients. For example, the ratio of the net change amplitudes changes strongly with the dephosphorylation threshold, while it is relatively independent of the phosphorylation threshold (see Fig. 5.5*D* and *E*). This behavior of the ratios cannot be explained from Eq. (5.15) and (5.13). (iii) Experimental data show the locations of the positive peak of STDP plasticity outcomes at positive Δt and of the transition from positive to negative plasticity changes at $\Delta t \approx 0$ ms. In the model, these locations crucially depend on the rise time of the NMDA-R-mediated calcium current. For very fast rise times of the NMDA-R component, both locations would shift to negative time differences. Naturally, slowing down the NMDA-R evoked calcium transient would move the peak and the transition from positive to negative changes to larger positive values of Δt.

Shouval and Kalantzis (2005) have shown that the occurrence of LTD at large positive time differences in response to STDP stimulation protocols depends on the stochastic properties of synaptic transmission. In particular, the small number of NMDA receptors present at one synapse yields a large variability and reduces considerably the amplitide of pre-post LTD (Shouval and Kalantzis 2005). Consistent with these results, we show that pre-post LTD vanishes for realistic levels of calcium transient fluctuations and STD in the investigated region of de- and phosphorylation thresholds (Fig. 5.4). We furthermore can classify models describing plasticity changes based on calcium dynamics and on an arbitrary form of the calcium control hypothesis in response to STDP spike-pair protocols with the general approach of the reduced model. Shouval et al. (2002) and Karmarkar and Buonomano (2002) chose that independent pre- and postsynaptic spikes (large Δt) do not change at all their synaptic state variable. Only interacting pre- and postsynaptically evoked calcium transients induce changes in their models. In terms of the calcium control hypothesis, they chose the single amplitudes of pre- and postsynaptic spikes to be below the calcium range inducing LTD. In the model of Abarbanel et al. (2003), the half activation concentrations of the Hill functions describing phosphorylation and dephosphorylation are chosen well above the calcium amplitudes of single pre- or postsynaptic transients. Such scenarios corresponds to region **DPD** in Fig. 5.4*A*. Since these models do not account for noisy calcium transients, they observe LTD at time differences at which the pre- and the postsynaptically evoked calcium transients start to interact, which happens for short negative and large positive Δt. Even in the absence of noise, we can show that if for large Δt phosphorylation and dephosphorylation are activated and chosen to counterbalance each other, LTD occurs at short negative time differences only (**DP** region in Fig. 5.4*A*).

We want to highlight the resemblance of the phosphorylation and dephosphorylation implementation in the reduced model (left hand terms in Eq. (5.1)) with the multiplicative learning rules (van Rossum et al. 2000; Kepecs et al. 2002; Gütig et al. 2003). The phosphorylation level of CaMKII, ρ, can be considered as a measure for the synaptic weight or efficacy, w. The more the ρ approaches the UP state the weaker phosphorylation gets and vice versa for dephosphorylation, *i.e.* the phosphorylation and dephosphorylation rates linearly attenuate as the corresponding boundaries are approached. The reduced competition in multiplicative models drives all synapses to similar equilibrium values in feedforward network studies (see section 2.7.2 on page 33 and Kepecs et al. (2002)). This cannot happen in the reduced model due to the bistability of the synaptic weight parameter. We would therefore expect that the reduced model can translate input pattern correlations into corresponding synaptic patterns which are furthermore stable in time.

Note that the net change considerations are only valid for small changes in the phosphorylation level in response to stimulation protocols, *i.e.* for small de- and phosphorylation rates (a and b). If, for example, the phosphorylation rate is larger than the dephosphorylation rate but activated for a short time interval, dephosphorylation is favored. This can be understood by inspecting Eq. (5.1): the de- and phosphorylation rates are scaled with the momentary phosphorylation level and therefore decrease as the minimal and the maximal phosphorylation levels, respectively, are approached. If the evoked phosphorylation changes are large (*i.e.* large a and b), this reduction of changes close to the maximal and minimal phosphorylation level creates an imbalance which is not accounted for in the net change curve. In particular, since the phosphorylation rate (a) is larger than the dephosphorylation rate (b), the attenuation is stronger for increases in phosphorylation level. As a result, the balance adjusted by means of the net change curve is disturbed and dephosphorylation is favored. This behavior stems from the multiplicative nature of the implementation of phosphorylation changes (see paragraph above).

In reality, the current mediated by the NMDA receptor is voltage dependent while the reduced model does not account for this voltage dependence of the NMDA-R. Recent experimental data show that the EPSP waveform, *i.e.* the calcium influx in turn, regulates the temporal window for pre-post pairings (Fuenzalida et al. 2007). Their results indicate that the Δt range evoking LTP is narrowed by a reduction of the amplitude and decay time constant of the EPSP. Thus, by ignoring the voltage dependence of the NMDA-R we underestimate the range of time differences evoking LTP in the reduced model (see Fig. 5.2D). Our investigations show furthermore that increasing the phosphorylation and dephosphorylation threshold decreases the range of time differences leading to LTP (see Fig. 5.4F). Taken together these results suggests that we probably chose dephosphorylation and phosphorylation activation levels which are below realistic values in order to compensate for the narrowing of the LTP range.

6.2.2 Transition outcomes in response to various stimulation protocols

We expose the reduced model to calcium transients evoked by stimulation protocols which are shown to evoke LTP and LTD in experiments. The transition results behave as suggested by the net change curves and therefore confirm the conclusions drawn from the net change considerations.

The reduced model reproduces qualitatively transition outcomes in response to STDP spike-pair stimulation. As already pointed out in the discussion of the six-subunit model, the model yields a larger range of time differences evoking LTP than LTD, whereas experimental results suggest the opposite trend (Bi and Poo 1998; Sjöström et al. 2001; Froemke and Dan 2002). Rubin et al. (2005) show that the strength of nonlinear buffer dynamics controls the extent of the Δt range of LTD. We chose a simpler approach and add a slow, single exponentially decaying component to the calcium transient evoked by the backpropagating action potential, while keeping its amplitude constant. Depending on the slow decay time constant of this component, the LTD range of the STDP results can be arbitrarily extended. Interestingly, the decay of calcium in spines of hippocampal neurons can be best fitted by two exponential functions with time constants of 8.6 and 93.7 ms (Holcman et al. 2005). Action potential evoked calcium transients in spines decay with a time constant of 143 ms (Koester and Sakmann 1998) (compare to 15 ms for the fast decaying component from Sabatini et al. (2002), and 60 or 100 ms for the slow component used here). Sabatini et al. (2002) estimate that 5 % of the calcium ions entering the spine remains free and decays with a time constant of $\sim$ 15 ms. Note that Sabatini et al. (2002) eliminate the effect of added calcium buffers and deduce this decay constant for undisturbed calcium transients. However, the slow calcium component could stem from slow release of the remaining 95 % calcium from calcium sequestration systems or from a slowly decaying tail of the backpropagating action potential, a so-called "after-depolarizing potential" (Magee and Johnston 1997; Larkum et al. 2001) (see also Shouval et al. (2002)).

Transition results in response to STDP spike-triplet stimulation protocols are reproduced with the same parameter set as for spike-pairs (see Fig. 5.7*B*). As pointed out by Cai et al. (2007), the implementation of short-term depression yields the experimentally observed difference in plasticity outcomes between pre-post-pre and post-pre-post triplets. Short-term depression causes on average a reduction of the second presynaptically evoked calcium transient due to the slow recovery of vesicle release. This reduced elevation crosses the dephosphorylation threshold and prevents down-to-up transitions normally evoked by the first two spikes in the pre-post-pre triplet. As a result, no transitions are observed for pre-post-pre triplets and down-to-up transitions occur in response to the large calcium transients evoked by post-pre-post triplets. This behavior is consistent with experiments (Wang et al. 2005) and shows how the stochastic nature of synaptic transmission shapes plasticity results (compare Fig. 5.7*B* with Fig. 4.4*B*, where the latter does not account for STD). The second, slow time constant of the calcium transient evoked by the backpropagating action potential has no impact on the transition outcomes for the considered ranges of times differences between the spikes in the triplet protocol.

For purely presynaptic stimulation protocols, we show that depending on the extent of short-term depression the plasticity outcomes can be converted from LTD to LTP for high stimulation frequencies. For STD parameters describing presynaptic vesicle dynamics for the hippocampus, the reduced model predicts moderate LTD for a frequency range from 3 to 50 Hz. Dudek and Bear (1992) observe LTD for a range from 1 to 10 Hz and LTP above 10 Hz in response to stimulation of Schaffer collaterals. The major difference between these experiments and the results presented here is the presence or absence of postsynaptic activity. Dudek and Bear (1992) do not block postsynaptic activity and record extracellularly at the apical dendritic layer of CA1 neurons. It is therefore very likely that the simulation of an ensemble of afferents drives the postsynaptic CA1 cell to firing of action potentials which would in turn also backpropagate into the dendritic tree. This postsynaptic activity can potentially transform the LTD observed at high stimulation frequencies here into LTP. In support for this, Christie et al. (1996) state that also the induction of LTD requires the simultaneous activity of the postsynaptic neuron. The block of postsynaptic activity prevents LTD induction at presynaptic stimulation frequencies of 2 Hz which is consistent with our results (see Fig. 5.8, relative change in the number of synapses in the UP state ≈ -0.15 for $f = 2$ Hz). Our model predicts that moderate LTD can be observed at higher stimulation frequencies provided postsynaptic activity is blocked.

Low presentation frequencies of post-pre spike-pairs result in LTD, while no changes are observed for pre-post pairs in the visual cortex (Sjöström et al. 2001). High presentation frequencies of spike-pairs evoke LTP for pre-post and post-pre stimulations. The reduced model suggests three possible scenarios to account for such frequency dependence of STDP in the visual cortex: (i) Dephosphorylation processes of CaMKII outweight phosphorylation for spike-pairs with large time differences. Consequently, simple spike-pair stimulation at 1 Hz would evoke LTD for all Δts except for a narrow range of short positive time differences (see Fig. 5.9*B*). Markram et al. (1997) investigate large time differences ($\Delta t = \pm 100$ ms) and see no changes for both cases. They stimulate, however, pre- and postsynaptic cells with bursts of 4 spikes occurring at 20 Hz which might compensate for strong dephosphorylation since high calcium transients are induced by such stimulation patterns. (ii) The ratio of amplitudes between the calcium transients evoked by a post- and a presynaptic spike determines the ratio of LTP and LTD amplitudes. We can show with simple considerations that the LTD amplitude is increased relative to the LTP amplitude by increasing the postsynaptically evoked calcium transient amplitude. Such a scenario is shown to lead to LTD at low spike-pair presentation frequencies for the visual cortex (see Fig. 5.9*A*). At the same time, presentation of spike-pairs at 1 Hz for 60 times recovers LTD at short negative Δt and LTP at short positive Δt, while large time differences evoke no changes. (iii) If the basin of attraction of the UP state is smaller compared to the DOWN state in the reduced model, the frequency dependence of the STDP in visual cortex can be reproduced. In this case, the plasticity outcomes in response to spike-pairs at 1 Hz for 60 times would resemble the transitions observed in case (i) (see Fig. 5.9*B*). The stabilities of the UP and the DOWN state are defined by the balance of autophosphorylation and dephosphorylation progresses. It is possible that PP1 activity is more pronounced in the visual cortex reducing the basin of attraction of the UP state, while still preserving bistability at resting calcium conditions. Which one of the proposed scenarios or which combination of them might be the case in the visual cortex remains unclear. Spike-pair stimulation at 1 Hz for 60 could help to distinguish case (ii) from cases (i) and (iii). We could not think of a stimulation protocol so far which might help to differentiate between (i) and (iii) though.

Using the insights obtained through the investigations of the reduced model, we can reexamine the choice of parameters in the six-subunit model and draw conclusions about the origin of the observed transition behavior of the six-subunit model. Simple analytical considerations of the reduced model (assuming immediate rise times and same decay time constants of the calcium transients) indicate that the positive and the negative peak amplitudes of the plasticity results in response to STDP spike-pairs are controlled by the calcium amplitudes and the activation thresholds of de- and phosphorylation (see Eqs. (5.13) and (5.15)). We furthermore evaluate the balance between the peak values and the integrals of the STDP curve in the presence of noise and with more realistic calcium transients in case of the reduced model (see Fig. 5.5). If we compare the relative location of the calcium transient amplitudes with the calcineurin and the PKA pathway activation levels, we can approximately locate the six-subunit model with respect to the reduced model in the Θ_{phos} - Θ_{dephos} plane (shown in Figs. 5.4*A, C, E* and 5.5). The calcium amplitude of the presynaptic spike ($Ca_{\mathrm{pre}} = 0.1 + 0.17\ \mu\mathrm{M}$) is larger than the calcineurin activation threshold ($\sim 0.25\ \mu\mathrm{M}$, from Fig. 3.5*A, B*), and the postsynaptically induced amplitude ($Ca_{\mathrm{post}} = 0.1 + 0.34\ \mu\mathrm{M}$) is larger than the level of PKA activation ($\sim 0.4\ \mu\mathrm{M}$, from Fig. 3.5*A, B*) (compare to amplitudes and thresholds in the reduced model: $D_{\mathrm{pre}} = 0.1\ \mu\mathrm{M}$, $D_{\mathrm{post}} = 0.2\ \mu\mathrm{M}$; $\Theta_{\mathrm{phos}} = 0.35\ \mu\mathrm{M}$, $\Theta_{\mathrm{dephos}} = 0.25\ \mu\mathrm{M}$). This places the six-subunit model in upper right hand part of the **DP** region in Fig. 5.4*C*. Adding noise to such a case yields a larger LTP to LTD ratio for the six-subunit model as compared to the reduced model, which can be read from Fig. 5.5*D*. These considerations are confirmed by the comparison of the six-subunit model and the reduced model in Fig. 5.10*A*, where the LTP to LTD peak- and integral ratio of the six-subunit model is larger compared to the reduced model.

In summary, the reduced model reproduces the behavior of the detailed model describing phosphorylation dynamics in the CaMKII six-subunit ring. Since we develop a detailed understanding about what controls the shape of plasticity outcomes in the reduced model, we can draw conclusions about the properties of the underlying biochemical pathways. In the specific case for STDP spike-pair stimulation protocols, we point out that the low activation thresholds of the calcineurin and the PKA pathway yield the larger amplitude of the LTP changes compared to LTD in the six-subunit model.

6.3 Outlook

Our future projects based on the CaMKII phosphorylation model presented in this thesis include two main directions: (I) On the level of a single synapse, we want to further pursue the analytical approach based on the reduced model with respect to various stimulation protocols; and (II) we want to investigate the effects of the reduced model on neural network dynamics.

(I) In the last part of the thesis, we determine the net change in phosphorylation for STDP protocols and for presynaptic stimulation protocols in the framework of the reduced model. It is shown that the net change can be seen as a window of opportunity for transitions of a bistable synapse to occur. The reduced model with the simplest version of pre- and postsynaptically evoked calcium transients (immediate rise times and same decay time constants) makes it possible to calculate the net change in phosphorylation for every possible pre- and postsynaptic activity pattern (spike-doublets, spike-triplets, spike-quadruplets, purely presynaptic stimulation, purely postsynaptic stimulation, etc.). The analytical expressions of the net changes for the different stimulation protocols allow to evaluate to which extent *one* parameter set can reproduce all the experimentally observed plasticity outcomes. Is it, for example, necessary to take short-term depression into account in order to obtain the unbalance in plasticity results between pre-post-pre and post-pre-post triplets (Wang et al. 2005)? Such an analytical approach to transition outcomes allows to evaluate whether experimental plasticity results obtained in response to different stimulation protocols and in different brain regions rely on the same biological mechanisms. And if this is not the case, we will be able to suggest specific differences in the biological machinery giving rise to the differences in observed plasticity results. This can potentially help to pin down more specifically the properties of biological relevant pathways involved in induction and maintenance of synaptic plasticity in different brain areas.

If we can reproduce plasticity results evoked by different stimulation protocols with the reduced model using the same parameter set, can we generalize across pre- and postsynaptic activity patterns which lead to LTP/LTD transitions? In other words, does a more general formulation of neuronal activity patterns which drive synaptic plasticity exist? The reduced model provides an easy-to-study and yet realistic synaptic model to derive a mapping between transition probabilities and pre- and postsynaptic activities. The idea is to specify the probability to evoke down-to-up or up-to-down transitions as a function of pre- and postsynaptic firing rates and higher order statistics such as autocorrelation and cross-correlation of the considered neurons. Previous efforts to describe plasticity outcomes in more general terms of pre- and postsynaptic activities use either rate-based or spike-timing based plasticity rules. However, the non-linearities inherent to plasticity results impose complicated spike-to-spike interactions in models based on spike-timing, for example, in order to account for experimental data (Froemke and Dan 2002; Pfister and Gerstner 2006; Sjöström et al. 2001). Since such phenomenological plasticity rules lack the relation to the underlying biology, it is difficult to assess the biological realism of the implemented non-linearities. The reduced model, based on biological realistic mechanisms, accounts for the non-linearities of synaptic plasticity in a natural way by determining synaptic changes based on the calcium dynamics evoked through neuronal activity. It is therefore a convenient plasticity rule to deduce possible generalizations of the know induction protocols. A more general plasticity rule based on firing rates and correlations of neurons can potentially be used to relate natural spike patterns to synaptic plasticity. It could therefore bridge the gap between artifical stimulation protocols evoking long-term modifications by repetitive activity patterns and synaptic plasticity occurring *in* *vivo* in response to natural spike trains.

(II) Another project we intend to pursue is the implementation of the reduced model in neural network studies to investigate the impact of realistic, plastic synapses on network dynamics. Numerous studies have implemented synaptic learning rules reproducing spike-timing dependent plasticity in feedforward (Kempter et al. 1999; Song et al. 2000; van Rossum et al. 2000; Kistler and van Hemmen 2000; Rubin et al. 2001; Gütig et al. 2003; Izhikevich et al. 2004; Guyonneau et al. 2005; Meffin et al. 2006) and feedback networks (Hertz and Prügel-Bennett 1996; Levy et al. 2001; Gütig et al. 2003; Izhikevich et al. 2004; Iglesias et al. 2005; Mongillo et al. 2005; Morrison et al. 2007). Studies in feedward models have investigated how STDP allows for unsupervised learning of input correlations, while feedback model have been used to investigate the occurrence of balanced random network activity and the collective dynamics of subgroups of neurons in the presence of plastic synapses. We expect different synaptic dynamics and resulting synaptic maps if the reduced model is implemented in such network studies. Three important differences between the spike-based learning rules and the reduced model likely give rise to different results:

(i) Synaptic changes evoked by spike-pairs or -triplets do not add in a linear fashion in the reduced model. Rather, the spiking patterns are transferred into calcium dynamics which drive de- and phosphorylation processes leading in turn to synaptic changes. As shown in this work, this signaling cascade leads to highly nonlinear summation of synaptic changes evoked by pre- and postsynaptic spiking activity.

(ii) We mention the resemblance of the phosphorylation and dephosphorylation implementation in the reduced model with multiplicative learning rules above (van Rossum et al. 2000; Kepecs et al. 2002; Gütig et al. 2003). Since multiplicative learning rules have been shown to reliably represent input correlations, we expect that the reduced model will exhibit input selectively for correlated subsets of presynaptic neurons. In contrast to preceding work however, such patterns will be stably maintained over time after the exposure to correlated input due to bistability of synapses. It needs to be studied whether this can lead to strongly connected subsets of neurons in recurrent networks, where the subset is able to sustain elevated activity in the absence of external inputs.

(iii) Commonly, neurons are considered as points without spatial extent in network studies. This means that the input integration properties of the dendritic tree is neglected. Experimental studies have, however, highlighted the importance of the dendritic location for evoked plasticity outcomes in STDP, for example (Froemke et al. 2005; Sjöström and Häusser 2006). In general, neuronal dendrites exhibit a range of linear and nonlinear mechanisms that allow them to implement elementary computations (London and Häusser 2005; Stuart et al. 2007). The biological realistic nature of the reduced model allows to implement properties of dendritic input integration, for example, the attenuation of action potential backpropagation (Stuart et al. 1997), or the effect of limited protein resources to maintain evoked synaptic states (Fonseca et al. 2004).

In summary, the implementation of the synapse model proposed here in neural network studies provides a biochemical basis for a synaptic learning rule. It should therefore advance our understanding of the role of synaptic plasticity in shaping spatio-temporal dynamics of recurrent networks. The implementation of biologically realistic synaptic dynamics in neural network models has the potential to participate in elucidating the basic mechanisms underlying short-term memory - through the selective activation of specific subsets of neurons - and long-term memory - through the emergence of a specific synaptic structure.

A

Six-subunit CaMKII model

Here, we present details of the CaMKII model describing auto- and dephosphorylation of the six-subunit ring introduced in chapter III. These details of the six-subunit model are not necessary to follow the logical flow in the main text and have therefore been moved to the appendix. In particular, the differential equations accounting for the time course of CaMKII phosphorylation and dephosphorylation are listed. Furthermore, the mathematical model used to describe the ion current dynamics according to the Hodgkin-Huxley formalism is shown. These ion currents are part of the synaptic activity implementation to generate the calcium currents in the six-subunit model. Finally, the derivation of the simplified description which allows to calculate the PP1 activity level after the presentation of one spike-pair is illustarted.

A.1 CaMKII autophosphorylation and dephosphorylation

The model of CaMKII autophosphorylation and dephosphorylation is represented by the following system of coupled differential equations

$$\dot{S_0} = \dot{S}_{000000} = -6k_6\gamma^2 S_0 + k_{10}S_1, \tag{A.1}$$

$$\dot{S_1} = \dot{S}_{100000} = 6k_6\gamma^2 S_0 - 4k_6\gamma^2 S_1 - k_7\gamma S_1 - k_{10}S_1 + 2k_{10}(S_2 + S_3 + S_4), \tag{A.2}$$

$$\dot{S_2} = \dot{S}_{110000} = k_7\gamma S_1 + k_6\gamma^2 S_1 - 3k_6\gamma^2 S_2 - k_7\gamma S_2 - 2k_{10}S_2 + k_{10}(2S_5 + S_6 + S_7), \tag{A.3}$$

$$\dot{S_3} = \dot{S}_{101000} = 2k_6\gamma^2 S_1 - 2k_6\gamma^2 S_3 - 2k_7\gamma S_3 - 2k_{10}S_3 + k_{10}(S_5 + S_6 + S_7 + 3S_8), \tag{A.4}$$

$$\dot{S_4} = \dot{S}_{100100} = k_6\gamma^2 S_1 - 2k_7\gamma S_4 - 2k_6\gamma^2 S_4 - 2k_{10}S_4 + k_{10}(S_6 + S_7), \tag{A.5}$$

$$\begin{aligned}\dot{S_5} = \dot{S}_{111000} =& k_7\gamma S_2 + k_7\gamma S_3 + k_6\gamma^2 S_2 - k_7\gamma S_5 - 2k_6\gamma^2 S_5 - 3k_{10}S_5 \\ &+ k_{10}(2S_9 + S_{10}),\end{aligned} \tag{A.6}$$

$$\begin{aligned}\dot{S_6} = \dot{S}_{110100} =& k_6\gamma^2 S_2 + k_6\gamma^2 S_3 + 2k_7\gamma S_4 - k_6\gamma^2 S_6 - 2k_7\gamma S_6 - 3k_{10}S_6 \\ &+ k_{10}(S_9 + S_{10} + 2S_{11}),\end{aligned} \tag{A.7}$$

$$\begin{aligned}\dot{S_7} = \dot{S}_{110010} =& k_6\gamma^2 S_2 + k_7\gamma S_3 + 2k_6\gamma^2 S_4 - k_6\gamma^2 S_7 - 2k_7\gamma S_7 - 3k_{10}S_7 \\ &+ k_{10}(S_9 + S_{10} + 2S_{11}),\end{aligned} \tag{A.8}$$

$$\dot{S_8} = \dot{S}_{101010} = k_6\gamma^2 S_3 - 3k_7\gamma S_8 - 3k_{10}S_8 + k_{10}S_{10}, \tag{A.9}$$

$$\begin{aligned}\dot{S_9} = \dot{S}_{111100} =& k_7\gamma S_5 + k_6\gamma^2 S_5 + k_7\gamma S_6 + k_7\gamma S_7 - k_6\gamma^2 S_9 \\ &- k_7\gamma S_9 - 4k_{10}S_9 + 2k_{10}S_{12},\end{aligned} \tag{A.10}$$

$$\begin{aligned}\dot{S_{10}} = \dot{S}_{111010} =& k_6\gamma^2 S_5 + k_6\gamma^2 S_6 + k_7\gamma S_7 + 3k_7\gamma S_8 - 2k_7\gamma S_{10} - 4k_{10}S_{10} \\ &+ 2k_{10}S_{12},\end{aligned} \tag{A.11}$$

$$\dot{S_{11}} = \dot{S}_{110110} = k_7\gamma S_6 + k_6\gamma^2 S_7 - 2k_7\gamma S_{11} - 4k_{10}S_{11} + k_{10}S_{12}, \tag{A.12}$$

$$\begin{aligned}\dot{S_{12}} = \dot{S}_{111110} =& k_7\gamma S_9 + k_6\gamma^2 S_9 + 2k_7\gamma S_{10} + 2k_7\gamma S_{11} - k_7\gamma S_{12} - 5k_{10}S_{12} \\ &+ 6k_{10}S_{13},\end{aligned} \tag{A.13}$$

$$\dot{S_{13}} = \dot{S}_{111111} = k_7\gamma S_{12} - 6k_{10}S_{13}. \tag{A.14}$$

S_i refers to the concentration of the 14 ($i = 0, ..., 13$) macroscopic distinguishable activation states of the CaMKII protein. The subscript in the second column shows the geometrical order of Thr^{286} phosphorylated sites in the CaMKII ring, 1 refers to a phosphorylated subunit, 0 to a dephosphorylated subunit. Attention should be drawn to the fact that for example, S_5, S_6, S_7 and S_8, all have three phosphorylated subunits, *i.e.* all of them have the same macroscopic level of activation, *i.e.* $m_5 = m_6 = m_7 = m_8 = 3$. However, in terms of symmetry all the four have to be distinguished since at S_5 the phosphorylated sites are adjoin,

S_{111000}, whereas at S_8 they are separated by a dephosphorylated subunit, S_{101010}, for example. With regard to this difference, the propagation of autophosphorylation is different for both, phosphorylation step shown in Fig. 3.2*C* can occur on two pairs of subunits at S_5 but cannot occur at S_8 at all. Taking into account that the different autophosphorylation steps, depicted in Fig. 3.2*C*, *D* and *E*, happen with different probabilities leads to differing occurrences of the activation states S_i (with $i = 0...13$). Note that we use the fact $k_7 = k_8$ and simplify $k_7\gamma\gamma^* + k_8\gamma(1-\gamma^*)$ to $k_7\gamma$.

$\sum_{i=0}^{n} \dot{S}_i = 0$, with $n = 13$ for 14 macroscopic distinguishable activation states of the 6 subunit CaMKII ring, yields the CaMKII protein mass conservation, $2CaMKII_0 = \sum_{i=0}^{n} S_i$. $2CaMKII_0$ gives the total concentration of functionally independent CaMKII clusters of six subunits and $CaMKII_0$ the total CaMKII concentration since one holoenzyme comprises two six subunit rings. Note that the number of macroscopic distinguishable activation states is 3, 6, 14 and 36 for the two, four, six and eight subunit model, respectively.

Numerical methods We solve the system of coupled, ordinary differential equations with a fourth-order Runge-Kutta method with adaptive stepsize control. This has been implemented in a C++ program. We use XPPAUT by G. Bard Ermentrout (http://www.pitt.edu/~phase/) for the steady-state calculations of the CaMKII system.

A.2 Ion currents dynamics

The description and the parameters of the ionic currents of the Hodgkin-Huxley model are taken from Poirazi *et al.* (I_{CaL}) as well as Purvis & Butera (I_{Na}, I_{K}) (Poirazi et al. 2003; Purvis and Butera 2005).

Leak Current: The leak current is given by

$$I_{\mathrm{L}} = g_{\mathrm{L}}(V - E_{\mathrm{L}}), \tag{A.15}$$

where g_{L} is the leak conductance. The leak potential is adjusted such that the resting potential is -70 mV.

The ionic currents listed here have the general form $I_{\mathrm{ionic}} = gy(V - E_{\mathrm{ionic}})$. E_{ionic} is the reversal potential for the respective ions carried, g refers to the maximum conductance of each current and y is the product of one or more gating variables. y determines the dynamics of the ion currents regulated by voltage-dependent activation and inactivation variables which are described according to

$$\begin{aligned}
\frac{dx}{dt} &= (x_\infty(V) - x)/\tau_x(V), && \text{(A.16)}\\
x_\infty(V) &= \frac{1}{1+\exp\left((V-\theta_x)/\sigma_x\right)}, && \text{(A.17)}\\
\tau_x(V) &= \frac{A}{\exp\left((V-\theta_1)/\sigma_1\right) + \exp\left((V-\theta_2)/\sigma_2\right)} + B. && \text{(A.18)}
\end{aligned}$$

Here $x_\infty(V)$ is the steady-state voltage-dependent (in)activation function of x and $\tau_x(V)$ is the voltage-dependent time constant. In terms of this formalism, the respective ion currents are given by:

Sodium current:

$$\begin{aligned}
I_{\mathrm{Na}} &= g_{\mathrm{Na}} m_{\mathrm{Na}}^3 h_{\mathrm{Na}} (V - E_{\mathrm{Na}}), && \text{(A.19)}\\
m_{\infty\mathrm{Na}}(V) &= \frac{1}{1+\mathrm{e}^{-(\mathrm{V}+36)/8.5}}, \quad \tau_{m\mathrm{Na}} = 0.1 \text{ ms}, && \text{(A.20)}\\
h_{\infty\mathrm{Na}}(V) &= \frac{1}{1+\mathrm{e}^{(\mathrm{V}+44.1)/7}}, && \text{(A.21)}\\
\tau_{h\mathrm{Na}}(V) &= \left(\frac{3.5}{\mathrm{e}^{(\mathrm{V}+35)/4} + \mathrm{e}^{-(\mathrm{V}+35)/25}} + 1\right) \text{ ms}. && \text{(A.22)}
\end{aligned}$$

Delayed-rectifier Potassium current:

$$\begin{aligned}
I_{\mathrm{K}} &= g_{\mathrm{K}} n^4 (V - E_{\mathrm{K}}), && \text{(A.23)}\\
n_\infty(V) &= \frac{1}{1+\mathrm{e}^{-(\mathrm{V}+30)/25}}, && \text{(A.24)}\\
\tau_n(V) &= \left(\frac{2.5}{\mathrm{e}^{(\mathrm{V}+30)/40} + \mathrm{e}^{-(\mathrm{V}+30)/50}} + 0.01\right) \text{ ms}. && \text{(A.25)}
\end{aligned}$$

Voltage-dependent calcium current (high-voltage activated L-type):

$$\begin{aligned}
I_{\mathrm{CaL}} &= g_{\mathrm{CaL}} m_{\mathrm{CaL}}^3 h_{\mathrm{CaL}} (V(t) - E_{\mathrm{Ca}}), && \text{(A.26)}\\
m_{\infty\mathrm{CaL}}(V) &= \frac{1}{1+\exp\left(-(V+37)\right)}, \quad \tau_{m\mathrm{CaL}} = 3.6 \text{ ms}, && \text{(A.27)}\\
h_{\infty\mathrm{CaL}}(V) &= \frac{1}{1+\exp\left((V+41)/0.5\right)}, \quad \tau_{h\mathrm{CaL}} = 29 \text{ ms}. && \text{(A.28)}
\end{aligned}$$

AMPA current: Excitatory postsynaptic potentials are mainly mediated by the AMPA receptor current given by

$$\begin{aligned}
I_{\mathrm{AMPA}} &= g_{\mathrm{AMPA}} s_{\mathrm{AMPA}}(t)(V(t) - E_{\mathrm{AMPA}}), && \text{(A.29)}\\
\dot{s}_{\mathrm{AMPA}} &= -s_{\mathrm{AMPA}}/\tau_{\mathrm{AMPA}} + \alpha_s x_{\mathrm{AMPA}}(1 - s_{\mathrm{AMPA}}), && \text{(A.30)}\\
\dot{x}_{\mathrm{AMPA}} &= -x_{\mathrm{AMPA}}/\tau'_{\mathrm{AMPA}} + \alpha_x \sum_k \delta(t - t_k), && \text{(A.31)}
\end{aligned}$$

Parameter	Definition	Value	Reference
E_{L}	leak reversal potential	-68.0331 mV	see text
E_{Na}	sodium reversal potential	60 mV	(Purvis and Butera 2005)
E_{K}	potassium reversal potential	-80 mV	(Purvis and Butera 2005)
E_{AMPA}	AMPA mediated current reversal pot.	0 mV	(Destexhe et al. 1998)
E_{NMDA}	NMDA mediated current reversal pot.	0 mV	(Destexhe et al. 1998)
E_{Ca}	calcium reversal potential	140 mV	(Poirazi et al. 2003)
g_{L}	maximum leak conductance	0.005 μS	(Purvis and Butera 2005)
g_{Na}	maximum sodium conductance	0.7 μS	(Purvis and Butera 2005)
g_{K}	maximum potassium conductance	1.3 μS	(Purvis and Butera 2005)
g_{AMPA}	maximum AMPA current conductance	0.0195 μS	see text
g_{NMDA}	max. NMDA-R current conductance	$4.5 \cdot 10^{-4}$ μS	for $\Delta Ca_{\text{pre}} = 0.17$ μM, see text
g_{CaL}	maximum CaL current conductance	$5.6 \cdot 10^{-4}$ μS	for $\Delta Ca_{\text{post}} = 0.34$ μM, (Sabatini et al. 2002)
$N_{\text{NMDA tot}}$	total number of NMDA receptors	20	(Kennedy 2000; Nimchinsky et al. 2004)
$p_{\text{NMDA o}}$	single channel opening probability	0.5	(Nimchinsky et al. 2004)
σ_{NMDA}	SD of the Gaussian noise added	3.3 % of g_{NMDA}	(Mainen et al. 1999)
$N_{\text{CaL tot}}$	total number of CaL channels	5	
$p_{\text{CaL o}}$	single channel opening probability	0.52	(Sabatini and Svoboda 2000)
σ_{CaL}	SD of the Gaussian noise added	10 % of g_{CaL}	

Table A.1: Parameters of the calcium and the voltage dynamics

with $\tau_{\text{AMPA}} = 2$ ms, $\tau'_{\text{AMPA}} = 0.05$ ms, $\alpha_s = 1$ ms^{-1} and $\alpha_x = 1$ (dimensionless) (Destexhe et al. 1998; Wang 1999). s_{AMPA} is a single exponentially decaying gating variable with a finite rise time (the time-to-peak is ≈ 0.2 ms). At each occurrence of a presynaptic spike at time t_k, the variable x_{AMPA} is increased by one (the sum on the right and side of Eq. (A.31) goes over all presynaptic spikes occurring at times t_k).

NMDA current: The current mediated be the NMDA receptor is described by

$$I_{\text{NMDA}} = -g_{\text{NMDA}} s_{\text{NMDA}} B(V)(V(t) - E_{\text{NMDA/Ca}}), \tag{A.32}$$

where the voltage dependence of the magnesium block is given by

$$B(V) = \frac{1}{1 + \exp\left(-0.062V\right)\frac{[Mg^{2+}]}{3.57}}. \tag{A.33}$$

The voltage dependence is controlled by the extracellular magnesium concentration $[Mg^{2+}] = 1.0$ mM (Jahr and Stevens 1990). The dimensionless gating variable s_{NMDA} obeys the same types of equations as s and x of the AMPA current (Eq. (A.30) and (A.31), respectively) but with $\tau_{\text{NMDA}} = 80$ ms and $\tau'_{\text{NMDA}} = 2$ ms (Wang 1999) (the time-to-peak is ≈ 8 ms).

The maximum leak conductance and the whole cell capacitance yield a membrane potential time constant τ_{m} of 20 ms, according to the equation $\tau_{\text{m}} = C_{\text{m}}/g_{\text{L}}$. The AMPA receptor conductance g_{AMPA} is chosen such that a single presynaptic spike evokes a maximal depolarization of 1 mV at -70 mV. g_{NMDA} and g_{CaL} are chosen such that the amplitudes of the NMDA-R mediated (ΔCa_{pre}) and the action potential-evoked calcium transient (ΔCa_{post}) in the spine are realized as stated in the text. The ratio of ~ 2 between the BPAP evoked calcium transient amplitude and the NMDA-R mediated contribution is taken from Sabatini et al.

(2002). Note that the VDCC- and the NMDA-mediated calcium currents in the calcium dynamics (Eq. (3.13)) are multiplied by the scaling parameters β_{NMDA} and β_{CaL} which account for fast calcium buffering ($\sim$ 99 %, Helmchen et al. (1996)) and for the fractional calcium current through NMDA-Rs of $\sim$ 10 % (see section 3.3.1 on page 62, Burnashev et al. (1995), Schneggenburger (1996)). The calcium reversal potential, E_{Ca}, is used to describe the fractional calcium current through NMDAs in the calcium dynamics (Eq. (3.13)) whereas the reversal potential of the compound sodium, potassium and calcium ion current, E_{NMDA}, mediated by NMDA-Rs is employed in the voltage equation (Eq. (4.27)). Note that the transmembrane voltage V is to be measured in mV to make Eqs. (A.19)-(A.33) valid.

Converting ionic currents into concentration changes The sources of intracellular calcium are currents mediated by NMDA receptors and VDCCs. Both currents enter in the equation describing the calcium dynamics (Eq. (3.13)). However, the currents are given in Ampere (or Coulomb per second) and have to be converted into concentration changes per time for the reference volume (spine $V_{\mathrm{spine}} \approx 1$ $\mu\mathrm{m}^3$). This conversion is accounted for by $\zeta = 5182.15$ μM/C. Here we show how to calculate ζ for the spine.

ζ is given by

$$\zeta = \frac{1}{z \cdot F} \cdot \frac{1}{V_{\mathrm{spine}}}, \tag{A.34}$$

where z is the valence charge of the calcium ion ($z = 2$) and $F = 96485$ C/mole is the Faraday constant. The Faraday constant is the amount of electric charge in one mole of electrons. This first factor, $1/(z \cdot F)$, converts Coulomb per second into mole per second, *i.e.* the electrical current into number of ions per time. V_{spine} refers to the volume of the spine and converts the number of calcium ions into a concentration for the respective volume.

The currents in Eq. (3.13) are given in Coulomb per second (C/s). How does the numerical value of ζ look like to get μM/s? Plugging in the values in Eq. (A.34) gives

$$\zeta = \frac{1}{2 \cdot 96485(\mathrm{C/mol})} \cdot \frac{1}{10^{-15}\mathrm{l}}, \tag{A.35}$$

since $1\mu\mathrm{m}^3 = 10^{-15}$ l. Using the concentration (molarity), M, which denotes the number of moles of a given substance per liter of solution, we can write $\zeta = 5182.15$ μM/C. This value is used in the simulations of the calcium dynamics in the six-subunit model (chapter III) and in the two-subunit model (chapter IV).

A.3 Approximation of the PP1 activity level after presentation of one spike-pair

As it can be seen in Fig. 3.7*C* and *D*, the change in PP1 activity as well as the change in I1P concentration (not shown) during the presentation of one spike-pair is small. We therefore separate both variables into two terms, a constant value and a small time-dependent change, *i.e.* $D(t) \to D^* + \epsilon\delta D(t)$ and $I(t) \to I^* + \epsilon\delta I(t)$, where D^* and I^* are the values before the spike-pair presentation, and $\delta D(t)$ and $\delta I(t)$ describe the changes during the presentation. Since these small changes are exclusively driven by changes in $v_{\mathrm{CaN}}(t)$ and $v_{\mathrm{PKA}}(t)$, we consider the time dependent part of both rates as small compared to k_{13} and k_{-13}, *i.e.* $v_{\mathrm{CaN}} \to k^0_{\mathrm{CaN}} + \epsilon\delta v_{\mathrm{CaN}}(t)$ and $v_{\mathrm{PKA}} = k^0_{\mathrm{PKA}} + \epsilon\delta v_{\mathrm{PKA}}(t)$. Inserting these expressions in Eqs. (3.10) and (3.11) yields at zero order in ϵ the steady-state values D^* and I^*. The first order equations in ϵ are

$$\begin{aligned}\frac{d\delta I}{dt} &= -(k_{13}D^* + v_{\mathrm{CaN}})\delta I - (k_{13}I^* + k_{-13})\delta D \\ &\quad -\delta v_{\mathrm{CaN}} I^* + \delta v_{\mathrm{PKA}} I_0, \qquad \text{(A.36)}\\ \frac{d\delta D}{dt} &= -k_{13}D^*\delta I - (k_{13}I^* + k_{-13})\delta D. \qquad \text{(A.37)}\end{aligned}$$

The Eigenvalues of the homogeneous system of Eq. (A.36) and (A.37) are

$$\begin{aligned}\lambda_\pm =& -(v_{\mathrm{CaN}} + k_{13}D^* + k_{13}I^* + k_{-13})/2 \qquad \text{(A.38)}\\ &\pm\sqrt{(v_{\mathrm{CaN}} + k_{13}D^* + k_{13}I^* + k_{-13})^2/4 - v_{\mathrm{CaN}}(k_{13}I^* + k_{-13})}. \qquad \text{(A.39)}\end{aligned}$$

Since v_{CaN} is much smaller than $k_{13}D^*$, $k_{13}I^*$ or k_{-13}, we expand the two Eigenvalues around v_{CaN}. This yields a fast and a slow Eigenvalue since λ_+ is zero at leading order. The Eigenvalues become

$$\begin{aligned}\lambda_-^{(\mathrm{fast})} \equiv \lambda_{\mathrm{fast}} &\approx -(k_{13}(D^* + I^*) + k_{-13}), \qquad \text{(A.40)}\\ \lambda_+^{(\mathrm{slow})} \equiv \lambda_{\mathrm{slow}} &\approx -\frac{(k_{13}I^* + k_{-13})v_{\mathrm{CaN}}}{k_{13}(D^* + I^*) + k_{-13}}. \qquad \text{(A.41)}\end{aligned}$$

With the initial conditions $\delta D(0) = \delta I(0) = 0$, the solution for the inhomogeneous system (A.36) and (A.37) becomes

$$\begin{aligned}\delta I(t) &= A_1 e^{\lambda_{\mathrm{fast}} t}\int_0^t e^{-\lambda_{\mathrm{fast}}\tau}S(\tau)d\tau + B_1 e^{\lambda_{\mathrm{slow}} t}\int_0^t e^{-\lambda_{\mathrm{slow}}\tau}S(\tau)d\tau, \qquad \text{(A.42)}\\ \delta D(t) &= A_2 e^{\lambda_{\mathrm{fast}} t}\int_0^t e^{-\lambda_{\mathrm{fast}}\tau}S(\tau)d\tau + B_2 e^{\lambda_{\mathrm{slow}} t}\int_0^t e^{-\lambda_{\mathrm{slow}}\tau}S(\tau)d\tau, \qquad \text{(A.43)}\end{aligned}$$

with $A_1 = -(k_{13}D^* + v_{\mathrm{CaN}} + \lambda_{\mathrm{slow}})/(\lambda_{\mathrm{fast}} - \lambda_{\mathrm{slow}})$, $B_1 = (k_{13}D^* + v_{\mathrm{CaN}} + \lambda_{\mathrm{fast}})/(\lambda_{\mathrm{fast}} - \lambda_{\mathrm{slow}})$, $A_2 = -k_{13}D^*/(\lambda_{\mathrm{fast}} - \lambda_{\mathrm{slow}})$ and $B_2 = k_{13}D^*/(\lambda_{\mathrm{fast}} - \lambda_{\mathrm{slow}})$. $S(\tau)$ is the inhomogeneous part in Eq. (A.36), *i.e.* $S(\tau) = (-\delta v_{\mathrm{CaN}}(\tau)I^* + \delta v_{\mathrm{PKA}}(\tau)I_0)$. The first term in Eq. (A.42) and (A.43) describes the fast dynamics of both variables and allows D and I to follow on a fast time scale the calcium transient. After the spike-pair presentation, this term decays rapidly with the time constant λ_{fast}. The second term determines the slow dynamics of the system and therefore gives rise to a slow build-up, that decays after the spike-pair presentation with the slow time constant λ_{slow}. Since $(\lambda_{\mathrm{slow}} \cdot t)$ is small at the scale of single presentations, we obtain for the slow dynamics

$$\delta D(t) = \frac{k_{13}D^*}{\lambda_{\mathrm{fast}} - \lambda_{\mathrm{slow}}} \int_0^t (-\delta v_{\mathrm{CaN}}(\tau)I^* + \delta v_{\mathrm{PKA}}(\tau)I_0)d\tau. \tag{A.44}$$

$\delta D(t)$ is shown in Fig. 3.15*B* as a measure for the slowly decaying PP1 build-up after the presentation of one spike-pair. $D^* + \delta D(t)$ is compared with the PP1 activity obtained from numerical integration of Eq. (3.10) and (3.11) after one spike-pair in Fig. 3.15*A*. Note that the product of δD, D^* and D with k_{12} is shown in Fig. 3.15*A* and *B*.

In section 3.3.6 on page 88 we point out that an increase in R beyond the value of 1 does not significantly affect the dynamics of the PP1 response, which is basically determined by $\lambda_+^{(\mathrm{slow})}$ (see paragraph above). This can be understood by considering $\lambda_+^{(\mathrm{slow})}$ (Eq. (A.41)), if $D^* << I^*$, k_{-13}/k_{13} its denominator will be controlled by $k_{13}I^*$ and k_{-13} only and changes in D^* will have no impact on the PP1 dynamics.

B

Net change curves

Phosphorylation and dephosphorylation of CaMKII activate above specific thresholds in the reduced model. De- and phosphorylation rates are zero below the dephosphorylation threshold, Θ_{dephos}, and the phosphorylation threshold, Θ_{phos}, and take the constant rates b and a above, respectively. If the pre- and postsynaptically evoked calcium transients have immediate rise times and the same single exponential decay time constants or decay time constants which differ by a factor of 2 or 3, it is possible to calculate the time the calcium transient spends above these thresholds. These times spent above a given threshold in response to STDP spike-pair stimulation are presented in this chapter. We introduce the net change in phosphorylation in chapter V, which is the time spent above the phosphorylation threshold weighted by a reduced by the time spent above the dephosphorylation threshold weighted by b. The net change curve allows to deduce possible transition results in response to the respective stimulation protocol. The net change curve is calculated explicitely for the STDP spike-pair stimulation protocol without noise here.

B.1 The time the calcium transient spends above a given threshold

The STDP spike-pair stimulation protocol evokes a compound calcium transient. This transient is composed of the transient mediated by NMDA receptors in response to a presynaptic spike and the contribution from VDCCs following a back-propagating action potential. For the calculation presented here, we assume that both calcium transients have immediate rise times. Furthermore, no noise is added to the calcium transients, *i.e.* their maximal amplitudes are *not* drawn from distributions.

Equal decay time constants of pre- and postsynaptic calcium transients Let us first consider the case that the NMDA-R- and the VDCC-mediated calcium transients have the same decay time constants τ, *i.e.* $\tau_{\text{pre}} = \tau^{f}_{\text{post}} = \tau$ ($r = 0$, see section 5.1.2 on page 118). We introduce η which refers to the ratio between post- and presynaptic decay time constants of the calcium transients, *i.e* $\tau = \tau_{\text{pre}} = \tau^{f}_{\text{post}}/\eta$. Consequently, $\eta = 1$ is used here, while η is changed below to discuss cases of different decay time constants. All calculations are done for $D_{\text{post}} > D_{\text{pre}}$. The results for $D_{\text{post}} < D_{\text{pre}}$ can be obtained by swapping D_{post} and D_{pre} and inverting the time, *i.e.* $\Delta t \to -\Delta t$.

We calculate the time the calcium transient evoked by a pre- and postsynaptic spike-pair spends above the threshold Θ_{T}. Three conceptually different cases are distinguished: (i) the threshold is larger than both calcium transients ($D_{\text{post}} < \Theta_{\text{T}}$); (ii) the threshold lies in between the two amplitudes ($D_{\text{pre}} < \Theta_{\text{T}} < D_{\text{post}}$); (iii) and the threshold is below both calcium amplitudes ($D_{\text{pre}} > \Theta_{\text{T}}$) (note that the case $D_{\text{pre}} < D_{\text{post}}$ is considered). These three cases are illustrated in Fig. 5.2*A*. We define some times in advance

$$t_a = \eta\tau \ln(D_{\text{post}}/\Theta_{\text{T}}), \tag{B.1}$$

$$t_b = \tau \ln(D_{\text{pre}}/\Theta_{\text{T}}), \tag{B.2}$$

$$t_\alpha = |\Delta t| + \tau \ln\left[\frac{1}{\Theta_{\text{T}}}, (D_{\text{post}} e^{-|\Delta t|/\tau} + D_{\text{pre}})\right], \tag{B.3}$$

$$t_\beta = |\Delta t| + \tau \ln\left[\frac{1}{\Theta_{\text{T}}} (D_{\text{pre}} e^{-|\Delta t|/\tau} + D_{\text{post}})\right]. \tag{B.4}$$

The times spent above Θ_{T} for the three different cases read as follows:

(i): $D_{\text{post}} < \Theta_{\text{T}}$:

$$\Delta t < 0 \ \text{ and } \ |\Delta t| > a\tau \ln(D_{\text{post}}/(\Theta_{\text{T}} - D_{\text{pre}})),$$
$$I'_1 = 0, \tag{B.5}$$
$$\Delta t < 0 \ \text{ and } \ |\Delta t| < a\tau \ln(D_{\text{post}}/(\Theta_{\text{T}} - D_{\text{pre}})),$$
$$I'_2 = t_\alpha - |\Delta t|, \tag{B.6}$$
$$\Delta t > 0 \ \text{ and } \ \Delta t < \tau \ln(D_{\text{pre}}/(\Theta_{\text{T}} - D_{\text{post}})),$$
$$I'_3 = t_\beta - |\Delta t|, \tag{B.7}$$
$$\Delta t > 0 \ \text{ and } \ \Delta t > \tau \ln(D_{\text{pre}}/(\Theta_{\text{T}} - D_{\text{post}})),$$
$$I'_4 = 0. \tag{B.8}$$

(ii): $D_{\text{pre}} < \Theta_{\text{T}} < D_{\text{post}}$:

$$\Delta t < 0 \quad \text{and} \quad |\Delta t| > a\tau \ln(D_{\text{post}}/(\Theta_{\text{T}} - D_{\text{pre}})),$$

$$I_1'' = a\tau \ln\left(\frac{D_{\text{post}}}{\Theta_{\text{T}}}\right), \tag{B.9}$$

$$\Delta t < 0 \quad \text{and} \quad |\Delta t| < a\tau \ln(D_{\text{post}}/(\Theta_{\text{T}} - D_{\text{pre}}) \quad \text{and} \quad |\Delta t| > t_a,$$

$$I_2'' = \tau \ln\left(\frac{D_{\text{post}}}{\Theta_{\text{T}}}\right) + t_\alpha - |\Delta t|, \tag{B.10}$$

$$\Delta t < 0 \quad \text{and} \quad |\Delta t| < t_a,$$

$$I_3'' = t_\alpha, \tag{B.11}$$

$$\Delta t > 0,$$

$$I_4'' = t_\beta - |\Delta t|. \tag{B.12}$$

(iii): $\Theta_{\text{T}} < D_{\text{pre}}$:

$$\Delta t < 0 \quad \text{and} \quad |\Delta t| > t_a,$$

$$I_1''' = \tau \ln\left(\frac{D_{\text{post}}}{\Theta_{\text{T}}}\right) + t_\alpha - |\Delta t|, \tag{B.13}$$

$$\Delta t < 0 \quad \text{and} \quad |\Delta t| < t_a,$$

$$I_2''' = t_\alpha, \tag{B.14}$$

$$\Delta t > 0 \quad \text{and} \quad \Delta t < t_b,$$

$$I_3''' = t_\beta, \tag{B.15}$$

$$\Delta t > 0 \quad \text{and} \quad \Delta t > t_b,$$

$$I_4''' = a\tau \ln\left(\frac{D_{\text{pre}}}{\Theta_{\text{T}}}\right) + t_\beta - |\Delta t|. \tag{B.16}$$

I_{x}', I_{x}'' and I_{x}''' (with $\text{x} = 1, 2, 3, 4$) refer to the times the calcium transient spends above Θ_{T} for the three different locations of the threshold. In each case, the Δt range is separated into 4 intervals, *i.e.* $\text{x} = 1, 2, 3$ and 4. Fig. 5.2*B* shows that the time spent above a threshold which lies in between D_{pre} and D_{post} (case (ii)) has two discontinuities across the whole Δt range, *i.e.* at $t = -t_a = -\tau \ln(D_{\text{post}}/\Theta_{\text{T}})$ and at $t = -\tau \ln(D_{\text{post}}/(\Theta_{\text{T}} - D_{\text{pre}})$ $(\eta = 1)$. These two discontinuities exist also in cases (i) and (iii), *i.e.* when Θ_{T} is larger than D_{post} and smaller than D_{pre}, respectively. Since we furthermore differentiate between $\Delta t > 0$ and $\Delta t < 0$, the whole Δt is separated into 4 subintervals ($\text{x} = 1, 2, 3, 4$). Note that the time spent above Θ_{T} is zero if $D_{\text{post}} < \Theta_{\text{T}}$ (case (i)) for large positive and negative Δt, *i.e.* $I_1' = I_4' = 0$. In other words, since the threshold is higher than the amplitude of the postsynaptically evoked calcium transient, the threshold is crossed only if the pre- and the postsynaptically evoked transients superimpose.

Different decay time constants of pre- and postsynaptic calcium transients We now switch to the case that the single exponential decay time constants of the pre- and the postsynaptically evoked calcium transients are not equal. Since η refers to the ratio of decay time constants of the post- and presynaptically evoked calcium transients, *i.e.* $\tau = \tau_{\rm pre} = \tau^f_{\rm post}/\eta$, we investigate how the times spent above a threshold change if η deviates from 1 here. In particular, since the NMDA-R-mediated calcium transient has a slower dynamics than the VDCC-mediated component (Sabatini et al. 2002), we study $\eta < 1$.

If $\eta \neq 1$, t_a and t_b are still given by Eq. (B.1) and Eq. (B.2), respectively, but with the respective η. The times t_α and t_β (compare Eqs. (B.3) and (B.4)) are given by

$$0 = (e^{-t_\alpha/\tau})^{1/\eta} + \frac{D_{\rm pre}e^{|\Delta t|/\tau}}{D_{\rm post}}e^{-t_\alpha/\tau} - \frac{\Theta_{\rm T}}{D_{\rm post}}, \tag{B.17}$$

and

$$0 = (e^{-t_\beta/\tau})^{1/\eta} + \frac{D_{\rm pre}}{D_{\rm post}e^{|\Delta t|/(\eta\tau)}}e^{-t_\beta/\tau} - \frac{\Theta_{\rm T}}{D_{\rm post}e^{|\Delta t|/(\eta\tau)}}. \tag{B.18}$$

The analytical soultion of these equations can be readily calculated if $\eta = 1/2$ or $\eta = 1/3$ since this yields quadratic or cubic equations in $e^{-t_\alpha/\tau}$ and $e^{-t_\beta/\tau}$, respectively. With t_a, t_b, t_α and t_β for $\eta = 1/2$ or $1/3$, it is possible to calculate analytically the time spent above thresholds using Eqs. (B.5)-(B.16) with the respective η. If $\eta \neq 1/2, 1/3$, t_α and t_β can be obtained by solving Eqs. (B.17) and (B.18) numerically. The results can be used in turn with Eqs. (B.5)-(B.16) to get the times spent above $\Theta_{\rm T}$ for an arbitrary choice of η.

B.2 Explicit expressions for the net change in phosphorylation

We calculate the time a calcium transient evoked by STDP spike-pair stimulation spends above a given threshold in the previous section. These times can be used to calculate the net change in phosphorylation for a specific pair of phosphorylation ($\Theta_{\rm T} = \Theta_{\rm phos}$) and dephosphorylation thresholds ($\Theta_{\rm T} = \Theta_{\rm dephos}$). We impose on the model that the net change in phosphorylation, N, goes to zero for large positive and large negative time differences, *i.e.* $N(\Delta t)_{|\Delta t| \to \infty} = 0$ (see Eq. (5.11)). This requirement determines the net change curve up to a multiplicative constant since multiplying N with a constant does not change the convergence $N(\Delta t)_{|\Delta t| \to \infty} = 0$.

For the case with $D_{\rm pre} \leq \Theta_{\rm phos} \leq D_{\rm post}$, $D_{\rm pre} \leq \Theta_{\rm dephos} \leq D_{\rm post}$ and the same single exponential decay time constants of the pre- and the postsynaptically evoked calcium transients ($\eta = 1$), the net change curve is given by the following expressions

$$
\begin{aligned}
&\Delta t > 0: \\
&\quad N_1(\Delta t) = \tau \ln\left[\frac{\Theta_{\text{phos}}}{\Theta_{\text{dephos}}}\right] \ln\left[\frac{D_{\text{pre}} e^{-\Delta t/\tau} + D_{\text{post}}}{D_{\text{post}}}\right], && \text{(B.19)} \\
&\Delta t < 0 \text{ and } |\Delta t| < \tau \ln\left(\frac{D_{\text{post}}}{\Theta_{\text{phos}}}\right): \\
&\quad N_2(\Delta t) = \ln\left[\frac{\Theta_{\text{phos}}}{\Theta_{\text{dephos}}}\right] \left(|\Delta t| + \tau \ln\left[\frac{D_{\text{post}} e^{-|\Delta t|/\tau} + D_{\text{pre}}}{D_{\text{post}}}\right]\right), && \text{(B.20)} \\
&\Delta t < 0 \text{ and } |\Delta t| > \tau \ln\left(\frac{D_{\text{post}}}{\Theta_{\text{phos}}}\right) \text{ and } |\Delta t| < \tau \ln\left(\frac{D_{\text{post}}}{\Theta_{\text{dephos}}}\right): \\
&\quad N_3(\Delta t) = \tau \ln\left[\frac{\Theta_{\text{phos}}}{\Theta_{\text{dephos}}}\right] \ln(D_{\text{post}} e^{-|\Delta t|/\tau} + D_{\text{pre}}) + \tau \ln(D_{\text{post}}) \ln\left[\frac{D_{\text{post}}}{\Theta_{\text{phos}}^2}\right] \\
&\qquad + \ln(\Theta_{\text{dephos}}) \ln(\Theta_{\text{phos}}) - |\Delta t| \ln\left[\frac{D_{\text{post}}}{\Theta_{\text{phos}}}\right], && \text{(B.21)} \\
&\Delta t < 0 \text{ and } |\Delta t| > \tau \ln\left(\frac{D_{\text{post}}}{\Theta_{\text{dephos}}}\right) \text{ and } |\Delta t| < \tau \ln\left(\frac{D_{\text{post}}}{\Theta_{\text{phos}} - D_{\text{pre}}}\right): \\
&\quad N_4(\Delta t) = \tau \ln\left[\frac{\Theta_{\text{phos}}}{\Theta_{\text{dephos}}}\right] \ln\left[\frac{D_{\text{post}} e^{-|\Delta t|/\tau} + D_{\text{pre}}}{D_{\text{post}}}\right], && \text{(B.22)} \\
&\Delta t < 0 \text{ and } |\Delta t| > \tau \ln\left(\frac{D_{\text{post}}}{\Theta_{\text{phos}} - D_{\text{pre}}}\right) \text{ and } |\Delta t| < \tau \ln\left(\frac{D_{\text{post}}}{\Theta_{\text{dephos}} - D_{\text{pre}}}\right): \\
&\quad N_5(\Delta t) = \tau \ln\left[\frac{\Theta_{\text{phos}}}{D_{\text{post}}}\right] \ln\left[\frac{D_{\text{post}} e^{-|\Delta t|/\tau} + D_{\text{pre}}}{\Theta_{\text{dephos}}}\right], && \text{(B.23)} \\
&\Delta t < 0 \text{ and } |\Delta t| > \tau \ln\left(\frac{D_{\text{post}}}{\Theta_{\text{dephos}} - D_{\text{pre}}}\right): \\
&\quad N_6(\Delta t) = 0. && \text{(B.24)}
\end{aligned}
$$

$N_{\text{x}}(\Delta t)$ (with $\text{x} = 1,2,3,4,5,6$) is the net change in CaMKII phosphorylation level after the presentation of one spike-pair consisting of a pre- and a postsynaptic spike with a time difference of Δt. Fig. 5.2*B* shows $N(\Delta t)$ for $D_{\text{post}} = 0.2$ μM, $D_{\text{pre}} = 0.1$ μM, $\Theta_{\text{dephos}} = 0.21$ μM and $\Theta_{\text{phos}} = 2.8$ μM (blue line). The 6 intervals of the net change expressions above (Eqs. (B.19)-(B.24)) correspond to the following intervals between the points marked in Fig. 5.2*B*: N_1: from point **5** to $\Delta t \to \infty$ (all positive Δt); N_2: from point **4** to point **5**; N_3: from point **3** to point **4**; N_4: from point **2** to point **3**; N_5: from point **1** to point **2**; and N_6: from $\Delta t \to -\infty$ to point **1**.

The expressions for the net change in phosphorylation are shown for the example $D_{\mathrm{pre}} \leq \Theta_{\mathrm{phos}} \leq D_{\mathrm{post}}$ and $D_{\mathrm{pre}} \leq \Theta_{\mathrm{dephos}} \leq D_{\mathrm{post}}$. However, by using Eqs. (B.5)-(B.16) the net change in CaMKII phosphorylation can be calculated for arbitrary locations of the phosphorylation and the dephosphorylation thresholds.

Bibliography

Abarbanel, H. D. I., L. Gibb, R. Huerta, and M. Rabinovich (2003, Sep). Biophysical model of synaptic plasticity dynamics. *Biol Cybern 89*(3), 214–26.

Abarbanel, H. D. I., R. Huerta, and M. I. Rabinovich (2002, Jul). Dynamical model of long-term synaptic plasticity. *Proc Natl Acad Sci U S A 99*(15), 10132–10137.

Abarbanel, H. D. I., S. S. Talathi, L. Gibb, and M. Rabinovich (2005, Sep). Synaptic plasticity with discrete state synapses. *Phys Rev E Stat Nonlin Soft Matter Phys 72*(3 Pt 1), 031914.

Abel, T., P. V. Nguyen, M. Barad, T. A. Deuel, E. R. Kandel, and R. Bourtchouladze (1997, Mar). Genetic demonstration of a role for PKA in the late phase of LTP and in hippocampus-based long-term memory. *Cell 88*(5), 615–626.

Abraham, W. C. and S. E. Mason (1988, Oct). Effects of the NMDA receptor/channel antagonists CPP and MK801 on hippocampal field potentials and long-term potentiation in anesthetized rats. *Brain Res 462*(1), 40–46.

Alberini, C. M., M. Ghirardi, Y. Y. Huang, P. V. Nguyen, and E. R. Kandel (1995, Jun). A molecular switch for the consolidation of long-term memory: cAMP-inducible gene expression. *Ann N Y Acad Sci 758*, 261–286.

Andersen, P., S. H. Sundberg, O. Sveen, J. W. Swann, and H. Wigström (1980, May). Possible mechanisms for long-lasting potentiation of synaptic transmission in hippocampal slices from guinea-pigs. *J Physiol 302*, 463–482.

Artola, A., S. Bröcher, and W. Singer (1990, Sep). Different voltage-dependent thresholds for inducing long-term depression and long-term potentiation in slices of rat visual cortex. *Nature 347*(6288), 69–72.

Artola, A. and W. Singer (1987). Long-term potentiation and NMDA receptors in rat visual cortex. *Nature 330*(6149), 649–652.

Bagal, A. A., J. P. Y. Kao, C.-M. Tang, and S. M. Thompson (2005, Oct). Long-term potentiation of exogenous glutamate responses at single dendritic spines. *Proc Natl Acad Sci U S A 102*(40), 14434–14439.

Barrionuevo, G. and T. H. Brown (1983, Dec). Associative long-term potentiation in hippocampal slices. *Proc Natl Acad Sci U S A 80*(23), 7347–7351.

Bayer, K. U., P. D. Koninck, A. S. Leonard, J. W. Hell, and H. Schulman (2001, Jun). Interaction with the NMDA receptor locks CaMKII in an active conformation. *Nature 411*(6839), 801–805.

Bear, M. F., W. A. Press, and B. W. Connors (1992, Apr). Long-term potentiation in slices of kitten visual cortex and the effects of NMDA receptor blockade. *J Neurophysiol 67*(4), 841–851.

Bekkers, J. M. and C. F. Stevens (1990, Aug). Presynaptic mechanism for long-term potentiation in the hippocampus. *Nature 346*(6286), 724–729.

Bell, C., V. Han, Y. Sugawara, and K. Grant (1997, May). Synaptic plasticity in a cerebellum-like structure depends on temporal order. *Nature 387*(6630), 278–81.

Bender, V. A., K. J. Bender, D. J. Brasier, and D. E. Feldman (2006, Apr). Two coincidence detectors for spike timing-dependent plasticity in somatosensory cortex. *J Neurosci 26*(16), 4166–4177.

Benke, T. A., A. Lüthi, J. T. Isaac, and G. L. Collingridge (1998, Jun). Modulation of AMPA receptor unitary conductance by synaptic activity. *Nature 393*(6687), 793–797.

Bhalla, U. and R. Iyengar (1999, Jan). Emergent properties of networks of biological signaling pathways. *Science 283*(5400), 381–7.

Bhalla, U. S. and R. Iyengar (2002). DOQCS database. *http://doqcs.ncbs.res.in/*.

Bi, G. and M. Poo (1998, Dec). Synaptic modifications in cultured hippocampal neurons: dependence on spike timing, synaptic strength, and postsynaptic cell type. *J Neurosci 18*(24), 10464–72.

Bi, G. Q. and H. X. Wang (2002, Dec). Temporal asymmetry in spike timing-dependent synaptic plasticity. *Physiol Behav 77*(4-5), 551–5.

Bienenstock, E. L., L. N. Cooper, and P. W. Munro (1982, Jan). Theory for the development of neuron selectivity: orientation specificity and binocular interaction in visual cortex. *J Neurosci 2*(1), 32–48.

Bland, B. H. (1986). The physiology and pharmacology of hippocampal formation theta rhythms. *Prog Neurobiol 26*(1), 1–54.

Bliss, T. and G. Collingridge (1993, Jan). A synaptic model of memory: long-term potentiation in the hippocampus. *Nature 361*(6407), 31–9.

Bliss, T. and T. Lømo (1973, Jul). Long-lasting potentiation of synaptic transmission in the dentate area of the anaesthetized rabbit following stimulation of the perforant path. *J Physiol 232*(2), 331–56.

Bliss, T. V. P., G. L. Collingridge, and R. G. M. Morris (2003, Apr). Introduction. Long-term potentiation and structure of the issue. *Philos Trans R Soc Lond B Biol Sci 358*(1432), 607–11.

Blitzer, R. D., J. H. Connor, G. P. Brown, T. Wong, S. Shenolikar, R. Iyengar, and E. M. Landau (1998, Jun). Gating of CaMKII by cAMP-regulated protein phosphatase activity during LTP. *Science 280*(5371), 1940–1942.

Blitzer, R. D., T. Wong, R. Nouranifar, R. Iyengar, and E. M. Landau (1995, Dec). Postsynaptic cAMP pathway gates early LTP in hippocampal CA1 region. *Neuron 15*(6), 1403–1414.

Bollmann, J., F. Helmchen, J. Borst, and B. Sakmann (1998, Dec). Postsynaptic Ca2+ influx mediated by three different pathways during synaptic transmission at a calyx-type synapse. *J Neurosci 18*(24), 10409–19.

Bolshakov, V. Y. and S. A. Siegelbaum (1995, Sep). Regulation of hippocampal transmitter release during development and long-term potentiation. *Science 269*(5231), 1730–1734.

Bozon, B., A. Kelly, S. A. Josselyn, A. J. Silva, S. Davis, and S. Laroche (2003, Apr). MAPK, CREB and Zif268 are all required for the consolidation of recognition memory. *Philos Trans R Soc Lond B Biol Sci 358*(1432), 805–814.

Bradshaw, J. M., A. Hudmon, and H. Schulman (2002, Jun). Chemical quenched flow kinetic studies indicate an intraholoenzyme autophosphorylation mechanism for Ca2+/calmodulin-dependent protein kinase II. *J Biol Chem 277*(23), 20991–8.

Burnashev, N., Z. Zhou, E. Neher, and B. Sakmann (1995, Jun). Fractional calcium currents through recombinant GluR channels of the NMDA, AMPA and kainate receptor subtypes. *J Physiol 485 (Pt 2)*, 403–418.

Cai, Y., J. P. Gavornik, L. N. Cooper, L. C. Yeung, and H. Z. Shouval (2007, Jan). Effect of stochastic synaptic and dendritic dynamics on synaptic plasticity in visual cortex and hippocampus. *J Neurophysiol 97*(1), 375–386.

Cajal, S. (1995). *Histology of the Nervous System of Man and Vertebrates*. Oxford University Press.

Carr, D. W., R. E. Stofko-Hahn, I. D. Fraser, R. D. Cone, and J. D. Scott (1992, Aug). Localization of the cAMP-dependent protein kinase to the postsynaptic densities by A-kinase anchoring proteins. Characterization of AKAP 79. *J Biol Chem 267*(24), 16816–16823.

Castellani, G. C., E. M. Quinlan, F. Bersani, L. N. Cooper, and H. Z. Shouval (2005). A model of bidirectional synaptic plasticity: from signaling network to channel conductance. *Learn Mem 12*(4), 423–432.

Castro-Alamancos, M. A., J. P. Donoghue, and B. W. Connors (1995, Jul). Different forms of synaptic plasticity in somatosensory and motor areas of the neocortex. *J Neurosci 15*(7 Pt 2), 5324–5333.

Chapman, P. F., E. W. Kairiss, C. L. Keenan, and T. H. Brown (1990). Long-term synaptic potentiation in the amygdala. *Synapse 6*(3), 271–278.

Chen, A., I. A. Muzzio, G. Malleret, D. Bartsch, M. Verbitsky, P. Pavlidis, A. L. Yonan, S. Vronskaya, M. B. Grody, I. Cepeda, T. C. Gilliam, and E. R. Kandel (2003, Aug). Inducible enhancement of memory storage and synaptic plasticity in transgenic mice expressing an inhibitor of ATF4 (CREB-2) and C/EBP proteins. *Neuron 39*(4), 655–669.

Chen, H. X., N. Otmakhov, S. Strack, R. J. Colbran, and J. E. Lisman (2001, Apr). Is persistent activity of calcium/calmodulin-dependent kinase required for the maintenance of LTP? *J Neurophysiol 85*(4), 1368–1376.

Chin, D. and A. Means (2000, Aug). Calmodulin: a prototypical calcium sensor. *Trends Cell Biol 10*(8), 322–8.

Cho, K., J. P. Aggleton, M. W. Brown, and Z. I. Bashir (2001, Apr). An experimental test of the role of postsynaptic calcium levels in determining synaptic strength using perirhinal cortex of rat. *J Physiol 532*(Pt 2), 459–466.

Christie, B. R., J. C. Magee, and D. Johnston (1996). The role of dendritic action potentials and Ca2+ influx in the induction of homosynaptic long-term depression in hippocampal CA1 pyramidal neurons. *Learn Mem 3*(2-3), 160–169.

Coesmans, M., J. T. Weber, C. I. D. Zeeuw, and C. Hansel (2004, Nov). Bidirectional parallel fiber plasticity in the cerebellum under climbing fiber control. *Neuron 44*(4), 691–700.

Cohen, P. and P. T. Cohen (1989, Dec). Protein phosphatases come of age. *J Biol Chem 264*(36), 21435–21438.

Colbran, R. J. (2004). Targeting of calcium/calmodulin-dependent protein kinase II. *Biochem J 378*, 1–16.

Collingridge, G. L., S. J. Kehl, and H. McLennan (1983, Jan). Excitatory amino acids in synaptic transmission in the schaffer collateral-commissural pathway of the rat hippocampus. *J Physiol 334*, 33–46.

Cooke, S. F. and T. V. P. Bliss (2006, Jul). Plasticity in the human central nervous system. *Brain 129*(Pt 7), 1659–1673.

Cooke, S. F., J. Wu, F. Plattner, M. Errington, M. Rowan, M. Peters, A. Hirano, K. D. Bradshaw, R. Anwyl, T. V. P. Bliss, and K. P. Giese (2006, Aug). Autophosphorylation of alphaCaMKII is not a general requirement for NMDA receptor-dependent LTP in the adult mouse. *J Physiol 574*(Pt 3), 805–818.

Coomber, C. (1998). Site-selective autophosphorylation of Ca(2+)/calmodulin-dependent protein kinase II as a synaptic encoding mechanism. *Neural Comput 10*(7), 1653–1678.

Cooper, D., N. Mons, and J. Karpen (1995, Mar). Adenylyl cyclases and the interaction between calcium and cAMP signalling. *Nature 374*(6521), 421–4.

Crick, F. (1984). Memory and molecular turnover. *Nature 312*(5990), 101.

D'Alcantara, P., S. N. Schiffmann, and S. Swillens (2003, Jun). Bidirectional synaptic plasticity as a consequence of interdependent Ca(2+)-controlled phosphorylation and dephosphorylation pathways. *Eur J Neurosci 17*(12), 2521–8.

Davies, S. N., R. A. Lester, K. G. Reymann, and G. L. Collingridge (1989, Apr). Temporally distinct pre- and post-synaptic mechanisms maintain long-term potentiation. *Nature 338*(6215), 500–503.

Debanne, D., B. Gähwiler, and S. Thompson (1998, Feb). Long-term synaptic plasticity between pairs of individual CA3 pyramidal cells in rat hippocampal slice cultures. *J Physiol 507 (Pt 1)*, 237–47.

DeFelipe, J. and I. Fariñas (1992, Dec). The pyramidal neuron of the cerebral cortex: morphological and chemical characteristics of the synaptic inputs. *Prog Neurobiol 39*(6), 563–607.

Degn, H. (1968, Mar). Bistability caused by substrate inhibition of peroxidase in an open reaction system. *Nature 217*(5133), 1047–1050.

Derkach, V., A. Barria, and T. Soderling (1999, Mar). Ca(2+)/calmodulin-kinase II enhances channel conductance of alpha-amino-3-hydroxy-5-methyl-4-isoxazolepropionate type glutamate receptors. *Proc Natl Acad Sci U S A 96*(6), 3269–74.

Destexhe, A., Z. F. Mainen, and T. J. Sejnowski (1998). *Methods in Neuronal Modelling.* MIT Press.

Dobrunz, L. E. and C. F. Stevens (1997, Jun). Heterogeneity of release probability, facilitation, and depletion at central synapses. *Neuron 18*(6), 995–1008.

Doi, T., S. Kuroda, T. Michikawa, and M. Kawato (2005, Jan). Inositol 1,4,5-trisphosphate-dependent Ca2+ threshold dynamics detect spike timing in cerebellar purkinje cells. *J Neurosci 25*(4), 950–961.

Dosemeci, A. and R. W. Albers (1996, Jun). A mechanism for synaptic frequency detection through autophosphorylation of CaM kinase II. *Biophys J 70*(6), 2493–2501.

Dudek, S. and M. Bear (1992, May). Homosynaptic long-term depression in area CA1 of hippocampus and effects of N-methyl-D-aspartate receptor blockade. *Proc Natl Acad Sci U S A 89*(10), 4363–7.

Dunwiddie, T. and G. Lynch (1978, Mar). Long-term potentiation and depression of synaptic responses in the rat hippocampus: localization and frequency dependency. *J Physiol 276*, 353–367.

Dupont, G., G. Houart, and P. de Koninck (2003). Sensitivity of CaM kinase II to the frequency of Ca(2+) oscillations: a simple model. *Cell Calcium 34*(6), 485–497.

Egger, V., D. Feldmeyer, and B. Sakmann (1999, Dec). Coincidence detection and changes of synaptic efficacy in spiny stellate neurons in rat barrel cortex. *Nat Neurosci 2*(12), 1098–105.

Ehlers, M. D. (2000, Nov). Reinsertion or degradation of AMPA receptors determined by activity-dependent endocytic sorting. *Neuron 28*(2), 511–525.

Ehlers, M. D. (2003, Mar). Activity level controls postsynaptic composition and signaling via the ubiquitin-proteasome system. *Nat Neurosci 6*(3), 231–242.

Endo, S., X. Zhou, J. Connor, B. Wang, and S. Shenolikar (1996, Apr). Multiple structural elements define the specificity of recombinant human inhibitor-1 as a protein phosphatase-1 inhibitor. *Biochemistry 35*(16), 5220–8.

Erickson, C., B. Jagadeesh, and R. Desimone (2000, Nov). Clustering of perirhinal neurons with similar properties following visual experience in adult monkeys. *Nat Neurosci 3*(11), 1143–8.

Errington, M. L., M. A. Lynch, and T. V. Bliss (1987, Jan). Long-term potentiation in the dentate gyrus: induction and increased glutamate release are blocked by D(-)aminophosphonovalerate. *Neuroscience 20*(1), 279–284.

Eschrich, K., W. Schellenberger, and E. Hofmann (1980, Nov). In vitro demonstration of alternate stationary states in an open enzyme system containing phosphofructokinase. *Arch Biochem Biophys 205*(1), 114–121.

Esteban, J. A., S.-H. Shi, C. Wilson, M. Nuriya, R. L. Huganir, and R. Malinow (2003, Feb). PKA phosphorylation of AMPA receptor subunits controls synaptic trafficking underlying plasticity. *Nat Neurosci 6*(2), 136–143.

Eurich, C. W., K. Pawelzik, U. Ernst, J. D. Cowan, and J. G. Milton (1999, Feb). Dynamics of self-organized delay adaptation. *Phys. Rev. Lett. 82*(7), 1594–1597.

Feldman, D. E. (2000, Jul). Timing-based LTP and LTD at vertical inputs to layer II/III pyramidal cells in rat barrel cortex. *Neuron 27*(1), 45–56.

Fink, C. C. and T. Meyer (2002, Jun). Molecular mechanisms of CaMKII activation in neuronal plasticity. *Curr Opin Neurobiol 12*(3), 293–9.

Fonseca, R., U. V. Nägerl, R. G. M. Morris, and T. Bonhoeffer (2004, Dec). Competing for memory: hippocampal LTP under regimes of reduced protein synthesis. *Neuron 44*(6), 1011–1020.

Fox, K. (2002). Anatomical pathways and molecular mechanisms for plasticity in the barrel cortex. *Neuroscience 111*(4), 799–814.

Frenzel, J., W. Schellenberger, and K. Eschrich (1995, Jan). Bistability and damped oscillations in the fructose 6-phosphate/fructose 1,6-bisphosphate cycle in cell-free extracts from rat liver. *Biol Chem Hoppe Seyler 376*(1), 17–24.

Frey, U., Y. Y. Huang, and E. R. Kandel (1993, Jun). Effects of cAMP simulate a late stage of LTP in hippocampal CA1 neurons. *Science 260*(5114), 1661–1664.

Froemke, R. C. and Y. Dan (2002, Mar). Spike-timing-dependent synaptic modification induced by natural spike trains. *Nature 416*(6879), 433–8.

Froemke, R. C., M.-M. Poo, and Y. Dan (2005, Mar). Spike-timing-dependent synaptic plasticity depends on dendritic location. *Nature 434*(7030), 221–5.

Froemke, R. C., I. A. Tsay, M. Raad, J. D. Long, and Y. Dan (2006, Mar). Contribution of individual spikes in burst-induced long-term synaptic modification. *J Neurophysiol 95*(3), 1620–1629.

Fuenzalida, M., D. F. de Sevilla, and W. B. no (2007). Changes of the EPSP waveform regulate the temporal window for spike-timing-dependent plasticity. *J Neurosci 27*(44), 11940–11948.

Fusi, S., M. Annunziato, D. Badoni, A. Salamon, and D. J. Amit (2000, Oct). Spike-driven synaptic plasticity: theory, simulation, VLSI implementation. *Neural Comput 12*(10), 2227–2258.

Gerkin, R. C., P.-M. Lau, D. W. Nauen, Y. T. Wang, and G.-Q. Bi (2007, Apr). Modular competition driven by NMDA receptor subtypes in spike-timing-dependent plasticity. *J Neurophysiol 97*(4), 2851–2862.

Gerstner, W., R. Kempter, J. L. van Hemmen, and H. Wagner (1996, Sep). A neuronal learning rule for sub-millisecond temporal coding. *Nature 383*(6595), 76–81.

Gerstner, W. and W. M. Kistler (2002, Dec). Mathematical formulations of hebbian learning. *Biol Cybern 87*(5-6), 404–415.

Giese, K., N. Fedorov, R. Filipkowski, and A. Silva (1998, Feb). Autophosphorylation at Thr286 of the alpha calcium-calmodulin kinase II in LTP and learning. *Science 279*(5352), 870–3.

Glantz, S. B., J. A. Amat, and C. S. Rubin (1992, Nov). cAMP signaling in neurons: patterns of neuronal expression and intracellular localization for a novel protein, AKAP 150, that anchors the regulatory subunit of cAMP-dependent protein kinase II beta. *Mol Biol Cell 3*(11), 1215–1228.

Goelet, P., V. F. Castellucci, S. Schacher, and E. R. Kandel (1986). The long and the short of long-term memory–a molecular framework. *Nature 322*(6078), 419–422.

Grastyan, E., K. Lissak, I. Madarasz, and H. Donhoffer (1959, Aug). Hippocampal electrical activity during the development of conditioned reflexes. *Electroencephalogr Clin Neurophysiol 11*(3), 409–430.

Graupner, M. and N. Brunel (2007). STDP in a bistable synapse model based on CaMKII and associated signaling pathways. *PLoS Comput Biol 3*(11), 2299–2323.

Green, J. D., D. S. Maxwell, W. J. Schindler, and C. Stumpf (1960, July). Rabbit EEG "theta" rhythm: Its anatomical source and relation to activity in single neurons. *J Neurophysiol 23*(4), 403–420.

Griffith, L. C. (2004, Sep). Regulation of calcium/calmodulin-dependent protein kinase II activation by intramolecular and intermolecular interactions. *J Neurosci 24*(39), 8394–8.

Gustafsson, B., H. Wigström, W. C. Abraham, and Y. Y. Huang (1987, Mar). Long-term potentiation in the hippocampus using depolarizing current pulses as the conditioning stimulus to single volley synaptic potentials. *J Neurosci 7*(3), 774–780.

Guyonneau, R., R. VanRullen, and S. J. Thorpe (2005, Apr). Neurons tune to the earliest spikes through STDP. *Neural Comput 17*(4), 859–879.

Gütig, R., R. Aharonov, S. Rotter, and H. Sompolinsky (2003, May). Learning input correlations through nonlinear temporally asymmetric Hebbian plasticity. *J Neurosci 23*(9), 3697–714.

Hahm, J. O., R. B. Langdon, and M. Sur (1991, Jun). Disruption of retinogeniculate afferent segregation by antagonists to NMDA receptors. *Nature 351*(6327), 568–570.

Hall, Z. W. (1992). *An introduction to molecular neurobiology.* Sinnauer, Sunderland.

Hammond, C. (1996). *Cellular and molecular neurobiology.* Academic Press, Paris.

Hanson, P., T. Meyer, L. Stryer, and H. Schulman (1994, May). Dual role of calmodulin in autophosphorylation of multifunctional CaM kinase may underlie decoding of calcium signals. *Neuron 12*(5), 943–56.

Hanson, P. I. and H. Schulman (1992). Neuronal Ca(2+)/calmodulin-dependent protein kinase. *Annu Rev Biochem 61*, 559–601.

Harris, E. W. and C. W. Cotman (1986, Sep). Long-term potentiation of guinea pig mossy fiber responses is not blocked by N-methyl D-aspartate antagonists. *Neurosci Lett 70*(1), 132–137.

Harris, K. M. and J. K. Stevens (1989, Aug). Dendritic spines of CA1 pyramidal cells in the rat hippocampus: serial electron microscopy with reference to their biophysical characteristics. *J Neurosci 9*(8), 2982–2997.

Hayashi, Y., S. H. Shi, J. A. Esteban, A. Piccini, J. C. Poncer, and R. Malinow (2000, Mar). Driving AMPA receptors into synapses by LTP and CaMKII: requirement for GluR1 and PDZ domain interaction. *Science 287*(5461), 2262–2267.

Hayer, A. and U. S. Bhalla (2005, Jul). Molecular switches at the synapse emerge from receptor and kinase traffic. *PLoS Comput Biol 1*(2), 137–154.

Hebb, D. (1949). *The Organization of Behavior: A Neurophsychological Theory*. New York: Wiley.

Helmchen, F., K. Imoto, and B. Sakmann (1996, Feb). Ca2+ buffering and action potential-evoked Ca2+ signaling in dendrites of pyramidal neurons. *Biophys J 70*(2), 1069–1081.

Hertz, J. and A. Prügel-Bennett (1996, May). Learning short synfire chains by self-organization. *Network 7*(2), 357–363.

Holcman, D., E. Korkotian, and M. Segal (2005, May). Calcium dynamics in dendritic spines, modeling and experiments. *Cell Calcium 37*(5), 467–475.

Holmes, W. R. (2000). Models of calmodulin trapping and CaM kinase II activation in a dendritic spine. *J Comput Neurosci 8*(1), 66–85.

Hopfield, J. J. (1982, Apr). Neural networks and physical systems with emergent collective computational abilities. *Proc Natl Acad Sci U S A 79*(8), 2554–2558.

Hsia, A. Y., R. C. Malenka, and R. A. Nicoll (1998, Apr). Development of excitatory circuitry in the hippocampus. *J Neurophysiol 79*(4), 2013–2024.

Huang, C., Y. Liang, and K. Hsu (2001, Dec). Characterization of the mechanism underlying the reversal of long term potentiation by low frequency stimulation at hippocampal CA1 synapses. *J Biol Chem 276*(51), 48108–17.

Hudmon, A. and H. Schulman (2002). Neuronal Ca(2+)/calmodulin-dependent protein kinase II: The role of structure and autoregulation in cellular function. *Annu Rev Biochem 71*, 473–510.

Iglesias, J., J. Eriksson, F. Grize, M. Tomassini, and A. E. P. Villa (2005). Dynamics of pruning in simulated large-scale spiking neural networks. *Biosystems 79*(1-3), 11–20.

Ingebritsen, T. S. and P. Cohen (1983, Jul). Protein phosphatases: properties and role in cellular regulation. *Science 221*(4608), 331–338.

Irvine, E. E., L. S. J. von Hertzen, F. Plattner, and K. P. Giese (2006, Aug). alphaCaMKII autophosphorylation: a fast track to memory. *Trends Neurosci 29*(8), 459–465.

Isaac, J. T., G. O. Hjelmstad, R. A. Nicoll, and R. C. Malenka (1996, Aug). Long-term potentiation at single fiber inputs to hippocampal CA1 pyramidal cells. *Proc Natl Acad Sci U S A 93*(16), 8710–8715.

Ismailov, I., D. Kalikulov, T. Inoue, and M. J. Friedlander (2004, Nov). The kinetic profile of intracellular calcium predicts long-term potentiation and long-term depression. *J Neurosci 24*(44), 9847–61.

Ito, M. (1984). The modifiable neuronal network of the cerebellum. *Jpn J Physiol 34*(5), 781–792.

Izhikevich, E. M. and N. S. Desai (2003, Jul). Relating STDP to BCM. *Neural Comput 15*(7), 1511–1523.

Izhikevich, E. M., J. A. Gally, and G. M. Edelman (2004, Aug). Spike-timing dynamics of neuronal groups. *Cereb Cortex 14*(8), 933–44.

Jahr, C. and C. Stevens (1990, Jun). A quantitative description of NMDA receptor-channel kinetic behavior. *J Neurosci 10*(6), 1830–7.

Jay, T., H. Gurden, and T. Yamaguchi (1998, Oct). Rapid increase in PKA activity during long-term potentiation in the hippocampal afferent fibre system to the prefrontal cortex in vivo. *Eur J Neurosci 10*(10), 3302–6.

Ji, R.-R., T. Kohno, K. A. Moore, and C. J. Woolf (2003, Dec). Central sensitization and LTP: Do pain and memory share similar mechanisms? *Trends Neurosci 26*(12), 696–705.

Jouvenceau, A., J.-M. Billard, U. Haditsch, I. M. Mansuy, and P. Dutar (2003, Sep). Different phosphatase-dependent mechanisms mediate long-term depression and depotentiation of long-term potentiation in mouse hippocampal CA1 area. *Eur J Neurosci 18*(5), 1279–1285.

Jörntell, H. and C. Hansel (2006, Oct). Synaptic memories upside down: bidirectional plasticity at cerebellar parallel fiber-purkinje cell synapses. *Neuron 52*(2), 227–238.

Kandel, E. R., J. H. Schwartz, and T. M. Jessell (1996). *Neurowissenschaften - Eine Einführung*. Spektrum, Heidelberg.

Kandel, E. R. and W. A. Spencer (1961, May). Electrophysiology of hippocampal neurons. II. After-potentials and repetitive firing. *J Neurophysiol 24*, 243–259.

Karmarkar, U. R. and D. V. Buonomano (2002, Jul). A model of spike-timing dependent plasticity: one or two coincidence detectors? *J Neurophysiol 88*(1), 507–513.

Karmarkar, U. R., M. T. Najarian, and D. V. Buonomano (2002, Dec). Mechanisms and significance of spike-timing dependent plasticity. *Biol Cybern 87*(5-6), 373–82.

Kemp, N. and Z. I. Bashir (2001, Nov). Long-term depression: a cascade of induction and expression mechanisms. *Prog Neurobiol 65*(4), 339–365.

Kempter, R., W. Gerstner, and J. L. van Hemmen (1999, Apr). Hebbian learning and spiking neurons. *Phys. Rev. E 59*(4), 4498–4514.

Kennedy, M. (2000, Oct). Signal-processing machines at the postsynaptic density. *Science 290*(5492), 750–4.

Kepecs, A., M. C. W. van Rossum, S. Song, and J. Tegner (2002, Dec). Spike-timing-dependent plasticity: common themes and divergent vistas. *Biol Cybern 87*(5-6), 446–58.

Kirkwood, A., S. M. Dudek, J. T. Gold, C. D. Aizenman, and M. F. Bear (1993, Jun). Common forms of synaptic plasticity in the hippocampus and neocortex in vitro. *Science 260*(5113), 1518–1521.

Kistler, W. M. and J. L. van Hemmen (2000, Feb). Modeling synaptic plasticity in conjuction with the timing of pre- and postsynaptic action potentials. *Neural Comput 12*(2), 385–405.

Kitajima, T. and K. Hara (2000). A generalized Hebbian rule for activity-dependent synaptic modifications. *Neural Netw 13*(4-5), 445–454.

Klee, C. (1988). *Calmodulin.* Elsevier, Amsterdam pp. 35-56.

Koester, H. J. and B. Sakmann (1998, Aug). Calcium dynamics in single spines during coincident pre- and postsynaptic activity depend on relative timing of back-propagating action potentials and subthreshold excitatory postsynaptic potentials. *Proc Natl Acad Sci U S A 95*(16), 9596–9601.

Kolodziej, S. J., A. Hudmon, M. N. Waxham, and J. K. Stoops (2000, May). Three-dimensional reconstructions of calcium/calmodulin-dependent (CaM) kinase IIalpha and truncated CaM kinase IIalpha reveal a unique organization for its structural core and functional domains. *J Biol Chem 275*(19), 14354–14359.

Koninck, P. D. and H. Schulman (1998, Jan). Sensitivity of CaM kinase II to the frequency of Ca(2+) oscillations. *Science 279*(5348), 227–30.

Konorski, J. (1948). *Conditioned reflexes and neuron organization.* Cambridge University Press.

Kubota, Y. and J. Bower (1999). Decoding time-varying calcium signals by the postsynaptic biochemical network:: Computer simulation of molecular kinetics. *Neurocomputing 26-27*, 29–38.

Kubota, Y. and J. M. Bower (2001). Transient versus asymptotic dynamics of CaM kinase II: possible roles of phosphatase. *J Comput Neurosci 11*(3), 263–279.

Kuhnt, U. and L. L. Voronin (1994, Sep). Interaction between paired-pulse facilitation and long-term potentiation in area CA1 of guinea-pig hippocampal slices: application of quantal analysis. *Neuroscience 62*(2), 391–397.

Larkum, M., J. Zhu, and B. Sakmann (2001, Jun). Dendritic mechanisms underlying the coupling of the dendritic with the axonal action potential initiation zone of adult rat layer 5 pyramidal neurons. *J Physiol 533*(Pt 2), 447–66.

Larson, J. and G. Lynch (1986, May). Induction of synaptic potentiation in hippocampus by patterned stimulation involves two events. *Science 232*(4753), 985–988.

Lee, H., M. Barbarosie, K. Kameyama, M. Bear, and R. Huganir (2000, Jun). Regulation of distinct AMPA receptor phosphorylation sites during bidirectional synaptic plasticity. *Nature 405*(6789), 955–9.

Lee, H.-K., K. Takamiya, J.-S. Han, H. Man, C.-H. Kim, G. Rumbaugh, S. Yu, L. Ding, C. He, R. S. Petralia, R. J. Wenthold, M. Gallagher, and R. L.

Huganir (2003, Mar). Phosphorylation of the AMPA receptor GluR1 subunit is required for synaptic plasticity and retention of spatial memory. *Cell 112*(5), 631–643.

Lengyel, I., K. Voss, M. Cammarota, K. Bradshaw, V. Brent, K. P. S. J. Murphy, K. P. Giese, J. A. P. Rostas, and T. V. P. Bliss (2004, Dec). Autonomous activity of CaMKII is only transiently increased following the induction of long-term potentiation in the rat hippocampus. *Eur J Neurosci 20*(11), 3063–3072.

Lev-Ram, V., S. T. Wong, D. R. Storm, and R. Y. Tsien (2002, Jun). A new form of cerebellar long-term potentiation is postsynaptic and depends on nitric oxide but not cAMP. *Proc Natl Acad Sci U S A 99*(12), 8389–8393.

Levy, N., D. Horn, I. Meilijson, and E. Ruppin (2001). Distributed synchrony in a cell assembly of spiking neurons. *Neural Netw 14*(6-7), 815–24.

Levy, W. B. and O. Steward (1979, Oct). Synapses as associative memory elements in the hippocampal formation. *Brain Res 175*(2), 233–245.

Levy, W. B. and O. Steward (1983, Apr). Temporal contiguity requirements for long-term associative potentiation/depression in the hippocampus. *Neuroscience 8*(4), 791–797.

Liao, D., N. A. Hessler, and R. Malinow (1995, Jun). Activation of postsynaptically silent synapses during pairing-induced LTP in CA1 region of hippocampal slice. *Nature 375*(6530), 400–404.

Linse, S., A. Helmersson, and S. Forsén (1991, May). Calcium binding to calmodulin and its globular domains. *J Biol Chem 266*(13), 8050–4.

Lisman, J. (1985, May). A mechanism for memory storage insensitive to molecular turnover: a bistable autophosphorylating kinase. *Proc Natl Acad Sci U S A 82*(9), 3055–7.

Lisman, J. (1989, Dec). A mechanism for the Hebb and the anti-Hebb processes underlying learning and memory. *Proc Natl Acad Sci U S A 86*(23), 9574–8.

Lisman, J. (2001, Apr). Three Ca(2+) levels affect plasticity differently: the LTP zone, the LTD zone and no man's land. *J Physiol 532*(Pt 2), 285.

Lisman, J. (2003, Apr). Long-term potentiation: outstanding questions and attempted synthesis. *Philos Trans R Soc Lond B Biol Sci 358*(1432), 829–42.

Lisman, J., H. Schulman, and H. Cline (2002, Mar). The molecular basis of CaMKII function in synaptic and behavioural memory. *Nat Rev Neurosci 3*(3), 175–90.

Lisman, J. E. and M. A. Goldring (1988, Jul). Feasibility of long-term storage of graded information by the Ca2+/calmodulin-dependent protein kinase molecules of the postsynaptic density. *Proc Natl Acad Sci U S A 85*(14), 5320–5324.

London, M. and M. Häusser (2005). Dendritic computation. *Annu Rev Neurosci 28*, 503–532.

Lynch, G., J. Larson, S. Kelso, G. Barrionuevo, and F. Schottler (1983). Intracellular injections of EGTA block induction of hippocampal long-term potentiation. *Nature 305*(5936), 719–721.

Lynch, G. S., T. Dunwiddie, and V. Gribkoff (1977, Apr). Heterosynaptic depression: a postsynaptic correlate of long-term potentiation. *Nature 266*(5604), 737–739.

Lynch, M. A. (2004, Jan). Long-term potentiation and memory. *Physiol Rev 84*(1), 87–136.

Magee, J. and D. Johnston (1997, Jan). A synaptically controlled, associative signal for Hebbian plasticity in hippocampal neurons. *Science 275*(5297), 209–13.

Mainen, Z., R. Malinow, and K. Svoboda (1999, May). Synaptic calcium transients in single spines indicate that NMDA receptors are not saturated. *Nature 399*(6732), 151–5.

Malenka, R. and R. Nicoll (1999, Sep). Long-term potentiation–a decade of progress? *Science 285*(5435), 1870–4.

Malenka, R. C. and M. F. Bear (2004, Sep). LTP and LTD: an embarrassment of riches. *Neuron 44*(1), 5–21.

Malenka, R. C., J. A. Kauer, R. S. Zucker, and R. A. Nicoll (1988, Oct). Postsynaptic calcium is sufficient for potentiation of hippocampal synaptic transmission. *Science 242*(4875), 81–84.

Malinow, R. and R. C. Malenka (2002). AMPA receptor trafficking and synaptic plasticity. *Annu Rev Neurosci 25*, 103–126.

Malinow, R. and R. W. Tsien (1990, Jul). Presynaptic enhancement shown by whole-cell recordings of long-term potentiation in hippocampal slices. *Nature 346*(6280), 177–180.

Malleret, G., U. Haditsch, D. Genoux, M. Jones, T. Bliss, A. Vanhoose, C. Weitlauf, E. Kandel, D. Winder, and I. Mansuy (2001, Mar). Inducible and reversible enhancement of learning, memory, and long-term potentiation by genetic inhibition of calcineurin. *Cell 104*(5), 675–86.

Mammen, A. L., K. Kameyama, K. W. Roche, and R. L. Huganir (1997, Dec). Phosphorylation of the alpha-amino-3-hydroxy-5-methylisoxazole4-propionic acid receptor GluR1 subunit by calcium/calmodulin-dependent kinase II. *J Biol Chem 272*(51), 32528–32533.

Manabe, T., P. Renner, and R. A. Nicoll (1992, Jan). Postsynaptic contribution to long-term potentiation revealed by the analysis of miniature synaptic currents. *Nature 355*(6355), 50–55.

Mansuy, I. M., M. Mayford, B. Jacob, E. R. Kandel, and M. E. Bach (1998, Jan). Restricted and regulated overexpression reveals calcineurin as a key component in the transition from short-term to long-term memory. *Cell 92*(1), 39–49.

Markram, H., J. Lübke, M. Frotscher, and B. Sakmann (1997, Jan). Regulation of synaptic efficacy by coincidence of postsynaptic APs and EPSPs. *Science 275*(5297), 213–5.

Matsushita, T., S. Moriyama, and T. Fukai (1995). Switching dynamics and the transient memory storage in a model enzyme network involving Ca2+/calmodulin-dependent protein kinase II in synapses. *Biol Cybern 72*(6), 497–509.

McNaughton, B. L. (1982, Mar). Long-term synaptic enhancement and short-term potentiation in rat fascia dentata act through different mechanisms. *J Physiol 324*, 249–262.

McNaughton, B. L., R. M. Douglas, and G. V. Goddard (1978, Nov). Synaptic enhancement in fascia dentata: cooperativity among coactive afferents. *Brain Res 157*(2), 277–293.

McNeill, R. B. and R. J. Colbran (1995, Apr). Interaction of autophosphorylated Ca2+/calmodulin-dependent protein kinase II with neuronal cytoskeletal proteins. characterization of binding to a 190-kDa postsynaptic density protein. *J Biol Chem 270*(17), 10043–10049.

Meffin, H., J. Besson, A. N. Burkitt, and D. B. Grayden (2006, Apr). Learning the structure of correlated synaptic subgroups using stable and competitive spike-timing-dependent plasticity. *Phys Rev E Stat Nonlin Soft Matter Phys 73*(4 Pt 1), 041911.

Meyer, T., P. I. Hanson, L. Stryer, and H. Schulman (1992). Calmodulin trapping by calcium-calmodulin-dependent protein kinase. *Science 256*(5060), 1199–1202.

Michaelis, L. and M. Menten (1913). Die Kinetik der Invertinwirkung. *Biochem Z 49*, 333–369.

Michelson, S. and H. Schulman (1994). CaM kinase: A model for its activation and dynamics. *J Theor Biol 171*(3), 281–290.

Miller, P., A. M. Zhabotinsky, J. E. Lisman, and X.-J. Wang (2005, Apr). The stability of a stochastic CaMKII switch: dependence on the number of enzyme molecules and protein turnover. *PLoS Biol 3*(4), e107.

Miller, S. G. and M. B. Kennedy (1986, Mar). Regulation of brain type II Ca2+/calmodulin-dependent protein kinase by autophosphorylation: a Ca2+-triggered molecular switch. *Cell 44*(6), 861–870.

Mizuno, T., I. Kanazawa, and M. Sakurai (2001, Aug). Differential induction of LTP and LTD is not determined solely by instantaneous calcium concentration: an essential involvement of a temporal factor. *Eur J Neurosci 14*(4), 701–8.

Mongillo, G., E. Curti, S. Romani, and D. J. Amit (2005, Jun). Learning in realistic networks of spiking neurons and spike-driven plastic synapses. *Eur J Neurosci 21*(11), 3143–3160.

Mooney, R., D. V. Madison, and C. J. Shatz (1993, May). Enhancement of transmission at the developing retinogeniculate synapse. *Neuron 10*(5), 815–825.

Morishita, W., J. Connor, H. Xia, E. Quinlan, S. Shenolikar, and R. Malenka (2001, Dec). Regulation of synaptic strength by protein phosphatase 1. *Neuron 32*(6), 1133–48.

Morishita, W., H. Marie, and R. C. Malenka (2005, Aug). Distinct triggering and expression mechanisms underlie LTD of AMPA and NMDA synaptic responses. *Nat Neurosci 8*(8), 1043–1050.

Morris, R. G., E. Anderson, G. S. Lynch, and M. Baudry (1986). Selective impairment of learning and blockade of long-term potentiation by an N-methyl-D-aspartate receptor antagonist, AP5. *Nature 319*(6056), 774–776.

Morrison, A., A. Aertsen, and M. Diesmann (2007, Jun). Spike-timing-dependent plasticity in balanced random networks. *Neural Comput 19*(6), 1437–1467.

Mulkey, R., S. Endo, S. Shenolikar, and R. Malenka (1994, Jun). Involvement of a calcineurin/inhibitor-1 phosphatase cascade in hippocampal long-term depression. *Nature 369*(6480), 486–8.

Munton, R. P., S. Vizi, and I. M. Mansuy (2004, Jun). The role of protein phosphatase-1 in the modulation of synaptic and structural plasticity. *FEBS Lett 567*(1), 121–8.

Murthy, V. N. and C. F. Stevens (1999, Jun). Reversal of synaptic vesicle docking at central synapses. *Nat Neurosci 2*(6), 503–507.

Naparstek, A., J. L. Romette, J. P. Kernevez, and D. Thomas (1974, May). Memory in enzyme membranes. *Nature 249*(456), 490–491.

Neveu, D. and R. S. Zucker (1996, May). Long-lasting potentiation and depression without presynaptic activity. *J Neurophysiol 75*(5), 2157–2160.

Nevian, T. and B. Sakmann (2006, Oct). Spine Ca2+ signaling in spike-timing-dependent plasticity. *J Neurosci 26*(43), 11001–11013.

Ngezahayo, A., M. Schachner, and A. Artola (2000, Apr). Synaptic activity modulates the induction of bidirectional synaptic changes in adult mouse hippocampus. *J Neurosci 20*(7), 2451–8.

Nguyen, P. V. and E. R. Kandel (1997). Brief theta-burst stimulation induces a transcription-dependent late phase of LTP requiring cAMP in area CA1 of the mouse hippocampus. *Learn Mem 4*(2), 230–243.

Nicoletti, F., V. Bruno, A. Copani, G. Casabona, and T. Knöpfel (1996, Jul). Metabotropic glutamate receptors: a new target for the therapy of neurodegenerative disorders? *Trends Neurosci 19*(7), 267–271.

Nimchinsky, E. A., R. Yasuda, T. G. Oertner, and K. Svoboda (2004, Feb). The number of glutamate receptors opened by synaptic stimulation in single hippocampal spines. *J Neurosci 24*(8), 2054–64.

Nishi, A., G. L. Snyder, A. C. Nairn, and P. Greengard (1999, May). Role of calcineurin and protein phosphatase-2A in the regulation of DARPP-32 dephosphorylation in neostriatal neurons. *J Neurochem 72*(5), 2015–2021.

Nishiyama, M., K. Hong, K. Mikoshiba, M. M. Poo, and K. Kato (2000, Nov). Calcium stores regulate the polarity and input specificity of synaptic modification. *Nature 408*(6812), 584–588.

Normann, C., D. Peckys, C. H. Schulze, J. Walden, P. Jonas, and J. Bischofberger (2000, Nov). Associative long-term depression in the hippocampus is dependent on postsynaptic N-type Ca2+ channels. *J Neurosci 20*(22), 8290–8297.

Nowak, L., P. Bregestovski, P. Ascher, A. Herbet, and A. Prochiantz (1984). Magnesium gates glutamate-activated channels in mouse central neurones. *Nature 307*(5950), 462–465.

O'Connor, D. H., G. M. Wittenberg, and S. S.-H. Wang (2005a, Aug). Dissection of bidirectional synaptic plasticity into saturable unidirectional processes. *J Neurophysiol 94*(2), 1565–73.

O'Connor, D. H., G. M. Wittenberg, and S. S.-H. Wang (2005b, Jul). Graded bidirectional synaptic plasticity is composed of switch-like unitary events. *Proc Natl Acad Sci U S A 102*(27), 9679–84.

Oja, E. (1982). A simplified neuron model as a principal component analyzer. *J Math Biol 15*(3), 267–273.

Okamoto, H. and K. Ichikawa (2000). Switching characteristics of a model for biochemical-reaction networks describing autophosphorylation versus dephosphorylation of Ca(2+)/calmodulin-dependent protein kinase II. *Biol Cybern 82*(1), 35–47.

Oliver, C. and S. Shenolikar (1998, Sep). Physiologic importance of protein phosphatase inhibitors. *Front Biosci 3*, D961–72.

Otani, S., O. Blond, J. Desce, and F. Crépel (1998, Aug). Dopamine facilitates long-term depression of glutamatergic transmission in rat prefrontal cortex. *Neuroscience 85*(3), 669–76.

Palay, S. L. and V. Chan-Palay (1974). *Cerebellar cortex - Cytology and organisation.* Berlin-Heidelberg-New York: Springer.

Persechini, A. and P. M. Stemmer (2002, Jan). Calmodulin is a limiting factor in the cell. *Trends Cardiovasc Med 12*(1), 32–37.

Persechini, A., P. M. Stemmer, and I. Ohashi (1996, Dec). Localization of unique functional determinants in the calmodulin lobes to individual EF hands. *J Biol Chem 271*(50), 32217–32225.

Petersen, C., R. Malenka, R. Nicoll, and J. Hopfield (1998, Apr). All-or-none potentiation at CA3-CA1 synapses. *Proc Natl Acad Sci U S A 95*(8), 4732–7.

Petersen, J. D., X. Chen, L. Vinade, A. Dosemeci, J. E. Lisman, and T. S. Reese (2003, Dec). Distribution of postsynaptic density (PSD)-95 and Ca2+/calmodulin-dependent protein kinase II at the PSD. *J Neurosci 23*(35), 11270–11278.

Pfister, J.-P. and W. Gerstner (2006, Sep). Triplets of spikes in a model of spike timing-dependent plasticity. *J Neurosci 26*(38), 9673–9682.

Philpot, B. D., A. K. Sekhar, H. Z. Shouval, and M. F. Bear (2001, Jan). Visual experience and deprivation bidirectionally modify the composition and function of NMDA receptors in visual cortex. *Neuron 29*(1), 157–169.

Piomelli, D. (2003, Nov). The molecular logic of endocannabinoid signalling. *Nat Rev Neurosci 4*(11), 873–884.

Poirazi, P., T. Brannon, and B. W. Mel (2003, Mar). Arithmetic of subthreshold synaptic summation in a model CA1 pyramidal cell. *Neuron 37*(6), 977–87.

Purvis, L. K. and R. J. Butera (2005, Feb). Ionic current model of a hypoglossal motoneuron. *J Neurophysiol 93*(2), 723–33.

Pyott, S. J. and C. Rosenmund (2002, Mar). The effects of temperature on vesicular supply and release in autaptic cultures of rat and mouse hippocampal neurons. *J Physiol 539*(Pt 2), 523–535.

Raastad, M. (1995, Sep). Extracellular activation of unitary excitatory synapses between hippocampal CA3 and CA1 pyramidal cells. *Eur J Neurosci 7*(9), 1882–1888.

Ranck, J. B. (1973, Nov). Studies on single neurons in dorsal hippocampal formation and septum in unrestrained rats. I. Behavioral correlates and firing repertoires. *Exp Neurol 41*(2), 461–531.

Roberts, P. D. (1999). Computational consequences of temporally asymmetric learning rules: I. Differential hebbian learning. *J Comput Neurosci 7*(3), 235–246.

Rosenberg, O. S., S. Deindl, R.-J. Sung, A. C. Nairn, and J. Kuriyan (2005, Dec). Structure of the autoinhibited kinase domain of CaMKII and SAXS analysis of the holoenzyme. *Cell 123*(5), 849–860.

Rubin, J., D. Lee, and H. Sompolinsky (2001, Jan). Equilibrium properties of temporally asymmetric Hebbian plasticity. *Phys Rev Lett 86*(2), 364–7.

Rubin, J. E., R. C. Gerkin, G.-Q. Bi, and C. C. Chow (2005, May). Calcium time course as a signal for spike-timing-dependent plasticity. *J Neurophysiol 93*(5), 2600–2613.

Sabatini, B. and K. Svoboda (2000, Nov). Analysis of calcium channels in single spines using optical fluctuation analysis. *Nature 408*(6812), 589–93.

Sabatini, B. L., T. G. Oertner, and K. Svoboda (2002, Jan). The life cycle of Ca(2+) ions in dendritic spines. *Neuron 33*(3), 439–52.

Sahin, B., H. Shu, J. Fernandez, A. El-Armouche, J. D. Molkentin, A. C. Nairn, and J. A. Bibb (2006, Aug). Phosphorylation of protein phosphatase inhibitor-1 by protein kinase C. *J Biol Chem 281*(34), 24322–24335.

Sajikumar, S., S. Navakkode, and J. U. Frey (2007, May). Identification of compartment- and process-specific molecules required for "synaptic tagging" during long-term potentiation and long-term depression in hippocampal CA1. *J Neurosci 27*(19), 5068–5080.

Salin, P. A., R. C. Malenka, and R. A. Nicoll (1996, Apr). Cyclic AMP mediates a presynaptic form of LTP at cerebellar parallel fiber synapses. *Neuron 16*(4), 797–803.

Sanhueza, M., C. C. McIntyre, and J. E. Lisman (2007, May). Reversal of synaptic memory by Ca2+/calmodulin-dependent protein kinase II inhibitor. *J Neurosci 27*(19), 5190–5199.

Schneggenburger, R. (1996, May). Simultaneous measurement of Ca2+ influx and reversal potentials in recombinant N-methyl-D-aspartate receptor channels. *Biophys J 70*(5), 2165–2174.

Senn, W., H. Markram, and M. Tsodyks (2001, Jan). An algorithm for modifying neurotransmitter release probability based on pre- and postsynaptic spike timing. *Neural Comput 13*(1), 35–67.

Sharma, K., D. K. Fong, and A. M. Craig (2006, Apr). Postsynaptic protein mobility in dendritic spines: long-term regulation by synaptic NMDA receptor activation. *Mol Cell Neurosci 31*(4), 702–712.

Shen, K. and T. Meyer (1999, Apr). Dynamic control of CaMKII translocation and localization in hippocampal neurons by NMDA receptor stimulation. *Science 284*(5411), 162–166.

Shen, K., M. N. Teruel, J. H. Connor, S. Shenolikar, and T. Meyer (2000, Sep). Molecular memory by reversible translocation of calcium/calmodulin-dependent protein kinase II. *Nat Neurosci 3*(9), 881–886.

Shenolikar, S. (1994). Protein serine/threonine phosphatases–new avenues for cell regulation. *Annu Rev Cell Biol 10*, 55–86.

Shifman, J. M., M. H. Choi, S. Mihalas, S. L. Mayo, and M. B. Kennedy (2006, Sep). Ca2+/calmodulin-dependent protein kinase II (CaMKII) is activated by calmodulin with two bound calciums. *Proc Natl Acad Sci U S A 103*(38), 13968–13973.

Shouval, H. Z. (2005, Oct). Clusters of interacting receptors can stabilize synaptic efficacies. *Proc Natl Acad Sci U S A 102*(40), 14440–14445.

Shouval, H. Z., M. F. Bear, and L. N. Cooper (2002, Aug). A unified model of NMDA receptor-dependent bidirectional synaptic plasticity. *Proc Natl Acad Sci U S A 99*(16), 10831–6.

Shouval, H. Z., G. C. Castellani, B. S. Blais, L. C. Yeung, and L. N. Cooper (2002, Dec). Converging evidence for a simplified biophysical model of synaptic plasticity. *Biol Cybern 87*(5-6), 383–91.

Shouval, H. Z. and G. Kalantzis (2005, Feb). Stochastic properties of synaptic transmission affect the shape of spike time-dependent plasticity curves. *J Neurophysiol 93*(2), 1069–73.

Sjöström, P., G. Turrigiano, and S. Nelson (2001, Dec). Rate, timing, and cooperativity jointly determine cortical synaptic plasticity. *Neuron 32*(6), 1149–64.

Sjöström, P. J. and M. Häusser (2006, Jul). A cooperative switch determines the sign of synaptic plasticity in distal dendrites of neocortical pyramidal neurons. *Neuron 51*(2), 227–238.

Sjöström, P. J., E. A. Rancz, A. Roth, and M. Häusser (2008, Apr). Dendritic excitability and synaptic plasticity. *Physiol Rev 88*(2), 769–840.

Sjöström, P. J., G. G. Turrigiano, and S. B. Nelson (2003, Aug). Neocortical LTD via coincident activation of presynaptic NMDA and cannabinoid receptors. *Neuron 39*(4), 641–654.

Sjöström, P. J., G. G. Turrigiano, and S. B. Nelson (2004, Dec). Endocannabinoid-dependent neocortical layer-5 LTD in the absence of postsynaptic spiking. *J Neurophysiol 92*(6), 3338–3343.

Skrede, K. K. and R. H. Westgaard (1971, Dec). The transverse hippocampal slice: a well-defined cortical structure maintained in vitro. *Brain Res 35*(2), 589–593.

Smolen, P. (2007). A model of late long-term potentiation simulates aspects of memory maintenance. *PLoS ONE 2*(5), e445.

Soderling, T. R. and V. A. Derkach (2000, Feb). Postsynaptic protein phosphorylation and LTP. *Trends Neurosci 23*(2), 75–80.

Song, S., K. Miller, and L. Abbott (2000, Sep). Competitive Hebbian learning through spike-timing-dependent synaptic plasticity. *Nat Neurosci 3*(9), 919–26.

Staubli, U. and G. Lynch (1987, Dec). Stable hippocampal long-term potentiation elicited by 'theta' pattern stimulation. *Brain Res 435*(1-2), 227–234.

Stemmer, P. and C. Klee (1994, Jun). Dual calcium ion regulation of calcineurin by calmodulin and calcineurin B. *Biochemistry 33*(22), 6859–66.

Stevens, C. F. and Y. Wang (1995, Apr). Facilitation and depression at single central synapses. *Neuron 14*(4), 795–802.

Strack, S., S. Choi, D. M. Lovinger, and R. J. Colbran (1997). Translocation of autophosphorylated calcium/calmodulin-dependent protein kinase II to the postsynaptic density. *J Biol Chem 272*(21), 13467–13470.

Stuart, G., N. Spruston, and M. Häusser (2007). *Dendrites 2nd edition*. Oxford University Press.

Stuart, G., N. Spruston, B. Sakmann, and M. Häusser (1997, Mar). Action potential initiation and backpropagation in neurons of the mammalian CNS. *Trends Neurosci 20*(3), 125–131.

Svenningsson, P., A. Nishi, G. Fisone, J.-A. Girault, A. C. Nairn, and P. Greengard (2004). DARPP-32: an integrator of neurotransmission. *Annu Rev Pharmacol Toxicol 44*, 269–296.

Sweatt, J. D. (2004, Jun). Mitogen-activated protein kinases in synaptic plasticity and memory. *Curr Opin Neurobiol 14*(3), 311–317.

Tsodyks, M. V. and M. V. Feigel'man (1988). The enhanced storage capacity in neural networks with low activity level. *Europhys Let 6*, 101–105.

van Rossum, M. C., G. Q. Bi, and G. G. Turrigiano (2000, Dec). Stable hebbian learning from spike timing-dependent plasticity. *J Neurosci 20*(23), 8812–8821.

Vanderwolf, C. H. (1969, Apr). Hippocampal electrical activity and voluntary movement in the rat. *Electroencephalogr Clin Neurophysiol 26*(4), 407–418.

Waltereit, R. and M. Weller (2003, Feb). Signaling from cAMP/PKA to MAPK and synaptic plasticity. *Mol Neurobiol 27*(1), 99–106.

Wang, F. (2004, Sep). Steering growth cones with a CaMKII/calcineurin switch. *Neuron 43*(6), 760–2.

Wang, H.-X., R. C. Gerkin, D. W. Nauen, and G.-Q. Bi (2005, Feb). Coactivation and timing-dependent integration of synaptic potentiation and depression. *Nat Neurosci 8*(2), 187–93.

Wang, S. S., W. Denk, and M. Häusser (2000, Dec). Coincidence detection in single dendritic spines mediated by calcium release. *Nat Neurosci 3*(12), 1266–1273.

Wang, X. (1999, Nov). Synaptic basis of cortical persistent activity: the importance of NMDA receptors to working memory. *J Neurosci 19*(21), 9587–603.

Ward, B., L. McGuinness, C. J. Akerman, A. Fine, T. V. P. Bliss, and N. J. Emptage (2006, Nov). State-dependent mechanisms of LTP expression revealed by optical quantal analysis. *Neuron 52*(4), 649–661.

Waters, J., M. Larkum, B. Sakmann, and F. Helmchen (2003, Sep). Supralinear Ca2+ influx into dendritic tufts of layer 2/3 neocortical pyramidal neurons in vitro and in vivo. *J Neurosci 23*(24), 8558–8567.

Watkins, J. and G. Collingridge (1994, Sep). Phenylglycine derivatives as antagonists of metabotropic glutamate receptors. *Trends Pharmacol Sci 15*(9), 333–342.

Weisskopf, M. G. and R. A. Nicoll (1995, Jul). Presynaptic changes during mossy fibre LTP revealed by NMDA receptor-mediated synaptic responses. *Nature 376*(6537), 256–259.

Whitlock, J. R., A. J. Heynen, M. G. Shuler, and M. F. Bear (2006, Aug). Learning induces long-term potentiation in the hippocampus. *Science 313*(5790), 1093–1097.

Winder, D., I. Mansuy, M. Osman, T. Moallem, and E. Kandel (1998, Jan). Genetic and pharmacological evidence for a novel, intermediate phase of long-term potentiation suppressed by calcineurin. *Cell 92*(1), 25–37.

Wittenberg, G. M. and S. S.-H. Wang (2006, Jun). Malleability of spike-timing-dependent plasticity at the CA3-CA1 synapse. *J Neurosci 26*(24), 6610–6617.

Yang, H.-W., X.-D. Hu, H.-M. Zhang, W.-J. Xin, M.-T. Li, T. Zhang, L.-J. Zhou, and X.-G. Liu (2004, Mar). Roles of CaMKII, PKA, and PKC in the induction and maintenance of LTP of C-fiber-evoked field potentials in rat spinal dorsal horn. *J Neurophysiol 91*(3), 1122–1133.

Yang, S., Y. Tang, and R. Zucker (1999, Feb). Selective induction of LTP and LTD by postsynaptic [Ca2+]i elevation. *J Neurophysiol 81*(2), 781–7.

Zhabotinsky, A. M. (2000). Bistability in the Ca(2+)/calmodulin-dependent protein kinase-phosphatase system. *Biophys J 79*(5), 2211–2221.

Zhabotinsky, A. M., R. N. Camp, I. R. Epstein, and J. E. Lisman (2006, Jul). Role of the neurogranin concentrated in spines in the induction of long-term potentiation. *J Neurosci 26*(28), 7337–7347.

Zhang, L., T. Kirschstein, B. Sommersberg, M. Merkens, D. Manahan-Vaughan, Y. Elgersma, and H. Beck (2005, Aug). Hippocampal synaptic metaplasticity requires inhibitory autophosphorylation of Ca2+/calmodulin-dependent kinase II. *J Neurosci 25*(33), 7697–7707.

Zhang, L. I., H. W. Tao, C. E. Holt, W. A. Harris, and M. Poo (1998, Sep). A critical window for cooperation and competition among developing retinotectal synapses. *Nature 395*(6697), 37–44.

Zhuo, M., W. Zhang, H. Son, I. Mansuy, R. A. Sobel, J. Seidman, and E. R. Kandel (1999, Apr). A selective role of calcineurin A-alpha in synaptic depotentiation in hippocampus. *Proc Natl Acad Sci U S A 96*(8), 4650–4655.

Zucker, R. S. (1999, Jun). Calcium- and activity-dependent synaptic plasticity. *Curr Opin Neurobiol 9*(3), 305–313.